Mechanisms of iron storage in *Escherichia coli*: a Molecular-genetic analysis

A thesis submitted for the degree of Doctor of Philosophy

by

Afrah Mohammed Hassan Salman

Division of Microbiology

School of Biological Sciences

The University of Reading

UK

June 2018

THE UNIVERSITY OF READING - DECLARATION

Declaration:

I confirm that this is my own work and the use of all material from other sources has been properly and fully acknowledged.

Signed: _____Afrah Salman

Date: _____

I would like to dedicate this thesis to my husband

Mr. Bassil Al-Shibani

whose wonderful devotion and support was greatly appreciated

as well as my family

my parents

Mr. Mohammed Hassan and Mrs. Bahira Muslem

and my kids

Hussain, Ali and Zahraa

Acknowledgements

Abstract

Organisms must balance their iron requirement to achieve iron homeostasis. This is achieved through several mechanisms, including sequestration of excess cellular iron by iron-storage proteins. Such proteins ('ferritins') act as an iron source under iron restriction; they also counter redox stress imposed by excess cellular iron that might contribute to Fenton chemistry. In *Escherichia coli*, there are three iron-storage proteins: ferritin A (FtnA), bacterioferritin (Bfr) and the 'DNA-protection during starvation' (Dps). Experiments were conducted to further investigate their respective functions and to determine whether these proteins are mutually interchangeable, i.e. can one of these iron-storage proteins be used in place of the other two. This aim was progressed by first generating a triple mutant of the corresponding iron-storage genes (BW25113 Δ*ftnA* Δ*dps* Δ*bfr*) and by complementing the triple mutant with inducible plasmids expressing *bfr*, *dps* or *ftnA*. The lack of FtnA did not increase redox stress sensitivity, however, mutants lacking Dps had a reduced capacity to withstand challenge by hydrogen peroxide. Bfr appeared to combat H_2O_2 toxicity, but only in the absence of Dps (in minimal medium). Growth studies showed that the triple mutant displays a major growth impairment under iron deficient conditions and that Dps can contribute to iron-restricted growth, but only when no other iron-storage protein is available. Both Bfr and FtnA contribute to the total iron stores of *E. coli* K-12 in stationary phase following aerobic growth in iron-supplemented M9 medium, with Dps contributing relatively little except in the absence of Bfr and FtnA. Up to 62% of cellular iron can be stored in the wildtype by a combination of Bfr, FtnA and Dps. Both Dps and Bfr (but not FtnA) proteins provided redox-stress resistance when expressed from pBADrha in the triple mutant. Bfr acted to provide an iron source that could promote iron-restricted growth whereas neither Dps nor FtnA pre-induction caused any notable growth advantage under Fe-restriction. Subsequent studies showed that the lack of any growth advantage for pBADrha-induced *ftnA* was due to weak FtnA levels caused by rapid turnover of the protein through an apparent 'N-end rule dependent' degradation. Indeed, replacement of the second FtnA amino acid (L→A/K) greatly elevated the levels of FtnA, allowing a notable support of growth under iron-restricted conditions. Inactivation of the protease-encoding *ftsH* gene resulted in increased the levels of FtnA in the wild type. Eight iron-storage proteins from diverse species failed to complement the triple iron-storage mutant; the reason for this is unclear. Recombinant Dps was purified and used to generate polyclonal antibodies to assist determination of Dps levels in *E. coli*. Encapsulin (linocin M18) of the hyperthermophile *Pyrococcus furiosus* was overexpressed in *E. coli* and purified. TEM analysis showed that the recombinant linocin M18 protein forms spherical particles of 30 nm diameter apparent. The isolated linocin M18 appeared to aggregate into a high-order oligomeric structure. SDS-PAGE analysis suggested that the linocin M18 protein is generated at low level when expressed from pBADrha in the triple mutant, which resulted in enhanced hydrogen peroxide resistance upon rhamnose induction, and also appeared to provide some support growth under low iron conditions. Thus, linocin M18 appeared to partly complement the iron-storage defect of the triple mutant.

Publication and Presentations

1. "Mechanisms of iron storage in *Escherichia coli.*"
   Salman A, Andrews SC.
   The Microbiology Research Day.
   University of Reading. 18th August 2016.

2. "The roles of the three iron-storage proteins of *Escherichia coli* in supporting low-iron growth and redox stress resistance"
   Salman A, Andrews SC.
   The 2017 Seventh Congress of the International BioIron Society conference (May 7-11, 2017).
   Los Angeles, CA.

3. "The roles of the three iron-storage proteins of *Escherichia coli* in supporting low-iron growth and redox stress resistance"
   Salman A, Andrews SC.
   The Edinburgh Microbiology Society meeting (March 2017).
   Edinburgh, UK.

Abbreviations

Amp	Ampicillin
Bfr	*E. coli* bacterioferritin
BSA	Bovine serum albumin
Cm	Chloramphenicol
Da, kDa	Dalton, kilo-daltons
DEAE	Diethylaminoethyl
DTT	Dithiothreitol
DTPA	Diethylenetriaminepentaacitic acid
Ent	Enterobactin
ESI-MS	Electrospray ionisation - mass spectroscopy
Eut	Ethanolamine utilization microcompartment
FAS	Ferrous ammonium sulphate
Fe^{2+}	Ferrous iron
Fe^{3+}	Ferric iron
Fig	Figure
FLP	Flippase site-specific recombinase
FtnA	*E. coli* ferritin type A
Fur	*E. coli* ferric uptake regulation protein
H	Hour (s)
H_2O_2	Hydrogen peroxide
HEPES	2-[4-(2-hydroxyethyl)piperazin-1- yl]ethanesulfonic acid
ICP-OES	Inductively coupled plasma - optical emission spectroscopy
IPTG	Isopropyl β-D-1- thiogalactopyranoside
Km	Kanamycin
Kn^R	Kanamycin resistance cassette
MAP	Methionine aminopeptidase
Min	Minute (s)
MWCO	Molecular weight cut off
NADPH	Nicotinamide adenine dinucleotide phosphate
Pdu	Propanediol utilisation microcompartment
Pfu	*Pyrococcus furiosus polymerase*
SDS	Sodium dodecyl sulphate
TBE	Tris Borate EDTA Buffer
TCA cycle	Tricaboxylic acid cycle
TCA	Trichloro-acetic acid
TEMED	Tetramethylethylenediamine

Contents

Figures

Tables

Chapter 1 Literature Review
Iron Metabolism in Bacteria

1. Introduction

1.1 Properties and role of Iron

Iron is considered the fourth most abundant metal in the Earth's crust (Price and Morel, 1998), and is a transition metal; its d-orbital electrons are organised to form various spin states (according to the ligand environment), this is due to the partially filled d-orbital (Andrews *et al*., 2003). As a result it has the ability to act as an electron acceptor or donor, and is mostly found either in the reduced Fe^{2+} form or in the oxidised ferric Fe^{3+} form (Beinert *et al.*, 1997). Besides its high availability, it is considered as an essential prosthetic component for integration into many protein as a biocatalyst or electron carrier in the form of iron-sulphur clusters and haem, and also can be integrated as a mono- or binuclear centre (Beinert *et al.*, 1997). It is considered as an essential requirement for nearly all organisms (Price and Morel, 1998; Fischbach *et al.,* 2006; Posey and Gherardini, 2000) as it is involved in many biological processes: oxidative phosphorylation, N_2 fixation, methanogenesis, respiration, production of H_2, DNA biosynthesis (see Figure 1-1) (Andrews *et al*., 2003). However, a few organisms are recognized as iron-independent such as *Lactobacillus* (Braun *et al.*, 1998) which efficiently grows in highly iron–restricted media (e.g. milk) and also comprises part of the normal flora of the breast fed infant gut (Bullen and Griffiths, 1999). Species of *Lactobacillus* can use other cofactors (e.g. Mn) to replace iron in mediating its essential reactions (Byer and Arceneaux, 1998). Both *Treponema pallidum* and *Borrelia burgdorferi* also have the ability to grow normally in iron-restricted conditions. For *Borrelia burgdorferi* (the causative agent of Lyme disease) this is due to the lack of genes encoding iron proteins (Posey and Gherardini, 2000). Although these bacteria are iron free, both are dependent on getting their energy sources and many biosynthetic requirements from processes of iron-dependent metabolism performed by the infected host. This lack of metabolic capacity can explain their status as obligate parasites with fastidious growth requirement (Andrews *et al*., 2003; Posey and Gherardini, 2000).

Glutamate synthetase [Iron & iron-sulphur]
Dihydro-orotate dehydrogenase   [iron-sulphur]

Methane monooxygenase [contain bridged di-iron centre (Fe-O-Fe)]

Ribonucleotide reductase [di-nucleur Fe-centre]

Amino acid and pyrimidine

Carbon fixation

Haemoglobin-like

DNA synthesis

O_2 binding

Toluate 1,2-dioxygenase [iron-sulphur]

Degradation of aromatic compounds

Photosynthesis

Light-harvesting complexes

Degradation of hydrogen

Respiration

Haem-catalase
Iron-superoxide dismutase
Peroxidase

Gene regulation

Nitrogen fixation

Cytochromes
Cytochrome oxidase
Ferredoxins
Other iron-sulphur proteins

FNR, SoxR [Fe-S cluster],
CooA [haem], PerR [Fe^{2+}],
Fur [Fe^{2+}]

Nitrogenase [Iron-sulphur cluster]

Anabolism

Catabolism, energy production

Figure 1.1: Processes requiring iron. Adapted from Andrews (1998).

1.2 Iron in the Environment

Bacteria can obtain many of their requirements for nutrients from their environment by passive diffusion, however they cannot do so for iron for many reasons. First it is available in concentration (10^{-18} M) at neutral pH at very low level and so it is necessary for bacteria to acquire this metal using specialised traansport systems (Ratledge and Dover, 2000). Iron is found either in the reduced Fe^{2+} form or in the oxidised ferric Fe^{3+} form (Beinert *et al.*, 1997) but it's mainly exists in the insoluble oxidized Fe^{3+} form at pH above 7 under aerobic conditions which cause a problem for the pathogenic bacteria because the availability of iron limited by the host proteins such as haemoglobin, cytochromes, the chelating effect of the glycoproteins (Andrews *et al.*, 2003). Ferrous

iron can be dangerous because it can generate the reactive hydroxyl radical ($\cdot$OH) from H_2O_2 via the Fenton reaction (Equation I), and the Harber-Weiss reaction (Eq. III) (Woodmansee and Imlay, 2002; Byers and Arceneaux, 1998).

$$Fe^{2+} + H_2O_2 \rightarrow Fe^{3+} + OH^- + \cdot OH \qquad \ldots\ldots\ldots \text{(Eq. I)}$$

$$Fe^{3+} + O_2^- \rightarrow Fe^{2+} + O_2 \qquad \ldots\ldots\ldots \text{(Eq. II)}$$

$$O_2^- + H_2O_2 \rightarrow \cdot OH + OH^- + O_2 \qquad \ldots\ldots\ldots \text{(Eq. III)}$$
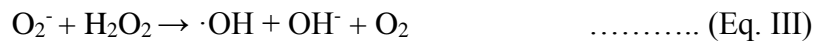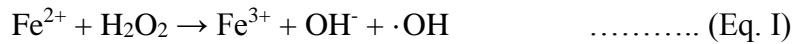
Hydroxyl radicals can cause damage not only to [Fe-S] clusters, and cause peroxidation for the membrane lipid but also to DNA; in order to prevent such damage the metabolism of iron has to be regulated to reduce the oxidative stress to the minimum level (Turner *et al*., 2007) because iron act as acofactor in the enzymes responsible for the toxic radical degradation such as superoxide dismutase, alkylhydroperoxidases catalases and peroxidases Thus, organisms need to employ mechanisms by which they can reach iron balance. Fe^{3+} can be reduced by the superoxide radical, O_2^-. This radical is produced by dioxygen acquiring an electron from one of many pigments, such as flavins, chlorophyll, porphyrins and retinal (Crichton, 2009).

The amount of hydroxyl radical and hydroxyl anion is increased by the sum of Eq. I and III) to produce extra $\cdot$OH and OH^- by so called Harber-Weiss reaction (Henle *et al.,* 1996). The competition between macrophages and the microbe also generate Reactive oxygen radical via the oxidative burst mechanism to kill and protect it selves from the pathogens (Nevo and Nelson, 2006).

1.3 Microbial iron transport and metabolism
The low concentration of the Fe^{3+} ion (Ratledge and Dover, 2000) can be overcome by bacteria by deploying iron acquisition systems, as explain below.

1.3.1 Siderophores
Many microorganism can overcome the problem of iron scarcity and increase their uptake of soluble iron by producing high-affinity compounds (with molecular weight <1000 Da) to bind Fe^{3+}, called siderophores (Byers and Arceneaux, 1998), which solubilise and strongly bind to ferric ion (Ratledge and Dover, 2000) to form Fe^{3+}-siderophore complexes (Neilands, 1995). In Gram-negative bacteria, these complexes can be

recognized by specific outer membrane (OM) receptors which help to transport them into the cell via periplasmic-binding proteins and cytoplasmic-membrane permeases (Fig1.2). Siderophores can be either reused after reduction or lysed to release iron in the cytoplasm (Payne and Mey, 2010). However, in Gram-positive bacteria, which do not contain OMs, these complexes can be taken up by membrane–anchored binding proteins (lipoproteins in nature) coupled with ABC permeases (Fig 1.3) (Köster, 2001).

The high specificity of siderophore uptake enables scientists to load antimicrobial agents on to siderophores (Ghysels *et al.*, 2005) as an antibacterial strategy. Indeed, some phage and bacteriocins utilise siderophore OM receptors as species-specific surface receptors for entry into the bacterial cell (Ratledge and Dover, 2000). A substantial number of siderophores are known (more than 500) and these are secreted from microorganism in conditions of iron scarcity (Ratledge and Dover, 2000). In addition, siderophores can be categorised into 5 groups according to their chemical nature: hydroxamates, catecholates, carboxylates, heterocyclic compounds and mixed types. Enterobactin is a well know siderophore that is predominately secreted from Gram-negative bacteria such as Enterobacteria and *Vibrio*, and is classified as a catechol (2,3-dihydroxybenzoic acid) and has high affinity to bind iron using its catechol groups as ligands (Winkelmann, 2002; Winkelmann and Drechsel, 1997). The enzymes mediating its synthesis in *E. coli* are encoded by *entA-F* (Ratledge and Dover, 2000). Furthermore, this type of siderophore can be easily recognized and neutralised by lipocalin-2, which is secreted from multiple tissues of the as part of a host bacterial defence mechanism (Fischbach *et al.*, 2006). However, the *iro* gene products in uropathogenic *E. coli* and *Shigella dysenteriae* enable salmochelin synthesis. Salmochelin is a C-glucosylated enterobactin which has the ability to escape from the neutralisation effect of lipocalin-2 (Payne and Mey, 2010; Hantke *et al.*, 2003). *E. coli* and other bacteria secrete aerobactin (hydroxamate-type siderophore) which has the same property as salmochelin (not bound to lipocalin-2) and so participates in the pathogenicity of bacteria. This role is confirmed by the presence of the *iucABCD* and *iut* genes (encoding the uptake and synthesis) in a genomic pathogenicity island or virulence plasmid (Payne and Mey, 2010).

E. coli (some strains only), *Pseudomonas putida, Vibrio anguillarum* and *Yersinia enterocottica* synthesize a complex heterocyclic siderophores called yersiniabactin, which can also take part in the bacterial pathogenicity as its production and uptake are encoded by genes located in the high pathogenicity island (HPI) of *Yersinia* spp. (Payne

and Mey, 2010). Many bacteria including *E. coli* can receive and transport siderophores (xenosiderophores) produced from other microorganism, such as ferrichrome, coprogen, rhodotorulic acid, ferrioxamine B and citrate (exogenous siderophores) (Braun *et al.*, 1998; Ratledge and Dover, 2000; Payne and Mey, 2010). In Gram-negative bacteria, several OM receptor proteins are involved in ferric-siderophore transport and each one specifically recognizes and differentiates between different siderophores. *E. coli* K-12 contains 6 such ferric transport systems. However, enterobactin is the only type of siderophore secreted from this strain (Braun *et al.*, 1998).

Importantly, enterobactin is not produced in conditions of iron availability, it is just produced in case of iron restriction, particularly in high redox condition (Griffiths and Williams, 1999). It has the strong ability to scavenge ferric iron from transferrin, lactoferrin (Hantke *et al.*, 2003) and ovotransferrin at pH 7 with pM value equal to 36.7 (the negative logarithms of the free ion concentration). In *E. coli,* this type of siderophore cannot be used again after it has delivered iron to the bacterial cell because during iron release esterase breaks the cyclic triester bond in enterobactin complexes with Fe^{3+} leading to loss of the ester bond that is necessary to produce a new complex with ferric iron. However, the aerobactin siderophore is synthesised in mild iron restricted condition (Griffiths and Williams, 1999). Enterobactin differs from aerobactin, which is produced from pathogens within the host, in that enterobactin can acquire iron from transferrin. However, for aerobactin, host cells and tissues are the source of iron (Brock *et al.*, 1991; Torres *et al.*, 2001).
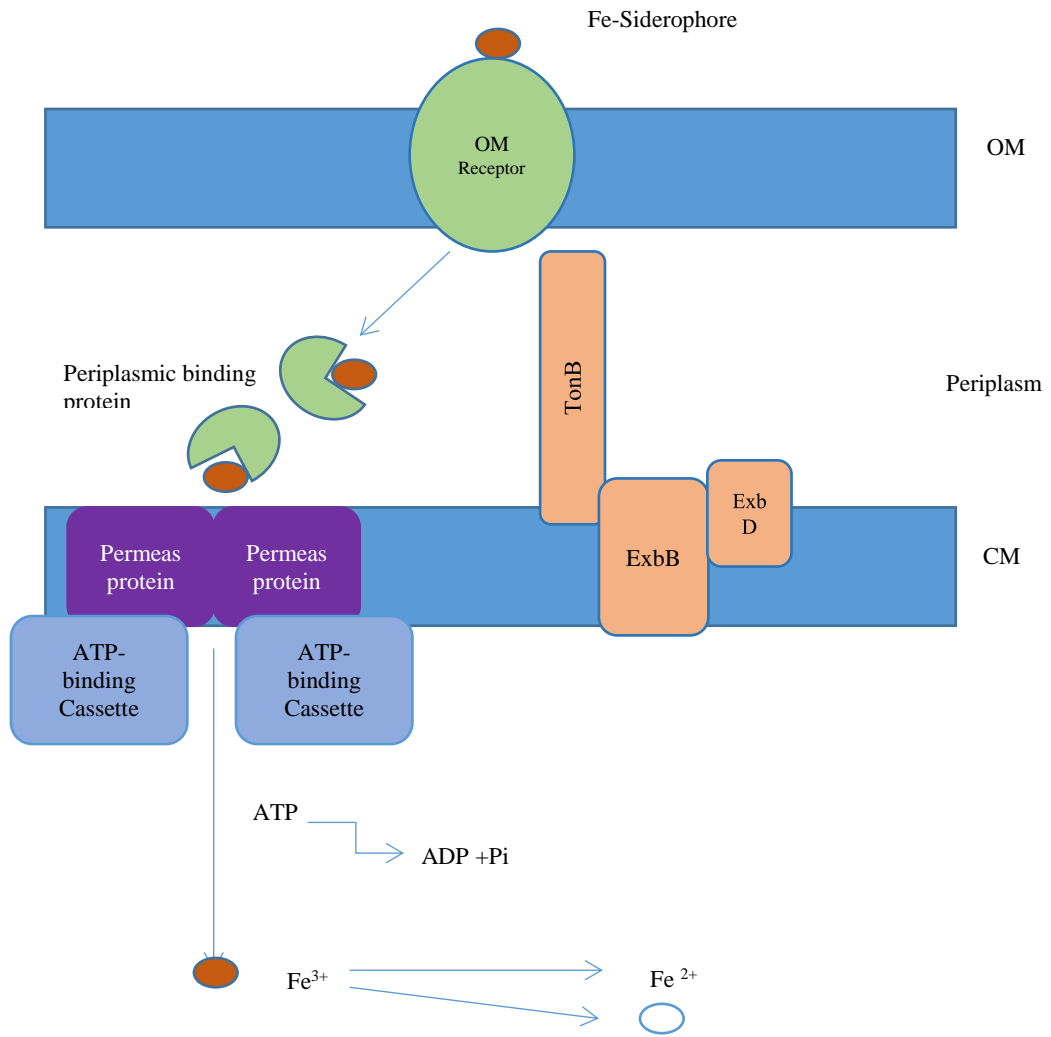
Figure 1.2 Schematic representation of iron-siderophore uptake in Gram-negative bacteria. OM (Outer Membrane); **CM,** (Cytoplasmic Membrane). Adapted from Andrews *et al*. (2003).
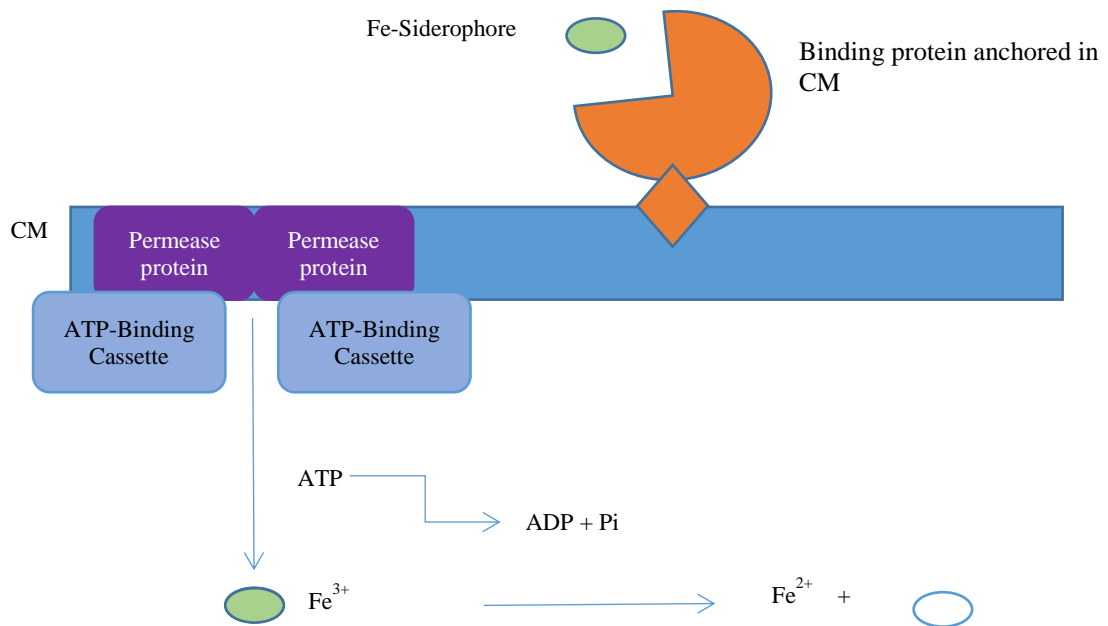
Figure 1.3 Schematic representation of iron-siderophore uptake in Gram-positive bacteria. CM**, c**ytoplasmic membrane. Adapted from Andrews *et al*. (2003).

1.3.2 Outer membrane receptor

Proteins comprise nearly half of the OM. Seven OM proteins have been recognised in *E. coli* K-12 (Braun and Braun, 2002) which are required for Fe-siderophore internalisation; the molecular mass of Fe^{3+}–siderophore complexes is too great to allow entry via porins (cut off of ~600 Da). Bacteria can scavenge ferri-siderophore by using these high-affinity OM receptors which have the ability to differentiate between different ferric-siderophores and function to translocate ferri-siderophores into the periplasm (Ratledge and Dover, 2000). This process requires energy generated from the TonB system. Some OM receptors also act as phage receptor or gateways for bacteriocins (Koebnik *et al.,* 2000). For example, FhuA, the ferrichrome receptor, acts as phage and colicin M receptor (Neilands, 1995), FhuE and IutA are hydroxamate receptors, FepA, Fiu and Cir act as ferric enterobactin receptors (Braun and Braun, 2002). However, FepA also acts as a colicin B and D receptor (Neilands, 1995). FecA is the receptor for ferric citrate. In *E. coli*, the *fepA* gene, which is located in the *ent-fep-fes* gene cluster on the chromosome, is responsible for the production of FepA protein (81 kDa, acts as enterobactin receptor) and the FhuA protein is the product of *fhuA*, which acts as ferrichrome receptor. This

receptor can also internalize other hydroxamates, namely coprogen and rhodotorulic acid (see Table 1.1) (Griffiths and Williams, 1999).

In addition to these ferri-siderophore receptors, *E. coli* contains a related non-iron TonB-dependent OM receptor, BtuB, which is the vitamin B12 receptor. The OM act as barrier in defence of the cell against toxins with molecular mass larger than 600 Da; without this property the enteric *E. coli* can be easily destroyed by bile salts created in the gastrointestinal tract (Braun *et al.*, 1998).

 The structures of all TonB-dependent OM receptors are similar. They are composed of two domains: a C-terminal β-barrel composed of 22 β strands inserted in the OM. They have a pocket in the outer face containing the recognition site for the ferric-siderophore complex; and an N-terminal domain (the cork) which acts as the gate in the middle of the β-barrel channel (Koebnik *et al.,* 2000) which is usually closed when the recognition site is opened. This gate is opened by binding at the β-barrel loops by the ferric-siderophore complex leading to transport to periplasm. Part of OM cork domain extends into the periplasm including a sequence of 7 amino acids called the 'TonB box' that acts as TonB interaction interface (Schramm *et al.,* 1987; Jordan *et al.,* 2013). To transport Fe-chelate complexes through the OM receptors, three proteins that interact via the TonB box are needed (TonB, ExbB and ExbD) to provide the energy for Fe complex transportation (Krewulak and Vogel, 2008). It was found that the 'FhuAΔ5-160' (a mutant where the N-terminal cork has been deleted such that the β-barrel channel is unplugged) mutant strain becomes susceptible to antimicrobial agents such as vancomycin and bacitracin, which were internalised by the large pores formed as a result of removing the N-terminal plug domain (Koebnik *et al.,* 2000). This work supports the role of the plug domain in restricting translocation of non-specific solutes across the OM via OM receptors.

Table 1.1TonB-dependent OM receptors in *E. coli* K-12 and their functions.

OM receptor	Function
FhuA	Ferrichrome receptor (Braun and Braun 2002; Coulton *et al*., 1986) Phage and colicin M receptore (Braun and Wollf 1973)
FhuE	Hydroxamate receptor (Braun and Braun 2002)
IutA	Aerobaction receptor (Torres *et al*., 2001)
FepA	Receptors for ferric enterobacter (Braun and Braun 2002) Colicin B and D receptor (Lundrigan and Kadner 1986)
Fiu	Receptors for ferric enterobacter.
Cir	DHB/DHBS (Hantke *et al*., 2003)
FecA	Receptor for ferric citrate (Braun and Braun 2002)
BtuB	Vitamin B12 receptor (Heller *et al*., 1985)

1.3.3 TonB

The process of transportation of ferri-siderophores across the OM requires energy which cannot be obtained from the OM. Gram-negative bacteria can overcome this obstacle by providing the energy from TonB which acts as an energy supplier required to actively transport these complexes across the OM to a corresponding periplasmic-binding protein (e.g. FepB and FhuD) (Griffiths and Williams, 1999). The TonB system is composed of a three protein complex TonB, ExbB and ExbD (Braun *et al.,* 1998; Moek and Coulton, 1998) that exists in the subunit proportion 1:7:2 (Higgs *et al*., 2005). In *E. coli,* an interaction between the carboxylic terminal region of TonB in its energised form and the OM receptor is required to lower binding with the ferric complex and open the channel for iron translocation (Braun *et al.,* 1998; Higgs *et al.,* 2002). This requires the utilization of the proton motive force (PMF) by ExbB and ExbD (Pawelek *et al*., 2006), and leads to transport of the ferric siderphore complex to the periplasm. This also results

in a disconnection of the TonB C-terminus from the OM receptors converting TonB back into its non-energised form (Gresock *et al.,* 2011).

Both TonB and ExbD are partially located in the periplasm and their N termini are in the cytoplasm, whereas most of the ExbB protein is integrated into the CM (Celia *et al*., 2016). The gene encoding TonB in *E. coli* K-12 is located away from *exbBD* genes on the chromosome, whereas in other bacteria of the *Enterobacteriacea* they are located next to each other. This separation may be needed to control their functional interdependence (Braun *et al.*, 1998).

1.3.4 Transport across the periplasm and cytoplasmic membrane

The translocation of ferric siderophore complexes across the periplasm and CM is dependent on periplasm-binding proteins (PBPs). All PBPs are divided into 8 groups according to their amino acid sequence similarities (Tam and Saier 1993) in addition to a new group which is specific for Zn and Mg permeases (Claverys, 2001). In *E. coli,* ferrichrome, coprogen, rhodotorulic acid, ferroxamine and aerobactin are delivered from their receptors by FhuD (periplasm-binding-protein) to its ABC transporter (ATP binding cassette) which is composed of two ABC domains opened into a channel formed by two membrane spanning domains (MSDs) (Mademidis *et al.,* 1997).

When the PBP loaded with ferric siderophore complex is attached to its ABC transporter, this induces the binding of two ATP molecules to provide the required energy to open the cytoplasmic gate located on the cytoplasmic side of the channel to facilitate passage into the cytoplasm. The released energy is also used to detach the binding protein to allow it to continue to work as a shuttle (Köster, 2001). The number of PBP-ABC systems is generally less than the number of OM receptors in any given bacterium (Köster, 2001), e.g. OM receptors in *E. coli* that bind to iron chelators are approximately seven (Braun and Braun, 2002) but it only has three cognate PBPs. This fact reflects the stronger specificity of OM receptors (Koster, 2001).

1.3.5 Iron release from ferric siderophores and ferric reductase

The mechanism of iron release from ferric siderophores involves ferric reductase enzyme activity for reduction of Fe^{3+} to Fe^{2+}. This weakens the binding of iron to its siderophore allowing dissociation and iron release. It appears that ferrireductases act non-specifically on ferric siderophores by indirect reduction of Fe^{3+}. These enzyme use NADH/NADPH

to provide electrons required for the reduction of flavin, which act as a co-factor that reduce Fe^{3+} to Fe^{2+} (Schröder *et al.,* 2003).

 Importantly, the process of releasing iron from ferric-enterobactin complexes in *E. coli* is esterase (Fes) mediated. Fes can hydrolyse the ester bonds of ferric-enterobactin complexes converting the cyclic trimer into monomeric dihydroxybenzoylserine units. This protein is the product of *fes* in *ent-fep* cluster which is the same cluster that is responsible for the production and uptake of enterobactin (Earhart, 1996). In *E. coli*, FhuF (a Fe-S protein) also acts as a ferroxamine reductase to utilise iron from this 'exogenous' siderophore (Andrews *et al.,* 2003; Patzer and Hantke, 1999).

1.3.6 Fe^{2+} transport systems in *E. coli*

E. coli is a facultative anaerobic bacterium so it can grow and survive in the gastrointestinal tract (GIT) (Kammler *et al.*, 1993). In this environment most of the iron is found in the Fe^{2+} form. Fe^{2+} high-affinity uptake requires three genes, *feoABC* (Hantke *et al.*, 2003), encoding two transport components: FeoA, which is composed of a 75 amino acids (Kammler *et al.*, 1993), and FeoB (84 KDa) composed of two domains. N-terminal domain, which is essential for Fe^{2+} uptake, functions as a GTPase with similarity to eukaryotic G proteins, and the C-terminal domain is a hydrophobic polytopic membrane component likely providing the transport channel for Fe^{2+} (Marlovits *et al.*, 2002). FeoB was believed to act as a transport ATPase, an ATP energy-dependent transporter for Fe^{2+}, as its sequence shows a similarity with this enzyme (Kammler *et al.*, 1993), but later it became apparent that it possesses GTPase activity. The *feoABC* operon is Fur and Fnr regulated allowing induction in response to low iron and oxygen, respectively (Kammler *et al.*, 1993; Hantke, 1997).

Fe^{2+} iron uptake is impaired in *feoA/feoB* mutants (Braun *et al.,* 1998). This observation emphasises the importance of FeoA and FeoB proteins in Fe^{2+} uptake. Ferrous iron can be also be taken up at low affinity by the CorA transporter, which is selective for Mg^{2+} (Braun *et al.*, 1998) as well as for other metals such as Mn^{2+} (Pazer and Hantke, 2001). In *Helicobacter pylori*, the Feo system is crucial for colonisation of the microaerobic stomach but under iron abundance (~10 µM) a non-specific mode (energy independent) mode of iron uptake is observed (Velayudhan *et al,* 2000). *feoB* mutation in both *E. coli* and *Salmonella* restricts the ability to invade and colonise the intestinal tract of mice as they lose the potential for ferrous transportation in the anaerobic condition present in the

gut (Tsolis *et al.,* 1996). FeoC is a small hydrophilic protein which contains an iron-sulphur (Fe-S) cluster carried on its 4-Cys residues (Hsueh *et al.,* 2013). Previous study reported that FeoC can protect FeoB from the activity of FtsH (which has a proteolytic activity) generated under iron/oxygen restricted condition. This can be achieved by the binding of FeoC to FeoB in *Salmonella enterica*. Hsueh *et al.* (2013) suggested that the activity of the Feo transporter can be regulated by FeoC protein via oxygen/iron sensitive coordination of the iron-sulphur cluster.

1.3.7 EfeUOB Transport system

Both pathogenic and non-pathogenic bacteria possess EfeUOB/YcdNOB, an acid-induced iron-transporter system which shows a functional similarity to Ftr1p, a high-affinity Fe^{2+} transporter in Saccharomyces (Fu *et al*., 2004; Debut *et al*., 2006). The functional EfeUOB system provides a growth advantage under iron deprivation, low-pH condition in aerobic and anaerobic condition. To be functional, this system requires three proteins: EfeU/YcdN which is an integral inner-membrane protein appearing to act as a permease involved in ferric iron transport; EfeB/YcdB is a haem peroxidase containing a *b*-type haem exported through the Tat pathway (the twin-arginine translocation pathway which acts as an exporting protein machinery in the CM); and EfeO, which is also periplasmic, and has an N-terminal cupredoxin-like domain and a C-terminal M75 metalloprotease domain (Cao *et al*., 2007; Rajasekaran *et al*., 2010). Cao *et al.* (2007) proved that the *efeUOB* operon of *E. coli* K-12 is cryptic as a result of frameshift mutation. However, the *efeUOB* operon of enterohaemorrhagic strain O157:H7 is completely functional when introduced to *E. coli* K-12 because it lacks this type of mutation.

1.3.8 MntH transport system (Nramp-1-like transporter)

In mammals the internal phagosomal environment presents engulfed pathogens with oxidative stress, low nutrients and low pH as well as an iron-restricted condition as a result of the transport activity of the 'host natural resistance-associated macrophage protein' (NRAMP-1), homologues of which are also present in bacteria such as *E. coli*. This transporter in the phagosomal membrane has the ability to take divalent cations out the phagosome (Jabado *et al*., 2000; Papp-Wallace and Maguire 2006). This has a negative impact on many intracellular pathogens because they cannot get adequate amounts of these cations, which leads to its inability to survive in such condition (Anderson *et al.,* 2009). MntH, a putative membrane bacterial protein, has a similar

function as Nramp-1 protein, in divalent cations transport. The MntH protein was thought to be a transporter for both Mn^{2+} and Fe^{2+} in *E. coli* (Makui *et al.,* 2000) and also have the ability to participate in the zinc and cobalt accumulation. However, later studies proved that it has higher affinity to transport Mn^{2+} than other divalent cations (Kehres and Maguire 2003). Kehres *et al.* (2000) also indicate that this protein may act as Fe^{2+} transporter. MntH protein is encoded by *mntH* in *E. coli* which is regulated by MntR (manganese-sensitive transcription factor) that acts as a repressor for *mntH* gene in response to sufficient manganese condition; it is also repressed by the Fe^{2+}-Fur complex (Patzer and Hantke 2001). This leads to homeostatic control of the MntH transporter in order to maintain Mn^{2+} levels (Kehres *et al.,* 2000). The MntH protein enhances the growth of *E. coli* in conditions of iron deficiency, by allowing a partial replacement of iron by Mn (Anjem *et al.*, 2009). The binding site of the MntR repressor is found associated with four genes: *mntH, mntR, yebN* (*mntP;* probably Mn^{2+} efflux pump)*,* and *dps* (Yamamoto *et al.*, 2011).

1.3.9 ZupT transport system

ZupT is a cytoplasmic membrane protein belonging to a group of eukaryotic divalent ion transporters known as the ZIP family. This protein was first identified as a Zn(II) transporter in *E. coli* (Grass *et al.*, 2002), but later research demonstrated that Fe(II) can be transported by ZupT, along with Co(II), Zn(II) and Mn(II). This protein is the product of the *zupT* gene, its expression is not affected by metal ions but it is independently expressed (Grass *et al.*, 2005). Its structure is similar to ZIP protein, composed of eight transmembrane helices (Grass *et al.*, 2005). Grass *et al.* (2005) show that the disruption in iron transport in *E. coli* by chelators can be relieved by *zupT* expression, and they also reported that ZupT has the same activity as MntH/Feo in the uptake of Fe^{2+}.

1.3.10 Siderophore independent Fe^{3+} transport system

Gram-negative bacteria also have pathways to take up ferric iron independently of siderophores, which are well identified in a number of pathogens including *Neisseria gonorrheae*, *N. meningitides* and *Haemophilius influenza*. These systems include OM receptors for transferrin (Tf), which are iron-binding proteins acting as iron providers for cells in the host fluids. There are two types of these proteins, Tf and lactoferrin (Lf) in addition to ovotransferrin (in egg white) (Ratledge and Dover, 2000). The process of iron utilisation and uptake from Tf and Lf by Tf and Lf receptors (TfR and LfR) also requires energy provided by the TonB system (Anderson *et al.*, 1994). These receptors

consist of the two OM proteins TbpA and TbpB for TfR, and LbpA and LbpB for LfR. The presence of these two subunits and their interaction is essential for creation of a suitable affinity for Tf and Lf towards diferric-transferrin or lactoferrin. Iron is liberated from these complexes at the OM by the energy supplied from the TonB system and the released iron is translocated by periplasmic Fbp (ferric binding protein) to an ABC permease which delivers iron to the bacterial cytosol (Aldhikari *et al.*, 1995).

1.3.11 Haem uptake

Pathogenic bacteria, including some *E. coli* strains, also have the ability to utilize haem or haemoglobin as iron sources in the host. This ability is found in *E. coli* O157:H7 where it requires a TonB-dependent OM receptor (69 kDa), which is the product of *chuA* (*E. coli* haem-utilization gene) induced in conditions of iron scarcity (Torres and Payne, 1997). In Gram-negative bacteria, haem can be taken up by haem-binding proteins called 'haemophores'; for example *Pseudomonas aeruginosa* secrets the HasA haemophore (Yukl *et al.,* 2010) which has the ability to bind with haem at a histidine/tyrosine pair (Lukat-Rodgers *et al.,* 2008). The released haem binds to the OM receptors and is then transported across the OM by the energy provided from TonB system. This step is followed by the process of delivering the haem across the CM into the cytoplasm which requires a periplasm-binding protein and ABC transporter. Following delivery to the cytoplasm, the complexed iron is liberated by haem degradation through the action of haem oxygenase (Genco and Dixon, 2001). Gram-positive bacteria can directly bind to haem through cell-wall-anchored haem-binding proteins, for example IsdH (Iron-regulated surface determinant) is employed as a haem-binding proteins in *Staphylococcus aureus* (Pilpa *et al.,* 2009). *Bacillus anthracis* takes up haem in the same way as some Gram-negative bacteria, by secreting haemophores (Fabian *et al.,* 2009).

1.4 Iron storage

Bacteria can get their requirement for iron not only from the extracellular environment but also from iron-storage proteins, which provide an endogenous iron in iron-restricted conditions. There are three types of iron-storage protein identified in bacteria, which have substantial similarities in their structure and function: the archetypal ferritins, the haem-containing bacterioferritins and the smaller Dps proteins which are only found in prokaryotes. These proteins consist of 24 similar subunits in both ferritin and bacterioferritins, and 12 in Dps proteins (Fig 1.4). The subunits are arranged to produce

spherical protein shells surrounding a space located in the centre which accommodates up to 4500 iron atoms in ferritin and bacterioferritin, and only 500 iron atoms in Dps due to its small size (~250 kDa) (Andrews et $al.$, 2003).

Iron is taken up in the Fe^{2+} form but is deposited as Fe^{3+}. This process is enabled by the action of ferroxidase sites which oxidise ferrous into ferric iron. This site is located in the centre of each ferritin and bacterioferritin subunit (Andrews et $al.,$ 2003). The mechanism of iron storage starts with the electrostatic attraction between Fe^{2+} and the iron-storage proteins which leads to its direction towards the ferroxidase centre (Douglas and Ripoli, 1998). Fe^{2+} then binds at this site and is oxidised by oxygen to form an oxobridged diferric intermediate or peroxo-diferric intermediate. This results in formation of Fe^{3+} that translocates and forms a ferrihydrite core or an amorphous ferric phosphate core in the centre of ferritin or bacterioferritin (Andrews et $al.$, 2003).

In $E.$ $coli$ there are two genes, $ftnA$ and $ftnB$, responsible for the production of ferritin, FtnA and FtnB (Abdul-Tehrani et $al.,$ 1999). The $ftnA$ mutation in $E.$ $coli$ results in lowering the percentage of cellular iron to half in the case of iron availability and decreases the ability to grow in low levels of iron (Andrews et al., 2003). These phenotypic results confirm the role of FtnA in iron storage in bacteria. Abdul-Tehrani et $al.$ (1999) also report that increasing the rate of FtnA production will reduce the redox stress stimulated by fur mutation in $E.$ $coli$. Previous study suggests that the role of FtnB is unclear. In addition to ferritin's function as a storage protein for iron, it is also prevents the toxic effect of hydroxyl radicals (·OH) generated by the Fenton reaction. This protection is performed by preserving iron in a nonreactive form during iron availability (Pandey and Rodriguez, 2012; Woodmansee and Imlay, 2002). Velayudnan et $al.$ (2007) showed that FtnB, which is expressed in iron scarcity conditions and is repressed by Fur, has an essential role in $Salmonella$ virulence due to its role in repairing the iron-sulphur clusters in aconitase enzymes following damage caused by oxidative stress. They also showed that the absence of Dps protein leads to increased DNA damage by hydroxyl radicals which is enhanced by FtnB due to it supply of Fe^{2+} acting as a catalyst in Fenton reactions.

The 12 haem groups per 24 subunits are found only in bacterioferritins (Bfr). These groups are present as protoporphyrin IX in the two-fold interface between subunits. However, the haem is found as coproporphyrin III (novel form of haem) in Bfr of

Desulphovibrio desulfuricans (Romao *et al.,* 2000). The function of haem groups is not clear. However, studies revealed that they play a substantial role in releasing iron from Bfr (Abdul-Tehrani *et al*., 1999; Yasmin *et al.*, 2011) with the haem group mediating electron transfer into the central cavity accelerating the rate of iron release from *E. coli* Bfr (Yasmin *et al.,* 2011). Co-crystalisation experiments provided a link between Bfr and the bacterioferritin associated ferredoxin (Bfd). Bfd acts as a 2Fe-2S ferredoxin that is thought to facilitate haem-mediated iron release from bacterioferritin in conditions of iron unavailability. The motifs at BfrB-Bfd the interaction site in both Bfr and Bfd are conserved in many bacteria, indicating the importance of this interaction in achieving iron balance in bacteria (Yao *et al*., 2012). Rivera (2017) proved that the BfrB/Bfd interaction in *Pseudomonas aeruginosa* is require to mobilize iron deposited in BfrB (Fig. 1.5).

Pandy and Rodrigues (2012) reported that in addition to the important role of Bfr in iron homeostasis, it is also contributes to *Mycobacterium tuberculosis* virulence. A *M. tuberculosis bfrB* mutant was sensitive to antibiotics (gentamicin, kanamycin, spectinomycin, ciprofloxacin, moxifloxacin, and isoniazid) and also was unable to invade the host. Furthermore, Bfr is shown to act as an iron supply in *Neisseria gonorrhoeae* under iron restricted condition (Chen and Morse, 1999). However, a *bfr* mutant phenotype has not been recognized yet in *E. coli* or *Brucella militensis* and so its function is unclear is some bacteria (Pandy and Rodrigues, 2012). The *bfr* mutant phenotype in *Pseudomonas aeruginosa* is redox stress sensitivity. This suggests a role for Bfr in redox stress resistance by supplying haem to peroxidases (Ma *et al*., 1999). Bfr also provides protection for *Salmonella typhimurium* from the toxicity of hydroxyl radical of Fenton reaction because this protein decreases the cellular level of free iron (Velayudnan *et al*., 2007).

The Dps protein has been categorized as a nonspecific DNA-binding protein produced in stress conditions such as carbon deficiency and redox stress caused by H_2O_2 (Stephani *et al*., 2003) . Its function starts once attachment occurs to DNA, as a DNA protector from damage caused by redox stress. In *E. coli*, Dps oxidizes ferrous iron at a ferroxidase centre located at the twofold axis between twofold-related subunits (Ilari *et al*., 2003). Dps isolated from the Gram-negative bacterium *Listeria innocua* was first described as a ferritin. However, in other bacteria this protein is not a ferritin (Bozzi *et al.,* 1997), i.e. does not act as an iron store. In *E. coli*, H_2O_2 stress can increase the induction of *dps*

which encodes the Dps protein (Velayudnan *et al*., 2007) Iron storage is not the main role of Dps but instead its essential function is in preventing DNA cleavage under redox condition (Andrews *et al.,* 2003). This protein can protect DNA from the effect of hydroxyl radical under iron-induced redox stress condition as it uses H_2O_2 as an antioxidant during iron deposition. This decreases the production of hydroxyl radical via Fenton reaction. Furthermore, recent studies reveal that Dps provides protection for *Salmonella enterica* serotype Enteritidis from radicals produced during antibiotic treatment (Calhoun and Kwon, 2011).
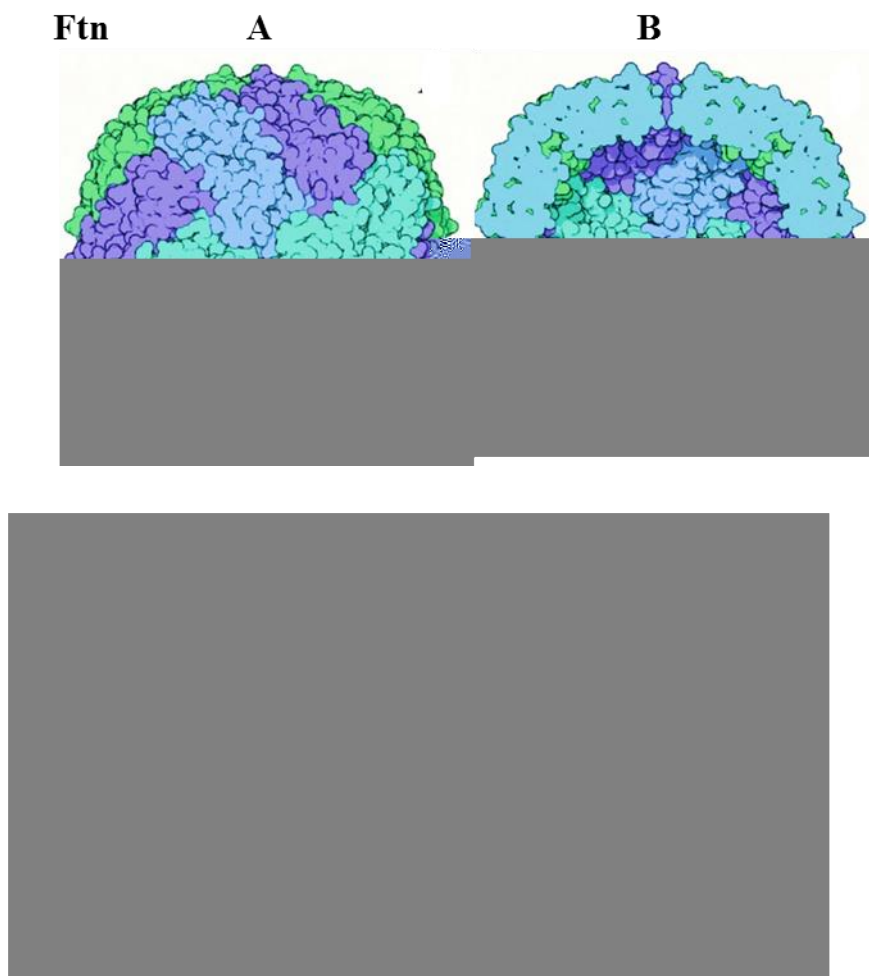
Figure 1.4 Structures of the three iron storage proteins of *E. coli*. Structures shown are of the 24-meric forms for both Ftn and Bfr, and the 12-meric Dps proteins (80-90 Å in diameter). A and B represent the outer and inner surfaces (respectively) of ferritin showing the spherical hollow structure, its outer diameter is ~ 120 Å and the inner diameter is ~ 80 Å. Pictures were obtained from the Protein Data Bank.
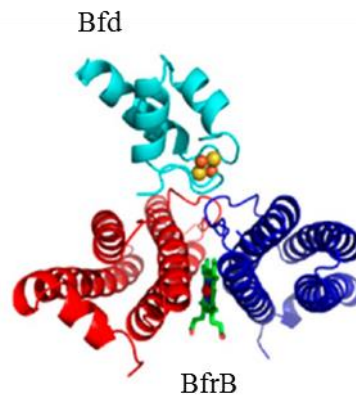
Figure 1.5 the structure of *Pseudomonas aeruginosa* BfrB/Bfd complex showing the binding of Bfd protein with the two BfrB subunits to mobilize iron deposited in BfrB. Rivera (2017).

1.5 Regulation of bacterial gene expression by iron

The mechanism of iron uptake and iron consumption in bacteria is regulated in response to iron availability. Most Gram-negative bacteria including *E. coli* achieve this regulation by the presence of the ferric uptake regulator protein, Fur (Hantke, 2001).

In *E. coli*, Fur is responsible for the regulation of more than 90 genes (Hantke, 2001) involved in many functions (McHugh *et al.*, 2003). It also controls the production of bacterial virulence factors such as shiga toxin in *Shigella dysenteriae* and haemolysin in *E. coli* (Ratledge and Dover, 2000). Fur regulates virulence factors in other bacteria also, e.g. endotoxin A in *Pseudomonas* (Crichton, 2009). Fur mutation in bacteria results in not only overexpression of siderophore receptors in the OM but also excretion of siderophores in the case of iron availability. This suggests that Fur protein is responsible for regulation of the biosynthesis of siderophores. So Fur plays a major role in *E. coli* iron-uptake systems, particularly enterobactin and ferrichrome transport systems, which appear to be found in most *E. coli* strain (Earhart, 1996).

Fur is considered as a global regulator for genes which define a modulon (Andrews *et al.,* 2003). In *E. coli,* Fur is a repressor for not only genes responsible for iron acquisition when the concentration of iron in the media is <5 µM (Chrichton, 2001; Andrews *et al.*, 2003), but also for genes which are responsible for non-iron functions such as respiration,

flagella mobility, the tricarboxylic acid cycle (TCA) cycle, glycolysis, methionine biosynthesis, DNA packaging of phage, DNA synthesis, purine metabolism and redox stress resistance (McHugh *et al*., 2003). The *fur* mutant phenotype has been identified in *E. coli* and *Salmonella*. In *E. coli*, this includes a growth inhibition on non-fermentable carbon sources. This leads to respiration deficiency and also susceptibility to redox stress caused by high level of labile iron in the cytoplasm (Hantke, 1987).

E. coli and *Salmonella* as pathogens can overcome the problem of gastrointestinal tract (GIT) acidity by the acid response reaction which has been suggest to be regulated by Fur. Although the proteins produced by Fur-dependent gene control under acid stress are not identified (Crichton, 2001) it is found that in *Salmonella*, *fur* mutants are more sensitive in low pH environment (acid stress) (Foster and Hall, 1992).

1.6 Positive regulation by Fur

Fur is also responsible for indirect induction of many genes in *E. coli* such as those encoding aconitase [4Fe-4S], SodB (Fe-containing), iron storage (FtnA and Bfr), and aerobic and anaerobic fumarases [4Fe-4S] (Massé and Gottesman, 2002; Tseng, 1998). However, it appears that Fur directly induces the *pfr* modulon (the ferritin gene of *Helicobacter pylori*) which is stimulated by iron (Delany *et al*., 2001). Massé and Gottesman (2002) showed that the $Fe^{2+}-Fur$ complex represses the *ryhB* gene, which encodes RyhB, a small non−coding RNA. Several genes in *E. coli* that are indirectly induced by Fur are negatively regulated by RyhB - these include as *acnA, bfr, sdh* and *sodB*. This gives an explanation for the ability of Fur to induce these genes under iron sufficiency: RyhB is a small regulatory RNA that itself is Fur repressed and that mediates the down-regulation of genes encoding iron-proteins in conditions of iron unavailability (see Fig. 1.6) (Massé and Gottesman, 2002). In this way, the demand of the cell for iron is reduced under iron deficiency – a phenomenon known as iron rationing or iron sparing. There are two types of RyhB, RyhB1 and RyhB2 in *Salmonella typhimurium*. Kim and Kwon (2013) suggest that they have essential regulatory functions in different cellular pathways such as motility and chemotaxis. For motility, they found that the *ryhB* deletion results in high expression of the gene which is responsible for motility (*flgJ, cheY* and *fliF*) which would probably increase bacterial motility.

Massé and Gottesman (2002) proposed that the induction of *ftnA* by $Fe^{2+}-Fur$ is mediated by RyhB. However, a subsequent study revealed a new mechanism for iron–induced gene

expression and proved that this induction is RyhB independent and results from the binding of $Fe^{2+}-$Fur complex in competition with H$-$NS (Histone-like nucleoid$-$associated protein), which is considered as an *ftnA* gene repressor, to the Fur-binding site upstream (-83) of this gene promoter (Nandal *et al*., 2010).
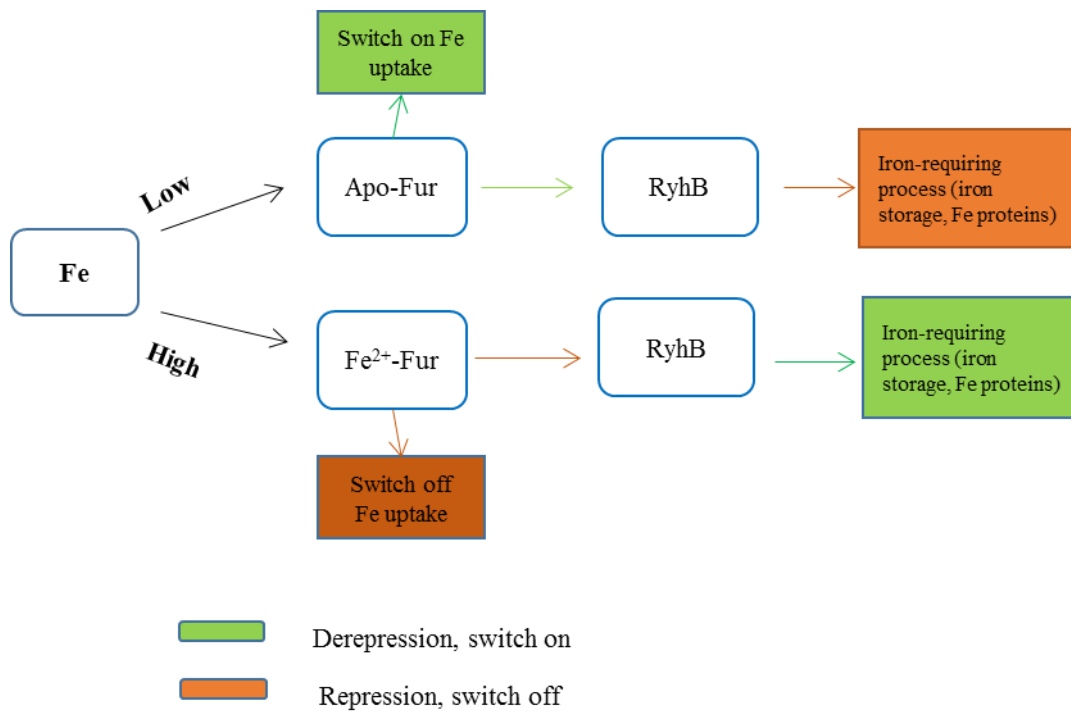
Figure 1.6 Schematic diagram showing the roles of Fur and RyhB in mediating Fe-dependent gene regulation in *E. coli*. Adapted from Masse and Gottsman (2002).

Fur is composed of two identical 17 kDa subunits, it binds with iron to produce a complex that can repress the transcription of genes, by binding to a Fur box, a specific 19-bp palindromic sequence (located between -35 and -10 box) at the promoter (GATAATGATAATCATTATC) (Neilands, 1995). Fe-Fur-DNA binding occurs in cases of a consensus match of no less than 11 bp using its N-terminal DNA-binding domain. The Fur fold is composed of an N-terminal DNA-binding domain and C-terminal domain which is rich in His residues. This domain is responsible for binding to ferrous iron and dimerization. The Fur protein in *E. coli* has a Zn-binding site in its C-terminal domain at Cys 92 and 95 (Andrews *et al*., 2003). It is believed that zinc binding is essential for maintaining the quaternary structure of Fur (Pecquenre *et al.,* 2006).

In *E. coli*, under oxidative stress conditions, Zheng *et al.* (1999) found that not only the level of Fur expression is increased but also flavodoxin, a flavin-containing protein which is encoded by *fldA* (the upstream gene of *fur*) in response to two redox stress regulators, OxyR and SoxRS. Flavodoxin may assist in maintaining iron in the ferrous form and thus may provide ferrous iron for the Fur protein. Fur levels elevate from 5000 to 10000 molecules/cell during transition to the stationary phase suggesting that the chromosome contains many Fur binding sites. Also, higher Fur levels may result in decreased cytoplasmic free iron which would probably reduce oxidative stress. Once Fur has complexed with Fe^{2+}, its affinity to its binding site (Fur box) is increased by 1000 fold, causing switching off of genes encoding for iron acquisition (Andrews *et al.,* 2003).

The SoxRS regulon is controlled by SoxS, produced by *soxS*, which in turn is induced by SoxR in response to redox cycling agents. The activation of this regulon is essential in bacterial defence mechanism particularly in this condition as it lead to expression of enzymes such as superoxide dismutases, endonuclease IV, fumarase, aconitase and glucose-6-phosphate dehydrogenase which perform essential role in DNA repairing and resistance to redox stress, as well as controlling iron flux (Daugherty *et al*., 2012). These finding lead to the suggestion that iron regulation is an essential component in the protection of bacteria from oxidative stress.

1.7 Iron and Pathogenicity

Iron in animals and human is withheld after assimilation from the diet. This occurs by binding of iron to the serum glycoprotein transferrin (Tf). This protein has an excess iron-binding capacity by which available iron in the blood stream is withheld from pathogenic bacteria as part of the innate host-defence mechanism. Invasive pathogenic bacteria can tolerate and survive in this condition by utilising iron from host sources (particularly haemoglobin and transferrin). Gram-negative pathogens may contain high-affinity OM receptors for haem or haem complexes (e.g. Hma and Chu in uropathogenic *Escherichia coli*) or for Tf (section 2 –9) that deliver haem or iron into the cytosol through periplasmic ABC transporters. Another option is the production of siderophores which have a specificity to scavenge iron from host sources (e.g. Tf) (Ratledge and Dover, 2000).

Salmonella and other intracellular pathogenic bacteria may exist in the phagosome inside the macrophage to escape from recognition of by the immune system. Pathogens compete with the host for acquiring iron from the host's iron-proteins e.g. *Mycobacteria* scavenges

iron from Tf, ferritin and Lf using mycobactin siderophores (Ratledge, 2004). In the host, macrophages provide self-protection against these invading pathogens with the assistance of Nramp1, (natural-resistance against macrophage pathogens) which is located in the phagosomal membrane and is responsible for lowering the iron levels of the phagosome. Nramp1 (as part of host defense mechanism), in competition with the pathogen, transports divalent ions (Fe^{2+} and Mn^{2+}) out of the phagosome and thus lowers metal levels within the phagosome such as ferrous iron to enhance the condition of iron restriction by preventing the acquisition of iron required for bacterial growth (see section 1.3.8 MntH transport system) (Nevo and Nelson, 2006). This mechanism of defense is supported and confirmed by the increased sensitivity of the host to infection by intracellular pathogenic bacteria when the NRAMP1 gene is mutated (Blackwell, 2001). A substantial number of enteric bacteria synthesise and produce aerobactin, particularly those causing septicaemia and extra intestinal infection. Aerobactin manufacture and utilisation requires genes (*iucABCD-iutA*) found either on the chromosome or on a plasmid. These genes are carried on the colicin V (pColV-K30) virulence-conferring plasmid in *E. coli* strains which cause septicaemia, and are only carried by virulent strains (Lafont *et al*., 1987). It also appears that there are a significant connections between its production and the ability to cause septicaemic infections in *Klebsilla pneumonia* (Nassif and Sansonetti, 1986). Aerobactin and salmochelin production by pathogenic *E. coli* provide an advantage during infection since these siderophores (unlike enteroobactin) have the ability to escape the neutralization effect of lipocalin 2 (a serum protein produced by the host as part of defence mechanism) (Cornelis and Andrews, 2010; Messenger and Barclay, 1983; Gao *et al*., 2012). Clemont *et al*. (2001) showed that the pathogenicity of *E. coli* responsible for causing bacteraemia and urosepsis is related to the presence of the yersinia high-pathogenicity island (HPI) which codes for the production of yersiniabactin. These finding emphasise on the role of siderophores in bacterial virulence.

Iron-storage proteins play an important role in sequestering excess iron in conditions of iron availability for later use in conditions of iron restriction to maintain iron homeostasis. They also serve to prevent the formation reactive oxygen species by the Fenton reaction in condition of redox stress. Dps in *E. coli* provides protection for DNA against hydroxyl radical through its ability to react with free ferrous iron (Zhao *et al*., 2002) and is associated with the ability to endure prolonged starvation through DNA-Dps co-crystallization (Frenkiel-Krispin et.al., 2001). It also contributes to *Mycobacterium*

smegmatis DNA protection under redox stress condition without direct contact to DNA; at temperature below 37 ˚C it forms trimers (rather than dodecamers) that cannot bind DNA or store iron, but sill protect DNA against hydroxyl radicals (Gupta and Chatterji, 2003). Halsey *et al*. (2004) proved that Dps significantly participates in the pathogenicity of *Salmonella enterica* by providing not only redox stress resistance but also enhancing survival in macrophages.

Aims and Objectives

- To further understand the *in vivo* mechanism of iron release from iron-storage proteins.

- To further understand the role of these protein in redox stress and determine which one is essential anti-redox agents.

- To determin the role of reduction in iron release from iron stores, using *E. coli* as the model.

This aim will be achieved through the following objectives:

- Determination of whether iron-storage proteins (FtnA, Bfr and Dps) act independently or specifically.

By generating single, double and triple mutant strains of iron-storage components:

> ➢ Testing their growth under iron-restriction conditions.

> ➢ Testing their growth under redox stress conditions.

> ➢ Complementation with iron-storage proteins from *E. coli* and other organisms.

- Determine whether the three different types of iron-storage protein can mutually complement and are thus functionally interchangeable.

> ➢ This will be achieved by complementing the mutants using the different classes of iron-storage protein under controlled expression conditions.

- If heterologous iron-storage proteins are found to be unable to fully complement corresponding *E. coli* mutants, then species-specific factors required for their function in intracellular Fe storage and release will be sought.

Chapter 2: Materials and Methods

2.1 Strain used for this work

All strains of *Escherichia coli* used in the research are listed in Table 2.1. These strains were stored at -80 ˚C in 20% (v/v) glycerol in L broth in sterile cryovials. P1 bacteriophage (virulent) (Miller, 1992) was used in transduction experiments.

Table 2.1: *E. coli* strains

Bacterial Strain	Genotype	Reference/Source
BW25113	F⁻ Δ(*araD-araB*)567 Δ*lacZ4787*(::*rrnB-3*) λ⁻ *rph-1* Δ(*rhaD-rhaB*)568 *hsdR514*	Baba *et al*., 2006
JW1893	BW25113 Δ*ftnA*::*kan*	Baba *et al*., 2006
JW3298	BW25113 Δ*bfr*::*kan*	Baba *et al*., 2006
JW0797	BW25113 Δ*dps*::*kan*	Baba *et al*., 2006
Top10	*E. coli* F⁻ *mcrA* Δ(*mrr-hsdRMS-mcrBC*) φ80*lacZΔM15* Δ*lacX74 nupG recA1 araD139* Δ(*ara-leu*)*7697 galE15 galK16 rpsL*(Str^R) *endA1* λ⁻	Sambrook *et al*., 2001
BL21/DE3*	F⁻ *ompT hsdSB* (rB-mB-) *gal dcm rne131* (λDE3)	Lab stocks
BW25113Δ*dps*	F⁻ Δ(*araD-araB*)567 Δ*lacZ4787*(::*rrnB-3*) λ⁻ *rph-1* Δ(*rhaD-rhaB*)568 *hsdR514* Δ*dps*	This work
BW25113Δ*ftnA*	F⁻ Δ(*araD-araB*)567 Δ*lacZ4787*(::*rrnB-3*) λ⁻ *rph-1* Δ(*rhaD-rhaB*)568 *hsdR514* Δ*ftnA*	This work
BW25113Δ*bfr*	F⁻ Δ(*araD-araB*)567 Δ*lacZ4787*(::*rrnB-3*) λ⁻ *rph-1* Δ(*rhaD-rhaB*)568 *hsdR514* Δ*bfr*	This work
BW25113Δ*ftnA*(Δ*dps*)::*kan*	F⁻ Δ(*araD-araB*)567 Δ*lacZ4787*(::*rrnB-3*) λ⁻ *rph-1* Δ(*rhaD-rhaB*)568 *hsdR514* Δ*ftnA* (Δ*dps*)::*kan*	This work
BW25113Δ*ftnA*(Δ*bfr*)::*kan*	F⁻ Δ(*araD-araB*)567 Δ*lacZ4787*(::*rrnB-3*) λ⁻ *rph-1* Δ(*rhaD-rhaB*)568 *hsdR514* Δ*ftnA* (Δ*bfr*)::*kan*	This work
BW25113Δ*bfr*(Δ*dps*)::*kan*	F⁻ Δ(*araD-araB*)567 Δ*lacZ4787*(::*rrnB-3*) λ⁻ *rph-1* Δ(*rhaD-rhaB*)568 *hsdR514* Δ*bfr* (Δ*dps*)::*kan*	This work
BW25113Δ*ftnA*Δ*dps*	F⁻ Δ(*araD-araB*)567 Δ*lacZ4787*(::*rrnB-3*) λ⁻ *rph-1* Δ(*rhaD-rhaB*)568 *hsdR514* Δ*ftnA* Δ*dps*	This work

BW25113Δ*ftnA*Δ*bfr*	F⁻ Δ(*araD-araB*)567 Δ*lacZ4787*(::*rrnB-3*) λ⁻ *rph-1* Δ(*rhaD-rhaB*)568 *hsdR514* Δ*ftnA*, Δ*bfr*	This work
BW25113Δ*bfr*Δ*dps*	F⁻ Δ(*araD-araB*)567 Δ*lacZ4787*(::*rrnB-3*) λ⁻ *rph-1* Δ(*rhaD-rhaB*)568 *hsdR514* Δ*bfr* Δ*dps*	This work
BW25113Δ*ftnA*Δ*dps* (Δ*bfr*)::*kan*	F⁻ Δ(*araD-araB*)567 Δ*lacZ4787*(::*rrnB-3*) λ⁻ *rph-1* Δ(*rhaD-rhaB*)568 *hsdR514* Δ*ftnA* Δ*dps* (Δ*bfr*)::*kan*	This work
BW25113Δ*ftnA*Δ*dps*Δ*bfr*	F⁻ Δ(*araD-araB*)567 Δ*lacZ4787*(::*rrnB-3*) λ⁻ *rph-1* Δ(*rhaD-rhaB*)568 *hsdR514* Δ*ftnA* Δ*dps* Δ*bfr*	This work
Stellar competent cell	F⁻, *ara*,Δ(*lac-proAB*) [Φ*80d lacZ*Δ*M15*], *rpsL*(*str*), *thi*, Δ(*mrr-hsdRMS-mcrBC*), Δ*mcrA*, *dam*, *dcm*	Clontech

2.2 Reagents.

All reagents were analytical grade or higher quality and were generally purchased from Bio-Rad Scientific, Fisher or Sigma.

2.3 Microbiological media

Medium components used in this work were purchased from Difco, Oxoid or Sigma and medium was prepared according to Sambrook *et al.* (2001). Media were sterilized by autoclaving for 20 min at 121 ˚C, 20 Ibs/in². Heat labile substances were filter sterilized using a 0.22 µm Millipore filters and added to the medium after it was cooled to 50 °C.

Luria Broth Medium (LB) contained 1% (w/v) tryptone, 0.5% (w/v) yeast extract, 0.5% NaCl in deionised water. LB-agar medium was prepared by adding 1.5% w/v agar in LB prior to autoclaving. These media were used for routine bacterial growth, with or without adding appropriate antibiotics (Table 2.2).

Table 2.2: Antibiotics used in this work

Antibiotic	Final concentration
Ampicillin (in H₂O)	100 µg/ml
Chloramphenicol (in ethanol)	50 µg/ml
Kanamycin (in H₂O)	25 µg/ml

Table 2.3: Oligonucleotides (from Eurofins UK)

Primers	Sequence 5' -3'	For. /Rev.	Tm	Length (nt)
bfr-**F**	CCCTCACTCGTTCCAGCAATTAAA	F	61.0	24
bfr-**R**	TATAACCACTATCGCATTCGGCCC	R	62.7	24
dps-**F**	TCCTGGCGAGCAGATAAATAAGAA	F	59.3	24
dps-**R**	TAAATAAGTGCGTTGAGGTGGGCT	R	61.0	24
ftnA-**F**	CAGCGAGGGGATCTTCGCTGATTAAAGAA	F	75.3	29
ftnA-**R**	AGAGCTGGTAGCGTTTCTGGCAGCAAAAGGC	R	79.3	31
pBad-*bfr*	TCAGCAGGATCACATATGAAAGGTGATACTAAAGTTATA	F	54	39
pBad-*bfr*	GACTCTCTCGGATCCTCAACCTTCTTCGCG	R	56	30
pBad-*dps*	TCAGCAGGATCACATATGAGTACCGCTAAATTAG	F	53	34
pBad-*dps*	GACTCTCTCGGATCCTTATTCGATGTTAGACTCG	R	53	34
pBad-*ftnA*	TCAGCAGGATCACATATGCTGAAACCAGAAATG	F	55	33
pBad-*ftnA*	GACTCTCTCGGATCCTTAGTTTTGTGTGTCGAGG	R	57	34
pBad-*ftnA* (L 2 K)	CAGCAGGATCACATATGAAAAAACCAGAAATGATTGA	F	61.1	37
pBad-*ftnA* (L 2 K)	AGGTCGACTCTAGAGGATCCTTAGTTTTGTGTGTCGA	R	65.6	37
pBad-*ftnA* (L 2 A)	TTCAGCAGGATCACATATGGCTAAACCAGAAATG	F	62	34
pBad-*ftnA* (L 2 A)	GTCGACTCTAGAGGATCCTTAGTTTTGTGTGTCGAG	R	65.6	36
pET21a- *dps*	CTCGAATTCGGATCCTTATTCGATGTTAGACTCG	F	68.3	34
pET21a- *dps*	GAAGGAGATATACATATGAGTACCGCTAAATTAG	R	64.7	34
T7 promoter	TAATACGACTCACTATAGGG	F	48	20

	GCTAGTTATTGCTCAGCGG	R	51	19
T7 terminator				
pBADrha	CTTTCCCTGGTTGCCAATG	F	64	19
pBADrha-A	AAGCTTGCATGCCTGCAGGT	R	55	20

Table 2.4: Plasmids

Plasmid name	Genotype	Antibiotic resistance	Source / Reference
pCP20	Knockout plasmid 9.4 kb, temperature-sensitive replication and thermal induction of FLP synthesis.	Ap^R and Cm^R	(Datsenko and Wanner, 2000)
pBADrha	Rhamnose induced expression vector, ori_{p15} *rhaR rhaS P_{rhaB}* Cat^r	Cm^R	Ford *et al*., 2014
pBADrha-*ftnA*	pBADrha containing the *E. coli ftnA* gene	Cm^R	This work
pBADrha-*bfr*	pBADrha containing the *E. coli bfr* gene	Cm^R	This work
pBADrha-*dps*	pBADrha containing the *E. coli dps* gene	Cm^R	This work
pET21a	Overexpression vector Optional C-terminal (His6)	Ap^R	Novagen
pET21a-*dps*	pET21a containing the *E. coli dps* gene	Ap^R	This work
pBADrha-*ftnA* (L 2 K)	pBADrha containing the *E. coli ftnA* gene (L 2 K)	Cm^R	This work
pBADrha-*ftnA* (L 2 A)	pBADrha containing the *E. coli ftnA* gene (L 2 A)	Cm^R	This work
pET*lin*M18	pET21a containing synthesised *Pyroccoucs furiosus linocin* M18 gene	Ap^R	This work
pBADrha-*lin*M18	pBADrha containing synthesised *Pyrococcus furiosus linocin* M18 gene	Cm^R	This work

2.4 DNA size markers

GeneRuler™ 1 kb DNA ladder from Fermentas was used to estimate the size and quantity of DNA following gel electrophoresis, using UV-induced fluorescence in the presence of Gel-Red (Cambridge Bioscience) (see Fig 2.1 for individual fragments and quantities).
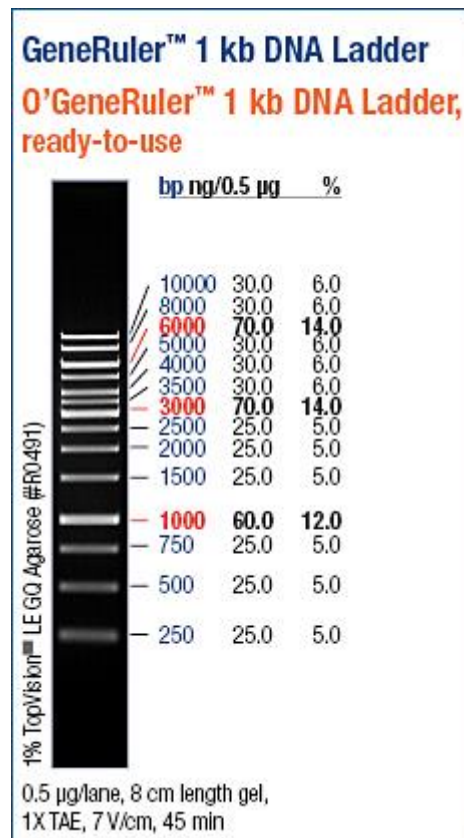
Figure 2.1: 1 Kb DNA ladder marker. Gene-Ruler by Fermentas.

2.5 Transformation of chemically competent cells

2.5.1 Preparation of chemically competent cells

Chemically competent cells were prepared by using calcium chloride. LB broth (50 ml) in a 250 ml conical flask was inoculated with 0.5 ml of an overnight culture of *E. coli* and grown up at 37 °C in a Gallenkamp orbital shaker (250 rpm). Once the culture reached mid-exponential phase and optical density of 0.4-0.5 at 650 nm, the cells were harvested in pre-cooled 50 ml Falcon tubes by centrifugation at 4 °C, 2880 x g (Eppendorf 5804 R with A-4-44 rotor) for 15 min. The supernatant was decanted, and the cells were re-suspended in 30 ml of ice-cooled 0.1 M $MgCl_2$ and placed on ice for 10 min, followed by centrifugation as before. The pellet was re-suspended in 30 ml of ice cold 0.1 M $CaCl_2$ and incubated on ice for 30 min. Cells were centrifuged again as in the previous step and

re-suspended in 8 ml ice cold 0.1 M of $CaCl_2$ plus 20% (v/v) glycerol. Finally, the cells were divided into 100 µl aliquots and stored at -80 ˚C.

2.5.2 Transformation of chemically competent cells of *E. coli*

Plasmid DNA (1-2 µl) was added to 100 µl *E. coli* chemically competent cells and mixed gently. The cells were incubated on ice for 30 min followed by heat shock at 42 ˚C for 2.5 min, then the reaction mixture was immediately placed on ice for 5 min. 1 ml of pre-warmed L-broth was added to the mixture, which was then incubated for 45 min at 37 ˚C. Next, the cells were harvested by centrifugation at 12000 x g for 5 min and 900 µl of supernatant were discarded, and the pellet was re-suspended in the remaining supernatant and plated out onto LA with appropriate antibiotic.

2.6 Agarose gel electrophoresis

For analysing plasmid DNA and PCR products, agarose gel electrophoresis was performed. Gels were generally 0.7% (w/v) agarose in 1X TBE buffer (0.4 M Tris, 0.4 M borate, 1 mM EDTA pH 8.0). Gel staining was performed with Biotium Nucleic Acid Stain GelRed^{TM} (dilution of GelRed^{TM} 10,000X stock reagent into the agarose gel solution; e.g. 1 µl of the GelRed^{TM} 10,000X stock reagent added to 50 ml of the gel solution). DNA samples (2 µl) were loaded with 2 µl of DNA loading dye (10 mM Tris-HCl pH 7.6, 0.03% bromophenol blue, 0.03% xylene cyanol FF, 60% glycerol, 60 mM EDTA) and 6 µl sterile ultrapure water (qH_2O) from a Reverse-Osmosis Nanopure Diamond (Barnstead) system. GeneRuler^{TM} 1 kb DNA ladder (Fermentas) was used as the DNA size marker (1 µl GeneRuler^{TM}, 2 µl of DNA loading dye, 7 µl qH_2O). Samples were electrophoresed for around 90 min in a BioRad horizontal gel tank containing 0.5X TBE buffer. Agarose gels were visualised under UV illumination provided by a short wave length UVP GelDoc-it ultraviolet transilluminator Bio-Imaging system.

2.7 DNA Digestion

DNA digestion of plasmid was generally performed in 20 µl volumes containing 4 µl (60-100 ng/µl) DNA, 10X digestion buffer and appropriate restriction enzymes (1-5 U). The mixture was incubated at 37 ˚C for 60 min without shaking.

2.8 DNA Extraction

2.8.1 Extraction of genomic DNA

Genomic DNA was extracted from *E. coli* strains by using GeneJET Genomic DNA Purification Kit (Thermo Scientific). One colony was inoculated in 2.5 ml LB and incubated with shaking (250 rpm) overnight at 37 ˚C. 0.5 ml of overnight culture were inoculated into 5 ml pre-warmed LB. Cells were harvested in the exponential phase and centrifuged at 4500 x g (5000 rpm) (Eppendorf 5804 R with A-4-44 rotor) for 10 min. The pellet was re-suspended in 180 µl of digestion solution and 20 µl of proteinase K and mixed thoroughly by vortexing, and then incubated at 56 ˚C in a shaking water bath for 30 min. RNase (20 µl) was added, and the reaction was mixed by vortexing and then incubated at room temperature for 10 min. After the incubation, 200 µl of lysis solution was added to the sample and mixed by vortexing for 15 s. 400 µl of 50% (v/v) ethanol were added and the sample mixed by pipetting. The mixture was transferred to a GeneJET^{TM} Genomic DNA Purification Column and centrifuged for 1 min at 6000 x g. Wash Buffer I (with ethanol added) (500 µl) was then added to the column and centrifuged for 1 min at 8000 x g followed by addition of 500 µl of Wash Buffer II (with ethanol added) and centrifuging for 3 min at 12000 x g. Finally, 200 µl of Elution Buffer (10 mM Tris-Cl, pH 9.0, 0.5 mM EDTA) were added to the centre of the column membrane to elute the genomic DNA; this was incubated at room temperature for 2 min. After the incubation, the column was centrifuged for 1 min at 8000 x g. The purified DNA was stored at -20 ˚C.

2.8.2 Plasmid extraction

A Thermo GeneJET Miniprep kit was used for plasmid extraction. LB broth (5 ml) supplemented with appropriate antibiotic and inoculated with a transformant *E. coli* colony harbouring the desired plasmid was grown at 37 ˚C for 16-18 h with 250 rpm shaking. After the incubation, the culture was centrifuged at 4500 x g for 10 min at 4 ˚C. The supernatant was discarded and the pellet re-suspended in 250 µl resuspension solution followed by 250 µl of lysis solution and 350 µl of neutralisation solution addition and then centrifuged at 12000 x g for 5 min. The supernatant (~800 µl) was added to the spin column and centrifuged for 1 min at 12000 x g, the column was washed twice with an ethanol based wash solution. Additional centrifugation for 1 min at 12000 x g was performed to remove residual ethanol. Finally, elution buffer (10 mM Tris-HCl, pH 8.5) (50 µl) was added to the centre of the column, followed by incubation for 2 min at room temperature and then centrifugation for 2 min at 12000 x g. The eluted plasmid DNA was stored at -20 ˚C.

2.8.3 Determination of DNA concentration

Cloning and sequencing reactions require a specific concentration of DNA. So estimation of DNA concentration using a Nanodrop spectrophotometer was performed before proceeding with any cloning or sequencing step. Plasmid DNA or PCR product (after cleaning) was placed onto the spectrophotometer's pedestal and the absorbance of the sample was recorded at 260 nm, and the concentration of DNA in ng/µl calculated. The purity of the DNA was determined from the ratio of 260/280 nm absorbance.

2.9 Polymerase Chain Reaction (PCR), Purification and Cloning

2.9.1 Colony Polymerase Chain Reaction (PCR)

A single colony chosen from an LB plate was suspended in 10 µl of sterile water and used as a template for PCR. Each 50 µl PCR reaction contained the following components in 0.5 ml thin wall PCR tube; 5 µl (10x) Dream Taq DNA polymerase buffer (Thermo Scientific), 1 µl (10 mM) dNTPs, 2 µl of (10 mM) of each primer, 1 unit of Dream Taq polymerase, 10 µl of template DNA and a final volume of 50 µl made up with qH$_2$O. tubes were placed in a Eppendorf Master Cycler gradient PCR machine, equipped a lid

heated to 105 ˚C, pre-heated at 95 ˚C for 1 min. PCR was performed using 30 thermal cycles (denaturation at 95 ˚C for 2 min, annealing at primer average Tm, -5 ˚C, for 30 s and extension at 72 ˚C for ~1-5 min) followed by a final extension step, 72 ˚C for 10 min.

2.9.2 Purification of PCR products

PCR products were purified using a GeneJET PCR Purification Kit (Thermo Scientific), according to manufacturer's instructions. 1:1 (v/v) of binding buffer to PCR product were combined, up to 800 µl of the re-suspension solution was transferred to the GeneJET Purification column which was then centrifuged for 60 s. 700 µl of wash buffer were added and the column was then centrifuged again for 60 s. The column was centrifuged for 1 min, then 50 µl of elution buffer were added and the column was centrifuged for 1 min the eluate was then stored at -20 ˚C.

2.9.3 Cloning of *ftnA*, *bfr* and *dps* DNA fragments into the pBADrha vector using Fusion Cloning Reaction.

For cloning *ftnA*, *bfr* and *dps*, PCR was employed using a high-fidelity polymerase such as Q5 with primers providing an *Nde*I site at the start codon and a *Bam*HI site just downstream of the stop codon. Primers used are indicated in Table 2.3 (dissolved in sterile qH$_2$O at 100 pmol/µl and then further diluted x10 to 10 pmol/µl; stored at -20 ºC). These primers were designed according to the procedures in the manual of In-Fusion® HD Cloning Kit User. PCR reaction mixtures of 25 µl were assembled on ice; these were composed of 5 µl 5x reaction buffer, 0.5 µl of 10 mM dNTPs, 1.25 µl of forward and reverse primers, 1 ng to 1 µg of template DNA and 0.25 µl (0.2 U/µl) of DNA polymerase, made to the final volume with qH$_2$O. Each PCR fragment was purified using a GeneJet PCR purification kit (Thermo Scientific) then cloned into the equivalent sites of pBADrha (vector linearized with *Bam*HI and *Nde*I restriction enzymes), according to manufacturer's instructions of Quick-Fusion Cloning Kit. To generate pBADrha-*ftnA*, pBADrha-*bfr* and pBADrha-*dps*, Fusion cloning reactions were prepared as follows: 10 µl final volume with insert to vector molar ratio 2:1, ~50 ng of vector DNA, 1 µl of Fusion Enzyme and 2 µl 5x Fusion Buffer. This reaction was incubated for 30 min at 37 °C. Following this, 5 µl of each reaction was transformed into Top10 competent (section 2.5.2). Transformants were picked using a sterile loop and grown overnight in LB and L-agar containing the appropriate antibiotic (Cm at 50 µg/ml) for plasmid extraction and analysis by restriction mapping (double digestion by *Bam*HI and *Nde*I restriction enzyme), followed by final confirmation by sequencing.

2.10 Elimination of the kanamycin resistance cassette

Single mutants were available as strains with a kanamycin resistance cassette flanked by *frt* sites inserted in place of the gene of interest (Baba *et al*., 2006). The Kn^R cassette was eliminated as described by Cherepanov and Wachernagle (1995) to give mutant strains acting as a recipients for horizontal transfer by transduction of further mutations to generate double mutants. The original mutant strains with Kn^R cassettes were transformed with pCP20 plasmid (see Table 2.4; Fig. 2.2). pCP20 (9.4 kb) is an ampicillin and chloromphenicol resistant plasmid that is a temperature-sensitive replicon and allows thermal induction of FLP synthesis (Cherepanove and Wakernagel, 1995). The transformed cells were plated onto L-agar plus ampicillin and incubated overnight at 30 ˚C. A few colonies were chosed and plated on L-agar and incubated overnight at 44 ˚C to delete the Kn^R cassette from the chromosome. Single colonies were selected and streaked onto L-agar, L-agar plus ampicillin, L-agar plus chloramphenicol and L-agar plus kanamycin. These plates were incubated overnight at 30 ˚C. The desired mutants were selected on the basis of growth on L-agar but not on the other plates (with antibiotic) – these were considered as mutants that had the kanamycin cassette eliminated and had lost the pCP20 plasmid. This was confirmed by colony PCR (section 2.9.1).
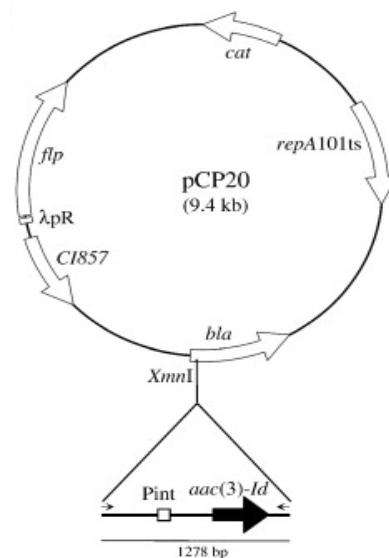
Figure 2.2 Features of pCP20. Restriction enzymes was used to confirm the identity of this plasmid. The plasmid is a Ts replicon encoding the 'flippase' site-specific recombinase that mediates FLP-FRT recombination at two adjacent and identical 13-bp sequences (5'-GAAGTTCCTATTC-3') flanking an 8 bp spacer. Source
http://www.yrgene.com/sites/default/files/images/vector/pcp20.png

2.11 Isolation and purification of P1 from P1 stock

P1 was isolated from the P1*vir* stock (10 µl stock from Gary Sawers [Germany] diluted in 200 µl P1 dilution fluid) by preparing x10 dilutions from 10^{-1} to 10^{-9}. Then, 0.1 ml from an overnight culture of *E. coli* BW25113 were combined with 0.1 ml of P1 phage for all dilutions. These phage-bacteria mixtures were incubated at 37 ˚C for 15 min, and then treated as described in section 2-12-1. After 6 h incubation, the plaque forming units were calculated. Next, in order to isolate single plaques, the plate showing discrete individual plaques was selected. From this plate, four plaques were picked up by using sterile 1 ml pipette tips and each transferred into an individual microfuge tube containing 1 ml of P1 dilution fluid (0.03 % NaCl, 0.1 % Peptone, 0.5 mM $MgSO_4$, 10 mM Tris, pH 7.8) plus two drops of chloroform. This mixture was mixed briefly and left for one hour at room temperature. Following this step, tubes were micro-centrifuged for 10 min at 12000 x g. Finally, the supernatant was transferred into a sterile microfuge tube and stored at 4 ˚C after adding one drop of chloroform. The concentration of P1 phage was expected to be 10^5-10^6 pfu/ml by this method. In order to increase concentration, the protocol for construction of P1 transducing phage (2.12.1) was followed by infecting 'wild type' bacteria (BW25113) with this phage lysate (~10^5-10^6 pfu/ml). The concentration of P1 lysate was expected to be ~ 10^8-10^9 pfu/ml by this method.

2.12 Transduction

Transduction can be defined as a mechanism, first discovered by Zinder and Lederberg (1952), involving horizontal transfer of bacterial DNA fragments from donor bacteria to the recipient as mediated by bacteriophage. There are two types of transduction, generalized and specialized. In generalized transduction, phage can transfer pieces of host genome of length up to that of the P1 chromosome. However, in specialized transduction the phage (e.g. lambda) is limited to the ability to carry only particular genes that are next to the insertion sequence site, which can be incorported into its DNA as a hybrid molecule. Generalized transduction occurs when new phage are being generated during infection and a transducing phage particle is produced by packaging any bacterial DNA fragment instead of phage DNA. This DNA can be transferred to the recipient cell by the transducing phage upon infection but the recipient bacterium cannot be lysed by the transducing phage because this phage does not carry its own genetic material.

2.12.1 Construction of P1 transducing phage

P1 transduction was performed as described in Miller (1992). One colony of donor strain was inoculated in 5 ml LB and incubated on a shaker (250 rpm) overnight at 37 ˚C. After overnight incubation, P1 phage stock was aerated under the flame of a Bunsen burner to evaporate chloroform away. Then a wide range of phage concentrations, from 10^1 to 10^9 pfu/ml, was prepared by diluting in P1 dilution buffer. Next, 0.1 ml of donor and 0.1 ml of phage (at all dilutions) were combined in sterile 4 inch tubes and incubated for 15 min at 37 ˚C. Then, 2.5 ml of pre-warmed L-agar soft top (1% Bacto tryptone, 0.5% Bacto yeast extract, 0.5% NaCl and 0.6% agar in water), containing 2.5 mM $CaCl_2$, 10 mM $MgSO_4$, at 50 ˚C in a 4 inch sterile tube, were added to the tube containing the infected donor strain, mixed briefly and poured immediately onto the pre-warmed Bottom-agar plates (1% Bacto tryptone, 0.5% Bacto yeast extract, 0.5% NaCl and 1% agar in water, and 2.5 mM $CaCl_2$, 5 mM $MgSO_4$) and spread by agitation. The plates were left to set and then incubated for about 6 h at 37 ˚C, top side up. Following the incubation, 3.5 ml of L broth (containing 5 mM $CaCl_2$, 10 mM $MgSO_4$) were added to the confluent lysis plates. These plates were left on a level surface overnight at 4 ˚C. The LB was then transferred to a Falcon tube and 1 ml of chloroform was added. This was mixed briefly and centrifuged at 4 ˚C for 5 min at 4500 x g to remove the debris. Finally, the lysate was stored at 4 ˚C in a sterile container after adding a few drops of chloroform.

2.12.2 Calculation of P1 levels (by P1 titration)

The collected lysate was diluted in dilution fluid to prepare x10 dilution series used to infect the recipient strain, as described above, and then the plates were incubated overnight at 37 ˚C. After incubation the plaques were counted and the plaque forming units per ml were calculated.

2.12.3 Construction of P1 transduction

The P1 transduction method from Miller (1992) was modified to perform transduction. A 3 ml overnight culture (in LB) of the recipient strain was harvested and the pellet was re-suspended in an equal volume of 5 mM $CaCl_2$, 10 mM $MgSO_4$ and shaken for 15 min at 37 °C. 0.1 ml of P1 lysate (4×10^8, 4×10^7, 4×10^6), after aeration to remove chloroform, were added to 0.1 ml of aliquots of the re-suspended bacterial cells and incubated for 20 min in a water bath at 37 °C then 200 µl of sodium citrate (prepared by adding 1 ml of 1 M sodium citrate to 9 ml of LB) were added. These tubes were then incubated for ~80 min in a water bath at 37 °C to allow the expression of antibiotic resistance. Following

the incubation, 0.1 ml of each mixture were plated out onto LB agar plates which contained an appropriate antibiotic (kanamycin, 25 µg/ml). The rest of the mixture was then centrifuged and the pellet was taken up in 0.1 ml of L-broth with sodium citrate and also plated out. All plates were incubated overnight at 37 °C. Two colonies were picked from the kanamycin plates and streaked on fresh L agar to get single colonies after incubation overnight at 37 °C.

2.13 SDS-PAGE and Western Blotting

2.13.1 SDS-PAGE

Protein samples were resolved using 15% SDS-polyacrylamide gels and the Bio-Rad Mini Protein II system. The 15% SDS- polyacrylamide gels contained: 5 ml Tris-HCl (0.5 M, pH 8.8), 10 ml 30% w/v acrylamide (Bio-Rad), 0.2 ml 10% w/v sodium dodecyl sulphate, 0.07 ml fresh 10% w/v ammonium persulphate, 0.015 ml TEMED, 4.7 ml distilled H_2O. The gel was cast at 1.0 mm thickness and, once set, the stacking gel applied to the top. The stacking gel was made up of: 2.5 ml Tris-HCl (0.5 M, pH 6.8), 1.5 ml 30% w/v acrylamide, 0.035 ml 10% w/v sodium dodecyl sulphate, 0.01 ml fresh 10% w/v ammonium persulphate, 0.015 ml TEMED, 4.9 ml distilled H_2O. Samples were suspended in SDS-loading buffer (1 OD_{600} unit in 200 µl of 50 mM Tris-Cl pH 6.8, 100 mM dithiothreitol, 2 % w/v SDS, 0.1 % bromophenol blue, 10 % v/v glycerol), heated to 100 °C for 10 min, micro-centrifuged for 5 min at 16,000 g and 10 µl of the supernatant were loaded into each well. The gel was resolved at 30 mA per gel in SDS-PAGE running buffer (25 mM Tris, 192 mM glycine, 0.1% w/v SDS). Following SDS-PAGE, gels were either stained or further processed for western blotting. For staining the gel was stained with Coomassie Brilliant Blue R-250 (0.2 % Coomassie Brilliant Blue R-250, 30 % v/v methanol, 10 % v/v glacial acetic acid in distilled H_2O). Finally, the gels were stained with destaining solution (30 % v/v methanol and 10 % v/v glacial acetic acid in H_2O until the background of the gels become clear.

2.13.2 Western Blotting

The electrophoresed gel was separated from the glass plates. Prior to electroblotting, the gel was rinsed for 20 min (1 mm gels) in 200 ml electroblot buffer (1x Tris-glycine: pH 8.3, 25 mM Tris-HCl, 0.2 M glycine, 20% v/v methanol and 2.4 litres ultra-pure water).

A nitrocellulose membrane (Whatman Protran BA 83 nitrocellulose paper) was then cut to size using sharp scissors. The membrane was then pre-wetted by soaking in pure water. It was lowered into the water by arching it into the surface of the water and then allowing the wetted area to spread gradually out from the centre of the membrane to the outer edges. Then the wetted nitrocellulose membrane was pre-equilibrated in electroblot buffer for 15 min.

Bio-Rad Trans-Blot cell with plate electrodes and Power Pac 200 power supply was used to transfer proteins from the gel to a nitrocellulose membrane. A blotting sandwich was assembled in the following order: the hinged plastic cassette was unfolded and laid out flat in a shallow vessel, a soaked fibre mat was placed on the grey side of the laid out cassette (not the clear side). Two layers of soaked Whatman 3MM (filter paper) were placed on top (these were about 1 cm bigger than the gel all round). The gel was then placed on top of filter papers (making sure it was the desired way up) with nicked corner positioned at the bottom left. The membrane was then carefully lowered on the gel (one corner nicked and aligned with nicked corner of gel). The membrane was carefully marked and all the air bubbles removed. Two layers of wet filter paper were then placed on the top of the membrane, then the other soaked fibre mat was placed on top, the cassette was closed and secured using the clip.

The electrobloting tank was half filled with electroblot buffer, and the cassette inserted with the grey side adjacent to the black spot (i.e. the cathode, negative terminal). The cooling coil was inserted and the tank filled to the bottom of the red anode disc. The lid was put on and the power turned on. A potential of 50 V was then applied for ~1 h (~500 mA). After the electrophoresis, the sandwich was disassembled and the gel separated from the nitrocellulose, which was then processed for immunodetection.

2.13.3 Immunodetection
The nitrocellulose membrane was washed for 5 to 10 min in Tris-buffer saline (TBS; 20 mM Tris-HCl, 500 mM NaCl, pH 7.5) and then blocked with 4% dried skimmed milk powder in Tris-buffered saline (TBS: 20 mM Tris-HCl, 500 mM NaCl, pH 7.5) for 1 h at room temperature with shaking or overnight at 4 ℃. The blocking solution was decanted and the membrane washed twice 5 min each in TTBS (TBS with 0.05% Tween 20). After washing, the primary antibody was added which comprised of a 1:1000 dilution of anti-FtnA antiserum (for FtnA detection) or 1:1000 dilution of anti-Bfr antiserum (for Bfr

detection), from rabbit. The membrane was left to react with the antibody on a shaking platform for 1 h. The primary antibody was then poured off and the membrane washed twice in TTBS. The secondary antibody solution consisted of 1/30,000 dilution of anti-rabbit IgG in 5% dried skimmed milk powder in TTBS buffer. This was then added to the membrane and left to react with the membrane on a shaking platform for 1 h at room temperature. The secondary antibody was then poured off and the membrane was washed with TTBS for 10 min on the shaker. After this, the membrane was washed in TBS twice to remove any Tween detergent from the membrane prior to development. The colour development solution was then prepared by dissolving one BCIP/NBT (5-bromo-4-chloro-3-indolyl-phosphate and nitro blue tetrazolium) (SIGMA-ALDRICH) tablet in 10 ml of distilled water. This was added to the membrane on a gently shaking platform. It was allowed to shake until the desired bands became clearly visible. Once the reaction had developed, the substrate was poured away and the membrane washed with copious volumes of deionized water for at least 10 min to stop further colour development. A photograph of the nitrocellulose membrane was taken while the membrane was still wet to enhance the colour. The membrane was then dried in between two filter papers and stored between polyester sheets.

2.14 Cloning of *dps* DNA fragments into the pET21a vector using Fusion Cloning Reaction.

A *dps* expression plasmid was generated to produce the authentic protein using the vector pET21a.

For cloning *dps*, PCR was employed using a high-fidelity polymerase, hot start Q5 with primers (Table 2.3) providing an *Nde*I site at the start codon and a *Bam*HI site just downstream of the stop codon. Primers were designed according to the procedures in the manual of In-Fusion® HD Cloning Kit. The PCR fragment was purified using GeneJet PCR purification kit (Thermo Scientific) then cloned into the equivalent sites of pET21a (linearized by *Bam*HI and *Nde*I restriction digestion), according to manufacturer's instructions. The In-Fusion cloning reaction was as follows: 10 µl final volume with insert to vector molar ratio 2:1, ~50 ng of vector DNA,1 µl of In-Fusion Enzyme and 2 µl 5x In-Fusion Buffer. This reaction was incubated for 30 min at 37 °C. Following this, 5 µl of the reaction was transformed into Stellar competent cells (section 2.5.2). Transformants were grown overnight in LB containing the appropriate antibiotic (ampicillin, 100 µg/ml), plasmids extracted and the size of the insert tested by restriction

mapping (double digestion by *Bam*HI and *Nde*I) and finally confirmed by sequencing (with primers 'T7 promoter' and 'T7 terminator'; Table 2.3). The sequence was identical to the *dps* gene and so the plasmid (pET21a-*dps*) was transformed into *E. coli* BL21/DE3* (used as host for protein expression).

2.15 Protein overexpression

2.15.1 Small-scale overexpression

To investigate the ability of pET21a-*dps* to overproduce the desired protein, a single isolated colony of a BL21/DE3 transformant containing pET21a-*dps* was inoculated into a 5 ml of LB containing 100 µg/ml of ampicillin and incubated overnight at 37 °C with 250 rpm shaking. This culture was used to inoculate a pre-warmed 50 ml of LB containing 100 µg/ml of ampicillin at a ratio of 1:100 (overnight culture; fresh LB) which was then incubated at 37 °C with 250 rpm shaking. Once the OD_{600} of the culture reached 0.5, IPTG inducer was added at final concentration of 0.5 mM. Samples were taken at the time of adding the inducer and every hour for 6 h, in addition to a final overnight sample. Cells were harvested from these sample by centrifugation at 13,225 x *g* for 8 min. Following this, the pellet was heated for 8 min at 95 °C with 100 µl of 1x SDS digestion buffer and microcentrifuged for 10 min at 13,000 rpm. The supernatant (10-20 µl) was then analysed by SDS-PAGE to determine the efficiency of induction.

2.15.2 Protein solubility

To determine the solubility of the expressed proteins, 5 ml of overnight culture with 100 µg/ ml ampicillin were inoculated from transformant colonies (containing the pET21a-*dps* or the empty vector as control). After incubation overnight at 37 ºC with shaking 250 rpm, 0.5 ml of the overnight culture was inoculated into 50 ml of LB with ampicillin in a sterile 250 ml conical flask, these were incubated at 37 ºC and 250 rpm until the OD_{600} reached 0.5. At this point, a sample equivalent to 0.5 OD units was taken and IPTG added as an inducer for protein overproduction. Cells were isolated by centrifugation and soluble protein released either with BugBuster (5 ml/g of cells) or with B-PER^{TM} (mild detergents that gently disrupt the bacterial cell wall to release the soluble protein contained). The mixture was incubated with gentle shaking at room temperature for 20 min. The lysed cells were then centrifuged at 12,000 x *g* (Eppendorf 5453) for 20 min at 4 °C. The supernatant which represent the soluble fraction was taken into a sterile 1.5 ml

centrifuge tube, and the cell debris representing the insoluble fraction was treated with SDS-digestion buffer (section 2.13.1). Both fractions were analysed by SDS-PAGE (section 2.13.1) and band intensity compared to determine the concentration of protein in each fraction.

2.15.3 Large-scale overexpression

When the time-point of maximum protein overproduction from the small-scale experiment had been determined and solubility established, large scale overproduction was performed. BL21/DE3 containing pET21a-*dps* was inoculated into a 5 ml of LB containing 100 µg/ml of ampicillin and incubated overnight at 37 °C with 250 rpm shaking. This culture was used to inoculate a pre-warmed 500 ml of LB containing 100 µg/ml of ampicillin (in a 2 litre flask) at a ratio of 1:100 (overnight culture; fresh LB) and incubated at 37 °C with 250 rpm shaking. Once the OD_{600} reached 0.5-0.6, the IPTG was added at 0.5 mM final concentration and incubation continued for the appropriate time as determined from the small-scale overexpression. At that time, the cells of the culture were harvested by centrifugation at 6000 x g (Sorval RC5B+ with SLA-3000 rotor) for 30 min at 4 °C and were then re-suspended in 25 ml ice-cold PBS (0.01 M phosphate buffer, 0.0027 M potassium chloride, 0.137 M sodium chloride, pH 7.4). This suspension then centrifuged at 4000 x g (Sorval RC5B+ with SS-34 rotor) to harvest the cell pellet which was maintained it at -80 °C for further work (protein extraction and purification).

2.15.4 Cell lysis and protein extraction by French pressure cell press

Cooling system was switch on for the Cell Disruptor, to allow it to cool to 4 °C before start working to protect the protein from denaturation and slow enzymatic processes resulting from cell lysis. The cells were resuspended in two volumes of appropriate buffer and were then lysed by applying 20,000 psi through the cell press, with a total of 2-3 passes through the press to ensure maximum cell lysis. The resultant solution was centrifuged at 51,428 x g at 4 °C for 40 min and the supernatant was quickly decanted and retained for protein purification by chromatography.

2.15.5 Anion-exchange chromatography

A column packed with 20 ml of DEAE-sepharose^{TM} from Amersham Biosciences was used for the separation of proteins based on charge on a BioLogic system (BioRad). A flow rate of 1 ml/min was maintained throughout the experiment, and fractions of 7 ml were collected. Equilibration of the column was carried out with 4 column volumes of buffer B (50 mM Tris, 1 mM DTT, pH 8.0, 1 M NaCl) and subsequently 8 column

volumes of buffer A (50 mM Tris, 1 mM DTT, pH 8.0). The column was first fully equilibrated, then the protein sample was loaded followed by washing with buffer A to remove unbound protein. The flow-through of this step was retained in case of the protein partially binding or failing to bind. Protein elution was carried out using a linear gradient of 0-1 M NaCl in eight volumes of buffer B. Finally, the fractions showing peaks on the chromatogram were analysed by SDS-PAGE to investigate the potential protein and its purity. The fractions containing the potential protein were maintained at 4 °C for further work.

2.15.6 Dialysis

The protein sample was dialysed for different reasons, mainly to alter the composition of buffer and to remove contaminating small particles. The Cellulose membrane Dialysis tubing (33 mm diameter, Sigma Aldrich) was rinsed with qH_2O Before use, then sealed at one end with closures and filled with qH_2O to detect any leakage; then the water was tipped out and the tubing 67% filled with protein sample and, after dispelling air bubbles and closing the other end of tubing, it was placed in 500-1000 ml of appropriate buffer and stirred at 4 °C for 24 h with two changes of buffer.

2.15.7 Centrifugal concentration of protein samples

The protein sample obtained from protein purification chromatography was concentrated using Vivaspin concentrators (Sartorius Ltd) of 5000 MWCO by centrifugation at 3074 x g (5000 rpm) for the appropriate time. The chromatography eluent was loaded into the upper chamber of the concentrator tube followed by centrifugation at 3250 x g for 20 min and the eluent regularly added to concentrate the required volume of protein.

2.15.8 Estimation of protein concentration

The concentration of the recombinant protein was determined using Bradford protein Assay reagent (BioRad) with bovine serum albumin (BSA) as standard. BSA standards in PBS were prepared in duplicate; 10 µl of standard and 10 µl of undiluted or diluted sample (5x and 10x were placed into a 96 well plate. Following this, 200 µl of 1:4 diluted dye reagent was added to each well. After 5 min incubation time at room temperature for colour development, the absorbance of each well was measured using a Spectramax 190 at 595 nm. The concentration of the protein was calculated from the standard curve created from the measurements of the standard.

2.16 Electron microscopy

Transmission electron microscopy (TEM) was used to analyse the shape and size of Linocin M18 nanocompartment moleculaes; 10 µl of the Linocin M18 protein sample was applied on the carbon-coated copper grid (Agar Scientific), after 1-2 min the excess was removed with filter paper, and then the grid was negatively stained with 1% (w/v) uranyl acetate and then dried with filter paper. The grid, after drying at room temperature, was examined under transmission electron microscopy. The principle of electron microscope work is depend on using electrons and their wavelength for improved the field resolution. The emitted electrons via the TEM column are focused to be a thin beam by electromagnetic lenses. The unscattered electrons formed a shadow image with different obscurity when hitting the fluorescent screen. According to its ability to get high resolution for particles (~ 0.14 nm) many nanoparticls structures had been studied and analysed by the TEM.

2.17 Whole-cell iron assay

Strains were grown overnight in 0.4% glucose-containing M9 medium with 20 µM ferric citrate, and then washed in 10 mM EDTA (pH 8.0). The cells were harvested (all cultures had equal OD units, for each experiment the pellet collected in equal OD e.x. 7 then the result calculated and adjusted to OD equal one) by centrifugation at 4 °C and 5000 rpm for 10 min; the cell pellets were then digested with 70 % (v/v) of Trace Metal Grade nitric acid at 80 °C overnight in screw capped plastic tubes (15 ml Falcons). Next day, the volume was adjusted with qH_2O to 5% of nitric acid as a final concentration; the resultant solution was yellow and fully dissolved. The iron contents of the pellets were measured using a Perkin Elmer 1100B atomic absorption spectrometer (Ann Dudley, Soil Science University of Reading). Standards were prepared in 5% nitric acid by serial dilution to give Fe at 0, 0.5, 1, 5 and 10 ppm.

2.18 Estimation of total cellular iron associated with Dps, Bfr and FtnA by immunoprecipitation

Bacteria were propagated in 5 ml overnight at 37 ºC with shaking at 250 rpm in 5 ml M9 supplemented with 20 µM ferric citrate with 100 µM of rhamnose; the overnight cultures were harvested by centrifugation at 4 ˚C, 5000 rpm, 15 min, in a benchtop centrifuge. The pellet was re-suspended in lysis buffer (lysozyme at 1 mg/ml, 0.1% Triton X100, 1 mg/ml DNase all in PBS) on ice for 15 min. The solution then centrifuged for 5 min at 13,000 rpm, 4 ˚C and the supernatant was aliquoted into three microfuge tube (for specific

iron-storage proteins). Following that, 2 µl neat antiserum (raised in rabbit, specific for the protein of interest) were added to each sample and mixed gently, and then left on ice to form the protein-antibody complex for 1 h. Then, 10 µl of Protein A (Dynabeads^R Protein A, ThermFisher Scientific) were added to the protein-antibody complex and mixed gently, and the reaction was left to incubate for 15 min on ice. Then the Dynabeads were recovered using a magnet (DaynaMag Magnet) and the protein bound to the Protein A Dynabeads was recovered from the beads by eluting with 500 µl of 0.2 M glycine buffer at pH 2.5. The supernatant was recovered and then then neutralised by adding 13 µl 2 M HEPES (pH 8) for each 100 µl supernatent. Then the recovered protein were subjected to analysis by SDS-PAGE and Western blotting to confirm the identity of the immune-precipitated proteins. Finally, the iron content of the immune-precipitated proteins were quantified by ICP-OES.

2.19 Estimation of total cellular iron by colorimetric ferrozine assay

Measurements of The whole cell iron content of the complemented triple mutant strains were conducted by a colorimetric assay using acidic ferrozine solution composed of 1 % ferrozine with 10% acetic acid and 750mM sodium sulphite. Transformants *E. coli* BW25113 Δ*ftnA* Δ*dps* Δ*bfr* carrying either the pBAD vector (A), pBAD-*bfr (*B), pBAD-*dps (*C) or pBAD-*ftnA* were grown overnight in minimal supplemented with 20 µM of iron, 50 µg/ml of chloramphenicol and 100 µM of rhamnose, the pellet then washed and mixed with the acidic ferrozine the mixture then exposed to 90 ºC temperature for one hour for cell lysis. After one hour heating, the absorbance at 562 nm was measured.

Ferrozine is act as an iron chelator has the ability to bind with ferrous iron, the acetic acid and sodium sulphite converts the iron to the ferrous form In order to measure the iron content.

2.20 Polyclonal Antibody against Dps Recombinant Protein

The purified Dps protein (3.5 mg/ml) was used to raise anti-Dps antibodies in two white New Zealand rabbits in Dundee Cell products Ltd. the 90-day protocol was performed for polyclonal antibody production in rabbits. The immunisation were given in three separated dose. The first injection was given in week 2, flowed by a booster in week four, and waiting for two week then bleed and testing. At week seven a third injection of antigen was given, this process was finalised by collecting a third bleed and testing. The

final immune sera was collected and testing for level of specific antibodies in the sera (dot-blot). The immune sera then used in the current work experiments (Western blot).

2.21 Iron –binding ability of Dps protein

To assess the ability of the purified recombinant Dps protein to store iron, an iron uptake assay was conducted, the Dps protein was treated with ferrous ammonium sulphate (FAS), anaerobically prepared (N2 purged), without and with hydrogen peroxide, in 20 mM HEPES (pH 7.0), A comparison of the UV-visible absorbance spectrum (200-400 nm) of 2 µM apo Dps, Dps with ferrous ammonium sulphate (FAS), without and with hydrogen peroxide conducted with the Unicam Helios alpha spectrophotometer at room temperature in 20 mM HEPES pH 7.0.

The Dps protein, with and without pre-incubated with ferrous ammonium sulphate (FAS), was then subjected to non-denaturing gel electrophoresis and was visualised by ferric-iron staining, by socking the gel in 2% potassium ferrocyanide with 5% trichloro-acetic acid (TCA), and after one hour the gel was destained in 5 % TCA.

2. 22 Non-denaturing 1% agarose gel electrophoresis

Non-denaturing 1% agarose gel electrophoresis was used to fractionate molecules of higher mass than can be achieved by PAGE. 1% agarose gel was prepared by dissolving 0.5 gm of agaros in 50 ml 1X running buffer (90 mM Tris base and 90 mM Boric acid, pH 8.0) then poured in thin layer, the gel was left to set for 20-30 min at room temperature.

2.23 Growth curve of *E. coli* strains under redox stress and iron restriction conditions

The phenotypic effects of the effect of mutations on growth of *E. coli* under redox stress and iron restriction conditions were assessed using a Bioscreen microbiology growth curve analysis system. An overnight culture form a single isolated colony of *E. coli* washed once with phosphate buffered saline pH 7.2 and adjusted to a final OD of 1. A microtitre (HONEYCOMB ®) plate was prepared with 200 µl of media per well and the standardised bacterial cultures used to inoculate individual wells to a starting OD of 0.01. Growth curves were monitored every 30 minutes for up to 24 h using a Bioscreen C (Labsystems) with continuous shaking. The experiment were carried out using different condition (with and without diethylenetriaminepenta acetic acid (DTPA), using different concentration of H_2O_2) and also using minimal medium (with/without ferric citrate).

DTPA was prepared by dissolving DTPA in ultra-pure water to 90% of final volume; this was neutralised with 5 M NaOH then ultra-pure water was added to 100% volume. The 0.5 M DTPA (pH 7) solution was then sterilized by filtration and used as an iron chelator (Fig. 2.3).
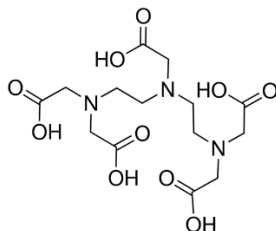
Figure 2.3 A structural diagram of diethylenetriaminepenta acetic acid (DTPA).

Chapter 3

3. Construction of a triple iron-storage mutant

3.1 Introduction

The mutations required for this project had already been generated. These were combined to produce double and triple mutants using P1 transduction method from Miller (1992) with modification to perform transduction (see section 2-12-3). This experiment was preceded by a step for removal of the kanamycin resistance cassette in recipient strains (the Kn^R inserted into the deleted genes carried by the recipient strains; this step was required to allow selection of transductants). This was performed by transformation of pCP20 plasmid, which shows thermal induction of FLP synthesis that enables non-homologous recombination at the FRT sites flanking the Kn^R cassette; (see section 2-10) into Kn^R mutants (see Table 2.4). The constructed mutants by transduction and the mutants generated following the removal of kanamycin resistance cassette were characterised by PCR using Taq DNA polymerase and specific primers for each gene listed in table 2.2 (see appendix 1 for schematic structure of single-gen deletion mutants and Kn^R cassette removal) the amplification fragment /gene size were compared with those amplified in both donor and recipient strains which were used as control, the transductants were confirmed when the gene product gave the same product size as that of the donor strain. For the constructed double mutant and triple mutant strains it was important to confirm that the first mutation (for the double mutants) and both first and second mutations (for the triple mutant) was maintained in mutants generated by transduction. After the confirmation of the genotypes of the generated mutants by PCR, Western blotting was done to additionally confirm the status of each mutant to ensure that the resulting strains were phenotypically correct ($FtnA^{+/-}$ / $Bfr^{+/-}$). $Dps^{+/-}$ status was assessed and confirmed for the generated mutants after generating the polyclonal antibodies using the purified recombinant Dps protein produced in this work (see chapter 6; section 6.11). The constructed mutant strains BW25113 Δ*ftnA* Δ*dps*, Δ*ftnA* Δ*bfr* and Δ*bfr* Δ*dps* double mutants and a Δ*ftnA* Δ*dps* Δ*bfr* triple mutant, in addition to the single mutant strains were required in the experimental work of this project.

3.2 Kanamycin cassette removal from Kn^R mutant strains

The kanamycin resistance cassette inserted into the corresponding deleted gene carried by the recipient strains, from the Keio collection (single gene deletion in *E. coli* K-12 Bw25113 was replaced with kanamycin cassette flanked by FLP recognition sites; in addition *araBAD*, *lacZ*, and *rhaBAD* were already disrupted in BW25113) was removed. This step was required to allow selection of transductants through their acquired Kn^R phenotype. Colony PCR was performed in order to confirm the absence of the kanamycin cassette in each colony. Then, the products were analysed by gel electrophoresis. The figures below show the successful removal of the Kn^R cassette (Fig. 3.1-3.3), as can be seen by the difference in the size of the PCR products for the original strain (with Kn^R cassette) and the resulting strains (BW25113 Δ*bfr*, BW25113 Δ*dps* and BW25113 Δ*ftnA*) in comparison with the wild type which gives the size for the wildtype gene.
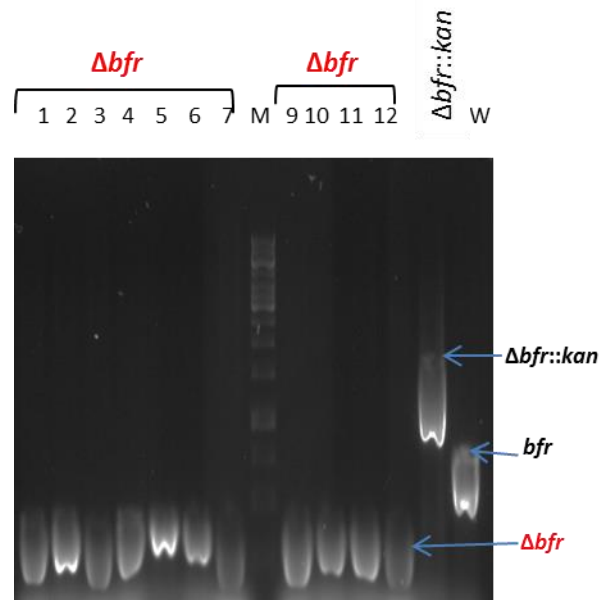
Figure 3.1 Electrophoretic analysis (agarose 0.7% w/v) of the PCR product for the potential BW25113 Δ*bfr* mutants. Removal of the Kn^R cassette by pCP20 and elimination of the plasmid. Primers employed were *bfr* F & R. **M**, 1 kb GeneRuler (Fermentas); **1-11**, mutant BW25113 Δ*bfr* 364 bp; (Δ*bfr*)::*kan*, JW3298 (Δ*bfr*)::*kan* 1598 bp; **W**, wild type 788 bp.
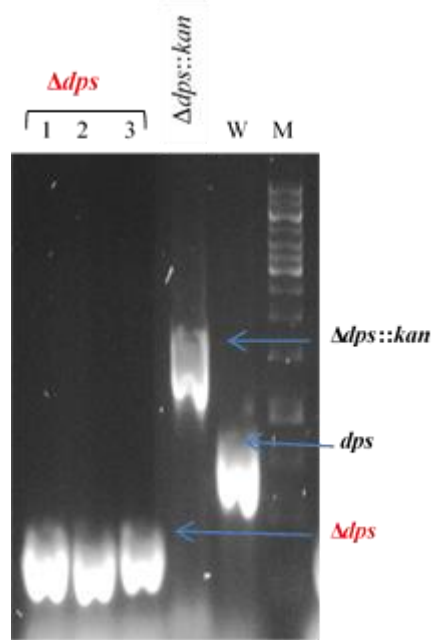
Fig. 3.2 Electrophoretic analysis (agarose 0.7%) of the PCR product for potential BW2513 Δ*dps*
mutants. Primers employed were *dps* F & R. M, Marker, 1 kb GeneRuler (Fermentas); **1-3**, mutant
colony BW25113 Δ*dps* 311 bp; **Δ*dps*::*kan*,** JW0797 (Δ*dps*)::*kan* 1536 bp; **W**, 791 bp wild type.
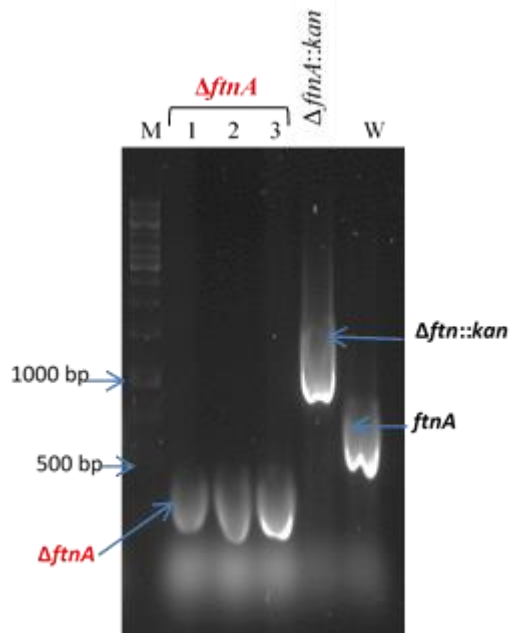
Fig. 3.3 Electrophoretic analysis (agarose 0.7%) of the PCR product for the potential BW25113 Δ*ftnA*
mutants. Primers *ftnA* F & R were employed. **M**, Marker, 1 kb GeneRuler (Fermentas); **1-3**, mutant colony
BW25113 Δ*ftnA* 312 bp; **Δ*ftnA*::*kan***, JW1893 (Δ*ftnA*)::*kan*, 1537 bp; **W**, 781 bp wild type.

3.3 P1 Transduction of *bfr*, *dps* and *ftnA* mutations into the single mutant BW25113 to generate double mutant strains.

Transduction was used to attempt to transfer the mutations of interest from corresponding strains of the KEIO collection (Baba *et al.*, 2006; Table 2.2) into the single mutant strains, BW25113 Δ*ftnA* and Δ*bfr*, to generate double mutants by bacteriophage P1 transductions. The transduction experiments (using BW25113 Δ*ftnA* and Δ*bfr* as recipients and phage from JW0797 (Δ*dps*)::*kan* and JW3298(Δ*bfr*)::*kan* donors) successfully generated Kn^R transductant colonies: BW25113Δ*ftnA*,(Δ*dps*)::*kan*, BW25113Δ*bfr*,(Δ*dps*)::*kan* and BW25113Δ*ftnA*, (Δ*bfr*)::*kan*. These were confirmed by testing their double mutant status using colony PCR. As shown in Fig. 3.4 and 3.5, the amplification products size of (Δ*dps*)::*kan* were the same size as the donor strain JW0797(Δ*dps*)::*kan* (1536 bp) and bigger than the recipient strain that gave a 791 bp *dps* amplification product. The status of the (Δ*bfr*)::*kan* mutations were also confirmed in the BW25113Δ*ftnA*, (Δ*bfr*)::*kan* double mutant (Fig. 3.6) as the PCR product gave the expected size of 1589 bp for (Δ*bfr*)::*kan* and gave the same product size as that of the donor strain, JW3298(Δ*bfr*)::*kan*

.
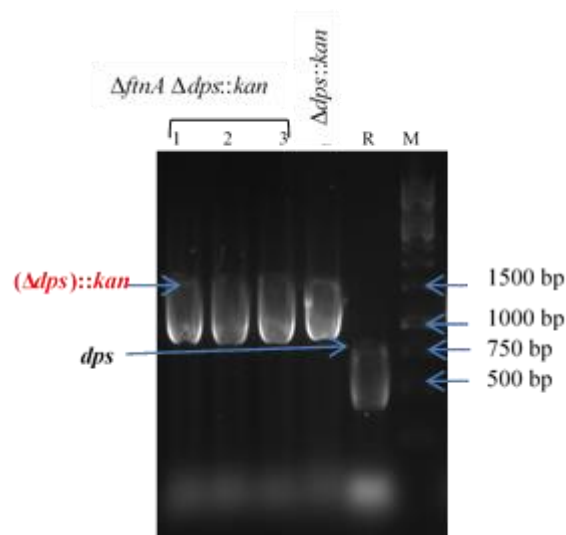
Fig.3.4 Electrophoretic analysis (agarose 0.7%) of the PCR product for potential BW25113 Δ*ftnA* (Δ*dps*)::*kan* mutants. Primers *dps*-F&R primers were employed. **M**, Marker, 1 kb GeneRuler (Fermentas); **1-3**, transductant colonies of BW25113 Δ*ftnA* (Δ*dps*)::*kan*; **Δ*dps*::*kan***, JW0797(Δ*dps*)::*kan* (1536 bp); **R**, *dps* amplification product of the recipient BW25113 Δ*ftnA* (791 bp).
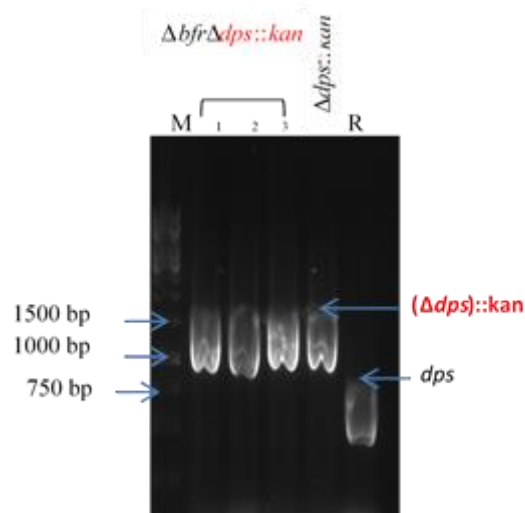
Fig.3.5 Electrophoresis analysis (agarose 0.7%) of the PCR product for the potential BW25113Δ*bfr* (Δ*dps*)::*kan* mutants. Primers *dps*-F&R were employed. **M**, Marker, 1 kb GeneRuler (Fermentas); **1-3**, transductant colonies - BW25113 Δ*bfr* (Δ*dps*)::*kan*; **Δ*dps*::*kan***, JW0797 (Δ*dps*)::*kan* (1536 bp); **R**, *dps* amplification product of the recipient BW25113 Δ*bfr* (791 bp) .
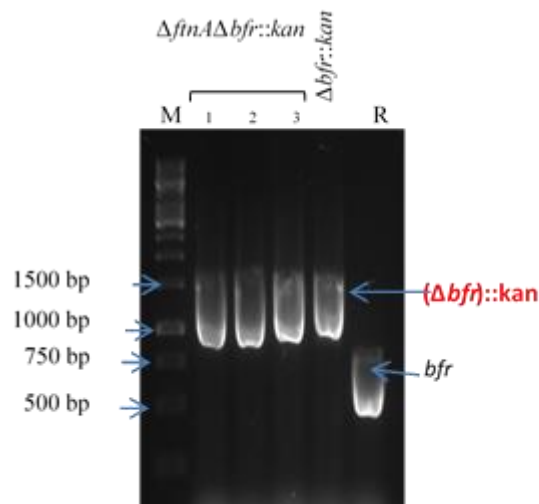
Fig. 3.6 Electrophoretic analysis (agarose 0.7%) of the PCR product for the potential BW25113 Δ*ftnA*, (Δ*bfr*)::*kan* mutants. Primers *bfr*-F&R were employed. **M**, Marker, 1 kb GeneRuler (Fermentas); **1-3**, transductant colonies - BW25113 Δ*ftnA* (Δ*bfr*)::*kan*; **Δ*bfr*::*kan***, JW3298(Δ*bfr*)::*kan* (1589 bp); **R**, *bfr* amplification product of the recipient BW25113 Δ*ftnA* (788 bp).

3.3.1 Analysis of the ΔftnA status of putative ΔftnA (Δdps)::kan transductants

It was also important to confirm that the first mutation was maintained in the double mutants generated by transduction. This was achieved by colony PCR using primers for identifying the status of the first mutation in the putative double mutants. Fig. 3.7 shows that the ΔftnA amplification size of the transductant colony BW25113 ΔftnA (Δdps)::kan was the same as the ΔftnA amplification of the recipient strain, BW25113 ΔftnA (~300 bp); this confirms that the first mutation was maintained. Fig. 3.8 and 3.9 also show that the Δbfr and ΔftnA mutations in BW25113 Δbfr (Δdps)::kan and BW25113 ΔftnA (Δbfr)::kan were also retained, as the PCR product of Δbfr and ΔftnA in these transductant colonies gave the same Δbfr and ΔftnA amplification size product as the recipient strains, BW25113 Δbfr (Δdps)::kan and BW25113 ΔftnA (Δbfr)::kan, respectively.
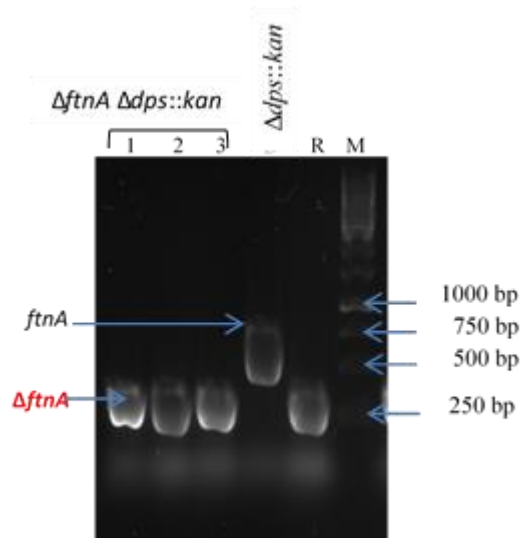
Fig 3.7 Electrophoretic analysis (agarose 0.7%) of the PCR product for the potential BW25113 ΔftnA (Δdps)::kan mutants. Primers *ftnA* F&R were employed. **M**, Marker, 1 kb GeneRuler (Fermentas), **1-3:** transductant colony - BW 25113 ΔftnA (Δdps)::kan (312 bp); **Δdps::kan**, *ftnA* amplification product of the donor JW0797(Δdps)::kan (781bp); **R**, the recipient BW25113 ΔftnA (312 bp).
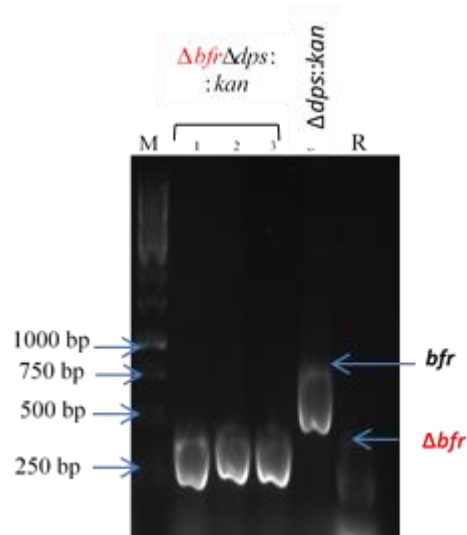
Fig 3.8 Electrophoretic analysis (agarose 0.7%) of the PCR product for the potential BW25113 Δ*bfr* **(Δ*dps*)::*kan* mutant.** Primers *bfr* F&R were employed. **M**, Marker, 1 kb GeneRuler (Fermentas); **1-3,** Δ*bfr* amplification of transductant colony - BW 25113 Δ*bfr* (Δ*dps*)::*kan* (364 bp); **Δ*dps*::*kan***, *bfr* amplification of the JW0797 (Δ*dps*)::*kan* 788 bp; **R**, the recipient BW25113 Δ*bfr*.
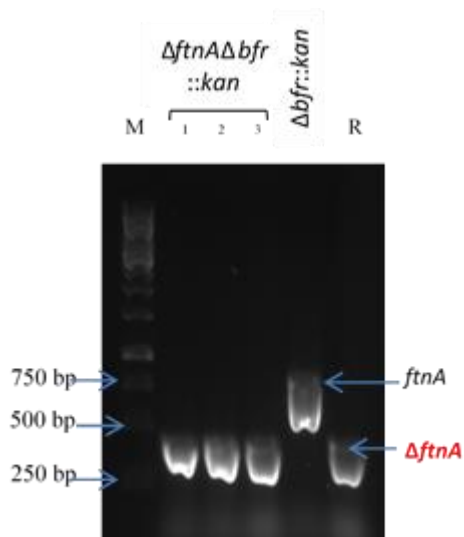
Fig.3.9 Electrophoretic analysis (agarose 0.7%) of the PCR product for the potential BW25113 Δ*ftnA* **(Δ*bfr*)::*kan* mutant.** Primers *ftnA* F&R were employed. **M**, Marker, 1 kb GeneRuler (Fermentas); **1-3,** Δ*ftnA* amplification of transductant colony - BW 25113 Δ*ftnA* (Δ*bfr*)::*kan* (312 bp); **(Δ*bfr*)::*kan***, ftnA amplification of the donor JW3298(Δ*bfr*)::*kan* (781bp), **R**, the recipient BW25113 Δ*ftnA*.

3.4 Removal of kanamycin resistance cassette from ΔftnA (Δdps)::kan mutant

PCR was carried out to confirm the removal of the Kn^R cassette from the double mutant transductants after treatment with plasmid pCP20. Gel electrophoretic analysis (Fig. 3.10 A) shows that the Kn^R cassette has been successfully removed from double mutant giving a PCR product of the expected size (311 bp) for the Δdps mutations, which is smaller than the product obtained for the donor JW0797 (Δdps::kan) of 1536 bp. The ΔftnA status was also confirmed in the double mutant strain BW25113 ΔftnA Δdps. The ftnA-amplification product (Fig. 3.10 B) of the putative ΔftnA Δdps double mutant was the same size as that gained from the recipient BW25113 ΔftnA, used as control. The resulting ΔftnA Δdps double mutant was then used as a recipient strain for transduction with P1 lysate containing transducing phage harbouring Δbfr:: kan to generate triple mutant.
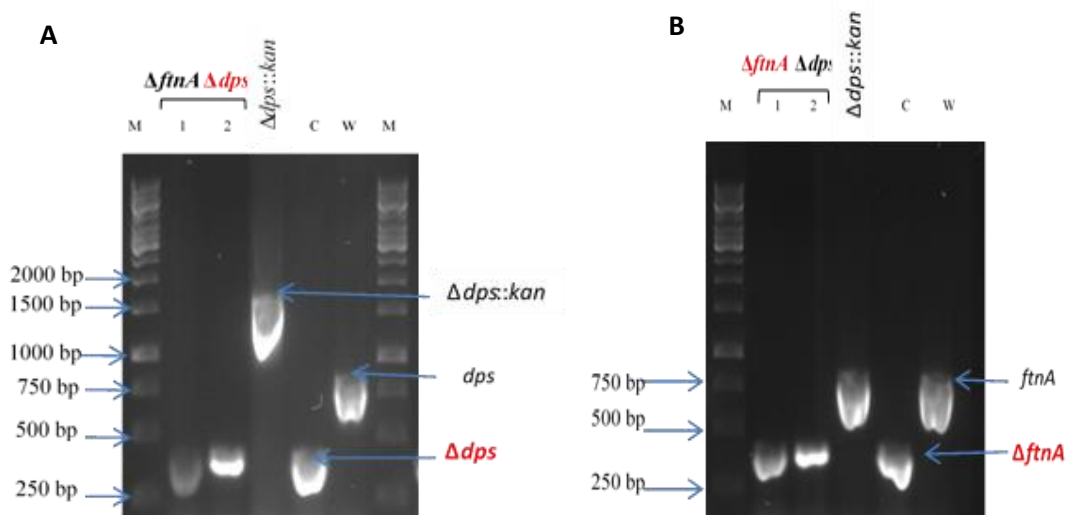
Fig. 3.10 Electrophoretic analysis (0.7 % agarose) A, showing *dps* amplification products of potential BW25113 ΔftnA Δdps mutants. Primers *dps*-F& R were employed. **M**, Marker, 1 kb GeneRuler (Fermentas); **1-2**, potential BW25113 ΔftnA Δdps mutants (311 bp); **Δdps::kan**, donor strain JW0797 Δdps:: kan (1536 bp)*;* **C**, BW25113 Δdps, 311 bp; **W**, wild strain BW25113 (791 bp). **B, showing *ftnA* amplification products of potential BW25113 ΔftnA Δdps mutants**. Primers *ftnA*-F& R were employed. **M**, Marker, 1 kb GeneRuler (Fermentas); **1-2**, potential BW25113 ΔftnA Δdps mutants (312 bp); **Δdps::kan**, donor strain JW0797 Δdps::kan (789 bp); **C**, BW25113 ΔftnA (312 bp); **W**, *ftnA* amplification product of wild type BW25113 (789 bp).

3.5 Generation of the triple mutant strains by combination of single mutant with double mutant using P1 Transduction.

Δ*ftnA* Δ*dps* (Δ*bfr*)::*kan* transductants were constructed by transduction of the (Δ*bfr*)::*kan* mutation into the Δ*ftnA* Δ*dps* double mutant.

3.5.1 Analysis of the *bfr* status of the putative Δ*ftnA* Δ*dps* (Δ*bfr*)::*kan*

The gel electrophoresis analysis (Fig. 3.11) showed that the (Δ*bfr*)::*kan* mutation had been successfully introduced (P1 transduction using lysate that contain transducing phage from the donor strain, (Δ*bfr*)::*kan*) into the double mutant recipient Δ*ftnA* Δ*dps*, as the (Δ*bfr*)::*kan* PCR amplification product size of the potential transductant colonies is the same as that of the donor (1589 bp) and larger than that of the recipient, BW25113 Δ*ftnA* Δ*dps* (*bfr* PCR product, 788 bp).
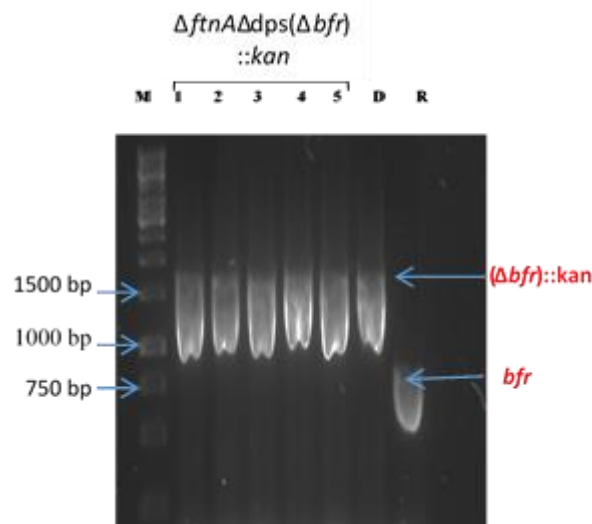
Fig. 3.11 Electrophoretic analysis (0.7 % agarose) showing *bfr*-amplification products of potential BW25113 Δf*tnA* Δ*dps* (Δ*bfr*)::*kan*. Primers *bfr*-F&R were employed. **M**, 1 kb GeneRuler (Fermentas); **1-5**, potential transductant colony - BW25113 (Δf*tnA* Δ*dps* (Δ*bfr*)::*kan*) mutants (1589 bp) ; **D**, donor strain JW3298 (Δ*bfr* ::kan)(1589 bp); **R**, *bfr* amplification product of recipient strain BW25113 Δf*tnA* Δ*dps* (788 bp).

3.5.2 Analysis of the *dps* and *ftnA* status of the putative Δ*ftnA* Δ*dps* (Δ*bfr*)::*kan*

After confirmation transfer of the (Δ*bfr*)::*kan* mutation to generate the triple mutant (Fig. 3.11), it was important to confirm that the Δ*ftnA* and Δ*dps* mutations were retained in the triple mutant. The *dps*- and *ftnA*-amplification products (Fig. 3.12-3.13) of the putative transductants were the same size as those of the recipient BW25113 Δ*ftnA* Δ*dps*. Thus, all five transductants (1-5) had the desired genotype.
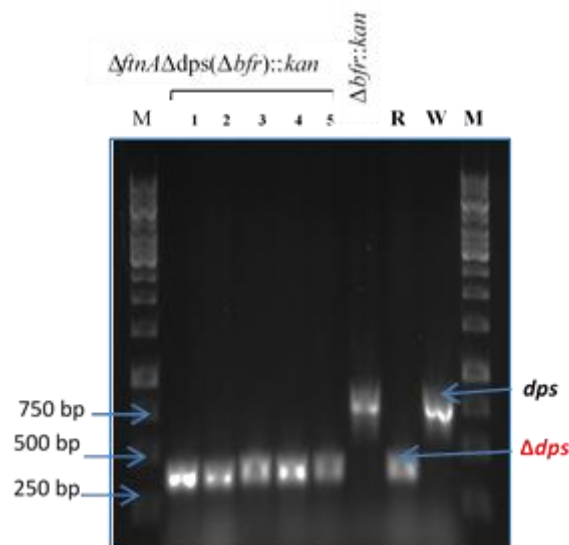
Fig. 3.12 Electrophoretic analysis (0.7 % agarose) showing *dps*-amplification products of potential BW25113 Δ*ftnA* Δ*dps* (Δ*bfr*)::*kan*. Primers *dps*-F&R were employed. **M,** 1 kb GeneRuler (Fermentas); **1-5,** potential transductant colony - BW25113 Δ*ftnA* Δ*dps* (Δ*bfr*)::*kan* (311 bp); **Δ*bfr* ::*kan*** , donor strain JW3298 (Δ*bfr*::*kan*) (791 bp); **R,** recipient strain BW25113 Δ*ftnA* Δ*dps*; **W,** wild type.
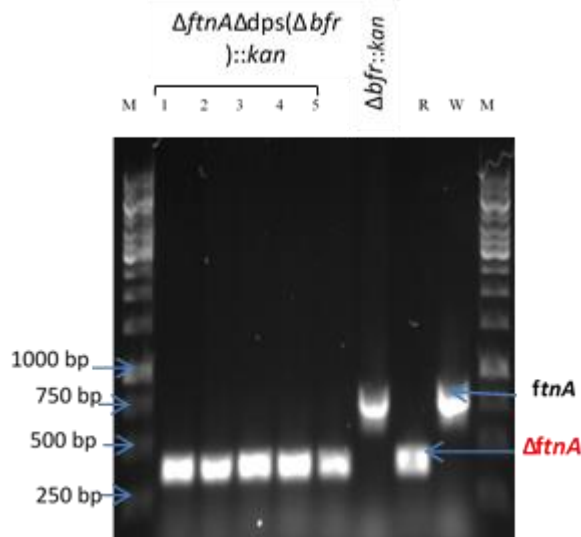
Fig. 3.13 Electrophoretic analysis (0.7 % agarose) showing *ftnA*-amplification products of potential BW25113 Δf*tnA* Δ*dps* (Δ*bfr*)::*kan*. Primers *ftnA*-F&R were employed. M, 1 kb GeneRuler (Fermentas); **1-5,** potential transductant colony - BW25113 Δ*ftnA* Δ*dps* (Δ*bfr*)::*kan*; **Δ*bfr* ::*kan*,** donor strain JW3298 (Δ*bfr* ::*kan*) (789bp); **R,** amplification product from recipient strain BW25113 Δ*ftnA* Δ*dps* (312 bp); **W,** *ftnA* amplification of wild type.

3.6 Removal of kanamycin resistance cassette from Δ*ftnA* Δ*dps* (Δ*bfr*)::*kan*, Δ*ftnA* (Δ*bfr*)::*kan* and Δ*bfr* (Δ*dps*)::*kan* mutants

In order to knockout the kanamycin cassette from the transductants (double and triple mutants), chemically competent cells of each mutant Δ*ftnA* Δ*dps* (Δ*bfr*)::*kan*, Δ*ftnA* (Δ*bfr*)::*kan* and Δ*bfr* (Δ*dps*)::*kan* mutants were prepared and treated with the pCP20 plasmid as described in section 2.10.

3.6.1 Analysis of the *bfr* status of the putative Δ*ftnA* Δ*dps* Δ*bfr*, Δ*ftnA* Δ*bfr*, Δ*bfr* Δ*dps*

PCR was carried out to confirm the removal of kanamycin cassette from double and triple mutant transductants after treatment with pCP20 plasmid. A PCR product for the Δ*bfr* mutation was obtained and was of the expected size (364 bp; Fig. 3.14). Thus, the Kn^R cassette had been successfully removed from each of the double and triple mutants generated by transduction. At the same time, Δ*bfr* status was also confirmed in BW25113 Δ*bfr* Δ*dps* and in BW25113Δ*ftnA* Δ*bfr* double mutants strains (Fig. 3.14).
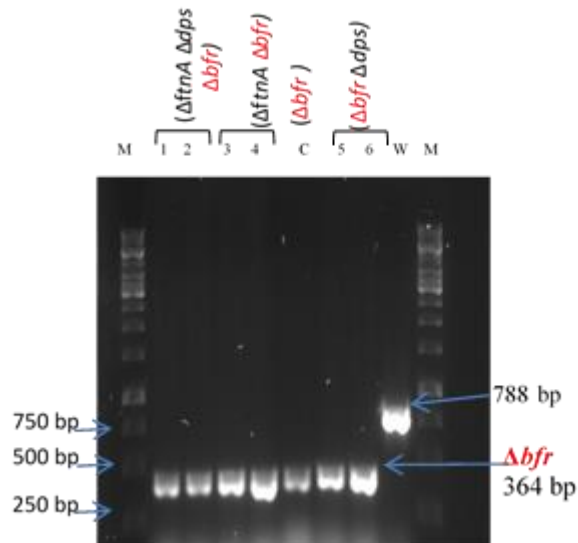
Fig. 3.14 Electrophoretic analysis (0.7 % agarose) showing *bfr*-amplification products of potential BW25113 Δf*tnA* Δ*dps* Δ*bfr*, BW25113 Δ*ftnA* Δ*bfr* and BW25113 Δ*bfr* Δ*dps* mutants. Primers *bfr*-F & R were employed. **M,** 1 kb GeneRuler (Fermentas); **1-6,** Δ*bfr* amplification product (**1-2,** BW25113 Δ*ftnA* Δ*dps* Δ*bfr*; **3-4,** BW25113 Δ*ftnA* Δ*bfr*; **5-6,** BW25113 Δ*bfr* Δ*dps* mutants) (364 bp); **C,** BW25113 Δ*bfr*; **W,** *bfr* amplification product from wild strain BW25113 (788 bp).

3.6.2 Analysis of the *ftnA* status of the putative Δ*ftnA* Δ*dps* Δ*bfr* and Δ*ftnA* Δ*bfr* mutants

The figure below (Fig. 3.15) shows that the Δ*ftnA* status was confirmed in both the BW25113 Δ*ftnA* Δ*dps* Δ*bfr* triple mutant strain and BW25113 Δ*ftnA* Δ*bfr* double mutant strain. These two strains both gave the expected PCR product (312 bp) which is the same size as that of the control, BW25113 Δ*ftnA*.
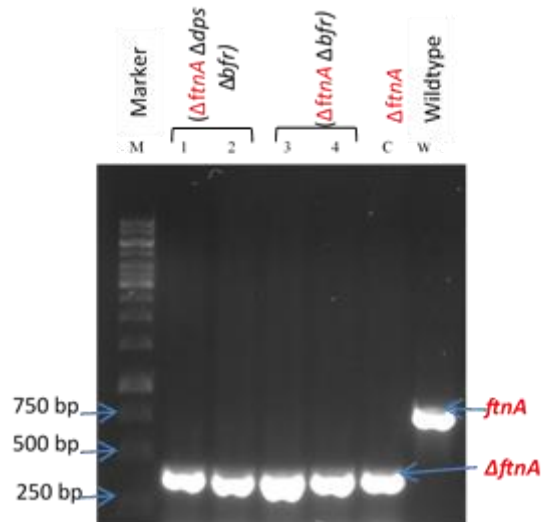
Fig. 3.15 Electrophoretic analysis (0.7% agarose) showing *ftn*-amplification products of potential BW25113 Δ*ftnA* Δ*dps* Δ*bfr*, BW25113 Δ*ftnA* Δ*bfr* mutants. Primers *ftnA*- F & R were employed. **M,** 1 kb GeneRuler (Fermentas); **1-4,** Δ*ftnA* amplification product of (**1-2,** BW25113 Δ*ftnA* Δ*dps* Δ*bfr*; **3-4,** BW25113 Δ*ftnA* Δ*bfr* mutants) (312 bp); **C,** BW25113 Δ*ftnA* (312 bp); **W,** *ftnA* amplification product from wild strain BW25113 (789 bp).

3.6.3 Analysis of the *dps* status of the putative Δ*ftnA* Δ*dps* Δ*bfr* and Δ*bfr* Δ*dps*

Fig. 3.16 shows the successful removal of the Kn^R cassette from the BW25113 Δ*bfr* (Δ*dps*)::*kan* transductant which is clear as the Δ*dps* amplification product size of the potential BW25113 Δ*bfr* Δ*dps* double mutant strain is the same as BW25113 Δ*dps*, at 311 bp. This is also indicated from the difference in size with respect to the wild type amplification product (791 bp). In addition, the Δ*dps* status was also confirmed in BW25113 Δ*ftnA* Δ*dps* Δ*bfr* triple mutant strain.
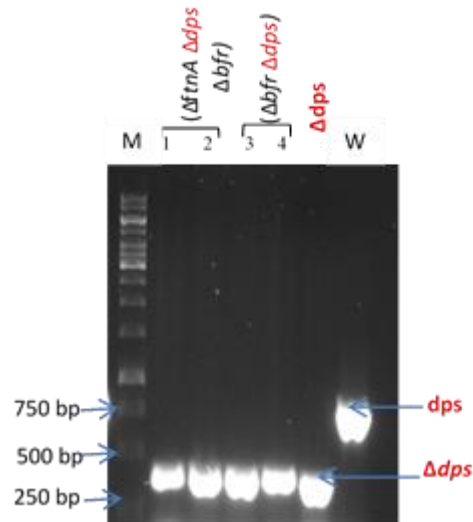
Fig.3.16 Electrophoretic analysis (0.7 % agarose) showing *dps*-amplification products of potential BW25113 Δ*ftnA* Δ*dps* Δ*bfr*, BW25113 Δ*bfr* Δ*dps* mutants. Primers *dps*-F&R were employed. **M,** 1 kb GeneRuler (Fermentas); **1-4,** Δ*dps* amplification product of (**1-2,** Δ*ftnA* Δ*dps* Δ*bfr*, **3-4,** Δ*bfr* Δ*dps* mutants) (311 bp); **C,** BW25113 Δ*dps*; **W,** *dps* amplification product from wild strain BW25113 (791 bp).

3.7 Phenotypic confirmation of knockout by Western blotting

After the confirmation of the genotypes of the P1 transductants by PCR, Western blotting was done to additionally confirm the status of each mutant to ensure sure that the resulting strains were phenotypically correct (FtnA$^{+/-}$ / Bfr$^{+/-}$).

3.7.1 Western blot analysis of FtnA status

To further confirm the *ftnA* status of relevant double and triple mutant strains, anti-FtnA western blotting as performed. The strains constructed by P1 transduction and Kn^R cassette removal, were grown in LB at 37 ˚C, 250 rpm. After incubation overnight, whole-cell extracts were subjected to SDS-PAGE followed by western blotting and anti-FtnA staining. From the figure below (3.17), western blot analysis confirmed that the FtnA protein is absent in the Δ*ftnA* Δ*dps*, Δ*ftnA* Δ*bfr* double and Δ*ftnA* Δ*dps* Δ*bfr* triple mutants. However, FtnA protein is present in the wild type, used as control. From this result the status of *ftnA* was confirmed in each mutant.
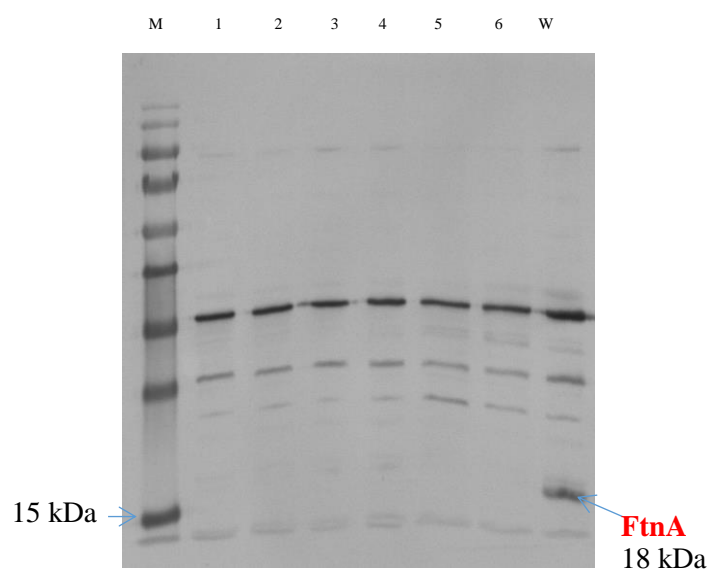
Fig.3.17 Western blot analysis of FtnA status. Whole-cell extracts were subjected to SDS-PAGE followed by western blotting and anti-FtnA staining. **Lane M,** Page Ruler pre-stained protein Ladder; **Lane W,** wild type BW25113; **Lane 1 and 2,** Δ*ftnA* Δ*dps* double mutants; **Lane 3 and 4,** Δ*ftnA* Δ*dps* Δ*bfr* triple mutant; **Lane 5 and 6,** Δ*ftnA* Δ*bfr* double mutant.

3.7.2 Western blot analysis of Bfr status

Western blot analysis using anti-Bfr staining was conducted for both double and triple mutant strains to confirm the deletion of *bfr* gene from the constructed mutants. Whole-cell extracts of the overnight culture of the mutant strains in LB were subjected to SDS-PAGE followed by western blotting and anti-Bfr staining. The figure below (3.18) shows that the Bfr protein is absent in the Δ*ftnA* Δ*bfr*, Δ*bfr* Δ*dps* double and Δ*ftnA* Δ*dps* Δ*bfr* triple mutants, although the wild type and Δ*ftnA* Δ*dps* double mutant controls possess Bfr protein. This confirms the *bfr* status of each mutants.
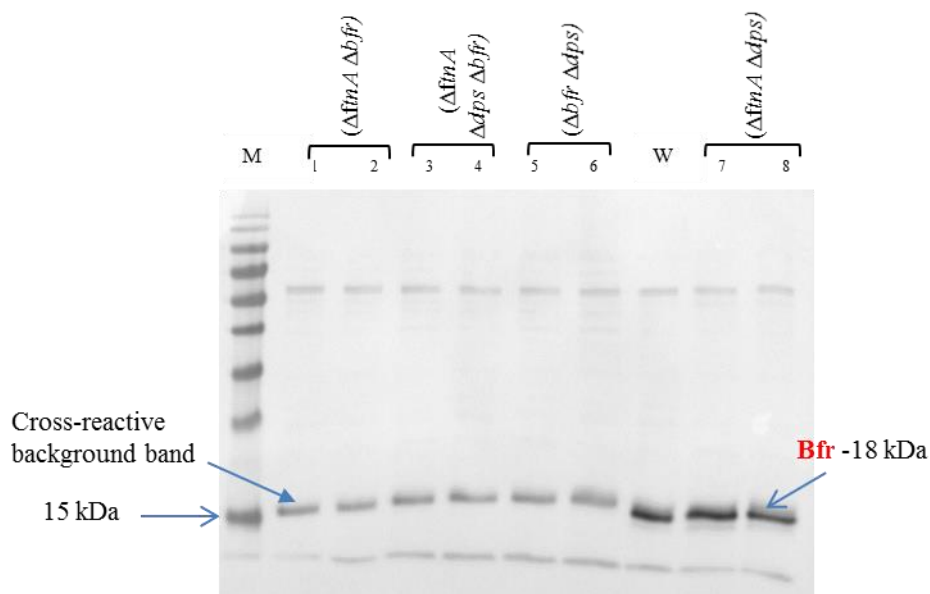
Fig.3.18 Western blot analysis of Bfr status. Whole-cell extracts were subjected to SDS-PAGE followed by western blotting and anti-Bfr staining. **Lane M,** Page Ruler pre-stained protein Ladder; **Lane W,** wild type BW25113; **Lane 1 and 2,** Δ*ftnA* Δ*bfr* double mutants; **Lane 3 and 4,** Δ*ftnA* Δ*dps* Δ*bfr* triple mutant; **Lane 5 and 6** Δ*bfr* Δ*dps* double mutant; **Lane 7 and 8,** Δ*ftnA* Δ*dps* double mutant.

The Dps status of the constructed mutant strains was not performed in this chapter, because the polyclonal antibodies for Dps was not available until a later stage of the PhD. However, the Dps phenotypic status was investigated and confirmed later in chapter 6 (see section 6.11).

3.8 Hydrogen peroxide sensitivity test

3.8.1 H_2O_2 sensitivity test on wild type, and Δ*dps* and triple mutants on L-agar plates

Dps is known to confer resistance to the combined toxic effects of iron and peroxides. Mutants lacking Dps possess a reduced capacity to withstand challenge by hydrogen peroxide (Almiron *et al.,* 1992; Choi *et al.,* 2000). This phenotype was tested in the *dps* mutants generated here, by comparing growth of three strains: the parent (wild type) and the Δ*dps* and triple mutant strains. This was achieved by applying serial dilutions of overnight cultures to rich agar plates containing various concentrations of H_2O_2. No effect was seen at 100-400 µM H_2O_2, but the growth of the Δ*dps* and triple mutants was clearly

decreased in the presence of 600 µM of H_2O_2 with respect to the wild type, which was not affected (Fig. 3.19).

The experiment was repeated as above with monitoring the growth on plates (L-agar with and without 600 µM of H_2O_2) over time. Growth of all strains first appeared after 5 h incubation on L-agar without H_2O_2, but on the 600 µM H_2O_2 plate no growth was seen at this time. After 9 h incubation, growth was clear for the wild type in the presence of 600 µM H_2O_2 (for the x1, x10 and x100 dilutions), but the Δ*dps* and triple mutants only produced growth for the x1 dilution. After 16 h incubation, the Δ*dps* and triple mutants continued to exhibit reduced growth on H_2O_2 with respect to the wildtype, with the single mutant showing slightly greater sensitivity than the triple mutant (Fig. 3.19). This phenotypic characteristic of the *dps* mutants matches the role of the Dps protein in survival under oxidative stress.
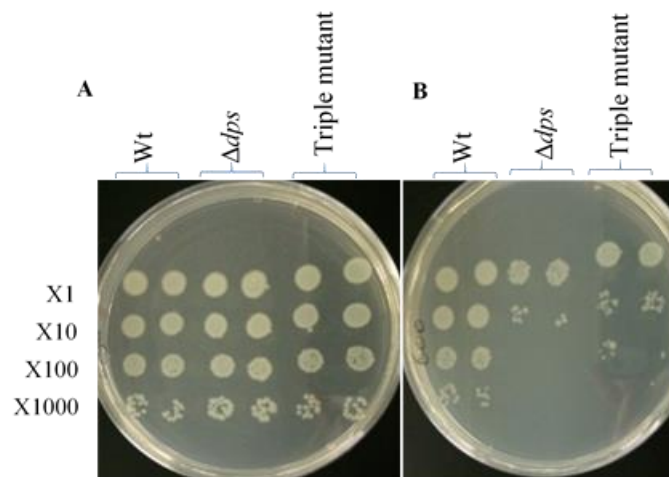
Figure 3.19 Sensitivity of the wild type, BW25113 Δ*dps* and BW25113 Δ*ftnA* Δ*dps* Δ*bfr* mutant strains to oxidative stress on LA with and without 600 µM H_2O_2. Bacterial suspension of 0.01 OD_{600} (from an overnight culture) indicated as x1 was diluted x10 , x100 and x1000 and 5 µL of each suspension were spot inoculated on LA plates with and without hydrogen peroxide, plates were then incubated overnight at 37 °C (Repeated once). **A**, the growth on LA; **B**, the growth on LA with 600 µM H_2O_2.

3.8.2 Effect of *dps* mutation on growth of *E. coli* in liquid medium under redox stress.

3.8.2.1 Effect of dps mutation on growth of *E. coli* in LB under redox stress.

The redox stress sensitivity of the *dps* mutants was further explored by monitoring growth with/without peroxide using a Bioscreen apparatus. The results (Fig. 3. 20 B) show that the growth of the Δdps and $\Delta ftnA$ Δdps Δbfr mutants was impaired in the presence of H_2O_2. H_2O_2 extended the lag phase of both mutants (by 7 h for Δdps and 3.5 h for the triple mutant from the wild type) particularly the Δdps mutant. This result is surprising because it was expected that the triple mutant would be more affected than the Δdps single mutant by hydrogen peroxide, due to its lack of iron-storage capacity which would be anticipated to result in raised levels of free iron participating in redox stress. However, this result was reproducible (twice) and the differences were significant ($P<0.05$) for Δdps and $\Delta ftnA$ Δdps Δbfr mutants with respect to the parent and also for Δdps with respect to the triple mutant, at 690 min of growth, as determined by Student's T test.

During growth in LB without H_2O_2, a slight growth difference was seen for the Δdps mutant with respect to the parent and $\Delta ftnA$ Δdps Δbfr mutant, and also with respect to all of the other iron-storage mutants (Fig. 3.20 A, Fig. 3.21 A-B). This modest growth defect was reproduced (twice) and was significant ($P<0.05$) at 810 min of the growth as determined by Student's T test and would thus appear valid.
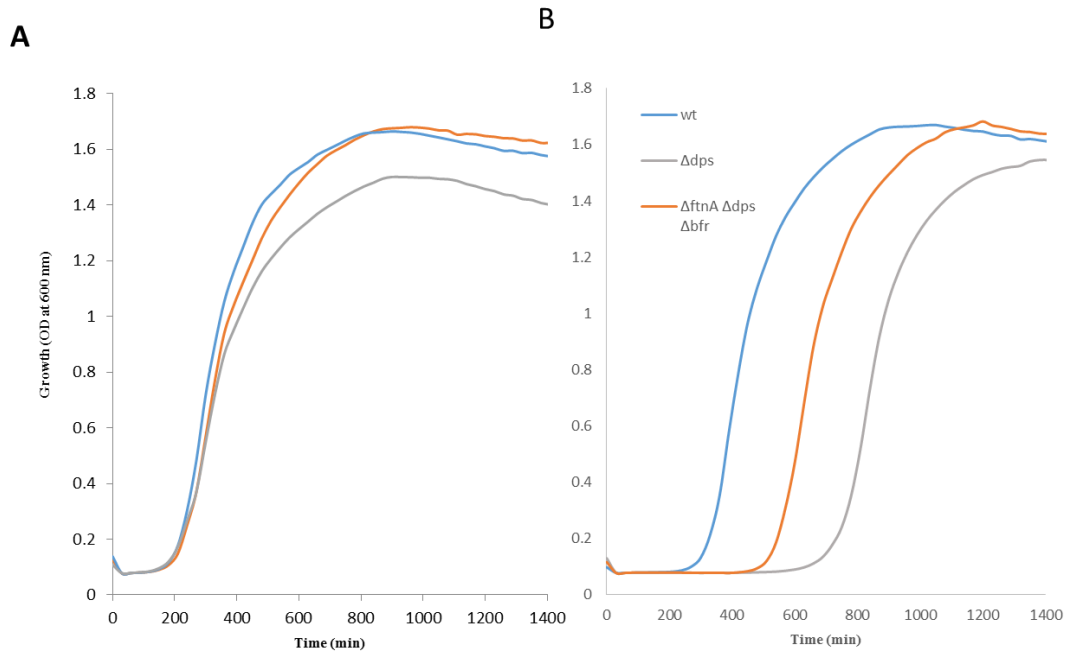
Figure 3.20 Growth curves of BW25113, BW25113 Δ*dps* and BW25113Δ*ftnA* Δ*dps* Δ*bfr* in LB with and without 600 μM H$_2$O$_2$. A, in LB; **B,** in LB with H$_2$O$_2$ in triplicate (Repeated once) at 37 ℃ using a Bioscreen apparatus.

.
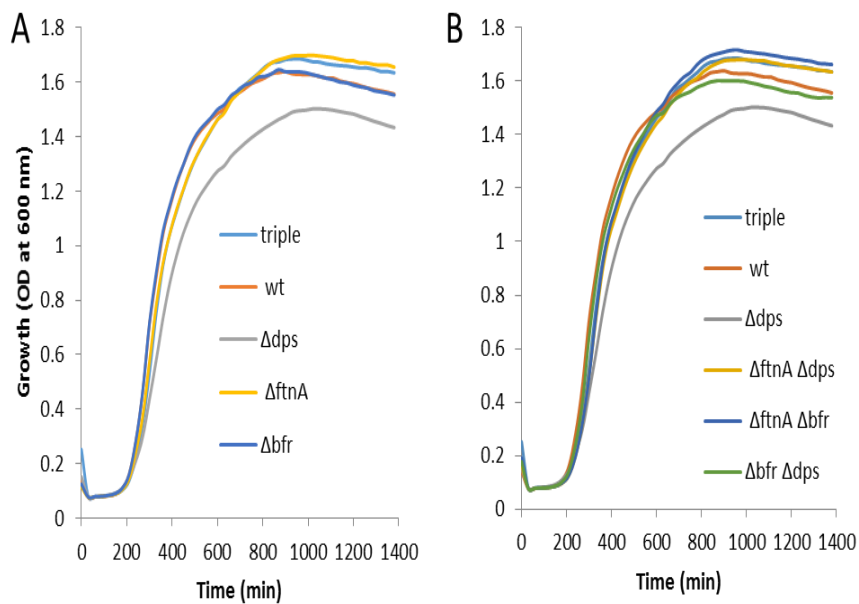
Figure 3.21 Growth curves of BW25113, and single, double and triple mutants strains in LB. A, wt, single mutants and triple mutant strains; **B,** wt, Δ*dps*, double mutants and triple mutant strains in LB in triplicate (Repeated once) at 37 ℃ using a Bioscreen apparatus..

The reason for the reduced peroxide sensitivity of the triple mutant with respect to the Δdps strain was explored by examining the sensitivity of double and single mutants to H_2O_2 (Fig. 3.22A & B). Neither the Δbfr nor $\Delta ftnA$ single mutants, nor the $\Delta ftnA$ Δbfr double mutant, exhibited an obvious phenotype with 600 μM H_2O_2 as their growth was approximately the same as wild type. This is consistent with previous work (Abdul-Tehrani *et al.,* 1999; Keyer and Imlay, 1996) showing that sensitivity to H_2O_2 is not increased by a lack of FtnA and/or Bfr. However, the lag phase of the Δdps and triple mutants was again clearly extended (by ~7 and ~3.5 h, respectively) in the presence of H_2O_2, as was seen above (Fig. 3.20 B). In addition, the growth of the $\Delta ftnA$ Δdps mutant was approximately the same as that of the Δdps single mutant (the difference was significant, $P<0.05$, at 870 min of growth with respect to the parent strain) (Fig. 3.22 A). Thus, loss of *ftnA* does not affect the sensitivity of the *dps* mutant to peroxide. However, combining the Δbfr mutation with the Δdps mutation resulted in an increased peroxide resistance with respect to the *dps* single mutant but remained significantly peroxide sensitive in comparison with the parent strain ($P<0.05$). The results thus indicate that the presence of *bfr* enhances sensitivity to peroxides in L broth when *dps* is nullified. This effect has not been reported previously and suggests that Bfr might act as an intracellular source of Fe^{2+} that aggravates hydroxyl radical production by Fenton reaction in the absence of Dps. Thus, a role for Dps may be to protect the cell against Bfr-enhanced peroxide stress. FtnA, unlike Bfr, seems to have no effect on Dps-dependent H_2O_2 resistance, yet FtnA stores a higher proportion of cellular iron (Abdul-Tehrani *et al.,* 1999). This suggests that the iron held by Bfr may be more labile than that sequestered within FtnA and so more prone to participation in peroxide stress. If so, this would point towards a clear physiological distinction between these two forms of iron store in relation to their cellular availability and potential toxicity.
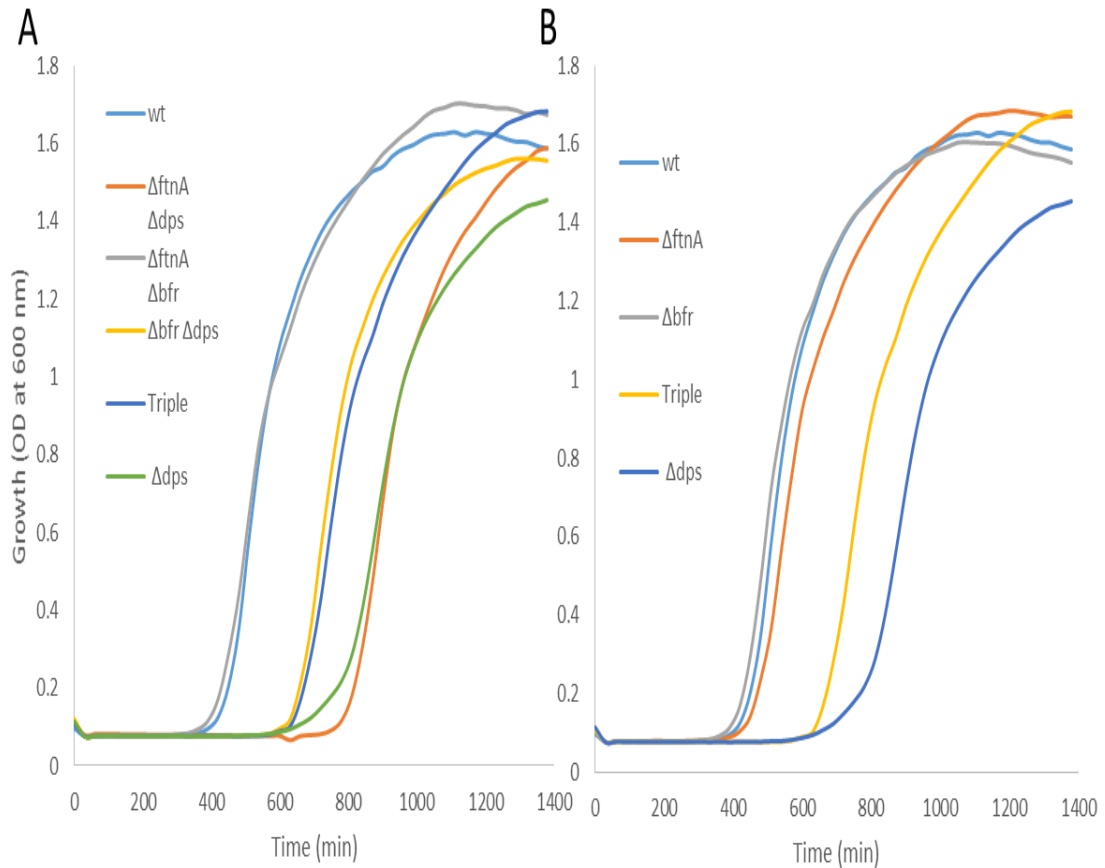
Figure 3.22 Growth curve of wt, and single, double and triple mutant strains under redox stress. A, wt, Δ*dps*, Δ*ftnA* Δ*dps* Δ*bfr* and double mutants; **B.** wild type, single and triple mutants strains, both A and B in LB with addition of 600 μM hydrogen peroxide in triplicate. Repeated once, at 37 °C using a Bioscreen apparatus.

3.8.2.2 Effect of dps mutation on growth of *E. coli* in LB under iron and redox stress.

Since the above suggests a role for Bfr in facilitating redox stress in a *dps* mutant, it appeared likely that iron stored within Bfr would be a requirement for this effect to be exhibited. Therefore, in order to determine the effect of iron status on redox stress, the above experiment was repeated one time using inocula grown with the iron chelator, 240 μM DTPA, to reduce cellular iron stores as far as possible. The concentration of DTPA employed was selected from trial experiments as the highest concentration that allowed good growth (two fold dilutions of DTPA from 5-480 μM). The results showed that presence of chelator in the pre-culture made no discernible difference to subsequent

growth in comparison with that for L-broth pre-cultures generated without chelator, although in both cases the growth of the Δ*dps* strain was slightly lower than the Δ*bfr* Δ*dps* strain and the wild type, which grew similarly. The presence of 240 µM DTPA in the post-cultures resulted in reduced growth in all cases (~0.2 OD unit lower final growth; Fig. 3.23 A).
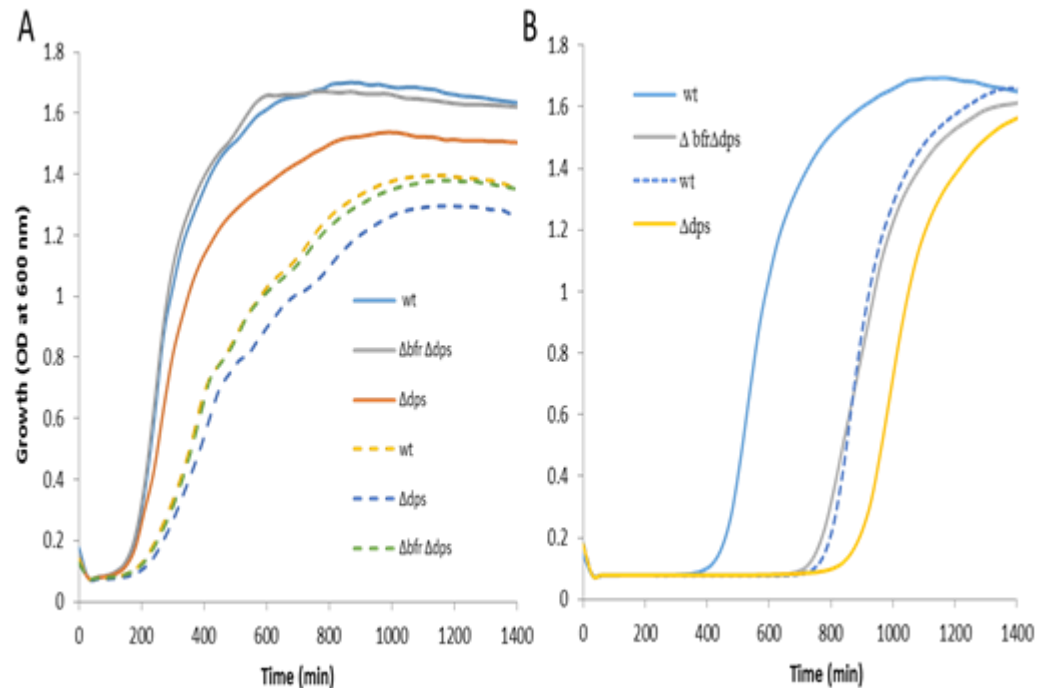
Figure 3.23 Growth curve of wt, and Δ*dps* and Δ*bfr*Δ*dps* mutants strains in LB with and without DTPA in the presence or absence of 600 µM H_2O_2. **A,** solid line, in LB without DTPA; dashed line, in LB with the addition of 240 µM DTPA in triplicate. Pre-culture were grown with the iron chelator, 240 µM DTPA. **B,** solid line, in LB with 600 µM H_2O_2 in triplicate (pre-culture in LB); dashed line, representative growth curve of wt in LB with 600 µM H_2O_2 (pre-culture in LB with addition of 240 µM DTPA).

The inclusion of 600 µM H_2O_2, along with 240 µM DTPA, in the post-culture resulted in enhanced toxicity with respect to conditions with 600 µM H_2O_2 alone (Fig. 3.23 B). The lag phase of the wild type was extended by ~5 h, whereas the Δ*dps* and Δ*bfr* Δ*dps* strains failed to grow. This suggests that DTPA enhances H_2O_2 toxicity, possibly by influencing iron availability.

3.8.2.3 Effect of dps mutation on growth of *E. coli* in minimal medium under iron and redox stress.

Since DTPA failed to have the desired effect in L broth, the experiment was repeated using minimal medium (instead of LB) to more readily control the iron concentration in the medium. Initially, an experiment was performed (one time) using M9 with 600 µM H_2O_2. However, the *dps* mutants failed to grow with this concentration (not shown) and so an experiment was performed to gauge the MIC of the three strains against 30, 75, 150, 300, 600 µM H_2O_2 in M9 medium. Both the Δ*dps* and triple mutant weakly grew in 150 µM H_2O_2 and failed to grow in 300 µM H_2O_2, however the wild type was able to grow at these concentrations. From the results, a concentration of 100 µM hydrogen peroxide was selected for future work since all three strains grew reasonably at this concentration.

Pre-cultures were grown in M9 medium with or without 20 µM ferric citrate to generate pre-cultures with low and high iron stores. Subsequently, growth was monitored in post-cultures with 100 µM hydrogen peroxide with/without 20 µM ferric citrate. Results show that the Δ*bfr* Δ*dps* and Δ*dps* mutants had lower growth than the wild type for both types of pre-culture (Fig. 3.24-3.25). However, in contrast to the result obtained in LB, the double mutant exhibited poorer growth than the single mutant. The reason for this difference in result between rich and defined medium is unclear and requires further investigation. However, the data are consistent with a role for Bfr in combating H_2O_2 toxicity in the absence of Dps in minimal medium, although in rich medium Bfr appears to enhance such toxicity. In the presence of peroxide the lag phase of the wild type was extended only by ~1.6 h relative to its growth in minimal medium supplemented with iron (the same condition in pre-culture) (Fig. 3.24). The wild type was slightly more peroxide sensitive when the inoculum was grown in M9 medium without iron; although the difference was significant but it was very slight in comparison to Δ*bfr* Δ*dps* and Δ*dps* mutants which were more significantly different in respect to the wild type. However, this is opposite to the far more substantial effect seen for the mutants (Fig. 3.25). Indeed, high iron in the inoculum is well reported to raise peroxide sensitivity (Abdul-Tehrani *et al.,* 1999). And the observed decreased sensitivity for the wild type pre-cultured in iron is thus unexpected, but the effect is modest.
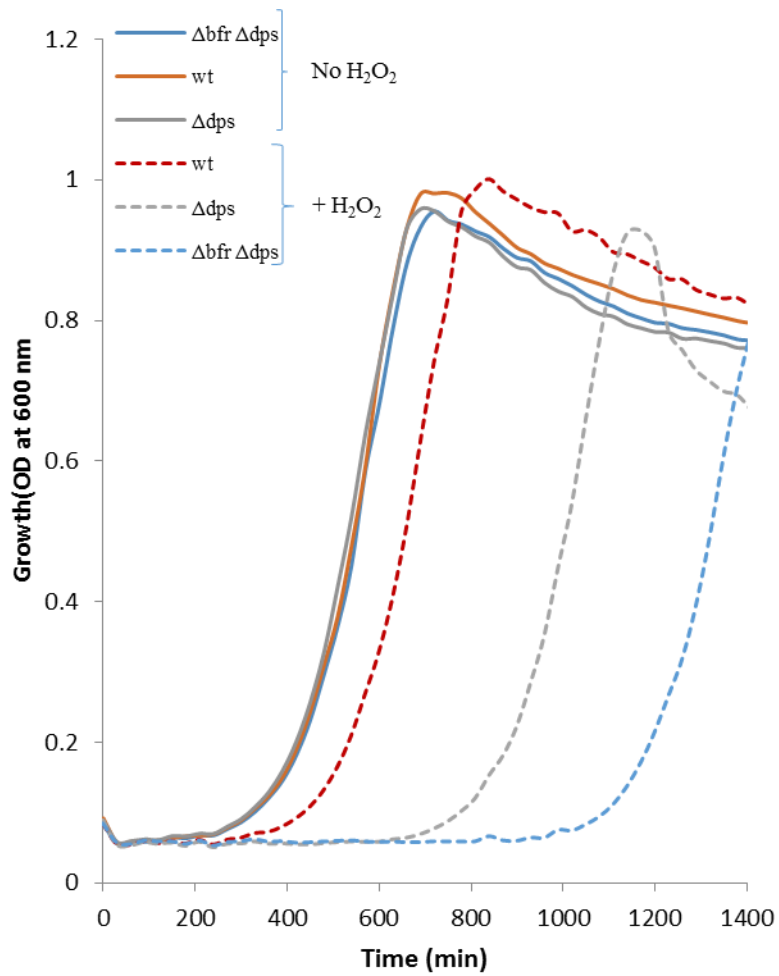
Figure 3.24 Growth curve of wt, and the Δ*dps* and Δ*bfr* Δ*dps* mutants strains in M9 medium supplemented with 20 μM ferric citrate with and without 100 μM H₂O₂. Pre-cultures were grown in M9 medium with 20 μM iron citrate. Results are an average of triplicate experiments. Solid line, without 100 μM H₂O₂. Dashed line, in the presence of 100 μM H₂O₂.
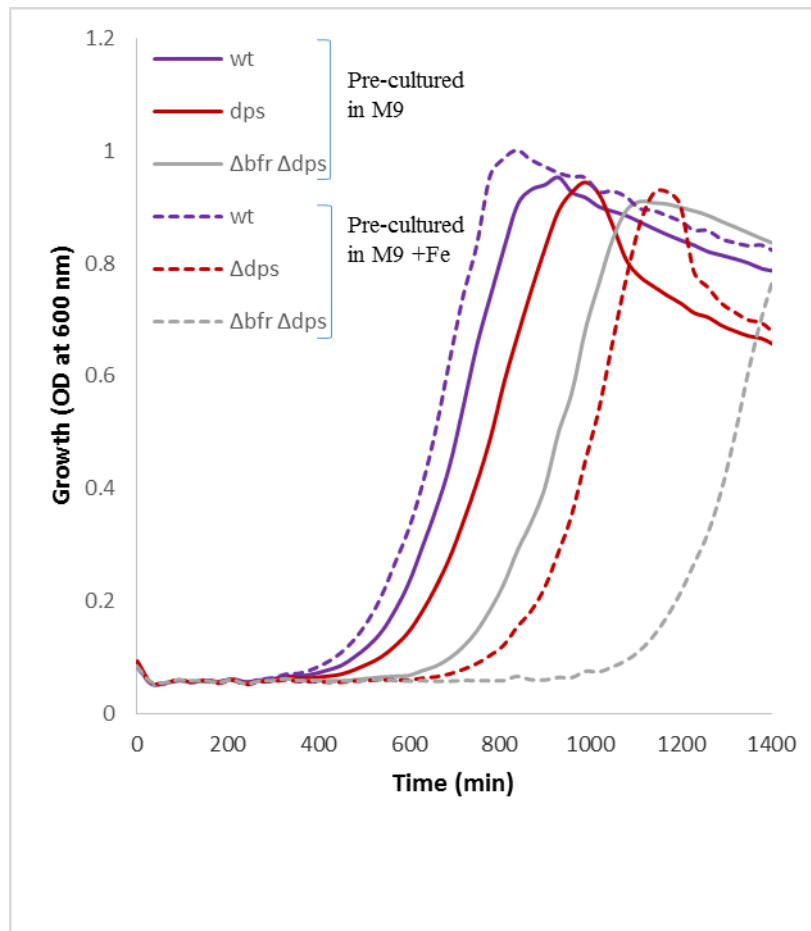
Figure 3.25 Effect of iron in pre-culture on subsequent peroxide sensitivity. Growth of the wt, and Δ*dps* and Δ*bfr* Δ*dps* mutants strains in M9 medium supplemented with iron in the presence of 100 μM H_2O_2. Data is the average of triplicate growths. Solid line, pre-cultures grown in M9 medium. Dashed line, pre-cultures grown in M9 medium with 20 μM ferric citrate.

Iron in the inoculum had little impact on the subsequent growth of the wt in the presence of peroxide when pre-culture with iron (Fig. 3.25). However, there was a dramatic effect on the single and double mutants as both exhibited far greater H_2O_2-induced lag phases (~5 h) when pre-cultured with iron, the differences was significant (at 1020 min) ($P<0.05$) with respect to the wild type under this condition. This is likely due to the combined effects of increase in free intracellular iron caused by iron supplementation of the pre-cultures and failure to appropriately sequester the increased free levels due to iron-storage deficiency (lack of Dps and Bfr) which would enhance peroxide mediated redox stress. No growth differences were observed for the strains in M9 medium without peroxide (Fig. 3.24).

The effect of high intracellular iron content in the presence of hydrogen peroxide on bacterial growth was consistence with the previous work of Abdul-Tehrani *et al*. (1999) which showed that the sensitivity of *E. coli* was increased in response to H_2O_2 when intracellular iron contents were high. This observation is also supported by Repine *et al*. (1981) who demonstrated that decreasing the intracellular iron content of *Staphylococcus aureus* decreases sensitivity to hydrogen peroxide.

Interestingly, neither the Δdps nor Δbfr Δdps mutant were able to grow in M9 medium combined with 100 µM when 20 µM ferric citrate was not also included in the medium, and only the wild type was able to grow in this condition. This is likely caused by enhanced H_2O_2 toxicity due to the absence of iron, since iron is well known to decompose hydrogen peroxide (Halliwell and Gutteridge 1986).

3.9 Impaired growth of the single mutants under iron-restriction conditions

In order to determine whether the iron-storage mutants display any defect in growth under iron restriction, as observed previously for *ftnA* mutants (Abdul-Tehrani *et al.,* 1999), their growth was compared with that of the wildtype under conditions of iron chelation (with DTPA). The results show that the growth of the *dps* mutant was comparable to that the wild type. This result reflects the low iron-storage capacity of Dps and its primary purpose in acting as an iron detoxifying protein. This perceived role matches that suggested in the literature and the absence of an iron storage function for Dps in *E. coli* (Choi *et al*., 2000; Velayudhan *et al*., 2007; Chiancone *et al*., 2004). The growth of *ftnA* and *bfr* mutant strains was impaired in the presence of DTPA (Fig. 2.26B & C), however, the *ftnA* mutant was more sensitive to iron restriction than the *bfr* mutant (80% growth for the *ftnA* mutant with respect to the wildtype at 23 h cf. ~90% for the *bfr* mutant; *P* = 0.02 and 0.03, respectively). This observation is consistent with the results of Abdul-Tehrani *et al*. (1999) who showed that FtnA supports low iron growth. However, Abdul-Tehrani *et al*. (1999) showed no role for Bfr in supporting low iron growth in *E. coli* K-12, although it should be noted that Bfr is the major iron storage protein in *Salmonella enterica* serovar Typhimurium (Velayudhan *et al*., 2007) since *bfr* mutation highly reduced the total cellular iron content, although not as much as *ftnA* mutation. This discrepancy suggests that Bfr is more highly expresses in *Salmonella* than *E. coli* allowing Bfr to contribute more so to iron storage. The Bfr of *Neiserria gonorrhoeae* provide iron under condition of iron restriction (Chen and Morse, 1999). Others have also

shown roles for Bfr and FtnA in supporting iron restricted growth in bacteria (e.g. Wai *et al*., 1996; Abdul-Tehrani *et al*., 1999; Ratnayake *et al*., 2000). The differences seen here for the effect of the *bfr* mutation on iron restricted growth likely reflects strain differences in the relative degree of *bfr* expression.

It should be noted that no significant growth difference was observed when iron (16 μM ferric citrate) was included in the medium or when DTPA was excluded (data not shown).

A. Δ*dps*

B. Δ*bfr*
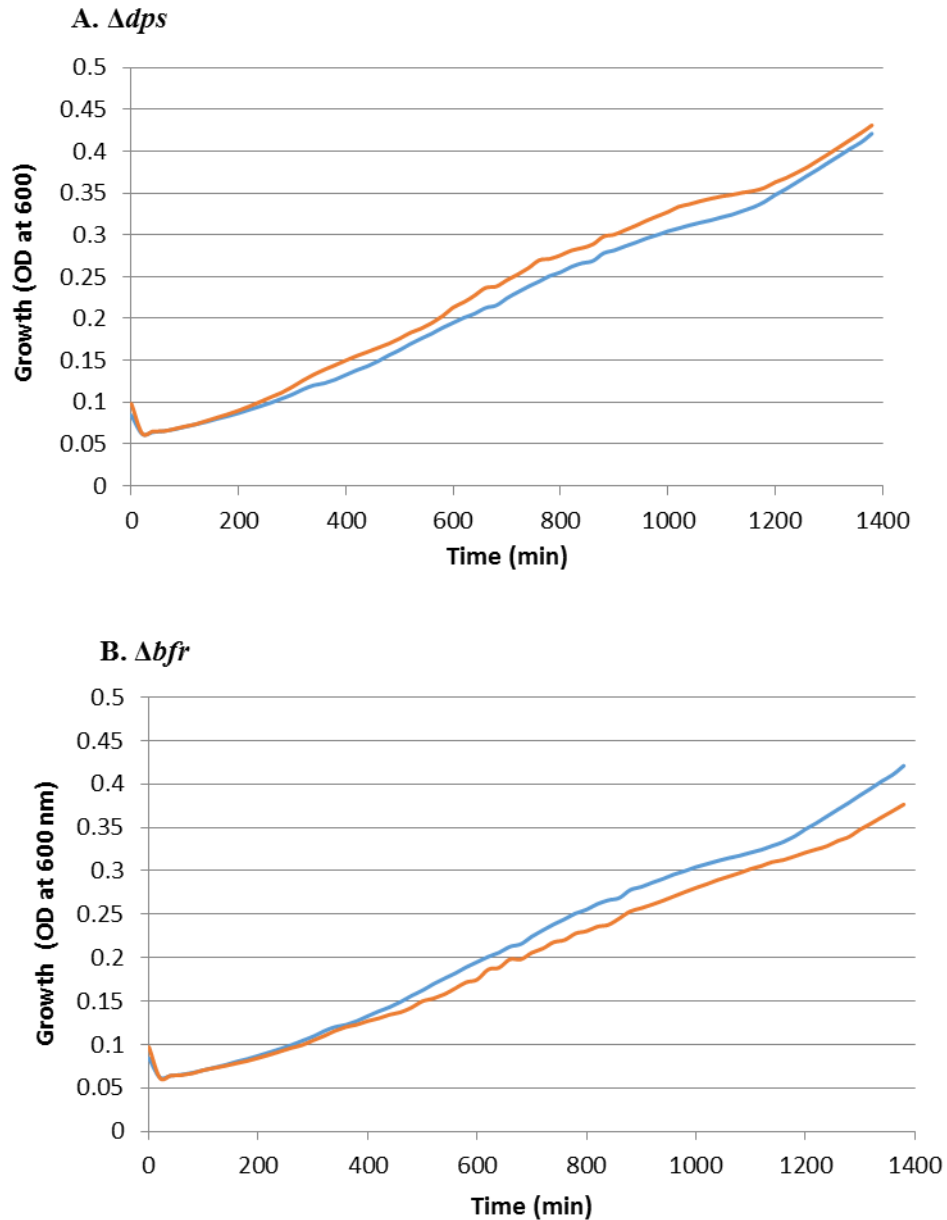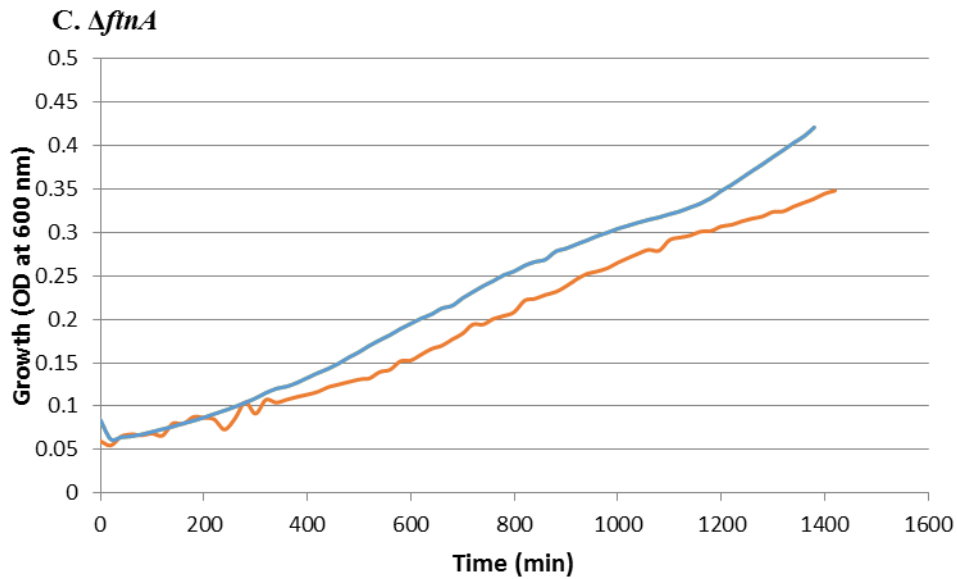
Figure 3.26 Impaired growth of the single mutants under iron-restriction conditions. Growth of the wild type (blue line), and **A**, Δ*dps*; **B**, Δ*bfr* and; **C,** Δ*ftnA* single mutants strains (orange line) in M9 medium in the presence of 0.5 µM DTPA. Repeated once. Pre-cultures grown in M9 medium with 16 µM ferric citrate.

3.9.1 Combination of iron-storage gene mutations results in reduced growth under iron restriction

The effect of combining the iron-storage gene mutations, to produce double mutant strains, was also tested in iron-restricted minimal medium (Fig. 3.27). The double mutant strains all showed growth impairment in comparison with the wild type in minimal medium with DTPA, with the growth of *ftnA bfr* mutant being weaker (69% that of the wildtype at 23 h; *P*= 0.002) than that of the *ftnA dps* and *bfr dps* mutants (81 and 86% that of the wildtype, respectively, at 23 h; *P*= 0.01 and 0.02). This result matches that obtained for the single mutants which indicated that the *ftnA* mutation had the greatest impact on iron-restricted growth, followed by *bfr*, with *dps* have no notable effect (Fig. 3.26). The result of the *ftnA bfr* mutants matches that of Abdul-Tehrani *et al*. (1999) who showed a similar trend in growth restriction for the respective double mutant *ftnA bfr* under iron limited conditions. No growth differences were noted in the presence of 16 µM ferric citrate nor in the absence of DTPA (data not shown), as was previously reported by Abdul-Tehrani *et al*. (1999).

A. Δ *ftnA* Δ*bfr*

B. Δ *ftnA* Δ*dps*

C. Δ*bfr* Δ*dps*
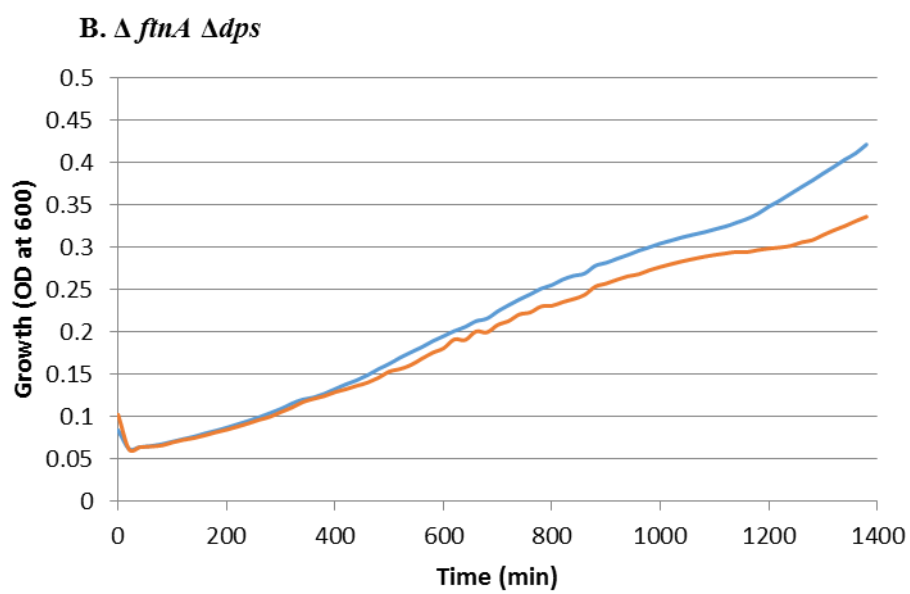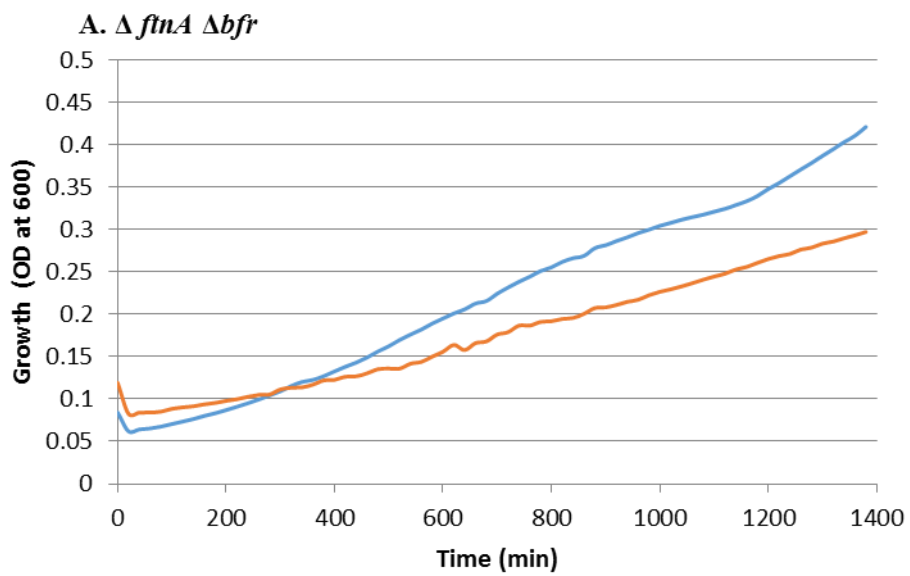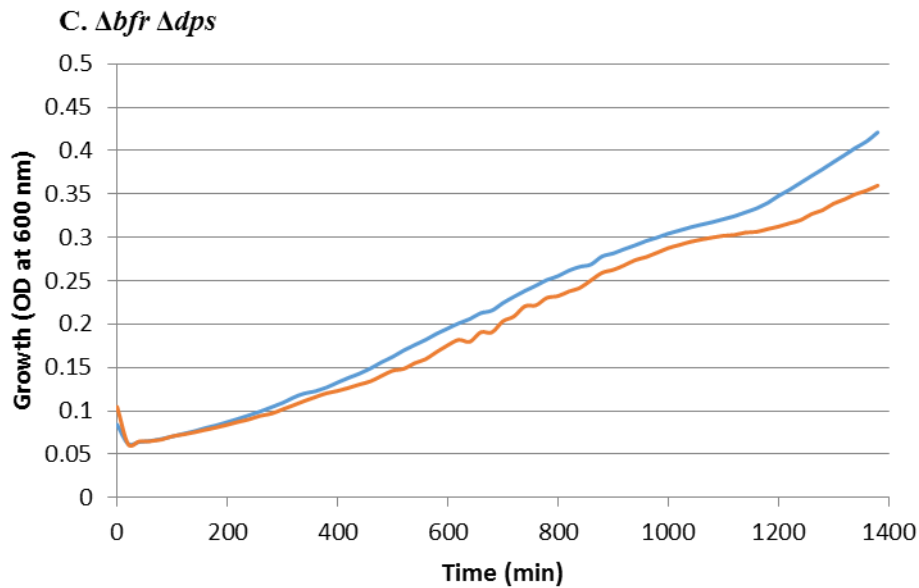
Figure 3.27 Impaired growth of the double mutants under iron-restriction conditions. Growth of the wild type (blue line), and **A**, Δ*ftnA* Δ*bfr*; **B**, Δ*ftnA* Δ*dps* and **C**, Δ*bfr* Δ*dps* double mutants strains (orange line) in M9 medium in the presence of 0.5 µM DTPA. Pre-cultures grown in M9 medium with 16 µM ferric citrate. Repeat once.

For the triple iron-storage mutant, the results of iron-restricted growth (Fig. 3.28) showed that lack of FtnA, Bfr and Dps reduces growth by 60% ($P = 0.0004$) compared to the wildtype, which is a greater growth effect than seen for any of the double mutant. This suggests that in the absence of both Bfr and FtnA, the additional absence of Dps reduces iron-restricted growth. Thus, it appears that Dps can contribute to iron-restricted growth, but only when no other iron-storage protein is available. This observation is consistent with the results of Velaydhan *et al*. (2007) who found that the additional absence of Dps on top of the *ftnA* and *bfr* mutations reduced the total cellular iron content.

No growth difference was seen under iron sufficiency for all mutant strains (data not shown), which is consistent the roles of the deleted genes in iron storage and/or redox resistance.
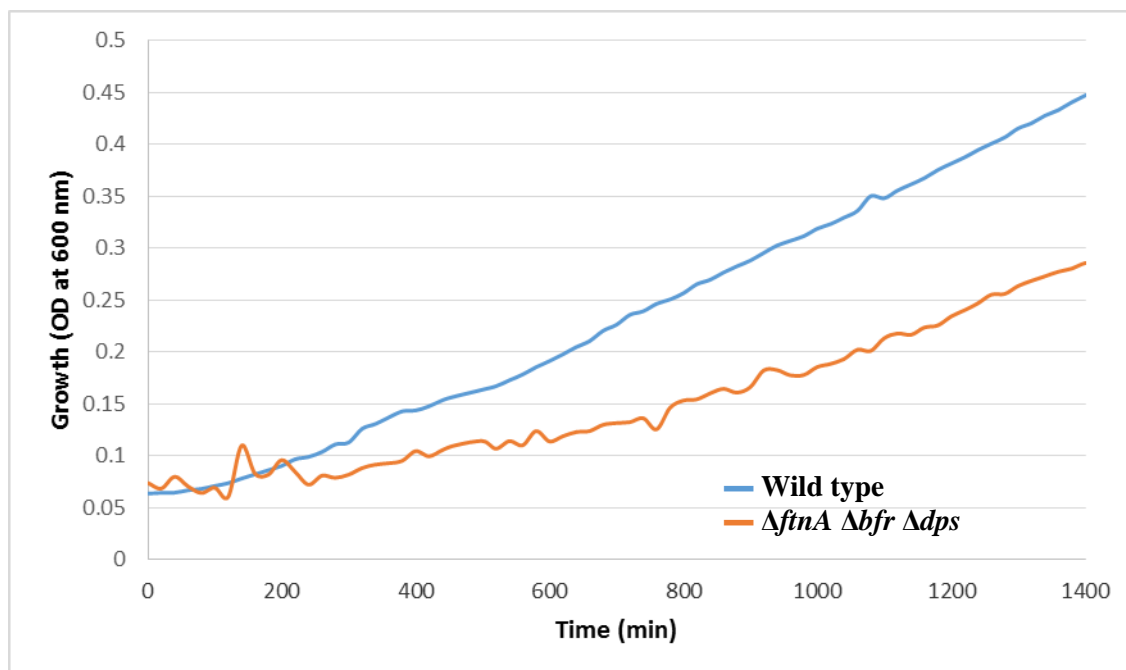
Figure 3.28 Impaired growth of the triple mutant's Δ*ftnA* Δ*dps* Δ*bfr* under iron-restriction conditions. Growth of the wildtype (blue line) and the Δ*ftnA* Δ*dps* Δ*bfr* triple mutant (orange line) in M9 medium in the presence of 0.5 µM DTPA. Pre-cultures grown in M9 medium with 16 µM ferric citrate. Repeat once.

In summary, results above show that the combination of the iron-storage mutations produce an additive iron-restricted growth phenotype effect such that the triple mutant revealed the highest degree of growth sensitivity under iron restriction (Fig. 3.29), and the lack of iron stores (FtnA, Bfr and Dps) significantly limit the intracellular sources available to compensate for lack of extracellular iron. It is probable that the reduced iron-restricted growth of the iron-storage mutants arises as a result of their lower iron-storage capacity. This hypothesis is explored in the following section.
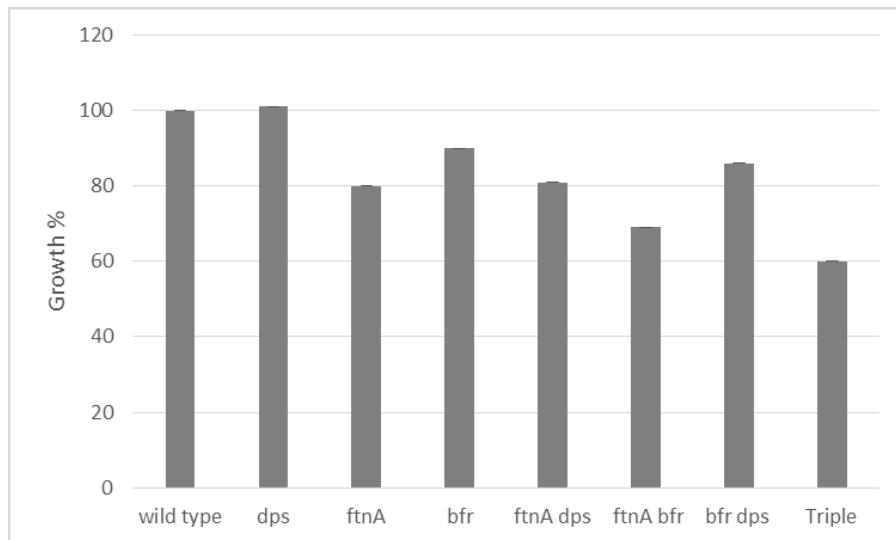
Figure 3.29. Summary of growth of the iron-storage mutant strains under iron-restricted condition as a percentage of that achieved by the wt. Data are from the graphs above and represent the final growth point (24 h). Error bars, too small, indicate standard error

3.10 Analysis of the iron content of *E. coli* iron-storage mutants

3.10.1 Introduction

The above experiments indicate a growth phenotype for the iron-storage mutants under iron restriction and show that combination of iron-storage mutations generates an addititve effect with respect to the iron-restricted growth phenotype, with the triple mutant exhibiting the greatest degree of iron restriction (Fig. 3.28). It is likely that the reduced iron-restricted growth of the iron-storage mutants arises as a consequence of their lower iron-storage capacity, as previously reported (Abdul-Tehrani *et al.,* 1999; Velayudhan *et al*., 2007). Therefore, to determine whether there is indeed a correlation between whole-cell iron levels and the observed iron-restricted growth phenotypes above, the mutant strains generated in this project were subjected to whole-cell iron analysis. It should be noted that relative contribution of iron-storage proteins to the total iron content of *E. coli* has been considered previously (Abdul-Tehrani *et al.,* 1999) but the previous work did not address the role of Dps and thus did not report the consequences of the elimination of all three iron-storage proteins on the total iron content of *E. coli*. Such work has however been reported for *Salmonella* (Velayudhan *et al*., 2007).

3.10.2 Effect of mutation of iron-storage genes on the whole-cell iron content of *E. coli* K-12

Strains included were the wild type, BW25113, and all of the isogenic iron-storage mutants described above: BW25113 Δ*ftnA,* BW25113 Δ*dps*, BW25113 Δ*bfr*, BW25113 Δ*ftnA* Δ*dps*, BW25113 Δ*ftnA* Δ*bfr*, BW25113 Δ*bfr* Δ*dps* and BW25113 Δ*ftnA* Δ*dps* Δ*bfr*. Strains were grown aerobically at 37 °C and 250 rpm, overnight, either in 5 ml of M9 or LB medium in test tubes, or in 50 ml of M9 medium in 250 ml flasks. In all cases the medium was supplemented with 20 µM ferric citrate the harvested cell pellets were analysed for metal content by ICP-OES as described in Methods (section 2.17). The samples were collected in the stationary phase because *ftnA*, *bfr* and *dps* are expressed in the post-exponential phase of the growth in iron sufficient condition and iron stores are deposited post-exponentially (Abdul-Tehrani *et al.,* 1999). For growth in 5 ml iron-supplemented glucose M9 salts medium (Fig. 3.30), the lack of Bfr and FtnA resulted in a modest reduction in iron content (78 and 82% cf wildtype; *P*= 0.03, 0.09) whereas the 8% reduction was seen for the Dps deficient strain was not significant. Also, the difference in iron contents between the *ftnA* and *bfr* single mutant was not significant (P= 0.64). All three double mutants showed lower iron contents than the single mutants, with the *ftnA bfr* double mutant showing the greatest reduction compared to the wildtype (60%; *P* = 0.01), followed by the *ftnA dps* mutant (65%; *P* = 0.03) and then the *bfr dps* mutant (70%; *P* = 0.01). However, the differences between the iron contents of the double mutants are no statistically significant. The triple mutant showed a dramatic decrease in iron content (~35% of that of the wildtype; *P* = 0.008), and a statistically significant lower iron content than that of the double mutants (*P* = 0.02).

The whole-cell iron contents (Fig. 3.30) correlate well with the iron-restricted growth phenotypes determined above (Fig. 3.26-28) which is fully consistent with the notion that the poor growth for the iron-storage mutants under low-iron conditions is proportion to the loss of iron storage capacity.
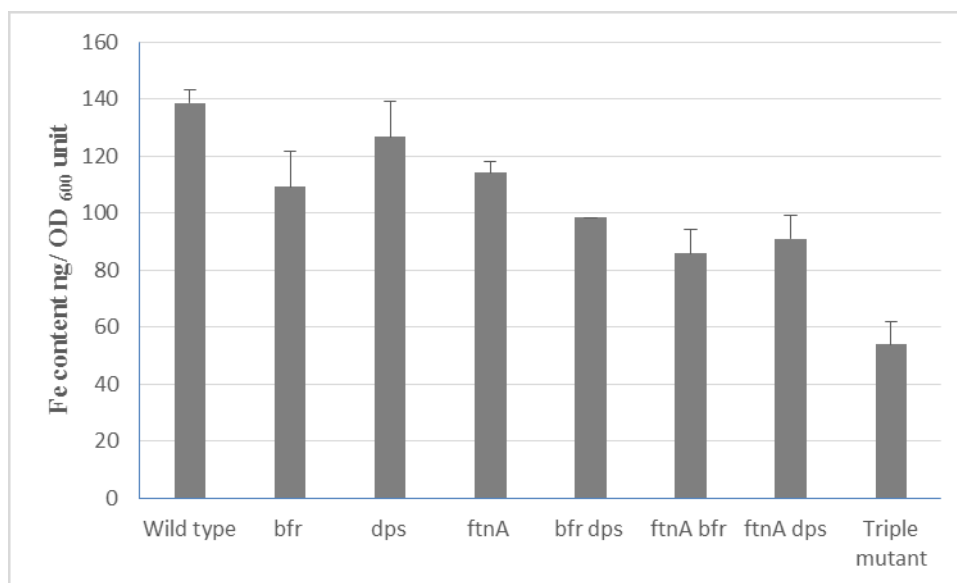
Figure 3.30. Effect of deletion of the three iron storage proteins on whole-cell iron content in *E. coli* iron-storage mutants grown aerobically in M9 medium with 20 μM Fe. The wild type and all mutant strains were grown overnight (18 h) in 5 ml of 40 mM glucose-containing M9 medium plus 20 μM ferric citrate, in test tubes. Repeated once.

The above experiment was repeated using LB, since the previous whole-cell iron content analyses of Abdul-Tehrani *et al*. (1999) was performed following growth in this medium. Following growth in LB, the effect of the iron-storage mutations on whole-cell iron levels (Fig. 3.31) was far less than that observed upon growth in M9 medium (Fig. 3.30). The results in LB show that the *ftnA bfr* and *bfr dps* double mutant, the triple mutant and the *ftnA* single mutant had the lowest iron content with respect to the other strains (Fig. 3.31), with similarly low levels at 77 (*ftnA bfr*), 81 (*bfr dps*), and 80% (triple and *ftnA* mutants) of those of the wildtype. However, of these values only differences for the triple mutant strain was statistically significant ($P < 0.05$). It should be noted that the cellular iron levels recorded were considerably lower in LB than in M9 medium, by 35% for the wild type, which would be expected to greatly reduce to the effect of the iron-storage mutations on whole-cell iron contents. This difference in cellular iron content caused growth in the two media appears to partly reflect a fivefold lower level of iron storage during growth in LB cf. M9 medium (85 ng/OD unit in M9 versus 17 ng/OD unit in LB; values represent respective differences between the wild type and triple mutant) and also the 1.4-fold higher requirement for iron during growth in LB cf. M9 medium (73 ng Fe/OD unit cf. 53 ng/OD unit for the triple mutants in LB and M9, respectively). The reasons for these differences in storage and non-storage iron levels during growth in rich

and poor medium are unclear. However, a key factor that might impact such effects is pH, since M9 medium becomes acid (pH ~5) during growth due to conversion of glucose into mixed acids, whereas LB becomes basic (pH ~9) due to production of ammonia from amino acid catabolism (Čepl *et al*., 2014; Christensen *et al*., 2017). The lower pH achieved in M9 medium would be expected to assist iron solubility and uptake. In addition, the different media might be expected to impact the expression of the iron-storage genes which would in turn influence iron-storage capacity.

The previous studies of Abdul-Tehrani *et al*. (1999) showed that the iron content of the *E. coli* K-12 *bfr ftnA* mutant was 50% reduced (with respect to wildtype) following aerobic growth in LB, whereas only a 22% difference was observed here. However, the experiments of Abdul-Tehrani *et al*. (1999) were performed using 250 ml flasks carrying 50 ml LB which affords a high rate of aeration whereas the growths reported here were in 5 ml of broth contained in test tubes, where aeration is far less vigorous. Thus, the differences observed between this and the previous study might relate to the degrees of aerobiosis achieved.
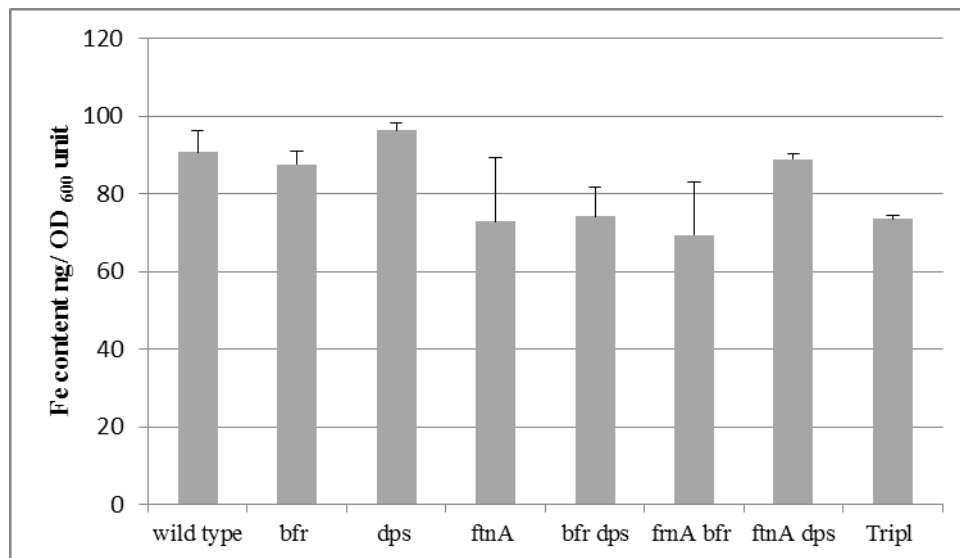
Figure 3.31 Effect of deletion of the three iron-storage protein genes on the whole-cell iron content of *E. coli* grown aerobically in LB with iron supplementation. Details are as for Fig. 3.29, except for the use of LB in place of M9 medium.

A further analysis of whole-cell iron content was performed in glucose M9 medium, as in Fig. 3.30, except for the use of 50 ml medium in 250 ml flasks to enhance the rate of aeration and aerobiosis. The results (Fig. 3.32) obtained are similar to those seen in the same medium but during growth in test tubes (Fig. 3.30), although the total iron contents are lower (93 versus 138 ng/OD unit), and similar to those seen in LB (90 ng/OD unit; Fig. 3.31). The triple mutant had a 61.3% lower total level of iron with respect to the wildtype, which is similar to that observed in the test tubes (61.6% lower).

For the single mutants, as before (Fig. 3.30) there was little effect of the *dps* mutation, which is consistent with the findings for *S. enterica* (Velayudhan *et al*., 2007). However, the *bfr* and *ftnA* mutations led to a 39 and 21% reduction in iron content relative to the wild type, which again reflects the results obtained with the growths in test tubes (Fig. 3.30), although the effect for the *bfr* mutation is greater than seen before.

For the *ftnA dps* and the *ftnA bfr* double mutants, the iron contents are similar to those observed for the corresponding *ftnA* and *bfr* single mutants. This indicates that the *dps* mutation does not affect cellular iron content, which is consistent with the result obtained for the *dps* single mutant.

In summary, the data obtained for growths in flasks and test tubes containing M9 medium are similar with the main difference being the overall lower total iron levels per OD unit. This difference may reflect a greater demand for iron during growth under low aeration cf. high aeration, possibly resulting from induction of iron-dependent anaerobic respiratory systems under conditions of lower oxygen availability.
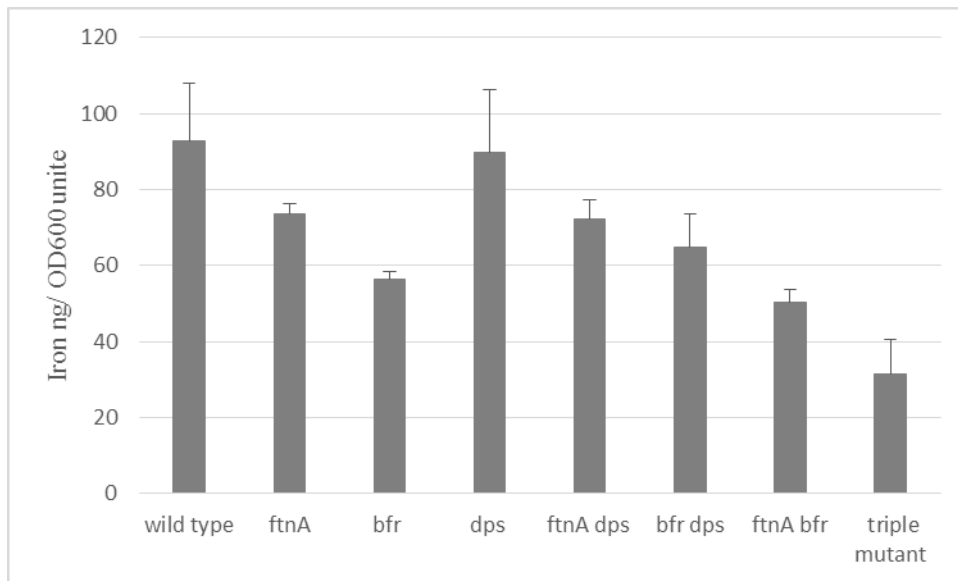
Figure 3.32 Effect of deletion of the three iron-storage proteins on the whole-cell iron content of *E. coli* grown aerobically in M9 medium with iron supplementation, in 250 ml conical flasks. Details are as for Fig. 3.29 except that growth was in 50 ml volumes in 250 ml conical flasks. Repeat once.

3.11 Discussion

The aim of this work was to further understand the roles of each of the three iron-storage proteins of *E. coli*. To facilitate these aims, single, double and triple iron-storage mutant strains were generated and confirmed genotypically and phenotypically, and their characteristics were determined during redox stress and also under iron restriction condition.

The role of ferritins is as iron-storage proteins and most prokaryotes contain either an Ftn or Bfr (or both) protein to perform such an iron storage role. Its appears that some species of prokaryotes contains more than one types of iron-storage protein including *E. coli*, *Mycobacterium tuberculosis* and *Vibrio cholera*; in these bacteria Ftn and Bfr can act as iron supplies in conditions of iron unavailability. The capacity of these proteins for iron is reported at around 2400 iron atoms per 24 subunits (Carrondo 2003). The detailed roles of these iron-storage proteins may differ somewhat in different bacteria. For example, previous studies suggest that the FtnA is the only significant iron-storage protein in *E. coli* (Abdul-Tehrani *et al*., 1999) and *Erwinia chrysanthemi* (Abdul-Tehrani *et al*., 1999; Boughammoura *et al*., 2008). However, the Bfr protein of some other bacteria is considered as the major iron-storage protein, e.g. in *Brucella abortus*, where it is the only iron-storage protein and it contributes 75% of the total iron content of the bacterial cell (Almirón & Ugalde 2010).

Thus, the aim of this chapter was to characterise iron-storage mutants to confirm the relative functions of the iron-storage proteins in *E. coli* and to enable subsequent experiments aimed at complementing any phenotype obtained through controlled expression of specific endogenous or foreign iron-storage proteins.

3.11.1 The construction of the mutant strains

The P1 transduction steps were preceded by a step for removal of the kanamycin resistance cassette inserted into the deleted genes carried by the recipient strains; this step was required to allow selection of transductants through their acquired Kn^R phenotype. Kn^R cassette deletion was performed by transformation with the pCP20 plasmid into the Kn^R deletion mutants. The pCP20 plasmid shows thermal induction of FLP synthesis that enables non-homologous recombination at the FRT sites flanking the Kn^R cassette. Thus, BW25113 Δ*ftnA* Δ*dps*, Δ*ftnA* Δ*bfr* and Δ*bfr* Δ*dps* double mutants and a Δ*ftnA* Δ*dps* Δ*bfr*

triple mutant were constructed as above. The genotypic status for the mutants generated by transduction and those resulting after treatment with pCP20 were confirmed by colony PCR. For transductant colonies, the amplification products sizes of (Δbfr)::*kan* and (Δdps)::*kan* were about (1589 and 1536 bp) which is the same as the donor strain JW3298 (Δbfr)::*kan* and JW0797 (Δdps)::*kan*, respectively and bigger than the wild type and the recipient that gave about ~800 bp and ~300 bp, respectively. In addition, the previous mutations associated with the recipient were confirmed as still present in the double and triple mutants. This was achieved by colony PCR. Following deletion of the Kn^R cassette, there was a corresponding reduction in size of PCR amplification products with respect to the parent strain. Western blotting was also performed to additionally confirm the status of the *bfr* and *ftnA* genes. The status of the Dps protein in the generated mutant strains was subsequently confirmed using polyclonal antibodies generated against the Dps protein, as overexpressed and purified in this study, as reported in chapter 6.

3.11.2 Phenotypic characteristic under redox stress on L-agar

Bacteria such as *E. coli* can protect themselves against hydrogen peroxide and superoxide by using different protection systems. One element of defence against redox stress is the production of enzymes, such as catalase, and also production of protective protein such as Dps which is known to confer resistance to the combined toxic effects of iron and peroxides. Mutants lacking Dps possess a reduced capacity to withstand challenge by hydrogen peroxide; this phenotype was tested on L-agar plates with and without H_2O_2 in different concentration. The growth of the Δdps and triple mutants was clearly decreased in the presence of 600 µM H_2O_2 with respect to the wild type, which was not affected. Furthermore, the growth of the *dps* mutants was delayed in the presence of the hydrogen peroxide (as described in section 3.10.1). This phenotype of the *dps* mutants matches the role of the Dps protein in survival under oxidative stress (Almiron *et al.,* 1992; Choi *et al.,* 2000).

The sensitivity of the Δdps mutant to hydrogen peroxide emphasises the protective role of Dps in agreement with Almiron *et al.* (1992) who found that this mutant in *E. coli* was unable to grow in the presence of 45 mM of H_2O_2. Choi *et al.*, (2000) also demonstrated that the presence of *dps* provides an oxidative redox and acid stress resistant property in *E. coli* O157:H7.

3.11.3 Phenotypic characteristic of the mutant strains under redox stress on LB

The *dps* mutation raised sensitivity to hydrogen peroxide, as found before in *Salmonella* (Velayudhan *et al.*, 2007) and *E. coli* (Almiron *et al.*, 1992; Choi *et al.*, 2000). It was expected that the growth of the triple mutant would be impaired more so than that of the single Δ*dps* mutant. However, hydrogen peroxide extended the lag phase by 7 h for the Δ*dps* strain but by just 3.5 h for the triple mutant. The sensitivity of double and single mutants to H_2O_2 was examined to explore the reason for the reduced sensitivity of the triple mutant with respect to the Δ*dps* strain. The sensitivity to H_2O_2 was not increased by a lack of FtnA and/or Bfr in a wildtype background. This result is consistence with previous reports indicating no role of FtnA and Bfr in redox stress resistance (Abdul-Tehrani *et al.*, 1999; Keyer and Imlay, 1996). The results suggested that the elimination of *ftnA* does not affect the peroxide sensitivity of a Δ*dps* mutant or the wild type, but indicate that combining the Δ*bfr* mutation with the Δ*dps* mutation results in increased peroxide resistance with respect to the *dps* single mutant, and so suggest that the presence of *bfr* <u>enhances</u> sensitivity to peroxide stress in LB when *dps* is nullified; this effect may be related to iron held by Bfr that might exacerbate peroxide stress (possibly because Bfr-iron may be more available than that located within FtnA).

3.11.4 Phenotypic characteristics of the mutant strains in LB under iron restriction and redox stress condition

In order to investigate the effect of the iron status with the addition of the hydrogen peroxide, iron chelator (240 µM DTPA) was added to reduce cellular iron stores as far as possible. The results show that the presence of 600 µM H_2O_2, along with 240 µM DTPA, in the post-culture resulted in enhanced toxicity with respect to conditions with 600 µM H_2O_2 alone. The lag phase of the wild type was extended by ~5 h, whereas the Δ*dps* and Δ*bfr* Δ*dps* strains failed to grow. This suggests that DTPA enhances H_2O_2 toxicity, possibly by influencing iron availability. So minimal medium was used in subsequent experiments to more readily control the iron concentration in the medium.

3.11.5 Phenotypic characteristic of the mutant strains in minimal medium under redox stress

In minimal medium with the addition of 100 µM hydrogen peroxide, the Δ*bfr* Δ*dps* and Δ*dps* mutants had lower growth than the wild type for pre-cultures with or without 20 µM ferric citrate (Fig 3.38). However, the double mutant exhibited poorer growth than

the single mutant, this result was opposite to that obtained in LB. The reason for this difference in result between rich and defined medium is unclear. However, the data are consistent with a role for Bfr in combating H_2O_2 toxicity in the absence of Dps in minimal medium, although in rich medium Bfr appears to enhance such toxicity. It also appeared that the presence of iron with the addition of the hydrogen peroxide causes an intense effect on the single and double mutants, by extending their lag phase by about ~5 h when pre-cultured with iron. However, it had less effect on the growth of the wildtype. This result is possibly due to an increase in free cytosolic iron levels arising from the iron-storage deficiency combined with a gain in iron due to the iron supplementation in the pre-culture, which together may lead to enhanced peroxide mediated redox stress. The effect of high intracellular iron contents in the presence of hydrogen peroxide on the bacterial growth was consistence with the previous work of Abdul-Tehrani *et al.* (1999) which show that the sensitivity of *E. coli* was increased to H_2O_2 in the condition of increasing the intracellular iron contents, this observation also supported by the Repine *et al.* (1981) work which demonstrate that decreasing the intracellular of iron content in *Staphylococcus aureus* decrease the sensitivity to hydrogen peroxide.

Importantly, the wild type was only able to grow in M9 medium with 100 µM peroxide when 20 µM ferric citrate was not also included in the medium. However, neither the Δ*dps* nor Δ*bfr* Δ*dps* mutant were able to grow in this condition. This may be as a result of an enhanced toxic effect of hydrogen peroxide in the absence of Dps.

There is some evidence for the ability of Bfr to participate in the detoxification process to protect the bacterial cell from oxidative stress, in bacteria such as *Bacterioides fragilis* (Chen & Morse, 1999) and *Neiserria gonorrhoeae* (Gauss *et al.*, 2012).

3.11.6 Impaired growth of the triple mutant under iron-restriction conditions

Results of the growth under iron-restricted condition showed that the deletion of *dps* does not affect growth in the presence of DTPA. However, the *ftnA* mutant was impaired in growth with DTPA which is consistence with previous work (Abdul-Tehrani *et al.,* 1999). The combination of the iron storage gene mutations to produce double mutant strains resulted in growth impairment under iron restriction, with the *ftnA bfr* mutant being more

impaired than the *ftnA dps* or *bfr dps* strains. The combined lack of FtnA, Bfr and Dps reduced iron-restricted growth by 60%, suggesting that in the absence of both Bfr and FtnA, the additional absence of Dps reduces iron-restricted growth. Thus, it appears that Dps can contribute to iron-restricted growth, but only when no other iron-storage protein is available. This is consistent with the results of Velaydhan *et al*. (2000) who found that the additional absence of Dps reduced the total iron content.

3.11.7 The effect of iron storage gene deletion on iron sequestering capacity

Experiments were conducted to evaluate the total iron content in the wild type and the mutant strains using whole-cell-iron assay. The deletion of all three type of iron storage protein genes resulted in a dramatic decrease in iron content (~35% of that of the wildtype) upon growth in iron-rich M9 medium. However, the reduction in iron content was less (1.24 fold) upon growth in iron-supplemented LB. Liu *et al*. (2016) also found that the level of iron was reduced in an *E. coli* BW25113 triple iron-storage mutant (by 1.5 fold) in comparison with the wild type in LB medium.

The single *dps* mutation did not affect cellular iron content which is consistent with the findings for *S. enterica* (Velayudhan *et al*., 2007). The deletion of *bfr* and *ftnA* resulted in a modest reduction in iron content, similar to *bfr dps* and *ftnA bfr* double mutants strains, respectively, and the combination of the *ftnA bfr* mutations showed the greatest reduction compared to that of the *ftnA dps* and *bfr dps* double mutant strains. In summary, it was found that both Bfr and FtnA contribute to the total iron stores of *E. coli* K-12 in stationary phase following aerobic growth in iron-supplemented M9 medium, with Dps contributing relatively little except in the absence of Bfr and FtnA. The data also indicate that up to 65% of cellular iron can be stored in the wildtype by a combination of Bfr, FtnA and Dps. Furthermore, the whole-cell iron contents of the mutant strains (Fig. 3.30) correlate well with the iron-restricted growth phenotypes determined (Fig. 3.26-28), which is fully consistent with the notion that the poor growth for the iron-storage mutants under low-iron conditions is in proportion to the loss of iron-storage capacity.

Chapter 4

4. Investigating the respective functions of the three iron-storage proteins of *E. coli* by determining whether these proteins are mutually interchangeable

4.1 Introduction

The phenotypic analysis of the triple mutant for the three iron-storage proteins in chapter three showed that the growth of the triple-mutant strain is impaired during redox stress and iron-restricted conditions. It was also observed that the largest decrease in total iron content was in the triple mutant, compared to the wild type (section 3.10.2). This indicates that the lack of iron-storage proteins resulted in diminished iron stores for supporting bacterial growth under iron-restricted conditions. In this chapter, the genes for iron storage were amplified and cloned into pBADrha, the constructed plasmids were then transformed into the triple iron-storage mutant (BW25113 Δ*ftnA* Δ*dps* Δ*bfr*) to perform complementation studies under conditions where expression of the iron-storage proteins genes is controlled by rhamnose rather than other factors (e.g. iron, stress and growth phase). In this way, the possibility that expression of a single specific iron-storage protein gene can compensate for the absence of the other genes can be tested. Thus, the mutual interchangeability of FtnA, Bfr and Dps can be explored in terms of the ability to support resistance of *E. coli* to growth under low-iron conditions or redox stress.

4.2 Cloning of iron-storage genes into the pBADrha vector

4.2.1 Gene amplification

PCR products of the *bfr*, *dps* and *ftnA* genes were required to allow complementing plasmids to be generated. These would be used to investigate the ability of each iron-storage protein gene to complement the triple mutant under different growth conditions (e.g. low iron and redox stress). A High Fidelity DNA polymerase kit and primers (Table 2.3) were used to amplify the iron-storage genes by PCR. Figs. 4.1-2 show the PCR products of *bfr*, *dps* and *ftnA* after purification using GeneJET™ PCR Purification Kit; these had the expected sizes.
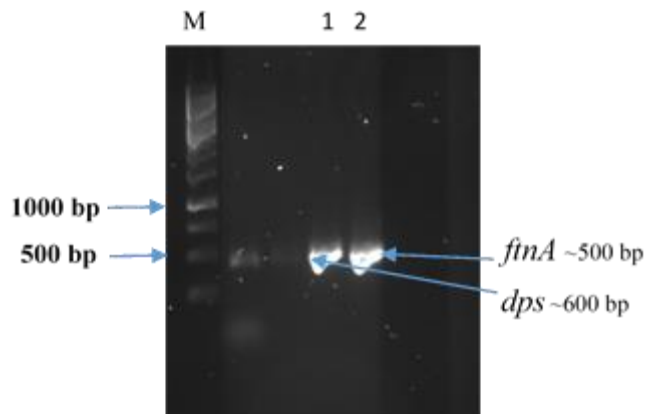
Figure 4.1 Gel electrophoresis of purified PCR products of *dps* and *ftnA*. 1, purified PCR product of *dps* (604 bp using pBADrha-*dps* F & R primers). 2, purified PCR product of *ftnA* (528 bp using pBADrha-*ftnA* F & R primers). M, marker, 1 kb GeneRuler (Fermentas)
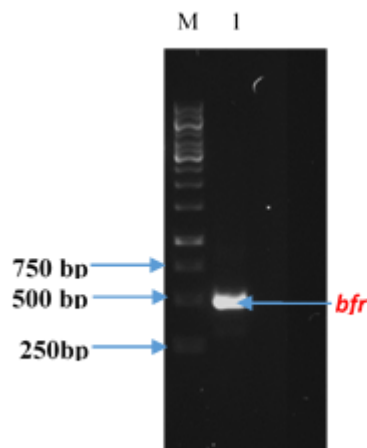
Figure 4.2 Gel electrophoretic analysis of the purified *bfr* PCR product. The 607 bp PCR product generated using pBADrha-*bfr* F & R primers is indicated. M, marker, 1 kb GeneRuler (Fermentas).

4.2.2 Transformation of *E. coli* Top10

The purified *bfr*, *dps* and *ftnA* DNA fragments were cloned into the pBADrha vector using the Fusion Cloning Reaction (FCR). Transformation of 3 µl of each cloning reaction (the linearised pBADrha plasmid plus insert (*dps*/*ftnA*/*bfr*)) into competent Top10 was as described in section 2.5.2. The expression of each cloned gene is under rhamnose control using the vector SD and AUG start codon.

4.2.3 pBADrha minipreps

After transformation, plasmid DNA was extracted from Cm^R transformant colonies (see the restriction map of uncut pBADrha with cloned inserts shown in Figs 4.3B, 4.4B and

4.5B) using a GeneJET Plasmid Miniprip Kit. All samples were digested with *Bam*HI and *Nde*I restriction enzymes to give bands corresponding to the insert (*dps* 574 bp, *bfr* 577 bp, *ftnA* 339 and 159 bp [due to an internal *Nde*I site]) and vector pBADrha (~6000 bp) (Fig. 4.3A, 4.4A and 4.5A, respectively). Selected plasmid samples which gave the expected DNA bands were confirmed by nucleotide sequencing. The plasmids were then designated pBADrha-*bfr*, pBADrha-*dps* and pBADrha-*ftnA*, accordingly. These plasmids were then used to complement the BW25113 Δ*ftnA* Δ*dps* Δ*bfr* triple mutant.
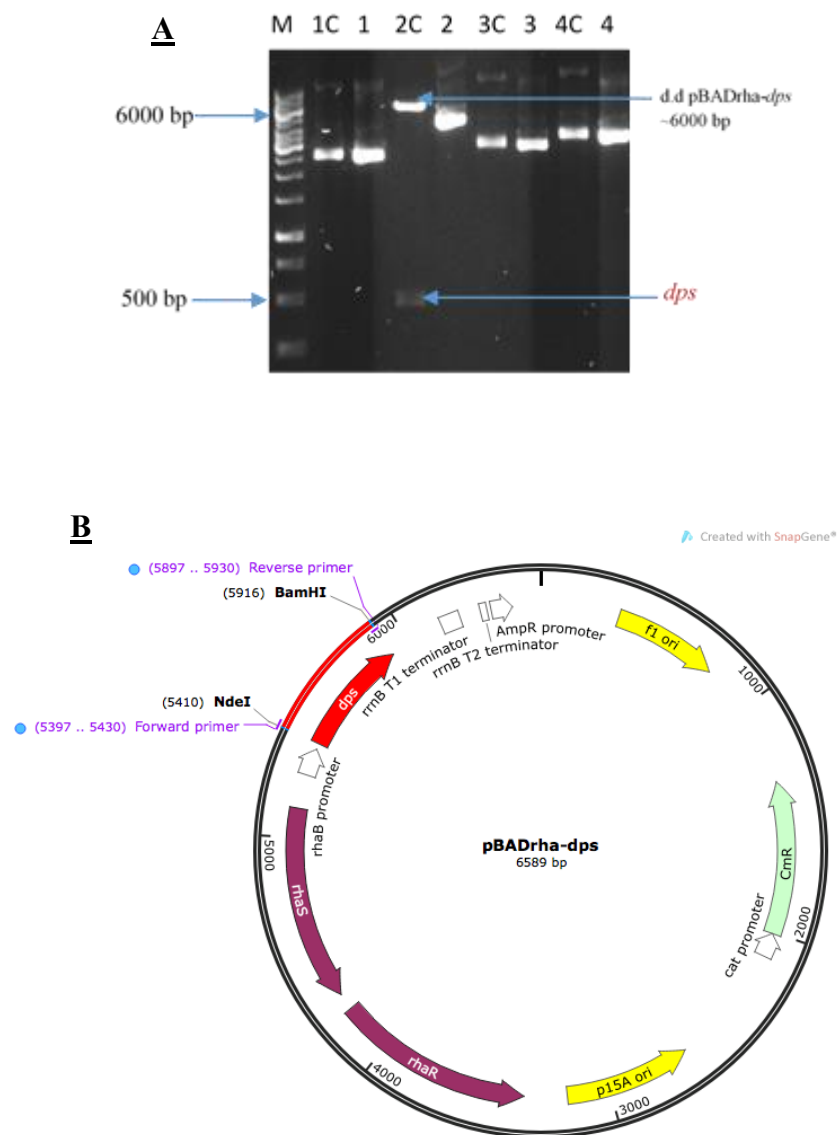
Figure 4.3 Gel electrophoretic analysis of *Bam*H1 and *Nde*I digested candidate pBADrha-*dps* plasmids and restriction map of pBADrha-*dps*. A. M, Marker, 1 kb GeneRuler (Fermentas); **1C-4C**, pBADrha-*dps* plasmid (cut); **1-4,** pBADrha-*dps* plasmid (uncut). Only

sample 2 digested correctly to give ~600 bp *dps* insert and the linearized pBADrha of ~6000 bp.
B. Restriction map of pBADrha-*dps* generated by using SnapGene
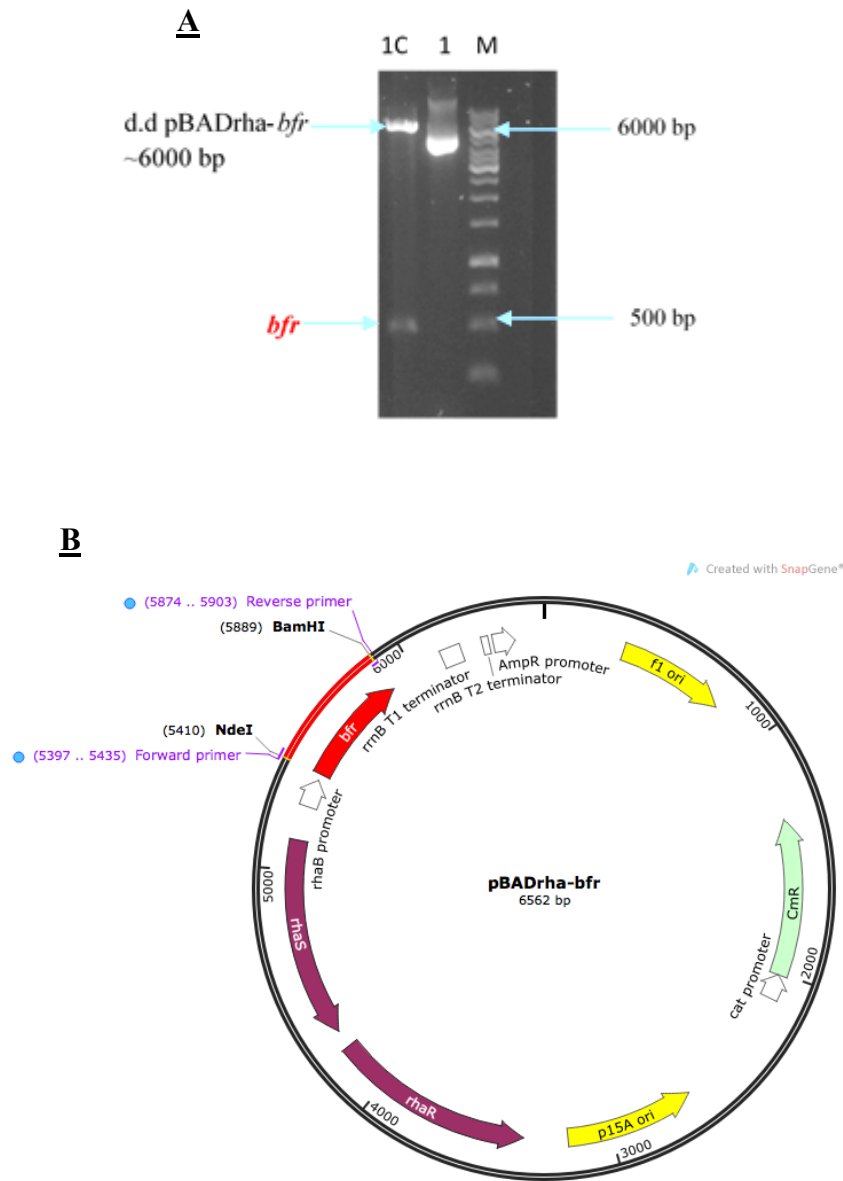
Figure 4.4 Gel electrophoretic analysis of *Bam*H1 and *Nde*I digested candidate pBADrha-*bfr* plasmid and restriction map of pBADrha-*bfr*. A. M, Marker, 1 kb GeneRuler (Fermentas); **1C,** pBADrha-*bfr* (cut); **1,** pBADrha-*bfr* plasmid (uncut). **B**. Restriction map of pBADrha-*bfr* generated by using SnapGene
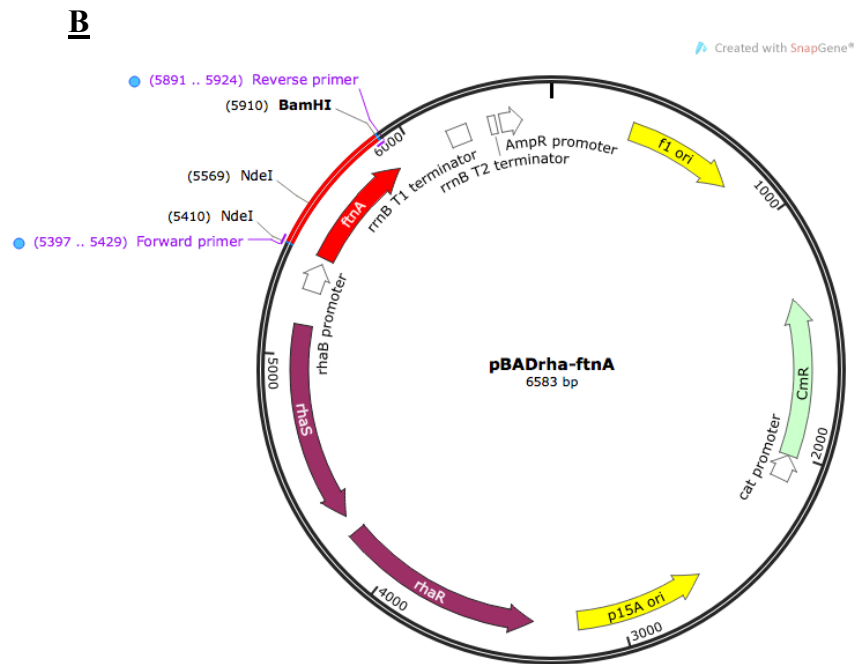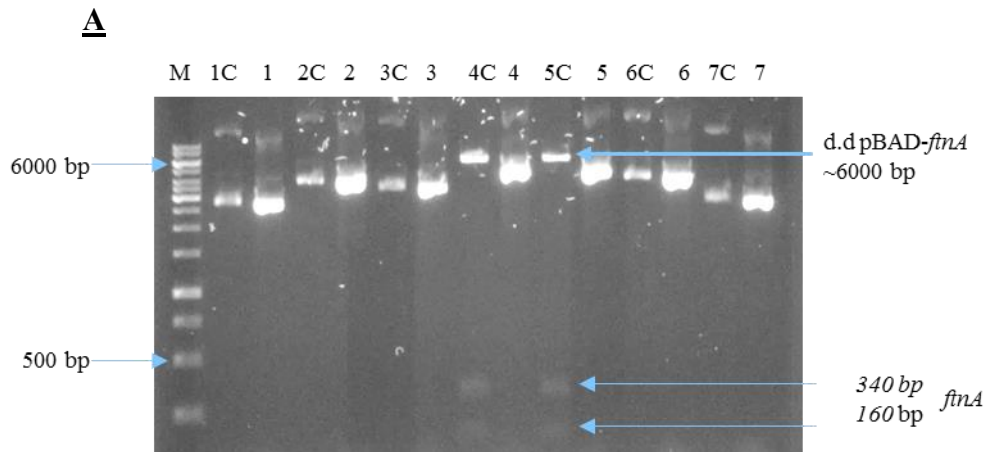
Figure 4.5 Gel electrophoretic analysis of *Bam*H1 and *Nde*I digested candidate pBADrha-*ftnA* plasmids and restriction map of pBADrha-*ftnA*. A. **M**, Marker, 1 kb GeneRuler (Fermentas); **1C-7C**, pBADrha-*ftnA* plasmid (cut); **1-7,** pBADrha-*ftnA* (uncut). Only sample 4 and 5 digested correctly to give 339 and 159 bp *ftnA* inserts and the linearized pBADrha of ~6000 bp. **B**. Restriction map of pBADrha-*ftnA* generated by using SnapGene

4.3 Complementation of the ΔftnA Δdps Δbfr triple mutant with the *ftnA*, *dps* or *bfr* pBADrha plasmids

4.3.1 Transformation into triple mutant

The plasmids constructed above were used for the the complementation (as in section 2.5.2) of the BW25113 ΔftnA Δdps Δbfr triple mutant to investigate the role of each iron-storage gene under specific growth conditions.

4.3.2 pBADrha minipreps

The status of the vector and pBADrha-*bfr* transformants was confirmed by plasmid isolation followed by digestion with *Bam*HI and *Nde*I. Bands of the expected sizes were obtained (Fig. 4.6 and 4.7). It was not considered necessary to confirm the remaining transformants since all had Cm^R status and the results below indicate success of the procedure.
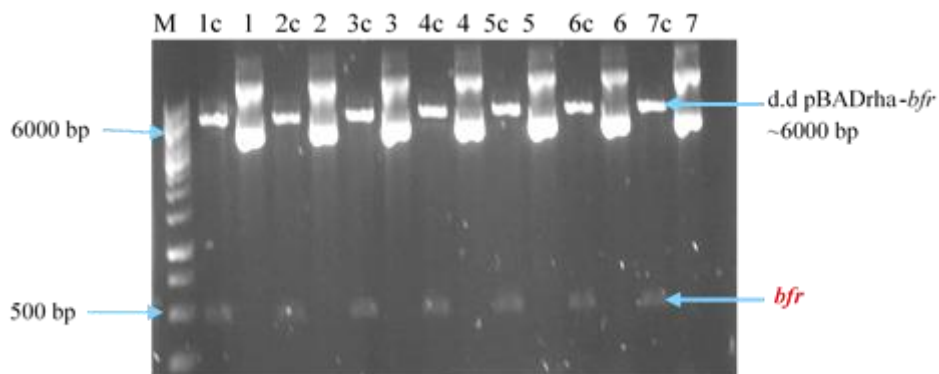
Figure 4.6 Confirmation of pBADrha-*bfr* status of the triple mutant. Plasmid DNA was isolated from seven transformants (1-7) of BW25113 ΔftnA Δdps Δbfr and then digested with *Bam*HI and *Nde*I ('c'). **M**, Marker, 1 kb GeneRuler (Fermentas); both digested and undigested DNA were subject to electrophoresis.
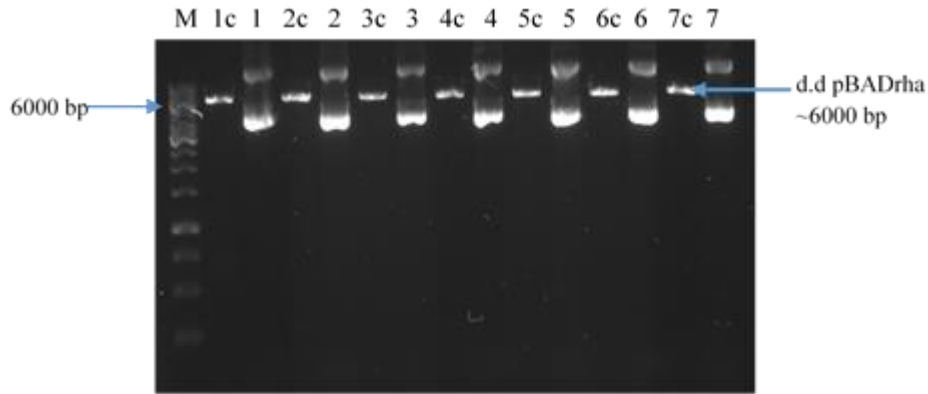
Figure 4.7 Confirmation of pBADrha empty-vector status of the triple mutant. Plasmid DNA was isolated from seven transformants (1-7) of BW25113 Δ*ftnA* Δ*dps* Δ*bfr* and then digested with *Bam*HI and *Nde*I ('c'). **M**, Marker, 1 kb GeneRuler (Fermentas); both digested and undigested DNA were subject to electrophoresis.

4.3.3 Phenotypic confirmation of the complementation of Δ*ftnA* Δ*dps* Δ*bfr* mutant with the *ftnA*, *dps* and *bfr* pBADrha plasmids.

Western blotting was used to test the phenotypic status of the complemented triple mutant. The western blots below (Fig. 4.8, 4.9, 4.10 and 4.11) show the FtnA and Bfr status of transformants of the triple mutant BW25113 Δ*ftnA* Δ*dps* Δ*bfr* with vector and pBADrha-*bfr*, pBADrha-*ftnA* and pBADrha-*dps*. The Dps status of the complemented triple mutant with pBADrha containing *dps* was not performed in this chapter, because the polyclonal antibodies for Dps had not been prepared at this time, however, the phenotypic status for Dps expression was investigated and confirmed later in chapter 6 (see section 6.12).
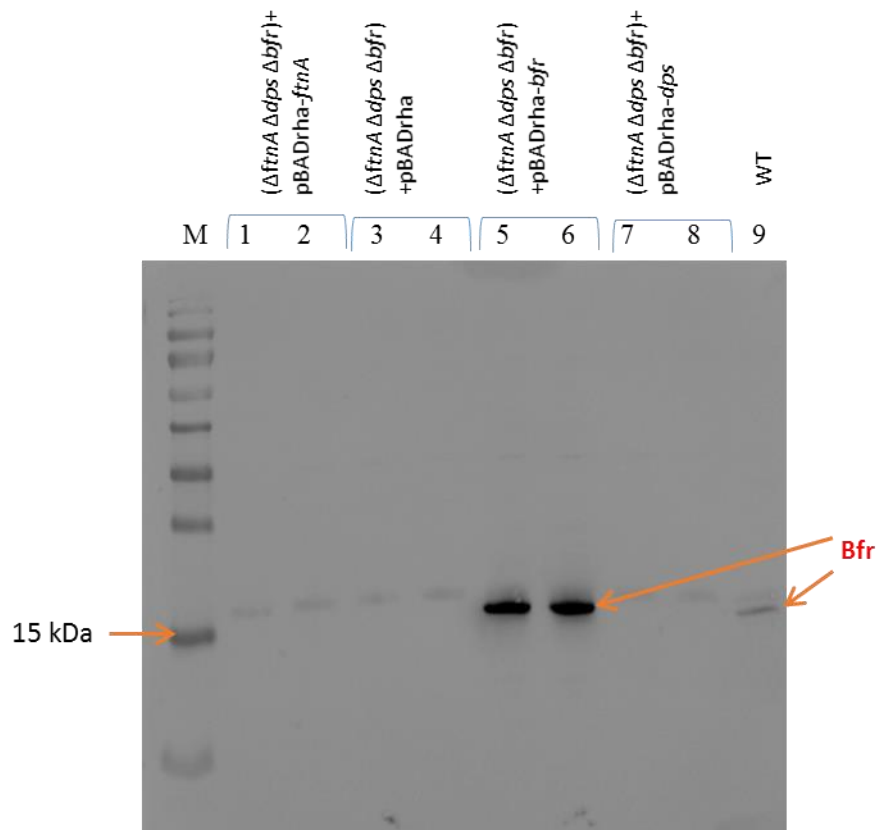
Fig. 4.8 Western blot analysis of Bfr status of transformants of BW25113 Δ*ftnA* Δ*dps* Δ*bfr*.
Transformants were pre-cultured in LB with chloramphenicol (50 µg/ml) plus rhamnose (0.02%
w/v). Cell pellets were subjected to SDS-PAGE followed by western blotting and anti-Bfr
staining. **Lane M,** Page Ruler pre-stained protein Ladder; **Lane 1 and 2,** triple mutant plus
pBADrha-*ftnA*; **Lane 3 and 4,** triple mutant plus pBADrha; **Lane 5 and 6,** triple mutant plus
pBADrha-*bfr*; **Lane 7 and 8,** triple mutant plus pBADrha-*dps*. **Lane 9,** wild type BW25113.
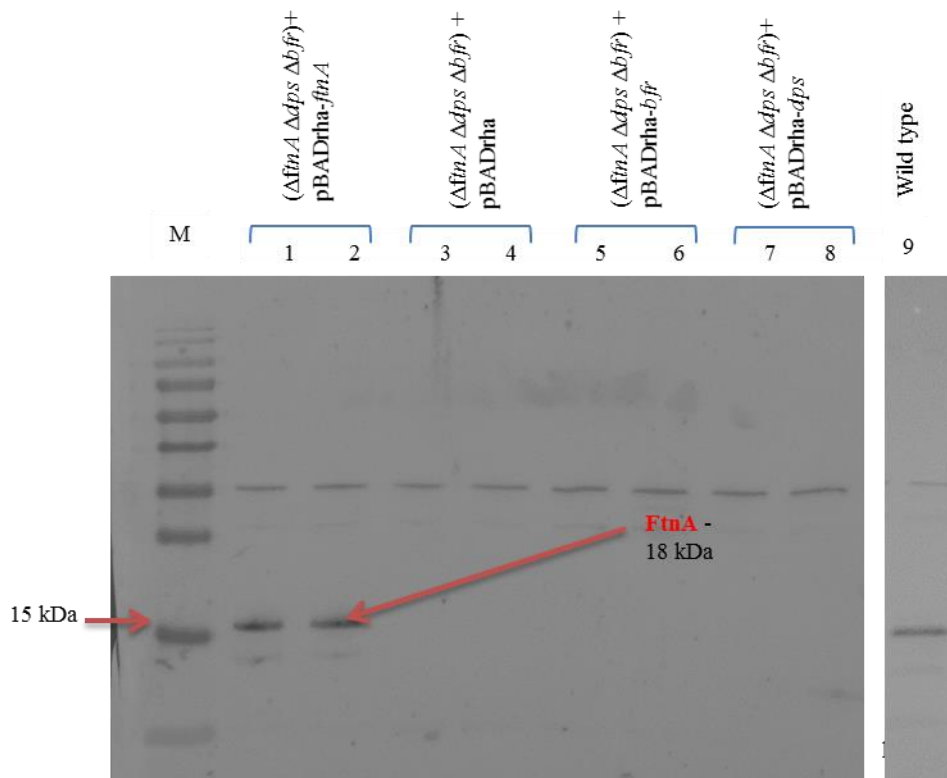
Fig. 4.9 Western blot analysis of FtnA status of transformants of BW25113 Δ*ftnA* Δ*dps* Δ*bfr* with pBADrha-*ftnA*. Transformants were pre-cultured in LB with chloramphenicol (50 µg/ml) plus rhamnose (0.02% w/v). Cell pellets were subjected to SDS-PAGE followed by western blotting and anti-FtnA staining. **Lane M,** Page Ruler pre-stained protein Ladder**; Lane 1 and 2,** triple mutant plus pBADrha-*ftnA*; **Lane 3 and 4,** triple mutant plus pBADrha; **Lane 5 and 6**, triple mutant plus pBADrha-*bfr*; **Lane 8 and 7**, triple mutant plus pBADrha-*dps*; **Lane 9,** wild type BW25113.

BW25113 Δ*ftnA* Δ*dps* Δ*bfr* transformants were pre-cultured in LB with chloramphenicol with 0.02% (w/v) rhamnose. Whole-cell extracts of the overnight culture were then subjected to SDS-PAGE followed by western blotting and anti-FtnA/Bfr staining (Fig. 4.8 and 4.9). The resulting western blot of anti-Bfr staining clearly showed the expression of Bfr in the triple mutant complemented with the pBADrha-*bfr* (Fig. 4.8). The expression of FtnA was also visualized by anti-FtnA western blotting of the corresponding complemented strains. The above results were obtained in the complemented strains induced with rhamnose. The procedure was repeated, with and without rhamnose, to test rhamnose induction capacity (Figs. 4.10 and 4.11). A clear induction effect was observed for both proteins. The immune-reactive bands were analysed using Gene Tools software

and comparison of their densities indicated that there is up to a threefold increase in Bfr levels upon induction (lanes 6 and 8; Fig. 4.10) and a fourfold induction for FtnA (lanes 1 and 3; Fig. 4.11). This relatively modest rhamnose induction effect, and the relatively high levels of Bfr and FtnA in the absence of inducer (similar to levels seen in the wildtype), may be due to the fact that LB is a rich medium lacking in any glucose which might exert a catabolic repression effect on the *rha* promoter (Ford *et. al*., 2014). Possibly, using minimal medium or including glucose may be helpful in ensuring more controlled expression in response to rhamnose. This possibility will be explored in the following chapter.
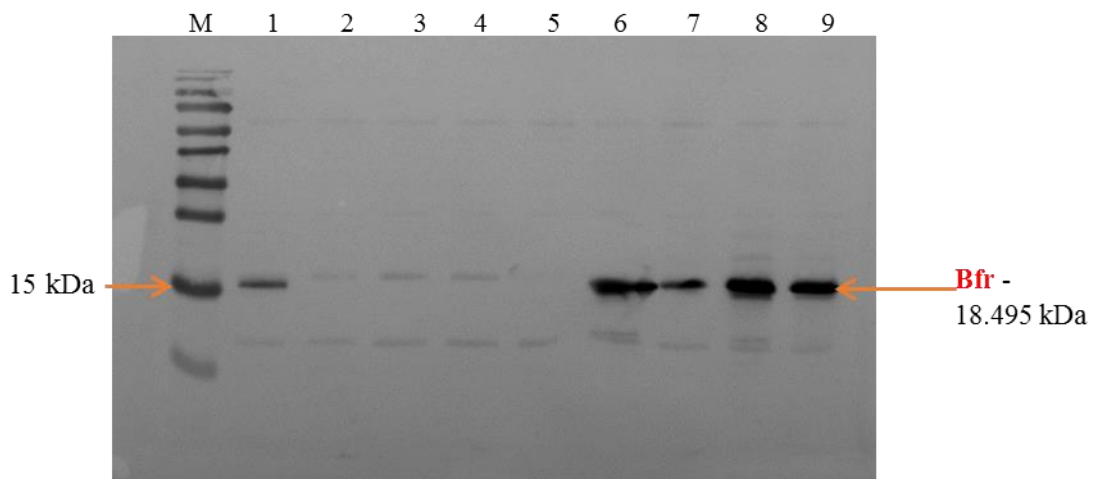
Fig. 4.10 Western blot analysis of the effect of rhamnose on the Bfr status in the *bfr* and *ftnA* complemented triple mutant (BW25113 Δ*ftnA* Δ*dps* Δ*bfr*) +/- rhamnose. Western blot analysis of whole-cell extracts of strains pre-cultured in LB (with chloramphenicol, as appropriate) with/without 0.02% rhamnose. Blot was subject to anti-Bfr immuno- staining. **Lane M,** Page Ruler pre-stained protein Ladder; **Lane 1,** wild type BW25113; **Lane 2 and 4,** triple mutant + pBADrha-*ftnA* with rhamnose; **Lane 3 and 5,** triple mutant + pBADrha-*ftnA* without rhamnose; **Lane 6 and 8,** Δ*ftnA* Δ*dps* Δ*bfr* + pBADrha-*bfr* with rhamnose; **Lane 7 and 9,** Δ*ftnA* Δ*dps* Δ*bfr* + pBADrha-*bfr* without rhamnose.

In conclusion, the expression of both *bfr* and *ftnA* in the triple mutant has been demonstrated in LB, indicating that the corresponding plasmids can be employed for complementation experiments. Although this has not been shown here for the *dps* gene,

experiments presented in chapter 5 confirm that *dps* is indeed expressed from pBADrha, and thus complementation can be attempted for all three genes.
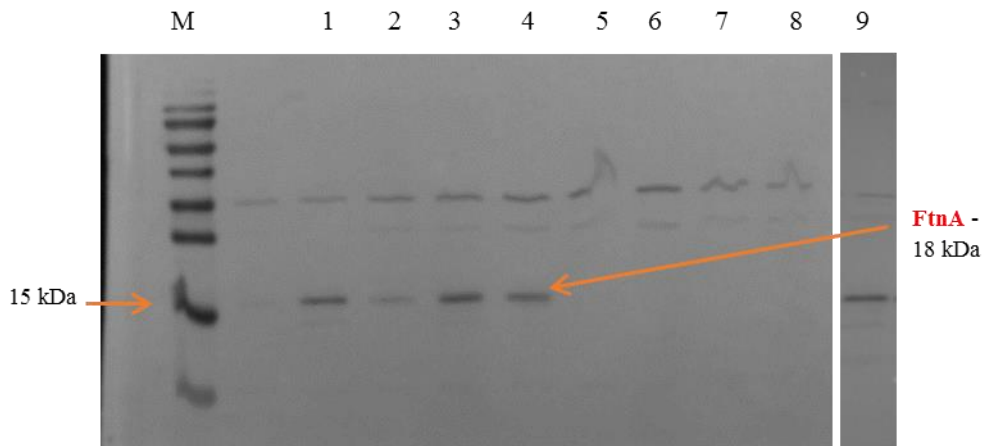
Fig. 4.11 Western blot analysis of the effect of rhamnose on the FtnA status in the *bfr* and *ftnA* complemented triple mutant (BW25113 Δ*ftnA* Δ*dps* Δ*bfr*) +/- rhamnose. Whole-cell extracts pre-cultured in LB with chloramphenicol 50 µg/ml -/+rhamnose 0.02% w/v were subjected to SDS-PAGE followed by western blotting and anti-Bfr staining. **Lane M,** Page Ruler pre-stained protein Ladder; **Lane 1 and 3,** Δ*ftnA* Δ*dps* Δ*bfr* + pBADrha-*ftnA* with rhamnose; **Lane 2 and 4,** Δ*ftnA* Δ*dps* Δ*bfr* + pBADrha-*ftnA* without rhamnose; **Lane 5 and 7,** Δ*ftnA* Δ*dps* Δ*bfr* + pBADrha-*bfr* with rhamnose; **Lane 6 and 8,** Δ*ftnA* Δ*dps* Δ*bfr* + pBADrha-*bfr* without rhamnose; **Lane 9,** wild type BW25113.

4.4 The role of the three iron-storage proteins of *E. coli* in supporting low-iron growth and redox-stress resistance.

4.4.1 Redox stress resistance

Transformants of *E. coli* BW25113 Δ*ftnA* Δ*dps* Δ*bfr* carrying pBADrha-*bfr*, pBADrha-*ftnA* or pBADrha-*dps* were used to assess the ability of each iron-storage protein to support the triple mutant lacking iron-storage capacity during growth in the presence of hydrogen peroxide, a mediator of redox stress that is enhanced by free intracellular iron.

Pre-cultures were in minimal medium (M9) with or without the inducer (rhamnose), in the presence of excess iron (20 µM) to allow iron stores to be deposited, where possible. Subsequent growth in M9 under H_2O_2-induced redox-stress conditions showed that the vector control (uncomplemented triple mutant) grew poorly under redox-stress

conditions (Fig. 4.12A). However, *bfr* pre-induction dramatically increased hydrogen peroxide resistance, decreasing the peroxide-induced lag phase by ~16 h (Fig. 4.12B). Induction of *dps* provided a similar increase in redox stress resistance (~17 h; Fig. 4.10C). However, the over increase in growth initiation (decrease in the length of lag phase) was greater for *dps* induction than for *bfr* induction (H_2O_2 induced lag phase was 3 and 6 h, respectively) indicating that Dps provided a greater resistance to peroxide than Bfr.

In contrast, *ftnA* expression failed to have any notable effect on redox-stress resistance (Fig. 4.12D). Bfr presumably combats peroxide toxicity by sequestration of iron (and possibly H_2O_2), whereas Dps does so by both sequestering iron and decomposing H_2O_2 to prevent iron-catalysed Fenton reactivity (Zhao *et al.*, 2002). The stronger redox-stress protection afforded by Dps cf. Bfr correlates well with its reported physiological role in redox-stress defence and protection against redox-stress mediated DNA damage. The failure of FtnA to provide peroxide resistance appears due to weak expression levels (see chapter 5), rather than to lack of ability to sequester excess iron.

B. pBAD-*bfr*

Growth (OD at 600 nm)

Time (hr)

+ Rha

− Rha

Bfr induction increase peroxide resistance

+ Rha +H$_2$O$_2$

− Rha +H$_2$O$_2$

C. pBAD-*dps*

Growth (OD at 600 nm)

Time (hr)

+ Rha

− Rha

Dps induction increases peroxide resistance

+ Rha +H$_2$O$_2$

− Rha +H$_2$O$_2$

101
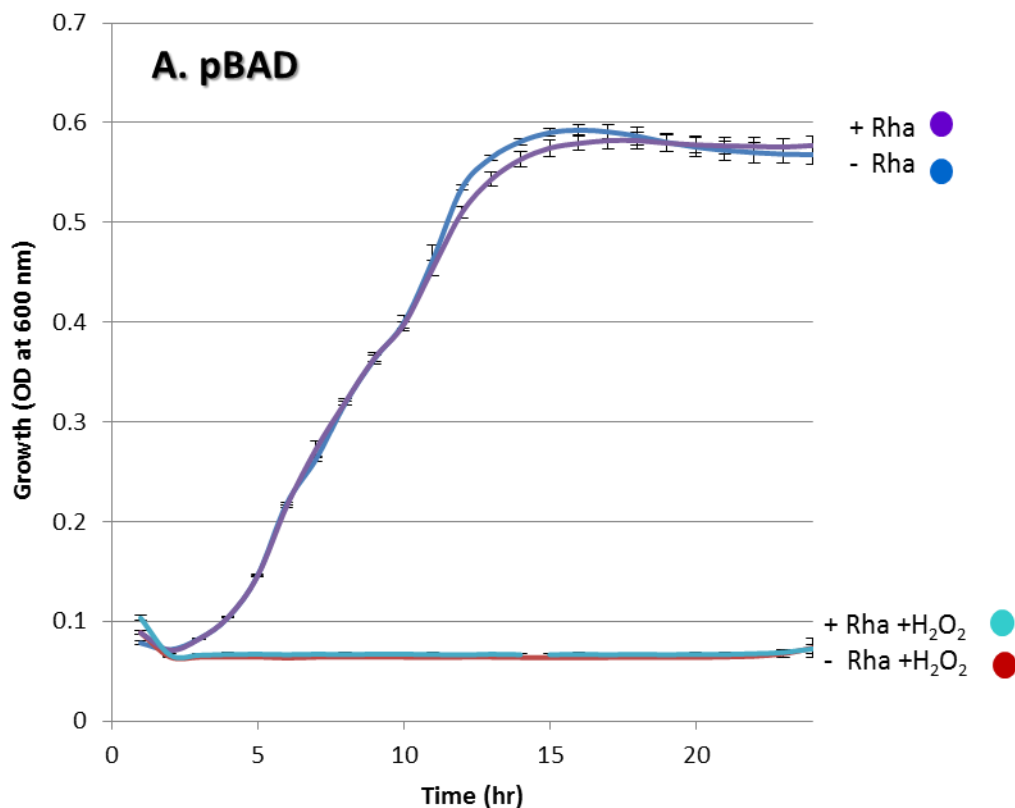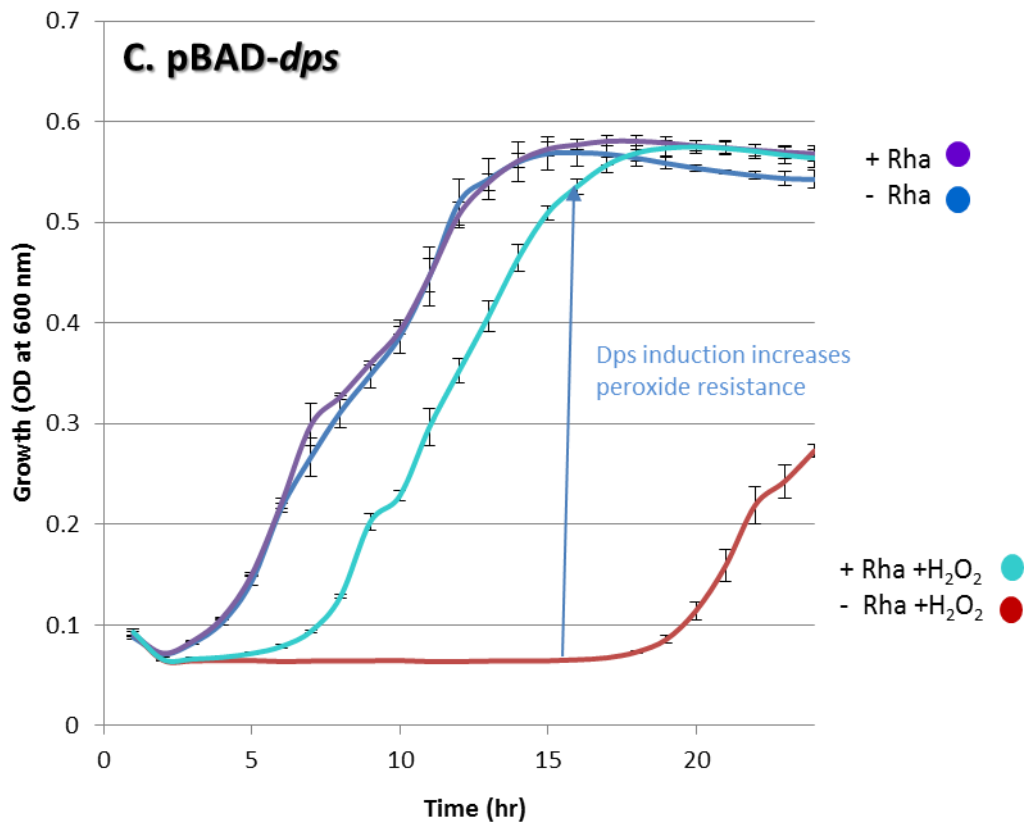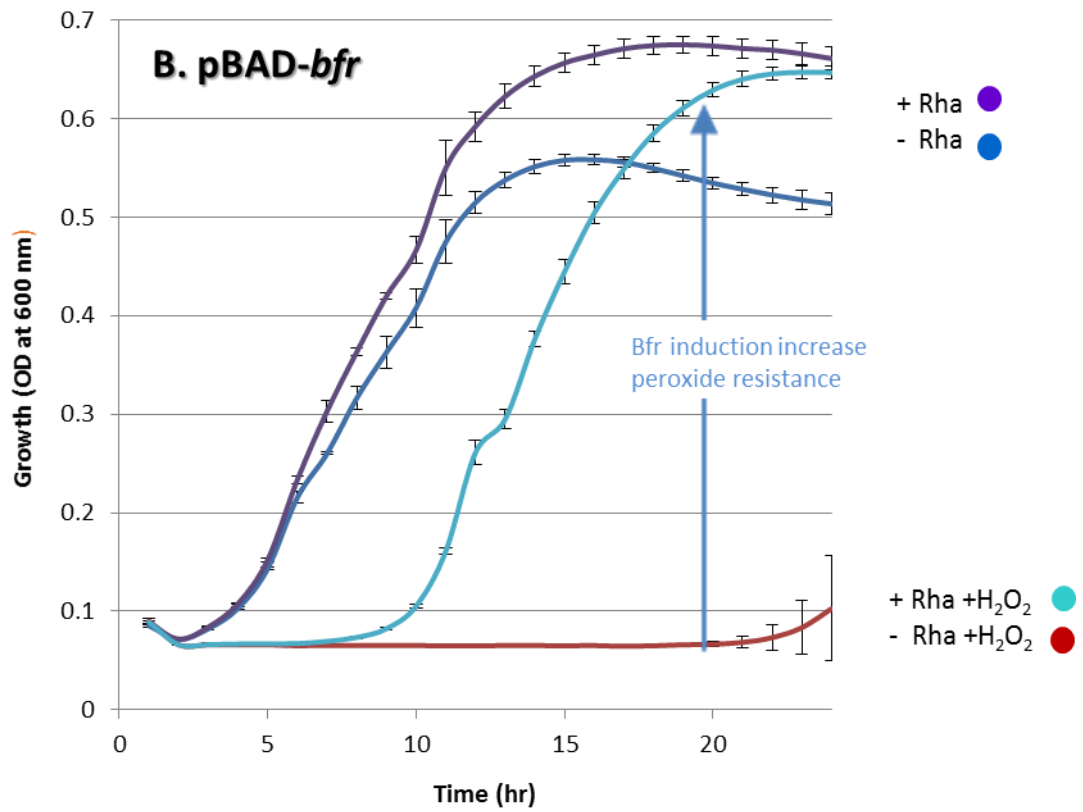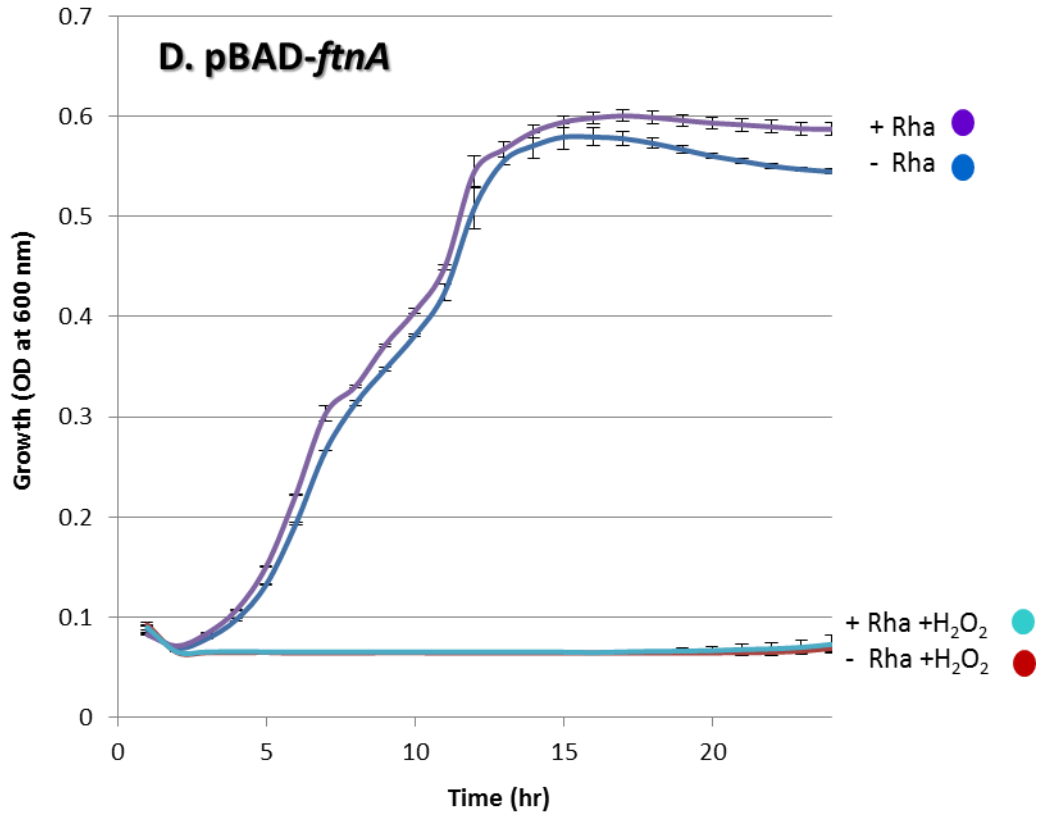
Figure 4.12 Effect of FtnA, Dps and Bfr on growth under redox-stress conditions.
Transformants of BW25113 $\Delta ftnA$ Δdps Δbfr carrying either the pBAD vector (A), pBAD-*bfr*
(B), pBAD-*dps* (C) or pBAD-*ftnA* (D) were grown in glucose M9 minimal medium with 200 µM
H_2O_2 or no additions. Pre-cultures were grown in the same medium but with 20 µM ferric citrate
with/without 100 µM rhamnose (there was no rhamnose in the final culture). Experiments were
performed in triplicate, and were repeated once with similar results obtained (not shown).

In summary, the results show that Bfr and Dps (but not FtnA) can provide resistance to
H_2O_2 when induced prior to exposure from the *rhaBAD* promoter. Note that when iron
was excluded from both the pre- and postcultures, only the wild type was able to grow in
the presence of 200 µM H_2O_2.

4.4.2 The role of the three iron-storage proteins under low-iron growth

The growth experiment, performed as above, was repeated but in the presence of the iron chelator DTPA (instead of hydrogen peroxide) to determine which of the three iron-storage proteins can support bacterial propagation (by supplying iron stores) under iron restriction. Growth under iron restriction was initially performed using 0.25, 0.5 and 1 μM of DTPA as a chelator to identify the concentration showing a significant phenotype of mutant complementation. DTPA at 0.5 μM was subsequently selected to assess the ability of Bfr, Dps and FtnA to support growth under low iron since this concentration gave a major growth inhibition whilst still allowing weak growth (data not shown). The results obtained show that the control (triple mutant with vector) grew very poorly in the presence of the chelator (Fig. 4.13A), increasing by just 0.06 OD units with DTPA but by 0.55 OD units in the absence of chelator (~ninefold difference). The presence of rhamnose had little impact on growth of the uncomplemented triple mutant (Fig. 4.13A). Pre-induction of *bfr* (but not *dps* or *ftnA*) enhanced growth both with and without chelator (Fig. 4.13B). In the presence of chelator, growth increase was 0.05 and 0.20 OD units, without and with rhamnose pre-exposure, respectively, indicating a fourfold increase in growth caused by *bfr* induction. In the absence of chelator, maximum growth increase was 0.49 and 0.61 OD units without and with rhamnose pre-induction, respectively, indicating that *bfr* induction increased growth (by ~25%) even without chelator (Fig. 4.13B). This effect presumably reflects the low iron content of non-iron-supplemented M9 medium. *dps* and *ftnA* induction gave much more modest growth increases with and without chelator, of ~0.025 OD units (Fig. 4.13C & D). The weak ability of FtnA to support iron-restricted growth (with and without chelator) is consistent with its inability to provide resistance to peroxide, whereas for Dps the weak iron-restricted growth effect likely relates to it perceived role in iron detoxification, as opposed to iron storage, together with its relatively low iron-storage capacity.

It should be noted, that when iron was also included in the post-culture, the transformants all grew equally well.

A. pBAD

Growth (OD at 600 nm)

+ Rha
- Rha

+ Rha +DTPA
- Rha +DTPA

Time (hr)

B. pBAD-*bfr*

+ Rha
- Rha

Bfr induction increases
Fe-restricted growth

+ Rha +DTPA
- Rha +DTPA

Time (hr)
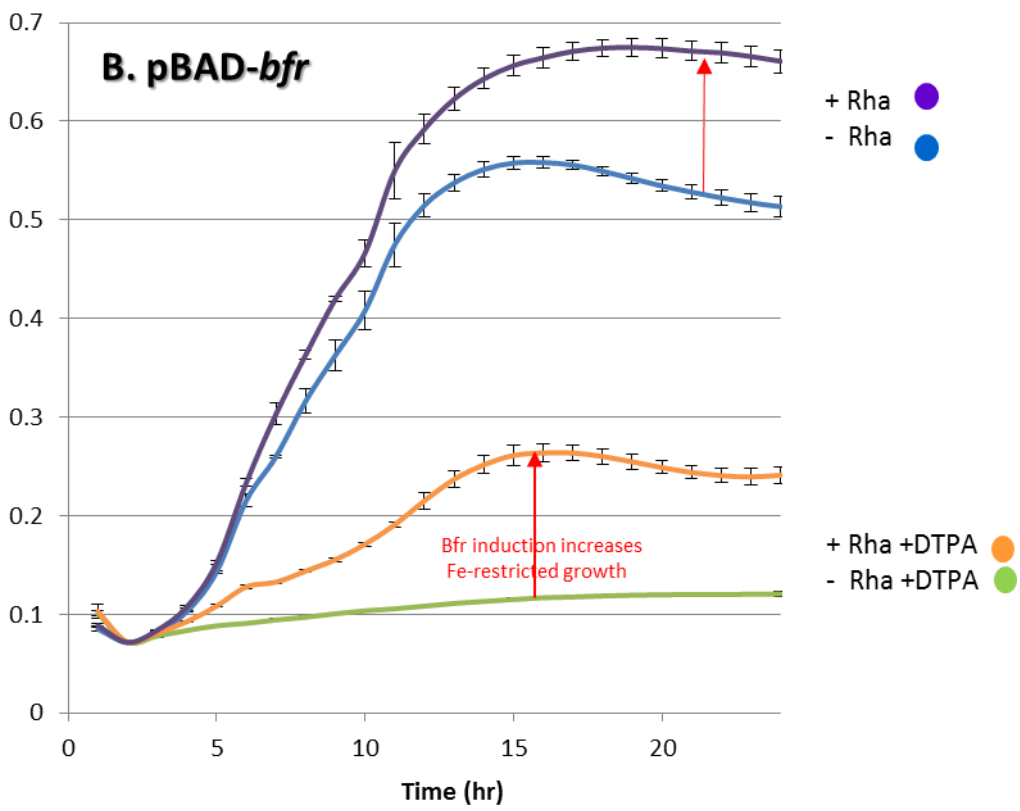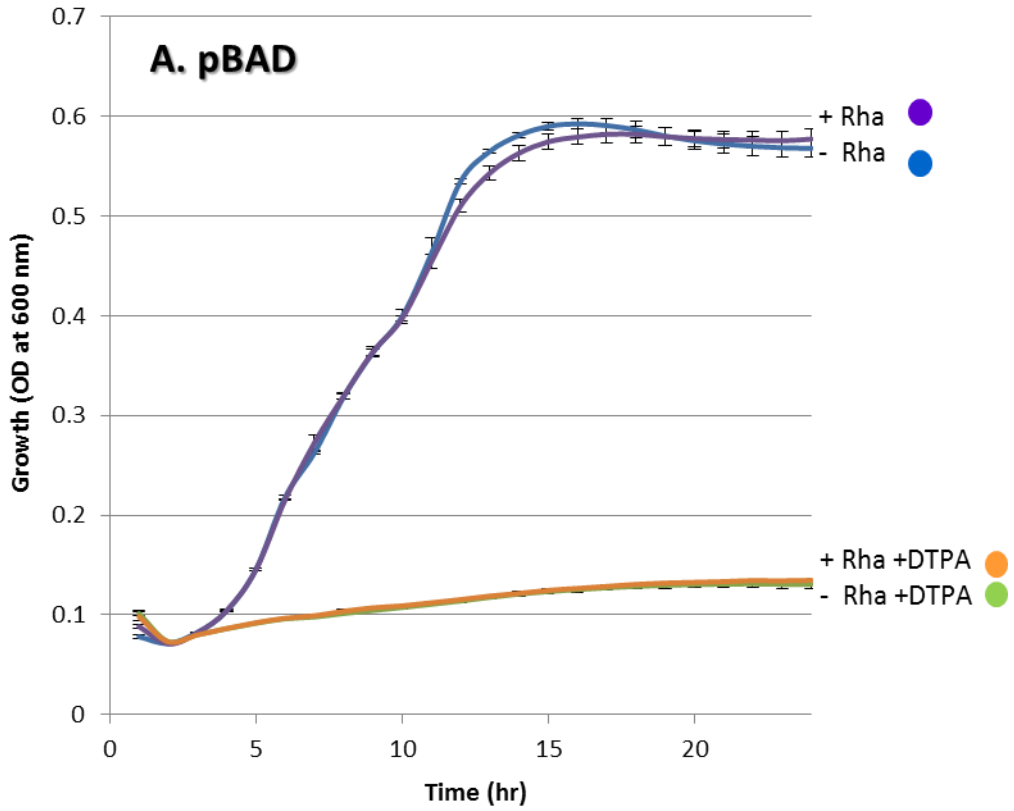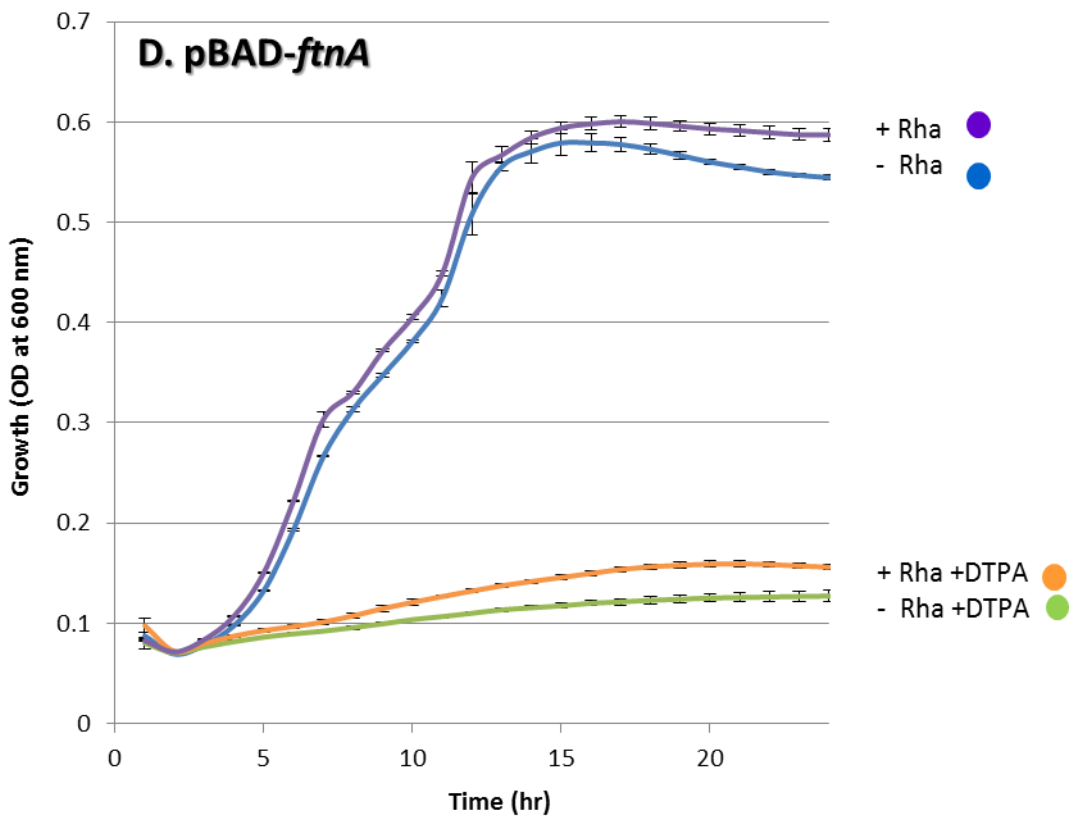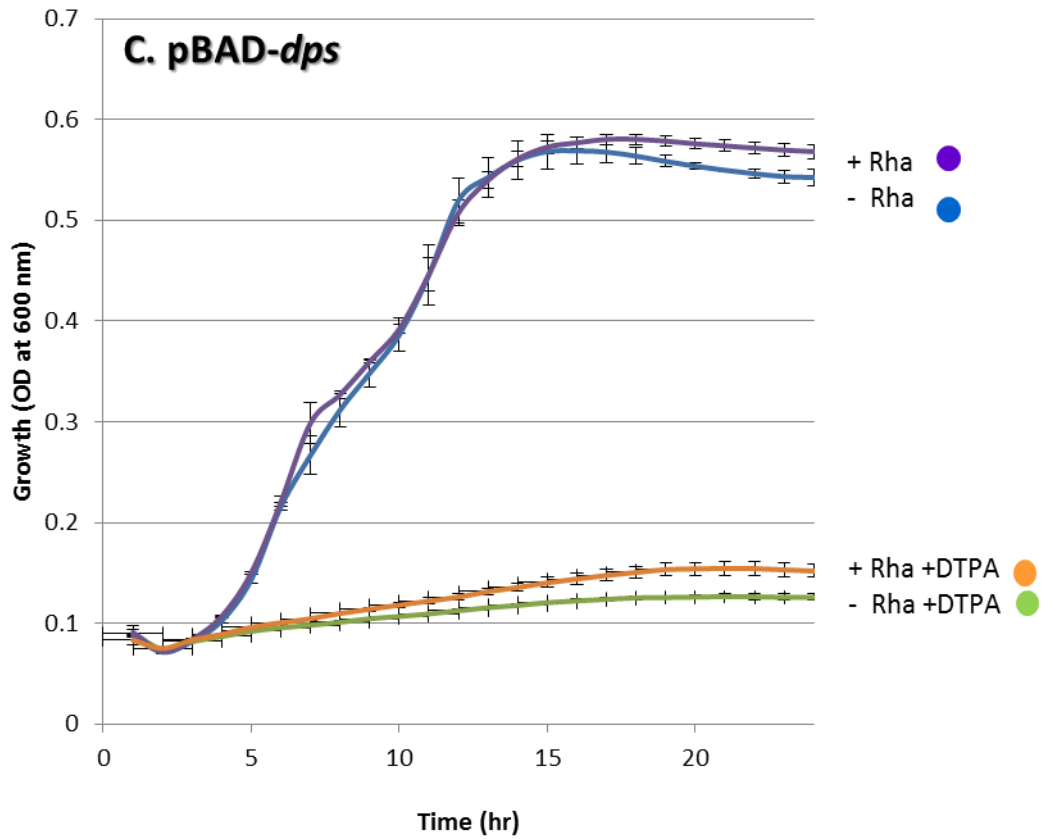
Figure 4.13 Effect of FtnA, Dps and Bfr on growth under low-iron conditions. BW25113 Δ*ftnA* Δ*dps* Δ*bfr* carrying either the pBAD vector (A), pBAD-*bfr (*B), pBAD-*dps (*C) or pBAD-

ftnA (D) was grown in glucose M9 minimal medium with 0.5 µM DTPA or with no additions. Precultures were grown in the same medium but with 20 µM ferric citrate with/without 100 µM rhamnose (there was no rhamnose in the final culture). Other details are as in Fig. 4.12.

4.5 The effect of *bfr*, *dps* and *ftnA* complementation on the total iron content of the *E. coli* iron-storage detective strain

To study the outcome of *bfr*, *dps* and *ftnA* induction on the iron content of *E. coli*, strains were grown overnight in minimal medium and the resulting cell pellet was subject to a ferrozine-based iron assay (Methods section 2.19). The results show that the triple mutant complemented with the empty vector had a significantly lower (46 and 47%) total iron content (Fig. 4.14) compared with the strains complemented with *dps* or *bfr*. However, the iron content of the vector control was only slightly lower (80%) than that of the *ftnA*-complemented strain which corresponds with the observation of the low *ftnA* mediates growth enhancement of the triple mutant under iron restriction condition and the failure of *ftnA* to provide resistance to H_2O_2.

The higher iron content of the *bfr*-complemented strain is consistent with the observed increase in redox-stress resistance and increase in low-iron growth afforded by *bfr* expression. The similarly high iron contents of the *dps*- and *bfr*-complemented stains suggests that the amounts of iron stored in these strains by Dps and Bfr is equivalent, yet the iron stored by Dps did not support iron restricted growth of the triple mutant, unlike that stored by Bfr. This finding thus suggests that although Dps can sequester excess cellular iron to a degree similar to that of Bfr, the iron that it acquires cannot support subsequent iron-restricted growth to the same degree as that sequestered by Bfr. This indicates that iron stored by Bfr is more mobilisable than that carried by Dps.
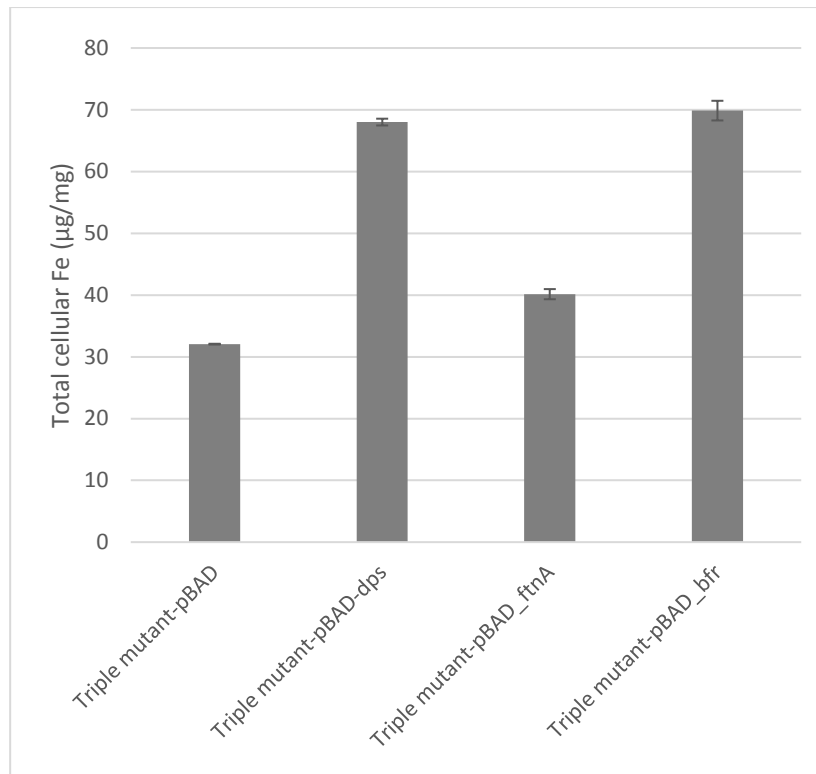
Figure 4.14 Comparison of the effect of *bfr*, *dps* and *ftnA* complementation on the total iron content of the *E. coli* iron-storage detective strain. Total iron content (Ferrozine assay) quantification of *E. coli* BW25113 Δ*ftnA* Δ*dps* Δ*bfr* transformed with the pBADrha-*bfr*, pBADrha-*ftnA* or pBADrha-*dps* or pBAD empty vector, following growth to stationary phase in M9 plus 20 μM . Data is presented as μg iron per mg of cellular protein (Bradford assay, section 2.15.8). Each sample was assayed in technical triplicate and biological duplicate. The experiment was repeated once with similar results obtained. The difference of the total iron content of the Bfr, Dps was significance in respect to the triple mutant complimented with empty vector and the *P*-value < 0.0005 and the defference of the FtnA expression was also significance in respect to the triple mutant with empty vector (*P*-value < 0.005)

4.6 Complementation of the *E. coli* triple iron-storage mutant with 'foreign' iron-storage genes

4.6.1 Selection of target proteins

The aim of this work was to determine whether the mutant phenotype of the triple mutant can be complemented using iron-storage proteins from diverse species. To enable this, an alignment of iron-storage protein amino acid sequences from a random selection of different bacteria and eukaryotes was performed (Fig 4.15). The conserved motifs were identified in an attempt to ensure that the proteins selected are functional (Fig. 4.15). Eight sequences were selected on this basis (in red below).
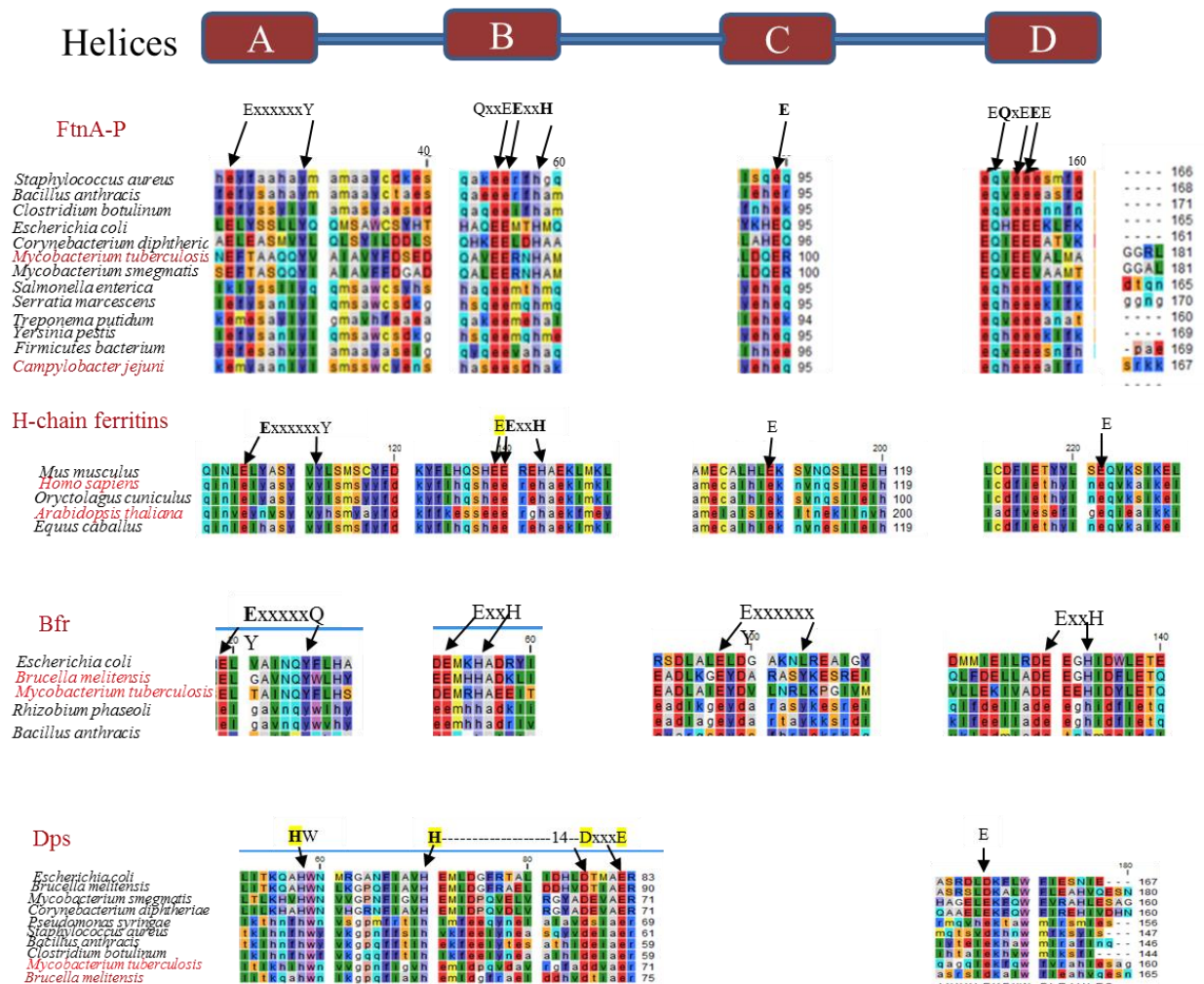
Figure 4.15 Alignment of selected iron-storage protein amino acid sequences for bacterial FtnA, Bfr and Dps proteins, and eukaryotic ferritins. Sequences are from NCBI. Alignment was performed using CLC Genomic Workbench using standard parameters. Sequences in red are those selected for complementation. Key motifs involved in the ferroxidase centre are

indicated, as is the regions predicted to correspond to helices (Andrews, 2010). Only highly conserved regions are shown in each case.

4.6.2 Cloning of the codon-optimized iron-storage genes into the pBADrha inducible vector.

The eight proteins selected above (Fig. 4.15) were as follows:

> FtnA of *Mycobacterium tuberculosis* and *Campylobacter jejuni*
>
> Ferritin of *Homo sapiens* and *Arabidopsis thaliana*;
>
> Bfr and Dps of *Brucella melitensis* and *Mycobacterium tuberculosis.*

The encoding genes were subjected to in silico codon optimisation (with 'GeneOptimizer') and then synthesised by GeneArt[TM], to include *Nde*I and *Bam*HI restriction endonuclease sites at the up- and down-stream ends (section 2.7), respectively. These target genes were PCR amplified using the pMA-T plasmid as a template and the resultant products were cloned into linearized pBADrha (also digested with *Nde*I and *Bam*HI) using a QuickFusion kit. Following transformation, plasmids were isolated and analysed by double digested with *Nde*I and *Bam*HI to confirm the successfully cloning (Fig. 4.16).   Electrophoresis showed the liberation of the inserted fragments which were of the expected sizes (~500 bp for all inserts, except for *ftnA* of *C. jejuni* and *dps* of *B. melitensis* which gave two bands due to internal *Nde*I restriction sites). Plasmid samples which gave the expected DNAbands were confirmed by nuclutied sequencing which confirmed the successful cloning.   The constructed plasmids were then used for complementation of BW25113 Δ*ftnA* Δ*dps* Δ*bfr* to determine their capacity to reverse the phenotypes of the iron-storage mutant strain.
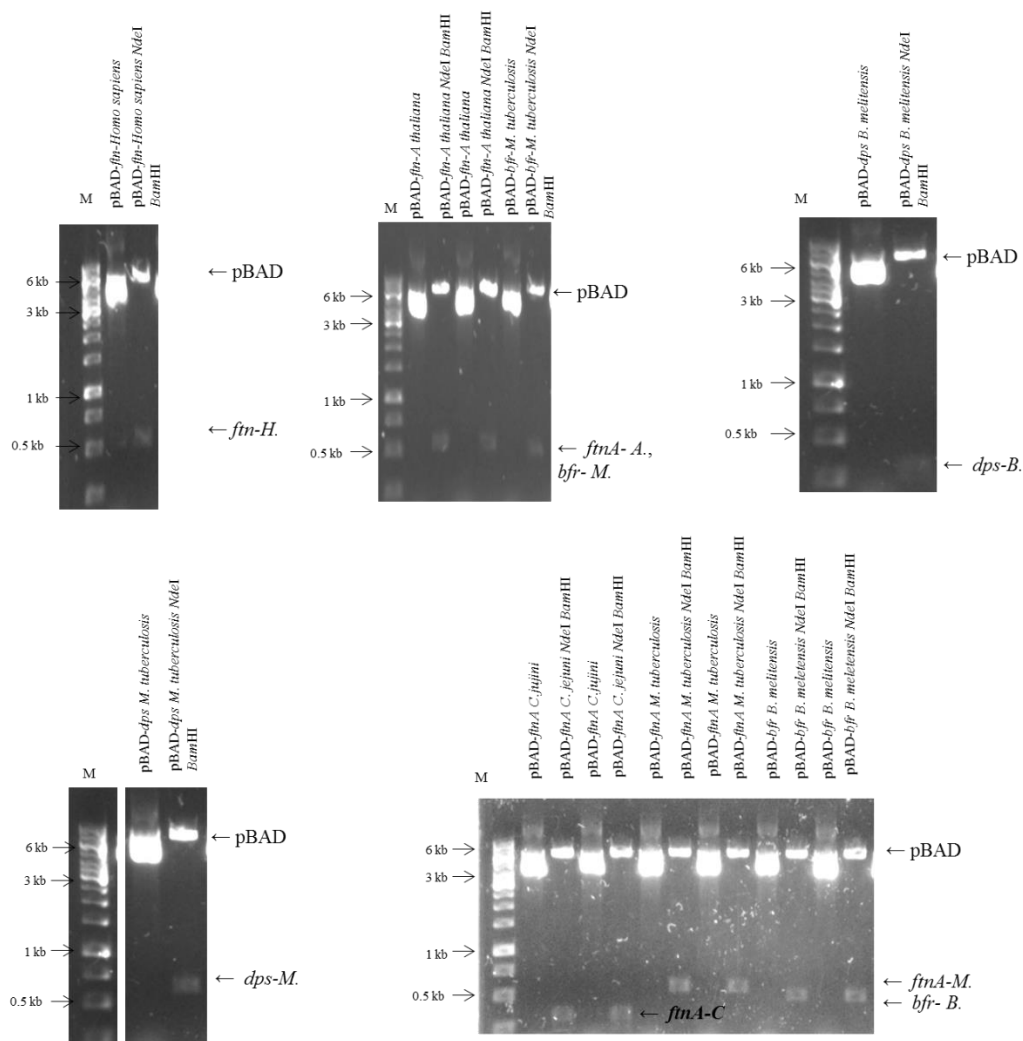
Figure 4.16 Gel electrophoretic analysis of *Bam*H1 and *Nde*I double digested candidate pBADrha clones carrying foreign iron-storage-protein genes. M, 1 kb GeneRuler (Fermentas). The iron storage genes and linearized pBADrha (~6000 bp) vector are indicated. Each plasmid is in digested and undigested form, as indicated.

4.6.3 Expression analysis of the foreign iron-storage protein genes in the *E. coli* triple iron-storage mutant.

Initially, the eight plasmids specifying the foreign iron-storage proteins were tested for their expression levels in BW25113 Δ*ftnA* Δ*dps* Δ*bfr*. Growth was in 0.4% glucose M9 medium with 20 μM ferric citrate, and with/without rhamnose, and was performed

overnight at 37 ˚C and 250 rpm. The production of each protein induced by rhamnose was assessed by the SDS-PAGE analysis of the whole-cell extracts protein. The resulting SDS-PAGE showed no evidence for any band that might suggest the presence of any of the foreign iron-storage proteins (Fig. 4.17). Results obtained with induced were similar to those without induced, and from vector-only controls with no overexpressed bands at expected mobility (~18 kDa). Thus, unlike Bfr and Dps of *E. coli*, no evidence for good expression was obtained (similar to the results obtained for *E. coli* FtnA).

4.6.4 Can the foreign iron-storage protein genes complement the *E. coli* triple iron-storage mutant?

Pre-cultures of all eight transformants (and the vector control) were propagated in M9 medium, with or without the inducer, in the presence of 20 µM iron citrate (to provide the opportunity for iron stores to be deposited). Subsequent growth in M9 under with 200 µM H_2O_2 redox- showed that the complementation had no effect on the growth of the triple mutant, either with or without inducer. Similarly, there was no growth advantage for the transformants with the foreign iron-storage proteins genes under iron restriction conditions (0.5 µM DTPA) (data not shown; repeated one time). This effect could be due to the poor production levels as indicated in Fig. 4.17, possible incorrect assembly (or poor solubility) of the foreign iron-storage proteins in *E. coli* or their failure to function in *E. coli* due to their heterologous nature.

Further work is required to establish whether the foreign iron-storage proteins are indeed weakly produced in *E. coli* and, if these proteins are indeed present, whether they are recoverable in an active form. Currently, it remains unclear why the foreign iron-storage proteins failed to provide any complementary activity in the triple iron-storage mutant.
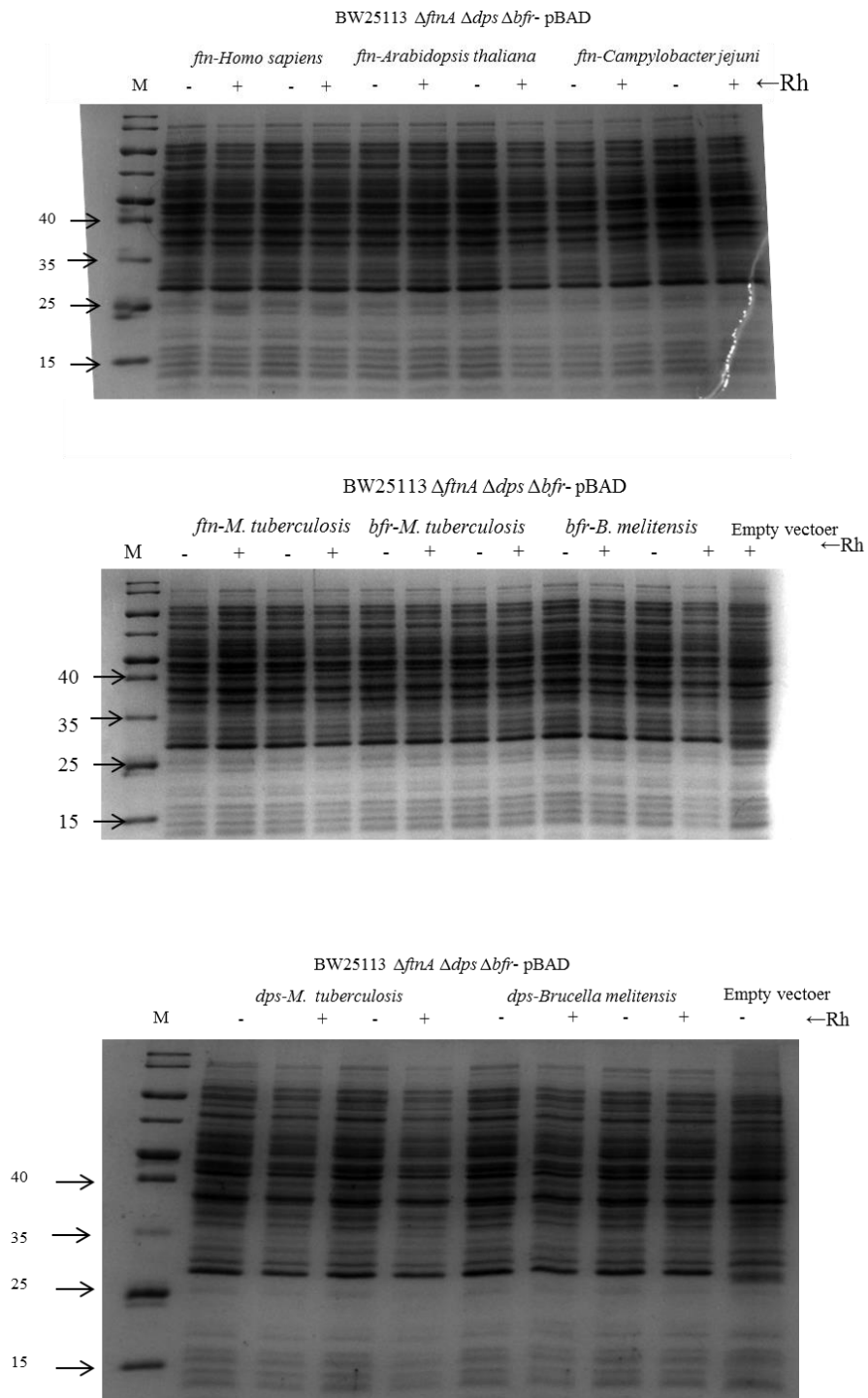
Figure 4.17 SDS-PAGE analysis of whole-cell extracts from BW25113 Δ*ftnA* Δ*dps* Δ*bfr* carrying pBADrha plasmids encoding foreign iron-storage protein genes. M, ladder. Strains were grown as described above, and +/- symbols indicate with/without rhamnose. All samples were analysed in biological duplicate.

4.7 Discussion

In order to assess whether the three iron-storage proteins of *E. coli* are mutually interchangeable when divorced from their natural promoters, and then expressed to similar levels and under equivalent conditions, plasmid pBADrha was used as an inducible vector. This enabled the controlled expression of each iron-storage protein gene from the inducible *rhaBAD* promoter in a mutant that was otherwise devoid of any apparent iron-storage capacity. An experiment to assess the expression levels and rhamnose induction capacity was conducted, and both Bfr and FtnA were found to be present in the absence of rhamnose at levels similar to those of the wildtype when grown in LB medium, as visualized by Western blotting. In addition, only a modest 3-4 fold rhamnose induction was observed. This is may be due to the fact that LB is a rich medium lacking in any glucose which might exert a catabolic repression effect (Ford *et al*., 2014). Analysis of Dps levels were performed subsequently (next chapter) once antibodies to Dps had been prepared.

The results of the experiment performed to assess the ability of each gene to provide redox-stress resistance for the complemented triple mutant showed that both Bfr and Dps enabled a large increase in the hydrogen peroxide resistance of the triple mutant by reducing the peroxide-induced lag phase by 12-14 h. In both cases, Bfr and Dps are presumed to act to resist H_2O_2 toxicity by sequestering intracellular iron and thus limiting iron-mediated Fenton chemistry. The protective role of the overexpressed Bfr in the triple mutant might be also be exerted in the same way as suggested by the Bfr of *Pseudomonas aeruginosa* and *Salmonella enterica* where it acts as an iron source for the haem prosthetic group of catalase (Velayudnan *et al*., 2007; Ma *et al*., 1999). Dps provided a somewhat better response to peroxide toxicity than did Bfr, giving a 3 h growth lag with H_2O_2 compared to 5 h with Bfr (Fig 4.10BC). This may reflect the perceived physiological role of Dps in providing peroxide/Fe toxicity resistance and protecting DNA from Fenton-reactivity-induced damage (Chiancone *et al*., 2004). Such Dps-mediated protection is also achieved by the ability of Dps to bind to DNA and thus limit Fenton-chemistry-induced DNA damage (Martinez and Kolter 1997). Choi *et al*. (2000) also observed that an *E. coli* O157 *dps* mutant shows sensitivity to redox stress and that complementation of the mutant with *dps* increased tolerance to hydrogen peroxide. A similar results of *dps* (or *dpr*) complementation was obtained with the *dpr* gene of *Strptococcus mutans* in an alkyl hydroperoxide reductase-deficient *E. coli* strain,

and it was shown that Dps (Dpr) lowered free cellular iron levels and increased cell viability and DNA integrity under aerobic conditions (Yamamoto *et al*., 2004). Ceci *et al*. (2003) also demonstrated that the Dps protein of *Agrobacterium tumefaciens* confers the same function as that in *E. coli*, through mitigate of the effect of the hydroxyl radicals generated from hydrogen peroxide. In other cases its appears that the Dps protein participates in the bacterial virulence and is required for bacterial survival within the host e.g. for Dps of *Helicobacter pylori* (Ceci *et al*., 2007) where it was demonstrated that Dps has the ability to bind DNA under the low pH conditions of the stomach and prevent its degradation.

Surprisingly, FtnA failed to show a notable growth enhancement under redox stress conditions. Since both Bfr and FtnA are considered to function primarily as iron stores, it is unclear why Bfr would provide an advantage under redox-stress conditions, but FtnA would not. Both Bfr and FtnA are reported to be able to use H_2O_2, as well as O_2, as an oxidant for iron core formation, so both should be able to consume peroxide as well as sequester excess cellular iron (Yang *et al*., 2000; Bou-Abdallah *et al*., 2014). However, the Dps protein prefers to exploit hydrogen peroxide as oxidant for iron core formation, rather than O_2 (Zhao *et al*., 2002; Su *et al*., 2005), which, along with its DNA affinity, explains the ability of Dps to provide DNA protection in response to Fenton chemistry (Chiancone *et al*., 2004)

Under iron-restriction conditions, only iron stored by Bfr was able to enhance growth of the triple mutant to a high degree. This effect was seen both with and without chelators, but was not observed in the absence of induction. Dps and FtnA gave only a weak growth enhancement under low-iron conditions (both with and without chelator). This was a surprising observation in the case of FtnA since Abdul-Tehrani *et al.* (1999) had shown that up to 50% of cellular iron is associated FtnA and that, unlike Bfr, FtnA is able it to act as a major iron source for growth stimulation under iron-restriction conditions. The results obtained above are thus opposite to those reported previously regarding the respective capacities of FtnA and Bfr to provide iron-stores to support iron-restricted growth of *E. coli*. The reason for this discrepancy might be related to the total cellular levels of FtnA and Bfr when expressed from the pBAD vector - a relatively low level of FtnA protein in the cell would prevent the deposition of significant quantities of iron store by FtnA. This possibility will be explored below (in chapter five). The finding of Liu *et al*. (2016) also show that the iron level of the *E. coli* BW25113 triple mutant of iron

storage proteins were not elevated when complemented with an *ftnA* gene carried by a pBAD rhamnose-inducible vector. This finding support the results of the weak growth enhancement generated by *ftnA* overexpression under iron restriction condition.

The failure of Dps to support low-iron growth of the triple mutant strongly reflects the low iron-storage capacity of Dps and its primary purpose in acting as an iron detoxifying protein. The results thus suggest a role in countering of iron/peroxide-induced toxicity but little function in iron storage. This perceived role matches that suggested in the literature (Choi *et al*., 2000; Velayudhan *et al*., 2007; Chiancone *et al*., 2004). However, it should be noted that Dps expression raised total cellular iron levels similar to those achieved by Bfr, which indicates that the Dps-stored iron is not readily available to counter iron restriction. This may reflect a high iron uptake activity, but relatively weak iron release activity.

Both FtnA and Bfr act as iron storage proteins, but the literature shows variation in their function in different microorganism. The main difference between FtnA and Bfr is that the later binds haem as a cofactor. The importance of haem was reveald when it was shown to act as a cofactor that mediates electron donation. This mechanism leads to increases in the formation of iron core in bacterioferitin (Wong *et al*., 2012). Not all Bfrs have the same number of haems per the 24 subunits, the number of haems is between 3-9 in *Pseudomonas aeruginosa* (Kader & Moore 1990), 12 in *E. coli* and less than 12 in *Neisseria gonorrhoeae* (Chen & Morse 1999). Yasmin *et al*., 2011 demonstrate that the heme groups perform an essential role in the pathway of iron release from the bacterioferritin protein in *E. coli*. Bacterioferritin of *Mycobacterium tuberculosis* appears to provide a protective effect in oxidative stress condition *in vivo*, this function was identified when it had been observed that the deletion of the *bfrA* and *bfrB* genes coding for this protein leads to inhibition of the ability of this bacteria to resist oxidative stress conditions created within macrophages as part of the host defence mechanism (Reddy *et al*., 2012). Another study, on the Bfr of *Sallmonella enterica,* also showed that deletion of *bfr* confers sensitivity to hydrogen peroxide and a decrease in the total cell iron content by up to 50% (Velayudhan *et al*., 2007).

Several studies on the *ftnA* gene of *Campylobacter jejuni* showed that FtnA can limit iron-mediated redox stress. However, FtnA protein of *E. coli* did not confer such a phenotype (Abdul-Tehrani *et al*., 1999; Ratnayake *et al*., 2000). The work of Keyer and

Imlay (1996) showed that *ftnA* and *bfr* inactivation did not affect free iron levels content nor redox stress sensitivity. In the plant pathogen, *Erwinia chrysanthemi*, deletion of *ftnA* caused a defect in growth in both iron restriction and redox stress, and both FtnA and Bfr were shown to be required for full pathogenicity (Boughammoura *et al*., 2008). A recent study of Eshelman *et al*. (2017) found that the main iron storage protein in *Pseudomonas aeruginosa* is represented by the BfrB protein, not by FtnA, and also found that the later did not compensate the lack of BfrB.

The variation in the function observed for Bfr and Ftn in different studies likely relate to differences in activity within different species.

The weak participation of pBADrha-encoded *ftnA* in enhancing growth of the triple iron storage mutant in low iron conditions was further explored by examination of the total iron content of the complemented triple mutant. The results showed that the expression of *ftnA* only slightly increased the total iron content of the triple mutant strain; this is probably due to the relatively low expression of ferritin. However, the expression of *bfr* or *dps* in the triple mutant strain significantly raised the total iron content (by ~two fold), thus indicating that the low iron restricted growth of the *ftnA*-complemented triple mutant is likely related its low iron storage content.

In summary, the work in this chapter supports the capacity of Dps to act in redox stress resistance as well as an iron store, and that of Bfr to act in both supporting iron-restricted growth (through providing an intracellular iron store) and in redox-stress resistance. The previous results (Keyer & Imlay 1996; Abdul-Tehrani *et al*., 1999) indicating that Bfr has no notable role in redox stress or iron storage in *E. coli*, presumably arise due to the weaker expression for *bfr* in wild type *E. coli* with respect to that achieved here where *bfr* was under control of a fully induced promoter. Indeed, lack of inducer markedly limited the positive impact of *bfr* on iron content, iron limited growth and redox stress resistance, which clearly demonstrates the need for good *bfr* expression in order for a *bfr*-dependent phenotypes to be observed. The reason for the surprising failure of pBADrha-encoded *ftnA* to exert a marked effect on iron limited growth or redox-stress resistance in the triple mutant is the subject of the following chapter.

Chapter 5

5. Investigation of factors influencing the stability of the FtnA protein in *E. coli*

5.1 Introduction

The results obtained in chapter 4 surprisingly indicate that FtnA provides little capacity to support iron-restricted growth when expressed from pBADrha, which is in contrast to the previous studies reported by Abdul-Tehrani *et al*. (1999) showing that FtnA is the major iron store for *E. coli*. A possible explanation for this effect is that FtnA cellular levels are relatively low when compared to those of Bfr upon induction from the pBAD vector. For this reason, the levels of the three iron-storage proteins were assessed in the BW25113 Δ*ftnA* Δ*dps* Δ*bfr* triple mutant strain complemented with the pBAD-*ftnA*, -*bfr* or -*dps* plasmid. Levels were estimated using SDS-PAGE analysis and by anti-FtnA, -Bfr or -Dps Western blotting. In addition, the second residue of the FtnA protein was altered by synthesis of a modified *ftnA* nucleotide sequence in an attempt to increase the relatively low levels of FtnA (as observed below by SDS-PAGE) and to determine whether FtnA is subject to degradation according to the 'N-end rule'. Furthermore, a preliminary study was performed to determine whether intracellular FtnA levels are influenced by the activity of the proteolytic enzymes of *E. coli*.

 Bacteria, including *E. coli*, possess a number of proteases, including: ClpA, ClpS ClpP ClpX, Lon and FtsH these all belong to AAA+ proteases enzymes (Ogura *et al*., 1999). Each is considered to play an important role in the degradation of cellular proteins which might be incorrectly folded or otherwise damaged. Some proteases, such as FtsH, degrade proteins that are unstable protein (Kihara *et al*., 1995). This is not the only function for proteases, they also participate in regulating several mechanism, which have essential role in the cell growth, including the replication of DNA (e.g. ClpX) and the expression of genes such as E. coli protein membrain by FtsH (Kihara *et al*., 1995). The general degradation mechanism employed can be summarised as the ability of these enzymes to unfold the target protein by identifying the substrate through signal motifs located ether at the N- or the C-terminus of the target protein; this step is followed by delivery of the unfolded protein to the proteolytic core of the protease (Gottesman, 2003) through an 'axial gate' in a hexameric ring formed by these type of protease (Sauer & Baker 2011). This mechanism allows removal of the damaged protein from the cell. The degradation

mechanism might require the presence of an 'adaptor' (e.g. SspB and RssB for ClpX) which facilitates substrate translocation to the enzyme for proteolysis (Dougan *et al.,* 2003). However, the details of the degradation mechanism for some proteases is still unclear regarding the substrate targeting sequences (Tsilibaris *et al.*, 2006).

Thus, the following study included an assessment of FtnA levels in five distinct *E. coli* protease-single-mutant strains, where one of five AAA+ proteases genes had been deleted. This approach was combined with modifying the second residue of the wild type FtnA to address the possibility that FtnA turnover is subject to the N-end rule.

5.2 Levels of FtnA, Dps and Bfr in *E. coli* BW25113 Δ*ftnA* Δ*dps* Δ*bfr* carrying pBADrha overexpressing constructs; estimation by SDS-PAGE and western blotting.

Transformants of the *E. coli* BW25113 Δ*ftnA* Δ*dps* Δ*bfr* triple mutant, carrying plasmids (pBAD-*ftnA*, pBAD-*bfr*, or pBAD-*dps*) expressing the *E. coli* iron-storage protein genes under control of an inducible promoter, were generated in chapter four. In order to determine whether expression from pBADrha succeeds in producing detectable quantities of the corresponding iron-storage, the transformants were propagated in M9 minimal medium supplemented with 20 μM ferric citrate, with and without inducer (100 μM rhamnose). Samples were taken at 16 h of incubation time, and 0.5 OD units of cells were then subjected to SDS-PAGE and western blotting. The results obtained show that the FtnA levels are much lower than those of Bfr and Dps when expressed from the pBAD vector in the triple iron-storage mutant (Fig. 5.1; see Appendices 2 and 3 for subunit molecular weight according to western blot and SDS-PAGE analysis; the standard curve gave estimated protein masses which are reasonable approximations to the mass predicted from its amino acid sequence). Indeed, Bfr and Dps are clearly visible by SDS-PAGE at 5 and 9 % of total protein, respectively. However, FtnA is not visible in the samples from the pBAD-*ftnA* strain, indicating that the levels are below the detectable limit of 1.7 %. However, *ftnA* is indeed expressed (as indicated by western blotting), albeit at a low level. It is notable that non of Bfr, Dps and FtnA are detectable by either PAGE or blotting in the absence of rhamnose. Thus, in glucose M9 medium, the pBADrha vector allows tight control of expression levels. This is in contrast to results obtained in LB where FtnA and Bfr were both generated in the absence of rhamnose and only a modest (3-4 fold)

induction was achieved. As suggested in chapter 4, this discrepancy is likely related to the effect of glucose in eliciting a catabolic repression effect on the *rha* promoter.

The results below correlate well with those in chapter 4 showing that the effect of Bfr or Dps complementation on iron restriction or peroxide resistance was only observed well upon rhamnose induction; it can be assumed that this is due to the strong induction of *bfr* and *dps* in glucose M9 medium by rhamsose. In addition, the results below explain the lack of any effect of FtnA complementation, since FtnA levels are far weaker (at least 5 fold) than those for Bfr or Dps with inducer in glucose M9 medium.

B BW25113 Δ*ftnA* Δ*dps* Δ*bfr* (pBAD/pBAD*ftnA*)

C
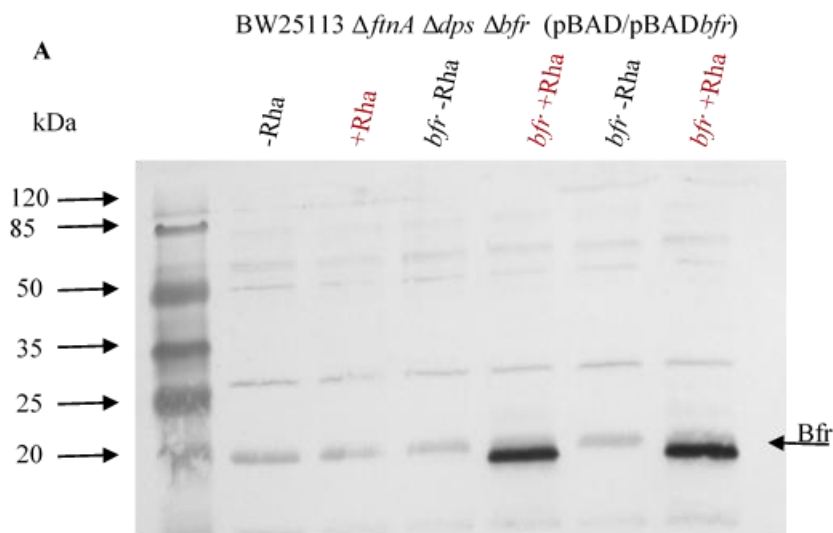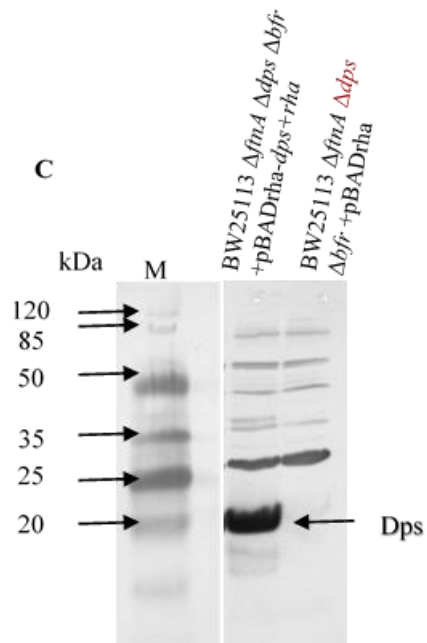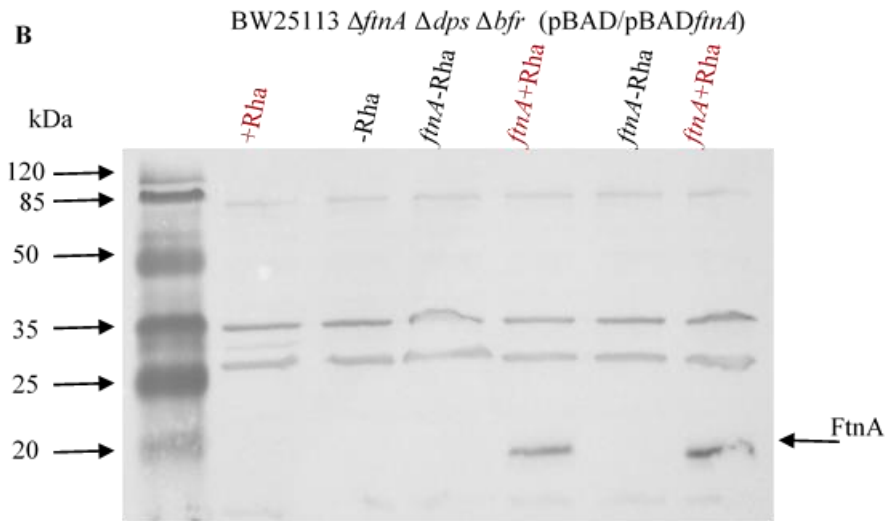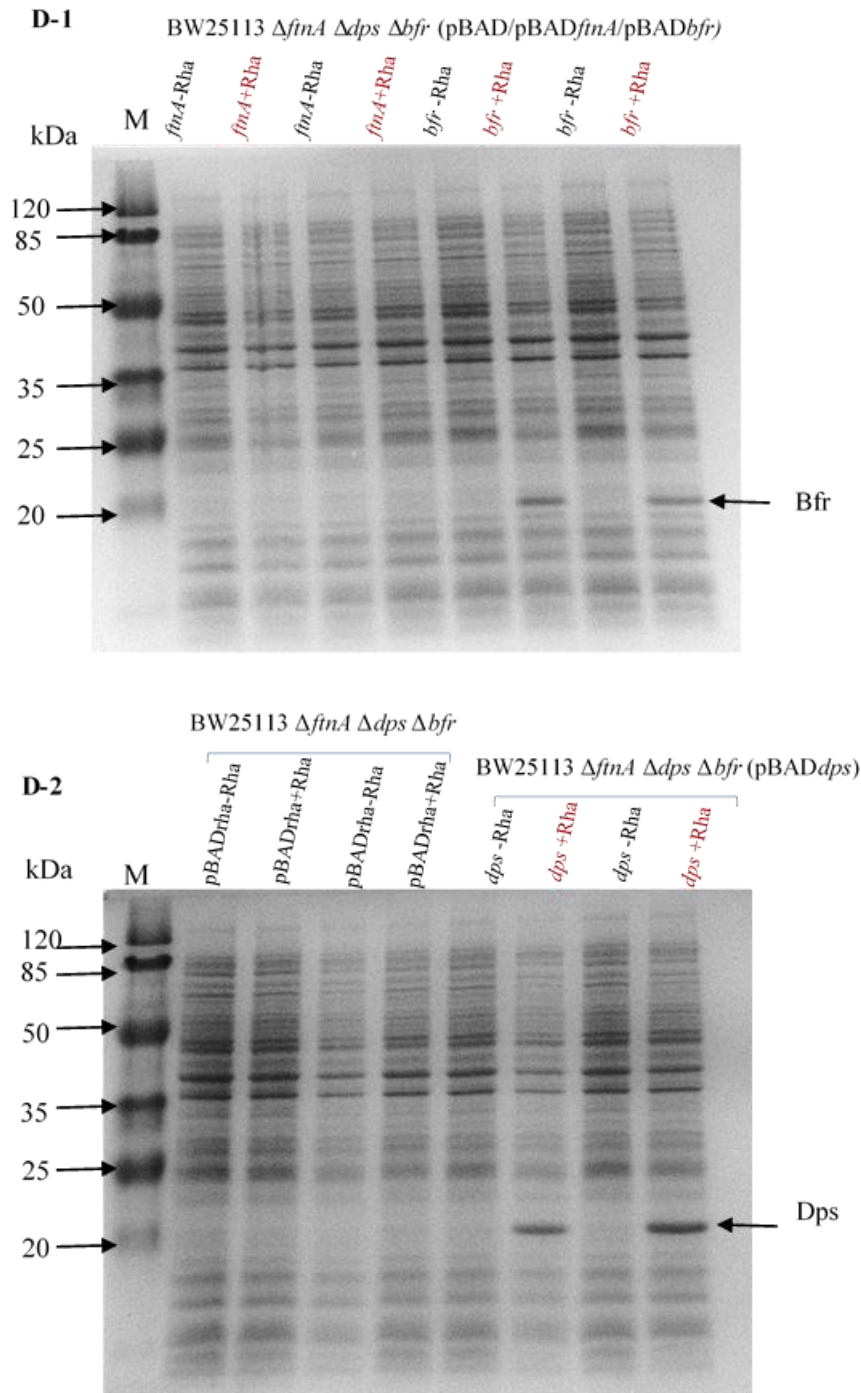
Figure 5.1 Western blotting and SDS-PAGE analysis of the levels of all three iron-storage proteins following expression from pBADrha. BW25113 Δ*ftnA* Δ*dps* Δ*bfr* with pBAD, pBAD-*bfr*, pBAD-*ftnA* or pBAD-*dps* was grown overnight (with/without 100 μM rhamnose) in 0.4% glucose M9 medium supplemented with 20 μM of ferric citrate for 16 h before analysis by SDS-PAGE and western blotting. All samples were analysed in biological duplicate. **A,** anti-Bfr Western blotting analysis; **B**, anti-FtnA Western blotting analysis; **C**, anti-Dps Western blotting analysis; **D,** SDS-PAGE analysis of Bfr, FtnA and Dps levels.

5.3 FtnA levels are greatly enhanced by replacement of residue 2 suggesting that FtnA degradation is subject to the 'N-end rule'.

Previous studies showed that the presence of specific amino acids at the second residue position of proteins provides them with a high level of stability. However, substitution with other types of amino acids decreases their half-life to minimal levels. This effect is explained by the so-called 'N-end rule' whereby in cases where Phe, Leu, Trp or Tyr are at the second amino acid residue of a polypeptide they act as 'destabiliser residues' leading to reduced levels. On the other hand, the presence of Ser, Ala or Thr at the second position provides proteins with high levels of stability and long half-lives (Varshavsky, 1996). The results of Bivone *et al*. (2010) also showed that the level of a protein varies according to the second residue of amino acid sequence according to the N-end rule.

Given the results above, it was decided to consider the N-terminal residues of Bfr, Dps and FtnA within multiple alignments of related iron-storage proteins to determine whether the amino acid at position 2 might be conserved and potentially correlate to the level of the protein as observed above and thus indicate a potential for a turnover process that is subject to the N-end rule. The second residues of *E. coli* Bfr, Dps and FtnA are Ser, Thr and Leu, respectively, and, according to the N-end rule, both Ser and Thr belong to the group of stabilising residues that lead to higher level of protein. However, the second residue of FtnA belongs to the group of amino acids which result in low stability. When the conservation of the second amino acid in the multiple alignment of FtnA was examined, it is apparent that Leu is the most frequent amino acid (at ~90%) among the group of aligned bacterial Ftn proteins, and T, I, S and K are present the remaining 10% (see Appendix 3). Whereas for Bfr multiple alignments, in no case is Leu at position 2; instead they these proteins tend to possess residues (such as Lys 90%, Gln, Phe and Ser these are present in 10 %), and for Dps only two cases (~1%) are Leu at the second residue, and the most frequent amino acid is Ser (at ~45%), followed by Arg and Lys (at ~22 and 9%, respectively). The high frequent residues for Dps and Bfr at position 2 are responsible for high protein stability (see Appendix 4). These observations thus suggest a distinction between Bfr/Dps and Ftn proteins regarding the identity and purpose of their second residues which might explain the differences in protein levels observed above, and that could have biological significance in terms of the manner in which the levels of these proteins are controlled. Thus, variants (L2A and L2K) of FtnA were expressed to test the impact of the second residue on FtnA levels and, specifically, to determine

whether the observed low FtnA level is caused by a high degradation rate resulting from the presence of a 'destabilising' Leu at position 2 of the FtnA polypeptide.

Residue 2 of FtnA was substituted for Ala or Lys ('stabilising' residues), these changes was based on the N-end rule. The two mutant *ftnA* genes were synthesised by GeneArt™, with *Nde*I and *Bam*HI restriction endonuclease sites at the up- and down-stream ends (section 2.7), respectively. The modified *ftnA* genes were provided in the GeneArt vector pMA-T; the corresponding plasmids were designated pMA-*ftnA*(L2K) and pMA-*ftnA*(L2A) (Table 2.4). These were used as a template for PCR using a High Fidelity DNA polymerase kit to amplify the synthesised target genes (Fig 5.2) with primers L2K (F/R) and L2A (F/R) (Table 2.3). The resulting PCR fragments were then cloned into the linearized pBADrha plasmid digested with *Nde*I and *Bam*HI in order to construct the derived pBAD-*ftnA*(L2K) and pBAD-*ftnA*(L2A) plasmids (Table 2.4). The identities of the plasmids thus generated were confirmed by double digestion with *Nde*I and *Bam*HI to release the inserted *ftnA* fragments; these were of same sizes as that of the gel-extracted fragments from the *Nde*I- and *Bam*HI-treated pMA-*ftnA* digestion (note, the wildtype *ftnA* was also included as a negative control). The pBAD-*ftnA*(L2K) or pBAD-*ftnA*(L2A) plasmids were subjected to nucleotide sequencing using primers pBADrha and pBADrh-A (Table 2.3) which confirmed the inclusion of the expected inserts and altered sequences at codon 2.

The constructed plasmids were then used for the complementation of the BW25113 Δ*ftnA* Δ*dps* Δ*bfr* triple mutant. Single colonies of transformants were used to inoculate 5 ml of M9 minimal medium supplemented with 20 µM ferric citrate and 50 µg/ml chloramphenicol with/without 100 µM rhamnose, in test tubes; these were incubated in 37 °C with shaking overnight. Cells were then isolated and whole-cell extracts analysed by western blotting. The bands of the western blots and SDS-PAGE analyses were analysed using ImageJ Tools software, the densities of the western blots bands were compared and this showed that the replacement of the second residue had resulted in a 7 and 6 fold increase in FtnA levels for pBAD-*ftnA*(L2K) and pBAD-*ftnA*(L2A), respectively (Fig. 5.3 A.1). The mutations also show expression of FtnA in the absence of inducer (Fig. 5.3 A.2), although a major rhamnose induction effect remained apparent.

The densitometric quantification of Bfr, Dps and FtnA (Wild type), and FtnA (L2A/ L2K) expression in SDS-PAGE were analysed and the results show that the difference of the

FtnA (of the wild type) expression in respect to Bfr, Dps and FtnA (L2A/ L2K), was significance and the *P*-value < 0.05 (Fig. 5.3 C).
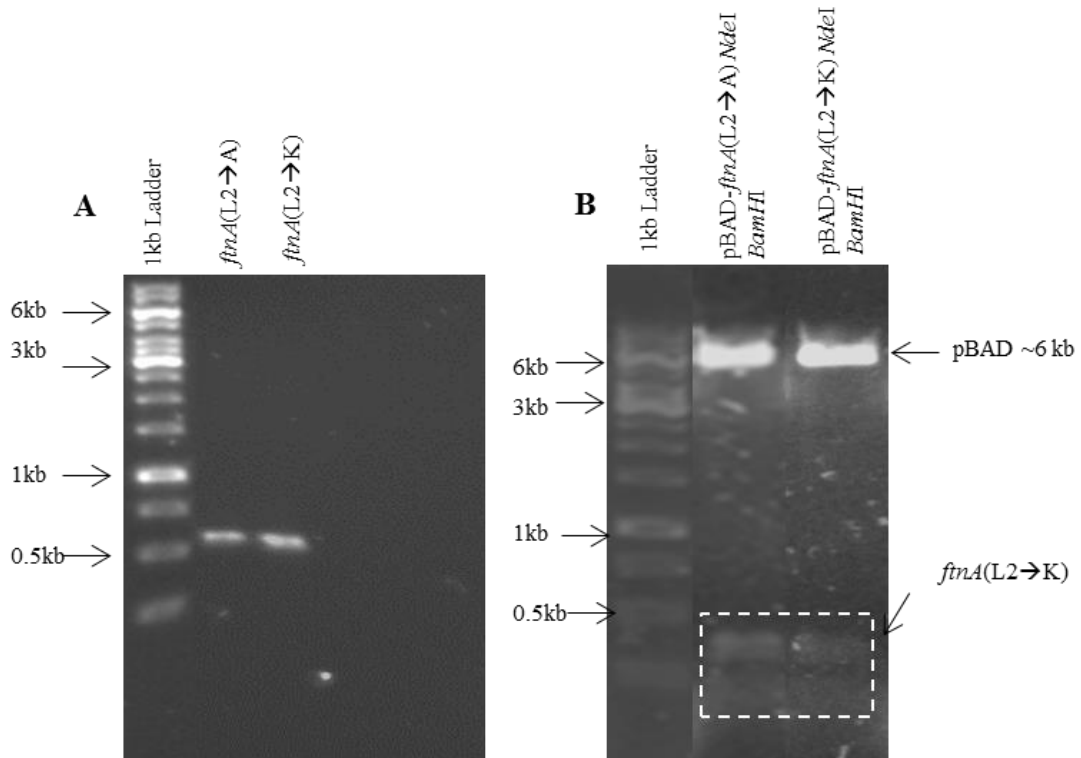
Figure 5.2 Restriction and electrophoretic analysis of the pBAD-*ftnA*(L2K) and pBAD-*ftnA*(L2A) constructs. A, agarose gel electrophoretic analysis of the isolated *ftnA*(L2A) and *ftnA*(L2K) gene fragments released by *Nde*I and *Bam*HI digestion from pMA-T plasmids*;* **B**, the pBAD-*ftnA*(L2A) and pBAD-*ftnA*(L2K) plasmids digested with *Nde*I and *Bam*HI.

A.1   BW25113 Δ*ftnA* Δ*dps* Δ*bfr*-pBAD-*ftnA* +Rha

Wild type   L2→K   Wild type   L2→A

A.2

BW25113 Δ*ftnA* Δ*dps* Δ*bfr*-pBAD-*ftnA* no Rha

Wild type   L2→A   L2→K

B

| | | *ftnA* L2A | | *ftnA* L2K | |

kDa   M   1   2   3   4

20 →   ← FtnA

C
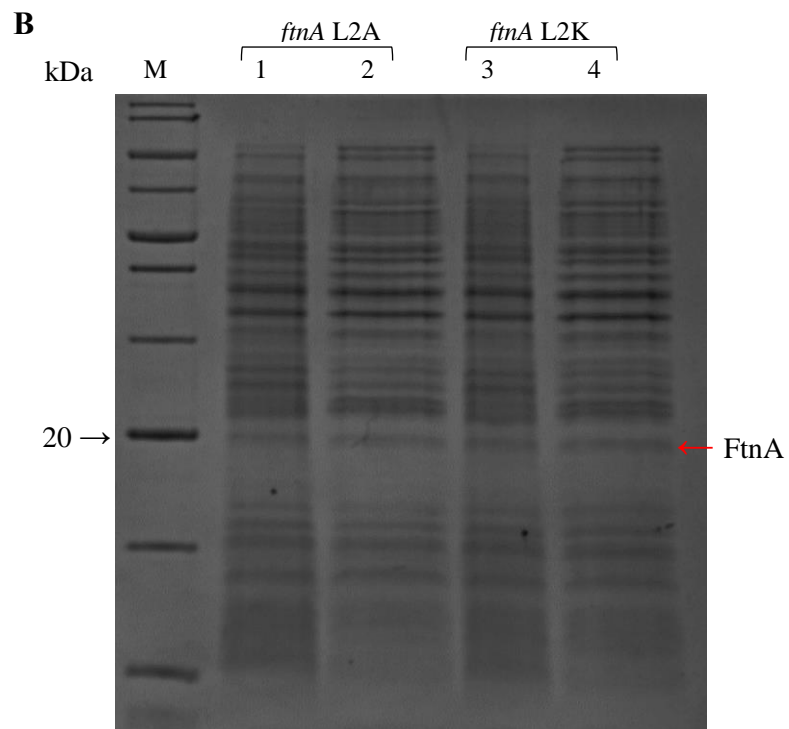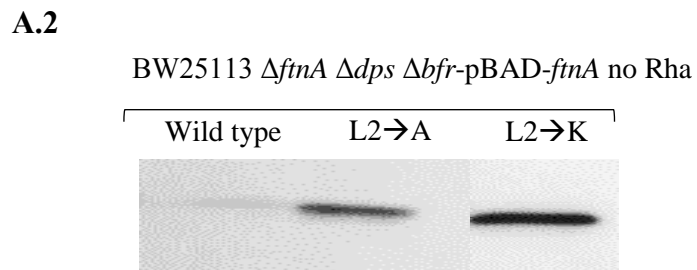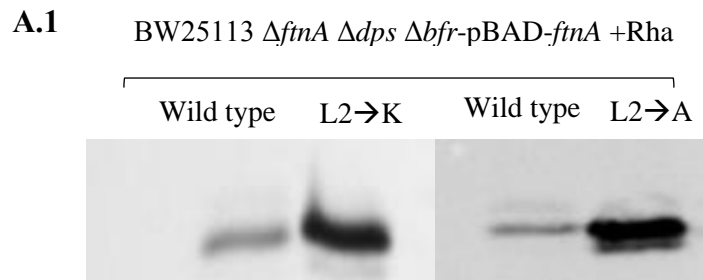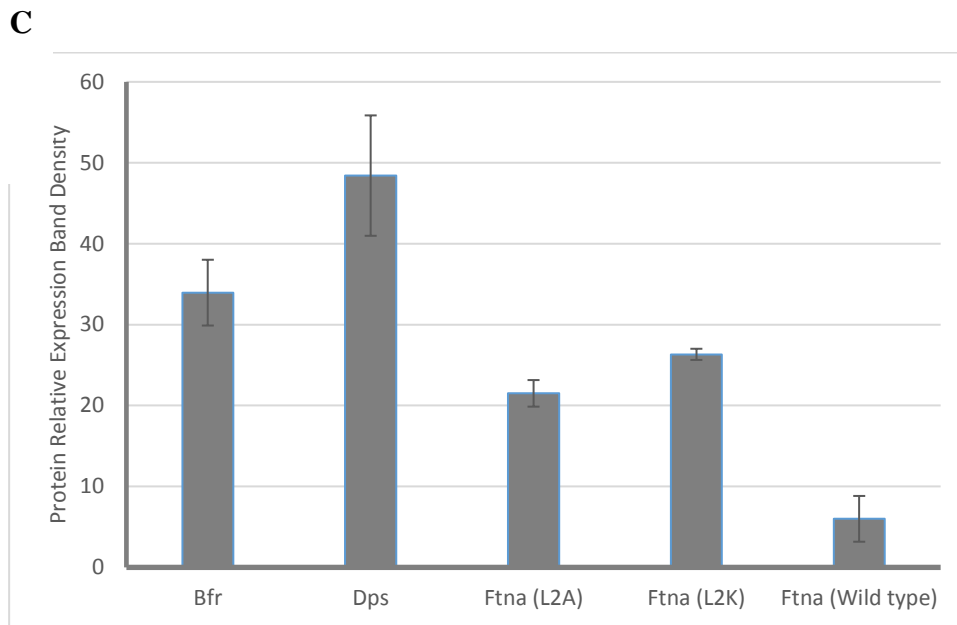
Figure 5.3 A, Western-blot analysis of FtnA levels before and after substitution of the Leu-2 with Ala or Lys. BW25113 Δ*ftnA* Δ*dps* Δ*bfr* with pBAD–*ftnA,* pBAD-*ftnA*(L2K) or pBAD-*ftnA*(L2A) were grown overnight in 0.4% glucose M9 medium with 20 µM of ferric citrate (**1,** with 100 µM rhamnose; **2,** without rhamnose) before analysis by western blotting using anti-FtnA serum.

B, SDS-PAGE analysis of the levels of FtnA (L2A/ L2K) following expression from pBADrha. BW25113 Δ*ftnA* Δ*dps* Δ*bfr* with pBAD-*ftnA*(L2K) or pBAD-*ftnA*(L2A) were grown overnight in 0.4% glucose M9 medium with 20 µM of ferric citrate, were grown overnight (with 100 µM rhamnose) in 0.4% glucose M9 medium supplemented with 20 µM of ferric citrate for 16 h before analysis by SDS-PAGE. Samples were analysed in biological duplicate.

C, **Densitometric quantification of Bfr, Dps and FtnA (Wild type), and FtnA (L2A/ L2K) expression of the SDS-PAGE analysis (from B and Fig.5.1, D)**. The difference was significance for FtnA (Wild type) in respect to the rest of proteins, and the P-value < 0.05. The density of the immune-reactive bands were measured using ImageJ Tools software

The above results thus suggest that FtnA turnover is subject to the N-end rule, which would explain the low levels of pBADrha-expressed FtnA with respect to levels seen for Bfr and Dps.

A further experiment was performed to determine the levels FtnA (L2, L2A and L2K) versions) in the triple mutant at different time points during the growth curve. Overnight

cultures in M9 minimal medium (with 20 µM ferric citrate and 50 µg/ml chloramphenicol) were used to inoculate 50 ml of the same medium, and then growth was achieved at 37 °C and 250 rpm. Once the OD reached 0.5, 100 µM rhamnose was added, as inducer, and samples taken at 1, 2, 4, 6, 8 and ~16 h after induction at 37 °C and 250 rpm. Western blot analysis showed that the replacement of the second residue for Ala or Lys resulted in the more rapid and greater appearance of FtnA following induction, with FtnA detected at 1 h post induction for the L2A/K mutants, rather than 4 h, as for the wildtype FtnA (Fig. 5.4 A).   In addition, the FtnA levels were far higher for the L2A/K variants than for the wildtype at all time points where FtnA was detectable. Plots of western-blot staining density against time suggest a 4.2 -4.6 fold increase in FtnA resulting for the L2A/K alterations after 4 h of the rhamnose induction (with respect to the overnight culture) and an even greater increase of ~8 and 9 fold (L2A/K) at 24 h post induction (Fig. 5.4 B) the difference was significant (P-value < 0.05). Note that no FtnA was observed at 0 h post induction – this is presumed to reflect the weak expression of the pBADrha encoded *ftnA* gene from the *rha* promoter in the absence of inducer.

 In summary, these results further suggest that FtnA is subject to rapid turnover through 'N-end rule'-dependent degradation (Dougan *et al.*, 2010). Such turnover could be important in the control of the build-up of FtnA iron stores and in the subsequent release of iron stores at the early stages of the growth cycle, and during iron-limited growth. Thus, N-end rule dependent FtnA turnover may assist the release of iron from FtnA in *E.coli*, and by inference this may be also the case in many other bacteria.
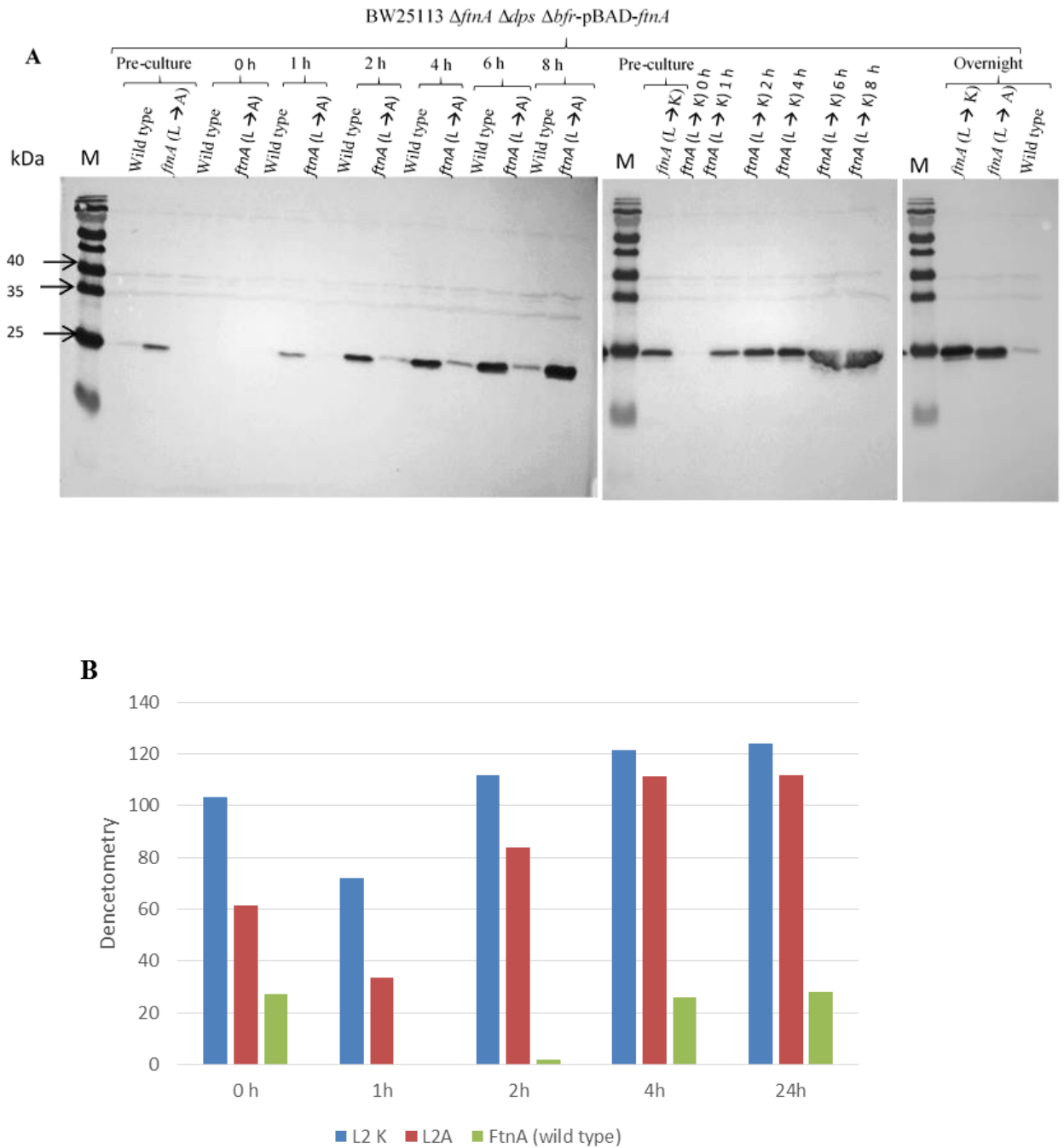
Figure 5.4 Representative western blot analysis of the effect of the L2A/K substitutions on FtnA levels over the course of the *E. coli* growth cycle. Cultures of the BW25113 Δ*ftnA* Δ*dps* Δ*bfr* with pBAD–*ftnA,* pBAD-*ftnA* (L2K) or pBAD-*ftnA* (L2A) were grown in M9 medium (with 20 μM ferric citrate).   Pre-cultures were grown in M9 medium with 20 μM ferric citrate. Chloramphenicol at 50 μg/ml was included throughout. Once the growth reach 0.5 OD, 100 μM rhamnose was added and whole-cell extracts (taken at the indicated time-points after induction with rhamnose; 0.05 OD600 units of bacterial cells) were subjected to SDS-PAGE followed by

anti-FtnA western blotting (**A**). **B**, densitometric quantification of FtnA levels (L2K, L2A and the FtnA of the wild type) v time.The immune-reactive bands were analyzed using ImageJ Tools software and their densities were compared.

It was considered important to determine whether the cellular half-life of FtnA is affected by the L2A/K substitutions, since although the above results indicate that overall FtnA levels are increased by the substitutions, the mechanism involved has not yet been investigated. In theory, the half-life of FtnA could be tested by inducing *ftnA* expression from pBADrha in the pre-culture and then measuring the persistence of the FtnA protein during subsequent growth in the absence of inducer. Since further *ftnA* expression should be largely repressed due to absence of inducer, any remaining FtnA would be expected to be derived from that expressed in the pre-culture and decline in levels would be due to degradation and/or dilution resulting from growth.

Thus, pre-cultures were grown overnight in M9 minimal medium in the presence 100 μM of rhamnose and 20 μM of ferric citrate (cells were then harvested and washed to remove rhamnose, before being used to inoculate 50 ml cultures of the same medium supplemented with iron, but without rhamnose). Samples were taken at various times during growth following inoculation and these were analysed by anti-FtnA western blotting.

The results show that wildtype FtnA as expressed from pBADrha, exhibits a rapid reduction in levels over the first 30 min of growth following inoculation (Fig. 5.5A); during this first 30 min period the culture exhibited only a slight increase in density (1.7-fold) suggesting that the initial reduction in levels is likely due to degradation. The FtnA L2A and L2K variants showed an initial reduction in levels (by 1.7 and 1.3, respectively) at 30 min post inoculation, but little further reduction in levels was observed at latter time points (Fig. 5.5A & B). This is surprising since the culture density increased by 0.07 OD unit over this time which would be expected to result in a reduction in FtnA-L2A/K levels through dilution effects. The lack of decline in FtnA-L2A/K levels beyond 30 min suggests that the FtnA protein is still being synthesised even in the absence of the inducer, this may arise as a result of leaky expression, or a hysteresis effect, from the inducible pBADrha promoter.

A — BW25113 Δ*ftnA* Δ*dps* Δ*bfr*-pBAD-*ftnA*

B — BW25113 Δ*ftnA* Δ*dps* Δ*bfr*-pBAD-*ftnA*

C

D

E
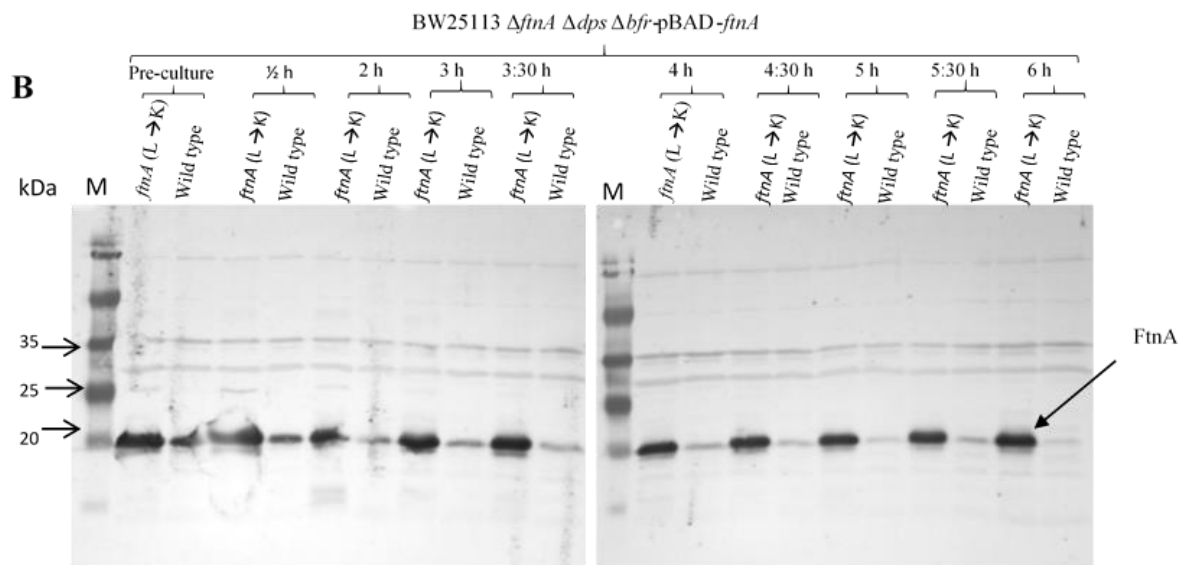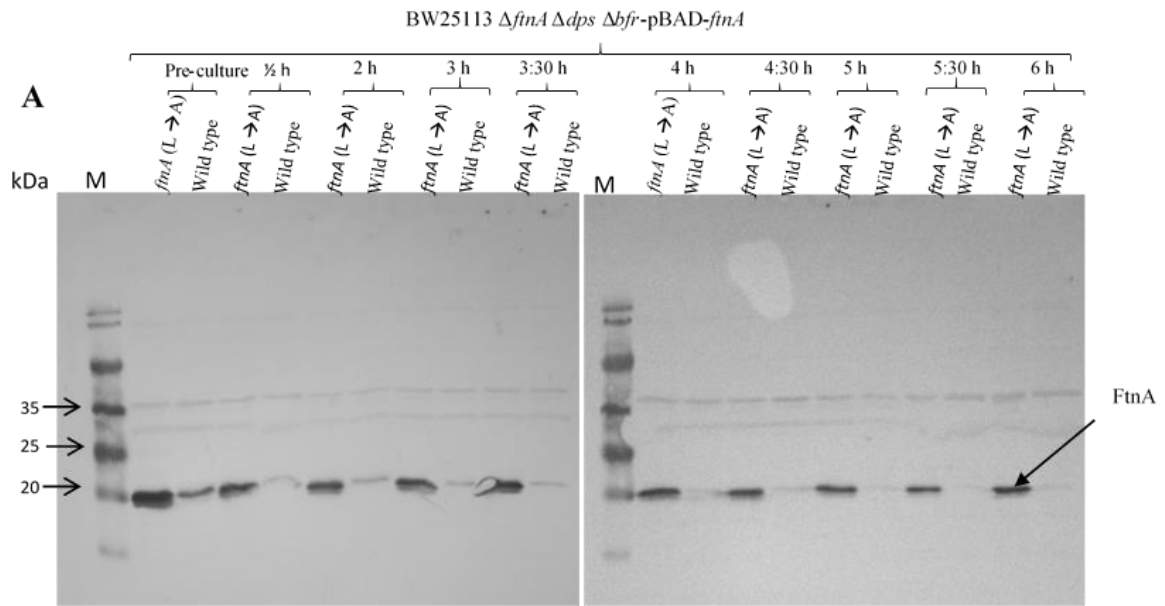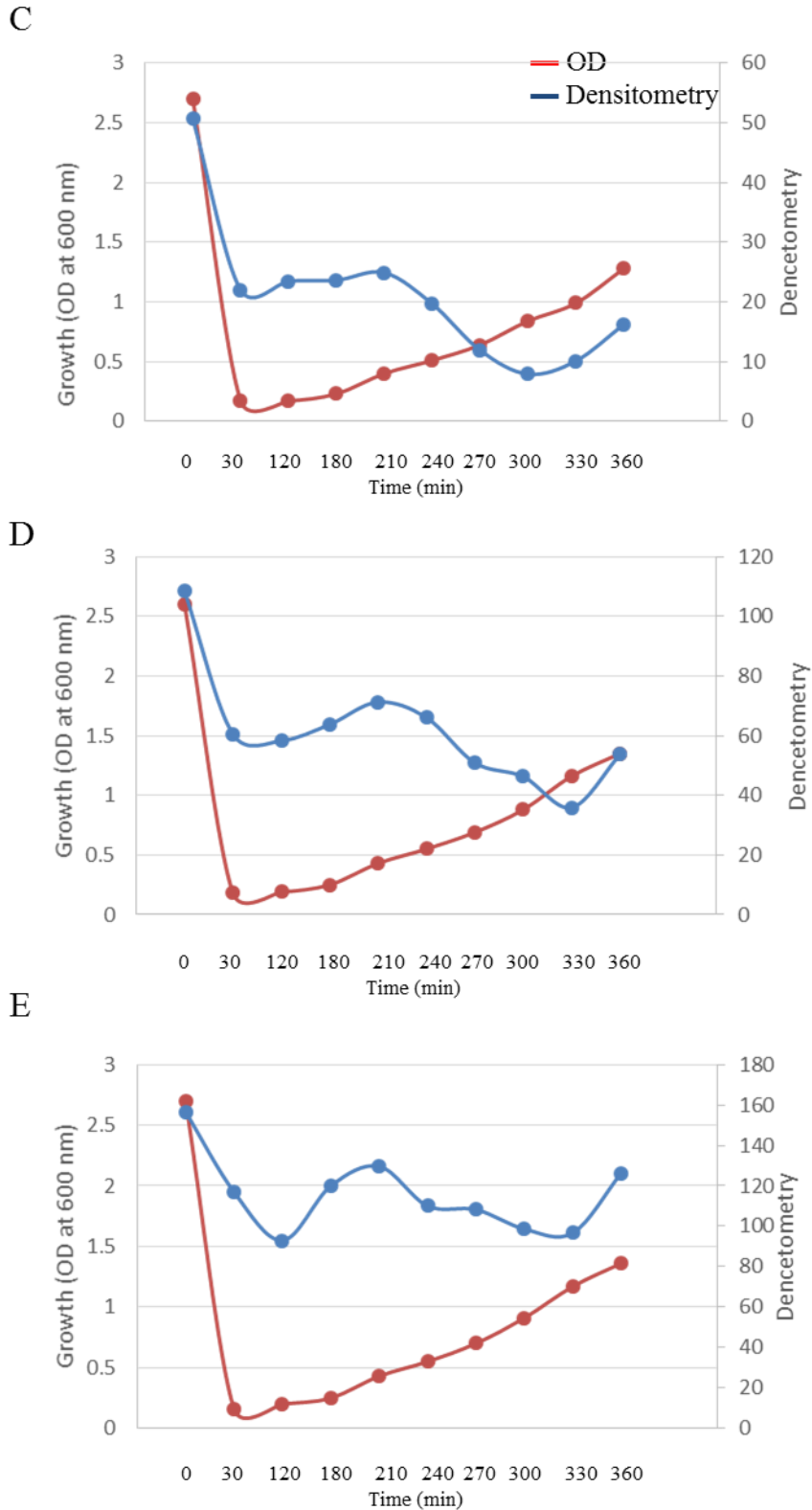
Figure 5.5 Western-blot analysis of the effect of the L2A (A) and L2K (B) substitution on FtnA stability. BW25113 Δ*ftnA* Δ*dps* Δ*bfr* carrying pBAD–*ftnA* or pBAD-*ftnA*(L2A/K) was grown in 50 ml of M9 medium with 20 µM of ferric citrate in the absence of inducer; pre-cultures were in grown in the same medium but with 100 µM of rhamnose. Inducer was removed from

the pre-culture before inoculation by washing cell pellets. Samples were taken at different time points following inoculation and analysed by anti-FtnA western blotting.
Plots of density and growth culture (OD) v time for BW25113 Δ*ftnA* Δ*dps* Δ*bfr* carrying pBAD–*ftnA,* **C**; pBAD-*ftnA*(L2A), **D**; pBAD-*ftnA*(L2K), **E**. the red line represent the OD and the blue line represent the densetometry.

In spite of the leaky expression as an explanation of the above observation, the differences in the degradation rate might be involved for more clarification. The densitometry quantification of the immune-reactive bands of the western blot of the FtnA expression (L2K, L2A and the FtnA of the wild type) show that the degradation rate of both FtnA L2K and L2A (in the time period between 30 min to 300) was about 1.1 and 1.3 fold, respectively. However the degradation rate of the FtnA (wild type) was about 2.7 fold (in the duration time between 30 min to 300 min); as shown in Figure 5.5B. So part of the high decline rate for the FtnA (of the wild type) is related to the degradation whereas the L2 mutants show low decline rate of FtnA levels, in addition to the leaky expression or a hysteresis effect of the vector promoter, might reflect that these protein are more stable than that of the wild type. This suggest that the replacement of the second residue with high stabiliser residues (A/K) leads to produce stable protein, this is agreement with previous publication (Varshavsky 1996; Bivone *et al*., 2010; Bittner *et al*., 2015).

5.4 The effect of the L2A/K replacements on the ability of FtnA to support growth under low-iron conditions

The previous studies reported in chapter 4 indicated that FtnA expressed from pBADrha could not support the low-iron growth of the *E. coli* iron-storage mutant effectively, nor was any notable resistance to redox stress provided. The results above indicate that this could be due to the low levels of FtnA arising as a result of 'N-end rule'-dependent turnover. Thus, growth experiments were performed to determine whether the increased levels of FtnA resulting from the L2→A/K substitutions enable the altered FtnA to enhance growth of the triple mutant under iron restriction. Growths were performed as before (Fig. 4.13) with rhamnose induction in the pre-culture in the presence of excess iron, and subsequent growth comparisons performed in the absence of inducer and added iron, but with or without 0.5 μM DTPA. The results show that the iron-restricted growth of the triple mutant is notably enhanced when complemented with pBAD-*ftnA* (L2A) or pBAD-*ftnA* (L2K) (Fig. 5.6). In the presence of 0.5 μM DTPA, induction of FtnA-L2A and –L2K production enhanced growth by 2.5- (from an OD increase of 0.2 to 0.5) and

2.1- (from an OD increase of 0.2 to 0.43) fold, respectively; and in the absence of DTPA induction increased low-iron growth density increase of 0.55 to 0.78) and 41% (from a density increase of 0.57 to 0.77), respectively (Fig. 5.6). This observation is consistent with the results of Abdul-Tehrani *et al*. (1999) who showed that up to 50% of cellular iron is associated FtnA and that iron stored in FtnA can support low iron growth. However, FtnA did not contribute to hydrogen peroxide resistance, except in a *fur* mutant background. This finding is consistence with previous work which showed that the sensitivity of an *E. coli fur* mutant to hydrogen peroxide is reversed by FtnA overexpression (Touati *et al*., 1995), where it was concluded that this effect arose due to the ability of FtnA to reverse of the high levels of 'free' cytosolic iron caused by the *fur* mutation.

The reason for the failure of FtnA to provide resistance to H_2O_2 when produced in the triple storage mutant may relate to an inability of FtnA(L2A/K) to utilise H_2O_2 as an oxidant for iron uptake as effectively as Bfr and Dps.
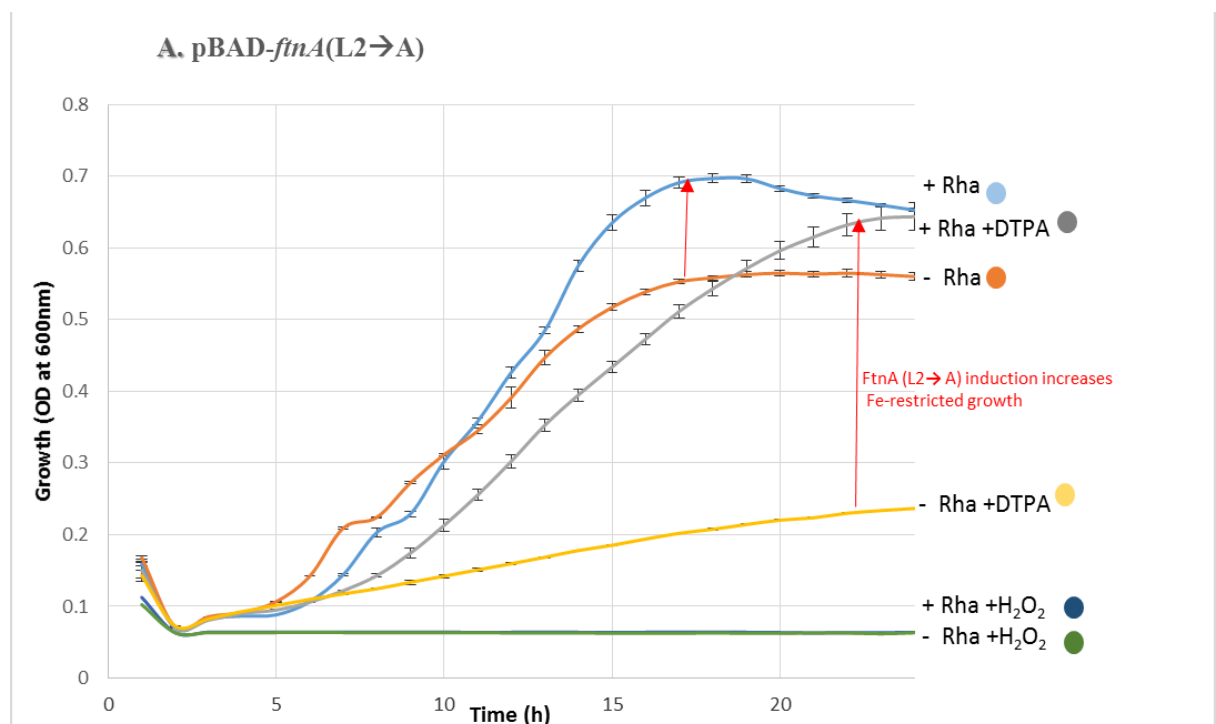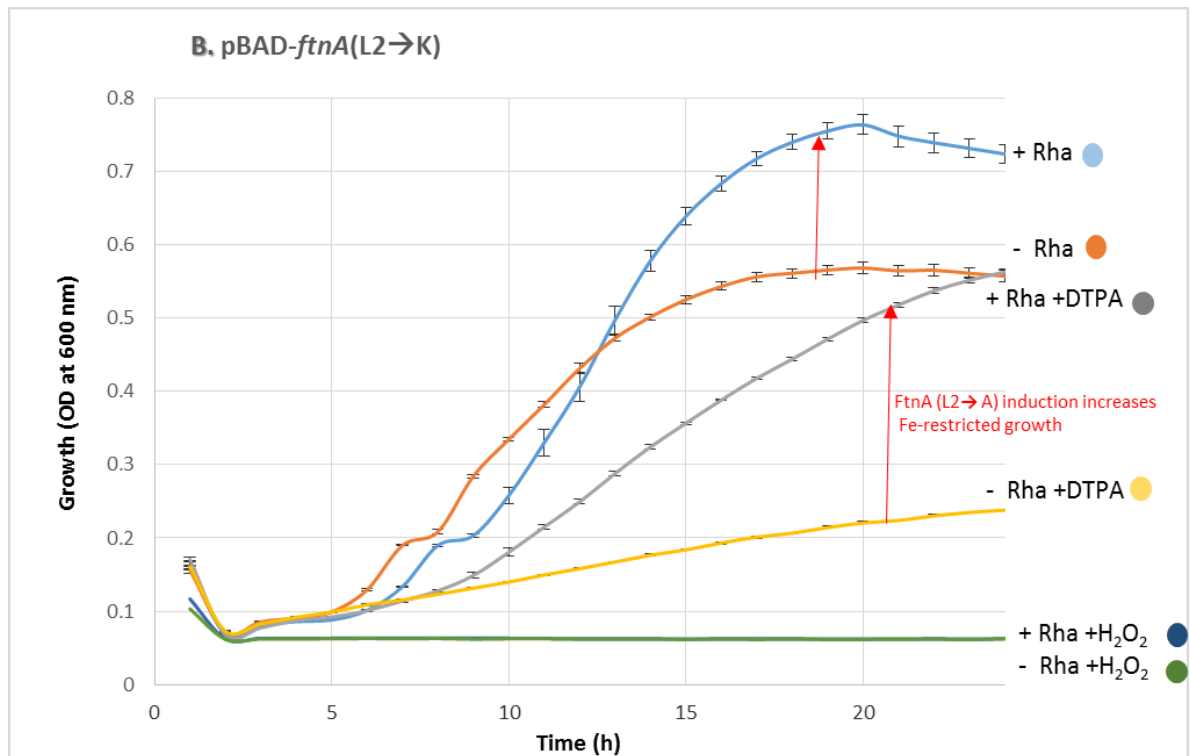
Figure 5.6 Effect of the L2→A/K substitutions of FtnA on iron-restricted and redox strees growth. Growth of the triple mutant with (A) pBAD-*ftnA*(L2A) or (B) pBAD-*ftnA*(L2K) in M9 minimal medium with and without 0.5 μM DTPA, and with / without 200 μM hydrogen peroxide . Precultures included iron and included or excluded rhamnose, as indicated. Repeated once.

5.5 The effect of mutations in genes encoding *E. coli* proteases FtnA levels.

The above data show that the second residue of FtnA influences its cellular levels, possibly due to its sensitivity to turnover through 'N-end rule'-mediated proteolytic degradation. To examine this possibility, the effect of mutations in genes encoding known cytoplasmic proteases was tested on levels of FtnA levels. The enzymes considered were as follow: FtsH, ClpS, ClpA, ClpP, ClpX and Lon. These enzymes/components are known to assemble as a ring-like structures to accommodate the protease active sites within their central lumen. Each enzyme attacks diverse sets of proteins as substrates for degradation. One of the ClpXP targets is the Dps protein. The process initiated by breaking down Dps which is then forwarded it to ClpAP for further degradation (Humbard *et al*., 2013). There is a recognition sequence in the N terminus of target proteins identified by either ClpX or ClpA (the 'unfoldases') which allows subsequent proteolysis by ClpP; both these proteases use substrates that follow the N-end rule pathway (Sriram *et al*., 2011), thus, this group of proteases is classified as a regulatory (Dougan *et al*., 2002). ClpS functions as an 'adaptor' to deliver substrates with an N-terminal F, Y, L or W residue to ClpAP for degradation. The FtsH protease degrades substrates by initially recognising their N- or C-termini (Chiba *et al*., 2000) and substrate degradation is initiated by unfolding by an AAA+ chaperon dependent process. FtsH was first thought to be a degrader of membrane proteins but subsequent study revealed that it has an essential role in degrading cytoplasmic as well as membrane proteins (Herman *et al.*, 2003). Lon is also an AAA+ protease and has a substantial role in processively degrading 'mutant' and abnormal, and selected proteins with short half-lives (Kowit & Goldberg 1977; Tsilibaris *et al*., 2006), as well as by damaged or misfolded proteins. One of the catalytic sites for Lon protease activity is Ser-Lys peptides (Rotanova *et al*., 2004). However, the Lon recognition motif is still unclear (Tsilibaris *et al*., 2006).

The corresponding *E. coli* protease gene mutants (Δ*ftsH*, Δ*clpS*, Δ*clpA*, Δ*clpP*, Δ*clpX* and Δ*lon*; see Table 2.1), in a BW25113 background, were grown in M9 minimal medium plus 20 μM ferric citrate (pre-cultured in the same medium) at 37 ℃ and 250 rpm. Samples of whole-cell extracts samples of the *ftsH*, *clpS*, *clpA*, *clpP*, *clpX* and *lon E. coli* mutants and wild type, as a control, were taken at 2, 4 and 6 h after an OD of 0.5 was achieved, and were used for subsequent anti-FtnA western blotting (Fig. 5.7). The results show that inactivation of *ftsH* results in high FtnA levels, in comparison with the wild

type, at all time points explored. Lack of the other five protease components caused no notable increase in FtnA levels, although did cause a modest decrease in some cases (ClpA, ClpP, ClpA, and Lon). This suggests that FtnA may be subject to proteolytic degradation by FtsH, but not by the other proteases explored (ClpXP, Lon, ClpS, and ClpAP) (Fig. 5.7). However, it should be pointed out that the proteases studied here could impact FtnA levels indirectly through their effects on other factors (e.g. transcription factors and iron metabolism components). Thus an increase in FtnA levels in the *ftsH* strain might not reflect direct degradation of FtnA by FtsH.
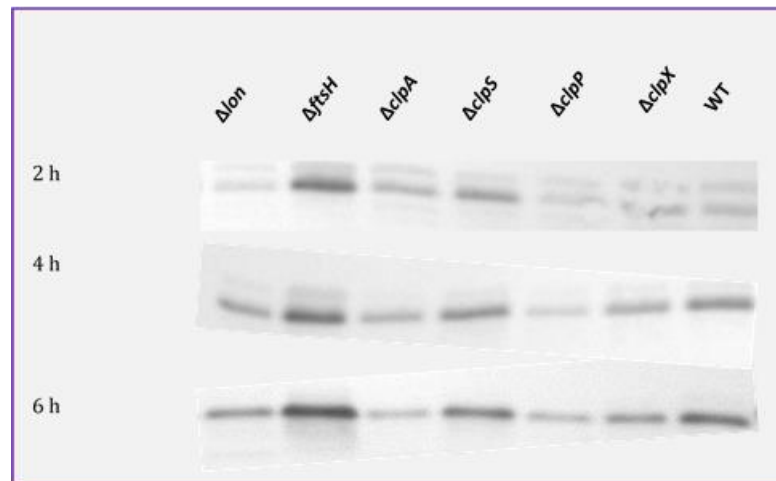
Figure 5.7 Western blot analysis of FtnA level in various *E. coli* protease-gene mutants. Anti-FtnA Western blot analysis of whole-cell extracts of the *ftsH*, *clpS*, *clpA*, *clpP*, *clpX* and *lon E. coli* mutants grown in M9 minimal medium supplemented with 20 μM of ferric citrate, at 2, 4 and 6 h (time past OD 0.5) with wildtype (BW25113) included as control.

FtsH ('filamentous temperature-sensitive'), also known as HflB ('high-frequency lysogenisation' by phage lambda) or TolZ (tolerance to colicins), is an ATP-dependent zinc-metalloprotease belonging to, as indicated above, the AAA$^+$ family (<u>A</u>TPases <u>a</u>ssociated with diverse cellular <u>a</u>ctivities) which combine ATP-dependent unfolding activity with protein degradation. *E. coli* possess four other AAA$^+$ proteases: Lon, HslUV, ClpAP and ClpXP. Of the five AAA$^+$ proteases in *E. coli*, only FtsH is considered essential for viability (Jayasekera *et al*., 2000), although mutants have been reported (Ogura *et al*., 1999) and were used in the work reported here. FtsH has a role in degrading both cytoplasmic and membrane-located proteins, although its major role is considered to be in the quality control of membrane proteins (Langklotz *et al*., 2012) and indeed it exhibits a membrane-anchored localisation (Tomoyasu *et al*., 1993). Membrane proteins

are recognised in a sequence independent fashion by virtue of exposed N- or C-termini of ~20 or 10 (respectively) amino acid residues which are subject to progressive degradation (Chiba *et al*., 2002). Membrane proteins targeted by FtsH include subunit A of the F_0 ATPase, SecY (protein secretion), FeoB (ferrous iron uptake) and YccA (a BI-1 family member of unclear function that inhibits FtsH activity) (Kihara *et al*., 1999). Cytoplasmic proteins degraded by FtsH include LpxC (lipid A biosynthesis), KdtA (WaaA; lipid A synthesis), and RpoH (heat-shock sigma factor) (Nonaka *et al*., 2006; Führer *et al*., 2006), and these appear to be recognised through internal structural motifs. FtsH also has a function in oxidative stress regulation by degrading SoxS (the regulator that induces genes required for superoxide-stress resistance) (Griffith *et al*., 2004) and potentially through its ability to degrade the apo-form (FMN-free) of flavodoxin (activity only observed *in vitro*) (Okuno *et al*., 2006).

The alteration of the second residue of FtnA might affect its FtsH sensitivity directly, perhaps by changing a key motif recognised by FtsH. However, since *ftsH* mutations causes pleiotropic effects, it remains possible that the raised levels of FtnA induced by *ftsH* mutation are a consequence of changes in other FtsH-influenced cellular functions (e.g. the heat shock or redox-stress responses). However, the apparent elimination of FtsH-sensitivity by alteration of FtnA residue 2 is consistent with a direct effect on protease sensitivity. Whether FtnA is indeed a direct substrate for FtnA would need to be tested by in vitro experiments with the purified proteins, with and without the modification to residue 2.

A second experiment was performed to further demonstrate the effect of *ftsH* inactivation on the cellular levels of FtnA; this was as above but at a range of time points. Overnight cultures grown in M9 minimal medium (plus 20 µM ferric citrate) were used to inoculate 50 ml of the same medium. Cultures were then grown at 37 °C and 250 rpm, and samples were collected 1, 2, 4, 6 and 16 h after the point at which the OD reached 0.5.

The anti-FtnA western blot analysis of the resulting whole-cell extracts shows that there is a distinct increase in the levels of the FtnA protein caused by the *ftsH* mutation at all time points measured (Fig. 5.8). It should be pointed out that the *ftsH* mutant grew poorly with respect to the wildtype (e.g. 3-4 fold lower growth at 4 h) which is as reported previously (Jayasekera *et al*., 2000); the deletion of FtsH protein has a consequential effect on the process of SecY translocation, which is an important protein for both growth

and viability of the bacterial cell (Kihara *et al*., 1995). Densitometric analysis show that FtnA levels were increased in the *ftsH* mutant by 2.5 fold. However, in both the wild type and mutant an increase in FtnA levels was observed over the time course of growth as reported previously for *ftnA* expression (Abdul-Tehrani *et al*., 1999; Andrews *et al.,* 2003). In summary, the time course analysis clearly shows that the absence of FtsH proteolytic activity raises the cellular abundance of FtnA throughout the course of growth.
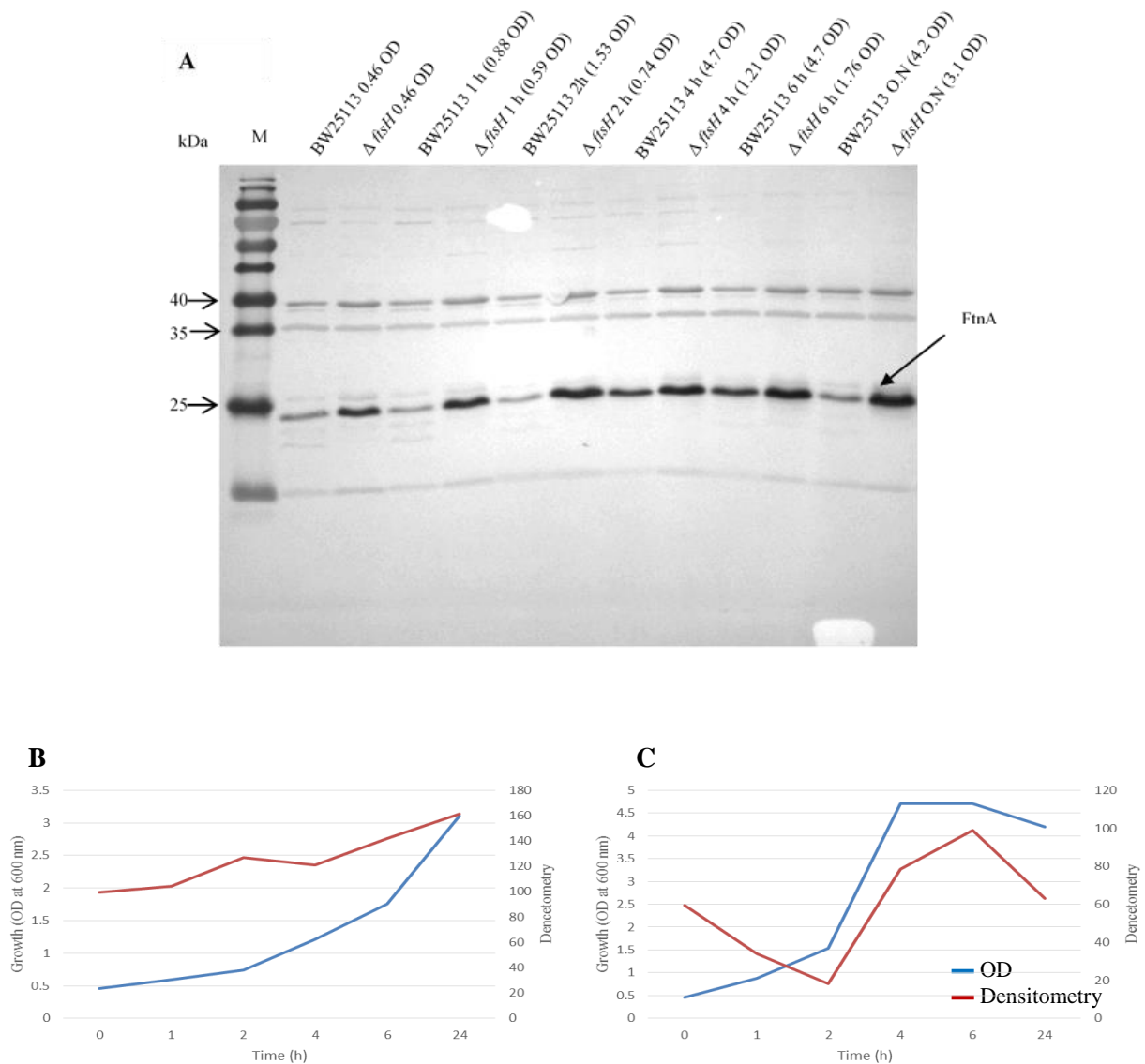
Figure 5.8 Western blot analysis of comparison of FtnA level in a Δ*ftsH* mutant of *E. coli* and the wild type (BW25113). A, Anti-FtnA western blot analysis of whole-cell extracts of the *ftsH* mutant and wild type at 1, 2, 4, 6 and 16 h after an OD of 0.5 was achieved. The OD of the culture at the time of harvesting is indicated. **Plots of density and growth culture (OD) v time B**, Δ*ftsH* mutant of *E. coli* and **C**, The wild type (BW25113).

5.6 Immunoprecipitation of FtnA, Bfr and Dps from *E.coli* to determine iron-storage protein iron contents

5.6.1 Introduction

This section describes an attempt to identifying the iron content, with or without labelling with Fe^{55}, of the iron-storage proteins of *E. coli*. The approach involved immunoprecipitation of the iron-storage proteins followed by iron assay or radioactivity measurement. This experiment was conducted in order to obtain the iron content of each type of iron storage protein within the cell.

The studies of total iron content using ICP-OES (Chapter 3) showed that both Bfr and FtnA contribute to the total iron stores of *E. coli* K-12 in stationary phase, with Dps contributing relatively little except in the absence of Bfr and FtnA. They also indicated that up to 62% of cellular iron can be stored in the wildtype by a combination of Bfr, FtnA and Dps. However, the above studies did not allow the respective contributions of each proteins in iron storage to be assigned, since mutations resulting in loss of one specific iron-storage protein could cause a redistribution to other pools and could also alter the physiology of the cell in a fashion leading to homeostatic changes that affect various aspects of iron accumulation. Thus, in order to determine the amount of iron in each type of iron-storage protein *in vivo*, an attempt was made to immune precipitate specific iron-storage proteins to measure the amount of cellular iron associated with each protein in the cell. Initially, trial experiments were performed with non-radioactively labelled cells (cold immunoprecipitation) which were then repeated using ^{55}Fe. Antiserum raised in rabbits was employed with protein A Dynabeads for precipitation of the antigen-antibody complex. Recovered immune-precipitated proteins were analysed by Western blotting. These results were sufficiently promising to prompt repeat experiments using ^{55}Fe to enable quantitation of the levels of iron incorporated into the isolated iron-storage proteins by scintillation counting.

5.6.2 Preliminary experiments with non-radioactive iron

Bacteria were propagated overnight in 0.4% glucose M9 medium supplemented with 20 μM ferric citrate with 100 μM of rhamnose overnight at 37 ºC and 250 rpm. Immunoprecipitation was as described in Methods 2.18, and in brief was performed as follows. Cells were harvested and then lysed in lysis buffer (lysozyme at 1 mg/ml, 0.1% Triton X100, 1 mg/ml DNase prepared in PBS). The supernatant was isolated and split into three 170 μl aliquots for immunoprecipitation of either Bfr, FtnA or Dps using 2 μl

of Ab (antiserum) and 10 µl of protein A Dynabeads[R]. The resulting complexes were recovered magnetically and proteins were eluted from the beads with 500 µl 0.2 M glycine buffer (pH 2.5). A 13 µl volume of 2 M HEPES (pH 8) was used to neutralize the recovered protein prior to analysis by Western blotting to confirm identities of immune-precipitated proteins (Fig. 5.9-11). The results of the Western blot revealed that the proteins has been successfully recovered since clear bands corresponding to each protein (FtnA/Bfr/Dps) were observed in the *ftnA/bfr/dps*-complemented triple mutant strains and the wild type.
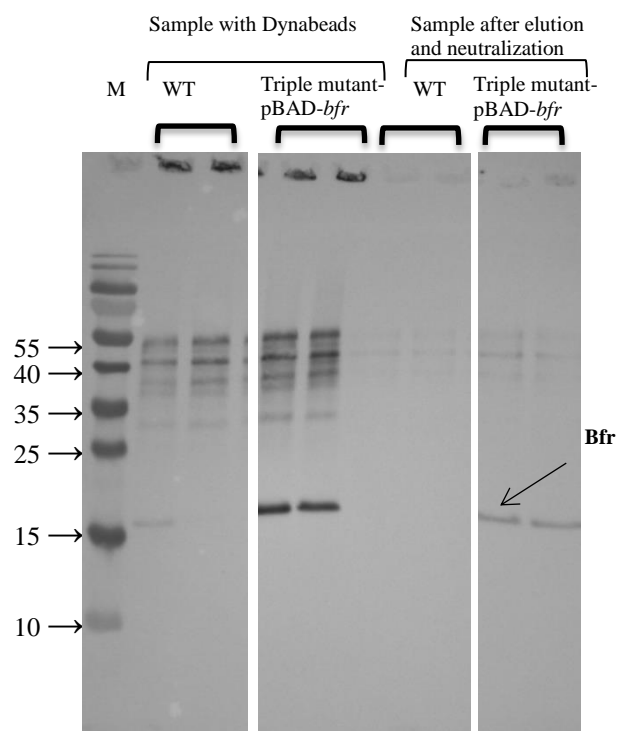
Figure 5.9 Anti-Bfr Western blot analysis of the Bfr protein recovered from *E. coli* by immunoprecipitation. Whole-cell extracts of the wild type (BW25113) and BW25113 Δ*ftnA* Δ*dps* Δ*bfr* pBAD-*bfr* (grown overnight in LB at 37 °C and 250 rpm) were treated with lysis and washing buffer, and the resultant supernatants were immunoprecipitated using anti-Bfr antiserum and protein A. The molecular weight marker (M) can be seen on the right hand side of the figure. The approximate size of the Bfr protein can be seen on the left. Additional bands are anticipated to represent protein A (42 kDa), and the small and large IgG subunits (25 and 52 kDa). One set of samples consists of the isolated Dynabeads/antiserum/soluble-cell extract directly loaded in digestion buffer, the other consists of the proteins eluted from the beads by glycine at pH 2. See Methods 2.18 and 2.13.2 for details of the immunoprecipitation and Western blotting protocols.
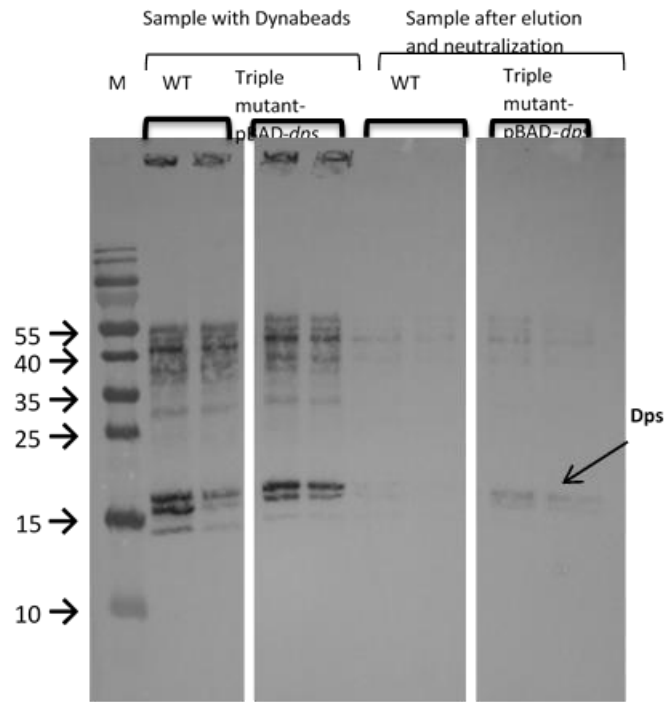
Figure 5.10 Anti-Dps Western blot analysis of the Dps protein recovered from *E. coli* by immunoprecipitation. See above for details.
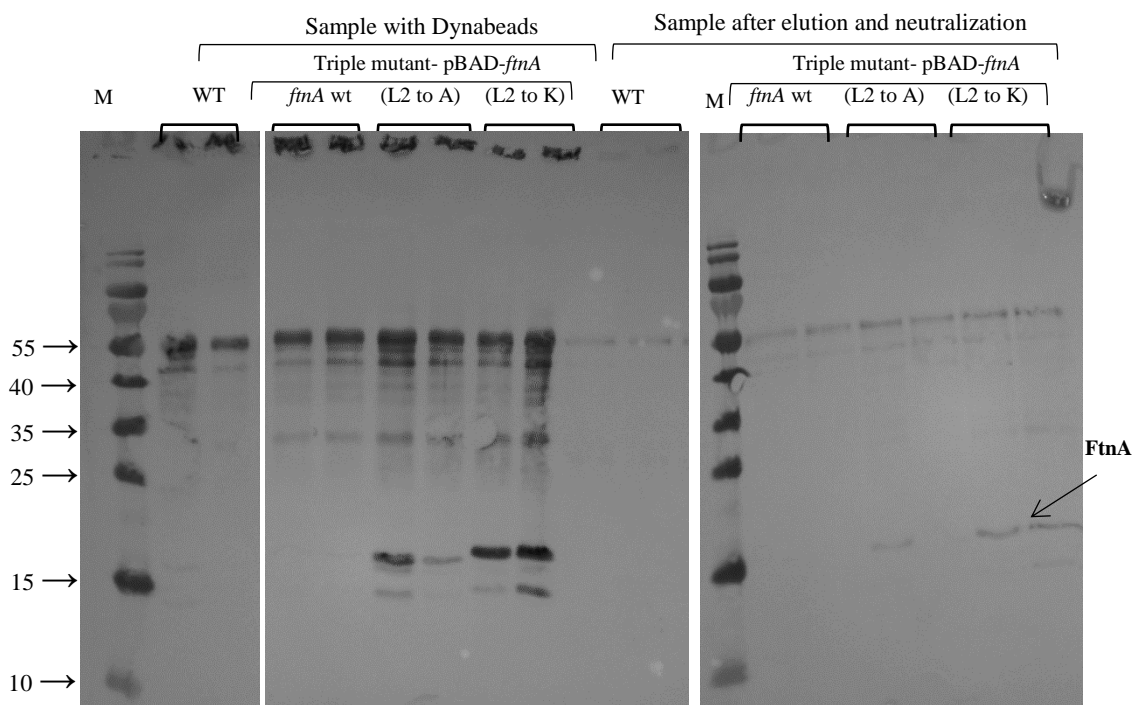
Figure 5.11 Anti-FtnA Western blot analysis of the wildtype, L2A and L2K FtnA protein recovered from *E. coli* by immunoprecipitation. See above for details.

This experiment was repeated by growing the bacteria overnight with ^{55}Fe instead of ferric citrate in the medium. The ^{55}Fe labelled proteins recovered as above by immunoprecipitation were counted using a scintillation counter. But, the experiment failed to give any indication of radioactivity above background. This is likely due to use of insufficient radioactive isotope. Thus, although the immunoprecipitation was successful, further work is needed in order to determine the iron content of the labelled, immunoprecipitated proteins.

5.7 Discussion

In this chapter, the weak effect of the FtnA iron storage protein, as encoded by the pBAD-*ftnA* plasmid, on the iron-restricted growth of the triple mutant was investigated. Western blotting analysis of whole cell extracts of the transformed triple mutants with *ftnA*, *bfr* or *dps* cloned in to pBADrha inducible vector showed that the expression of the FtnA is weak compared to the expression level of Bfr and Dps, and according to the densitometric measurements of the corresponding bands, Bfr and Dps were present at ~5 and ~7 fold higher levels ($P < 0.05$) than for FtnA. Given that the promoter and translational-initiation regions are identical for the *bfr*, *dps* and *ftnA* genes as expressed from pBADrha, this difference in protein levels is suggestive of a lower stability for FtnA than for Bfr and Dps. This effect is most likely due to a higher rate of turnover (proteolytic degradation) for FtnA than for the other two iron-storage proteins.

From this possibility the research in this chapter led to the suggestion that FtnA degradation is subject to the 'N-end rule'. This proposal was based on the presence of a 'destabilising' Leu at position 2 of the FtnA polypeptide (Dougan *et al*,. 2010; Tobias *et al*., 1991). This possibility was also thus investigated. The substituted of Leu-2 with Ala or Lys ('stabilising' residues) elevated the level of FtnA and throughout the bacterial growth phases by about 7 and 6 fold for L2K and L2A substitutions, respectively (at 24 h post-rhamnose induction). The results are consistence with previous work (Varshavsky, 1996; Bivone *et al*., 2010) which showed that the presence of Phe, Leu, Trp and Tyr at the second position of the protein sequence leads to reduced protein levels, however, the presence of Ser, Ala and Thr in the second residue provides high levels of stability.

Following overnight induction, the levels of FtnA declined during subsequent growth (without inducer) by about 2.7 fold (from 30 min to 300); however, the degree of decline for FtnA-L2A and FtnA-L2K was only about 1 fold, over the same time period. This indicates that the half-life of the FtnA had been increased by the L2A/K substitutions which would be consistent with wild type FtnA being subject the N-end rule. However, mutations in *clp* genes that specify the proteases involved in degradation of proteins that are subject to the N-end rule had little effect on FtnA levels, which indicates that the L2 substitutions are affecting degradation by another pathway. Also, the *clpS* mutation did not affect the levels of the FtnA-L2 variants with respect to levels seen in the wildtype (Appendix. 4).

We also assume that the FtnA protein might be selectively targeted by one or more proteolytic proteins for degradation in *E. coli.* Thus, several proteolytic mutant strains were used to assess the level of FtnA by western blotting. The results of the western blotting analysis show that the level of FtnA increases from 2 to 4 h, and then again from 4 to 6 h (post OD 0.5) in the wild type, and this effect was reiterated in all of the protease mutant strains except for the *clpA* mutant (Fig. 5.7). The observation of FtnA levels elevated over the time course of growth was as reported previously for *ftnA* expression (Abdul-Tehrani *et al*., 1999; Andrews *et al* 2003) when under control of its own promoter. The levels of FtnA at the 6 h stage (Fig. 5.7) in the *lon*, *clpX*, *clpP* and *clpA* mutant strains were lower than for the wildtype which suggests that the Lon, ClpXP, and ClpAP proteases are not involved in the proteolytic degradation of FtnA. In addition, the *clpS* mutation had little notable effect on FtnA levels indicating that ClpS, the ClpAP 'N-end rule' targeting component, also does not participate in FtnA degradation (see appendix 5). However the *ftsH* mutant strain was the only protease mutant that showed an increase in the level of FtnA (Fig. 5-8). FtnA levels were increased by the *ftsH* mutation by approximately 1.8-2.6 fold in the mid logarithmic phase and in the stationary phase, respectively. It is thus likely that FtsH degrades FtnA, a soluble protein, and thus lowers the cellular levels of FtnA; this finding is in keeping with previous work showing that FtsH not only degrades integral membrane proteins but can also degrade those that are soluble and cytosolic (Langklotz *et al*., 2012).

Previous work revealed that the substitution of the second residue (E2; located in the cytoplasm) of the YfgM membrane-anchored protein with A, K, D or Q resulted in a stable protein with greatly reduced sensitivity to FtsH degradation (Bittner *et al*., 2015). This study indicates a precedent for FtsH-dependent degradation that is affected by the identity of the second residue. Thus, it is possible that the L2 substitutions reduced FtnA degradation by FtsH. This possibility could be tested by determining whether FtnA levels in the *ftsH* mutant are affected by the L2 substitutions. It should be pointed out that the characteristics of the recognition site or substrates for FtsH degradation is still unclear (Langklotz, & Narberhaus, 2012).

The L2 modification not only raised FtnA levels but also clearly enhanced the ability of the triple mutant (with pBAD-*ftnA*L2→A/pBAD-*ftnA*L2→K) to support growth under

low iron condition (Fig. 5.6) but did not affect resistance to H_2O_2. This observation is consistent with the results of Abdul-Tehrani *et al*. (1999) and is presumed to be due to raised iron store levels in the form of FtnA-L2A/K; however, due to lack of time it was not possible to show this experimentally.

Chapter 6

6. Overexpression and purification of the Dps protein from *E. coli*, and generation of antiserum

6.1 Introduction

The Dps protein was first isolated from *E. coli* and determined as a new type of bacterial ferritin, composed of 12 subunits arranged in a tetrahedral cage form that can accommodate approximately 500 iron atoms (Grant *et al*., 1998). Each subunit is a four-helix bundle, similar to those in ferritin, except of a short additional helix between helix B and C within the long interconnecting loop (Fan *et al*., 2009). The combination of hydrogen peroxide and ferrous iron have a degradation effect on DNA, however, the iron sequestering properties of Dps provide the ability to protect DNA from the hydroxyl radicals that would normally be generated, and this DNA protective property is enhanced by Dps's ability to bind DNA (Su *et al*., 2005). To understand the function of the Dps protein in the metabolism of iron and haemostasis in *E. coli*, it is important to detect the presence/absence of the Dps protein in the constructed mutant strains, so anti-Dps antiserum is required to allow determination of cellular levels of Dps and for estimation of total cellular iron associated with Dps upon immune-precipitation. The availability of Dps antibodies would also aid in the confirmation of *dps* complementation in the *E. coli* iron-storage triple mutant. For this purpose, it was necessary to overproduce and purify Dps.

This chapter includes experiments for Dps protein production enabled through *dps* overexpression. The *dps* gene was PCR amplified using the chromosomal DNA of the wild type as a template and Gibson cloning was used to construct a pET21-*dps* plasmid which was then transformed into *E. coli* BL21/DE3 for Dps overproduction through IPTG induction of the T7 promoter controlling *dps* expression. The overexpression was firstly performed using 50 ml LB as a trial to assess the preferred conditions for overexpression of the recombinant protein. Then, after overexpression in larger volumes of LB, Dps was purified from the cytoplasmic fraction of the bacterial cells by DEAE chromatography for molecular characterisations and to raise anti-Dps antibodies.

6.2 Dps protein overproduction for purification and antiserum generation

6.2.1 *dps* gene amplification

A PCR product for *dps* was first required for generation of a *dps* overexpression plasmid using pET21a. High-fidelity DNA polymerase and primers (Table 2.3) were used to amplify *dps* by PCR. Fig. 6.1 shows the *dps* PCR product after purification using a GeneJET PCR Purification Kit, with the expected size of ~600 bp.
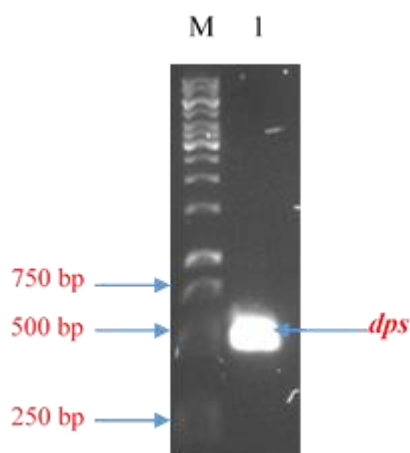
Figure 6.1 Gel electrophoretic analysis of the purified *dps* PCR product (604 bp). The hot start Q5 polymerase enzyme was used for amplification with primers pET21a-dps F & R Table 2.3).

6.2.2 Cloning of *dps* into pET21a

The *dps* PCR fragment was cloned into the pET21a vector using the Gibson cloning method, as described in section (2.9.4). Resulting Ap^R transformants were obtained in the *E. coli* Stellar strain and plasmid DNA was subsequently isolated and subjected to digestion with *Bam*HI and *Nde*I (Fig. 6.2 A and B). Two bands were obtained of the expected sizes, ~600 bp for the insert and ~5400 bp for the vector. Selected plasmid samples which gave the expected restriction pattern were also confirmed by nucleotide sequencing. After the sequencing confirmation, the pET21a empty vector (as control) and pET21a-*dps* plasmid were transformed into *E. coli* BL21/DE3* which was used as a host for protein overexpression.
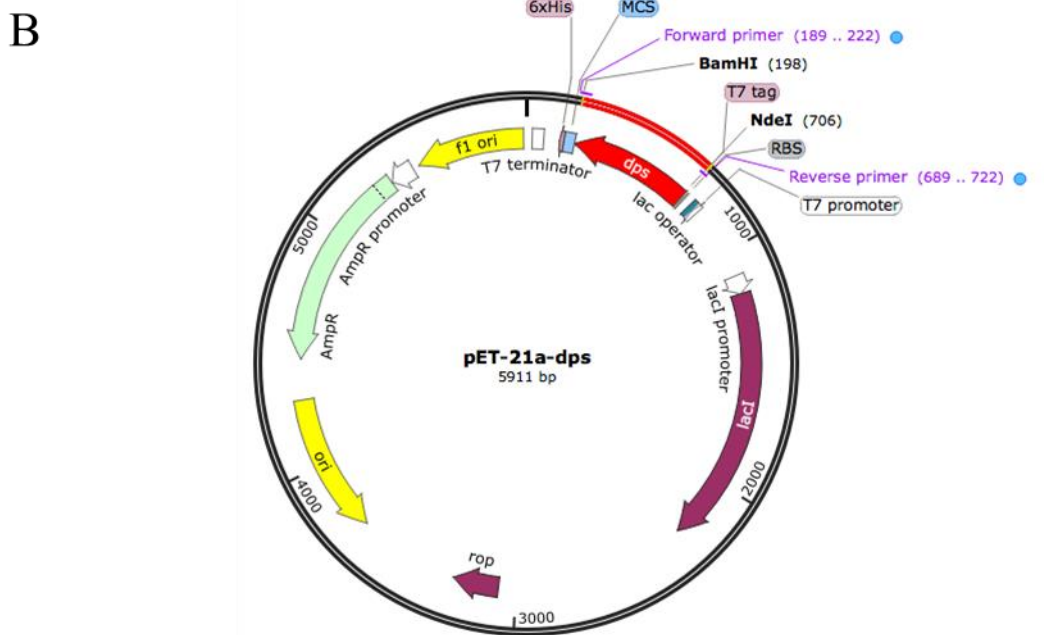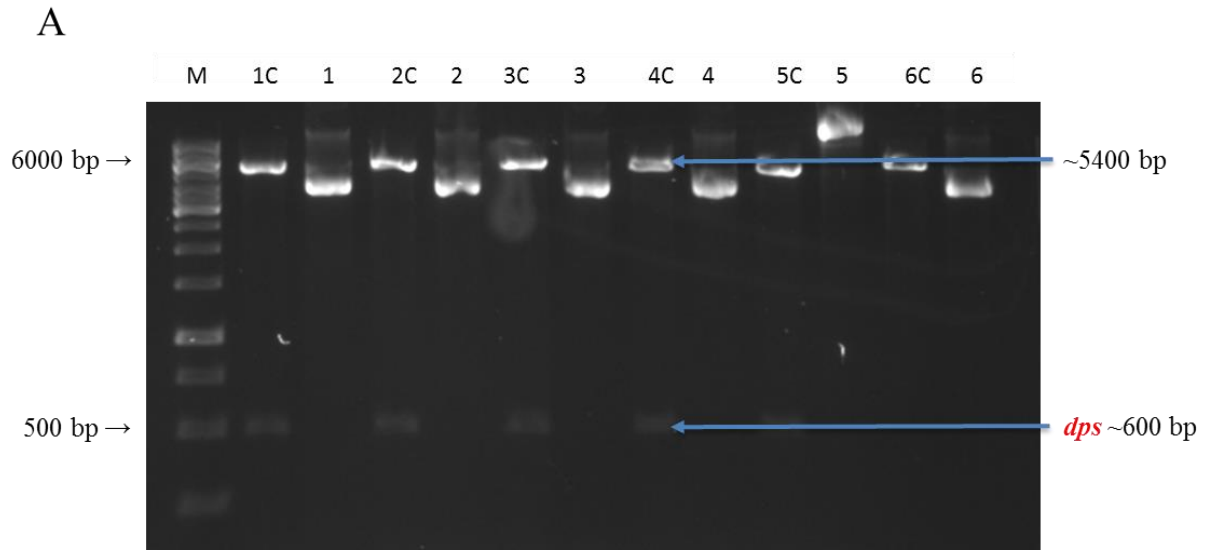
Figure 6.2 Gel electrophoretic analysis of *Bam*H1 and *Nde*I digested candidate pET21a-*dps* plasmid and restriction map of pET21a-*dps*. A. M, Marker, 1 kb GeneRuler (Fermentas); **1C-6C**, **pET21a-*dps*** plasmid (cut); **1-6, pET21a-*dps*** plasmid (uncut). All samples digested correctly to give ~600 bp *dps* insert and the linearized **pET21** of ~5400 bp. **B.** Restriction map of **pET21a-*dps*** generated by using SnapGene.

6.2.3 Overexpression of the Dps protein

The overexpression of *dps* was carried out using the pET21a-*dps* plasmid (isolate 1), following its transformation into BL21/DE3* competent cells (section 2.5.2). The resulting transformant colonies were used for small-scale overexpression (section 2.15.1). The degradation of recombinant proteins expressed in BL21/DE3* strain is minimised due to its lack of Lon and OmpT proteases. It is also carries the gene for T7 RNA polymerase, induced by IPTG, required for expression of genes cloned into pET21a downstream of the T7 promoter. In addition, it lacks RNase E which stabilises mRNA transcripts.

Before the induction using IPTG, no production of the Dps protein was observed (Figure 6.3A), but after the IPTG induction Dps protein started to appear and its levels increased significantly over time with maximal expression was seen at 3 h post-induction. The intensity of the Dps band seen by SDS-PAGE decreased after 4 h induction and its intensity after overnight incubation returned to the same low levels as for the pre-induction. Thus, from the small scale overexpression, the 3 h time point was selected for the large scale Dps production to harvest the cell pellet for protein purification. At the same time, using the same conditions of growth, a transformant of BL21/DE3* with empty pET21a vector was also induced with IPTG, as a control (Fig. 6.3B). The SDS-PAGE analysis of the whole-cell extract showed that no band of overproduction corresponding to Dps is apparent which indicates that the overproduced protein visualised in Fig. 6.3A, with a molecular weight estimated as 18.7 kDa, corresponds to Dps.
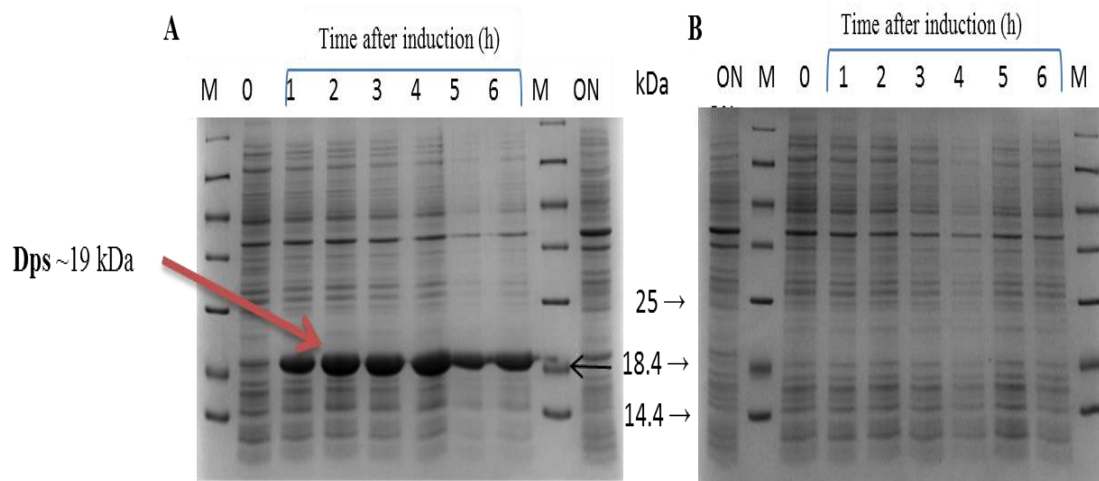
Figure 6.3 Small scale overexpression of Dps. 15% SDS-PAGE of the small scale overexpression of the Dps. Growth was carried out aerobically in LB containing 100 µg/ml ampicillin at 37 °C to an OD_{600} of 0.5. **A**; BL21/DE3*(pET21a-*dps*). **B**;.BL21/DE3*(pET21a). Once the growth reached mid-log, 0.5 mM of IPTG was added (time 0) 0.5 OD units of the whole-cell samples were taken at the indicated time-points (0-6 h and overnight incubation) to analyse basal levels of Dps production. Lanes contained 0.05 OD units of cells.

6.2.4 Solubility assessment

To test the solubility of the Dps at room temperature, 1x BugBuster (Novagen) was added to a set of cell pellets from small-scale overexpression (above) to release the soluble cellular protein (section 2.15.2), and both soluble and insoluble fractions (separted by centrifugation) were analysed in 15% SDS-PAGE (Fig. 6.4). The results showed that the Dps protein is only located in the pellet fraction and is thus likely to be insoluble.
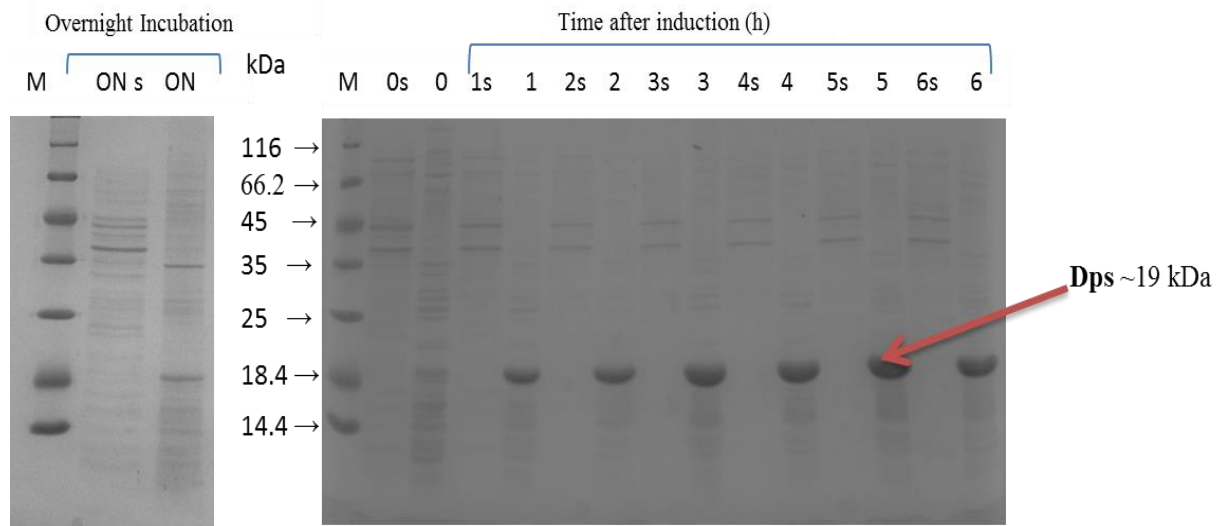
Figure 6.4 Analysis of solubility of overproduced Dps. 15% SDS-PAGE analysis of the solubility of Dps using 1x BugBuster (Novagen). The cell pellets (0.5 OD units) of the BL21/DE3*(pET21a-*dps*) samples were taken (before and after IPTG induction) and treated with 100 µl 1x BugBuster™; S; soluble fraction.

The overexpression of the recombinant *dps* gene appears to lead to the production of insoluble Dps protein; this may due to the production of inclusion bodies which are formed to protect the host cell from the toxic effect of excess cytosolic protein. This result was consistence with previous work showing that the overexpression of Dps in *E. coli* results in the aggregation of overexpressed protein as insoluble particles in inclusion bodies (Azam & Ishihama 1999; Villaverde & Carrió 2003).

However, previous studies performed by Almiron *et al.* (1992) showed that the Dps protein of *E. coli* can be purified by precipitation using ammonium sulphate followed by two gel filtration steps. The overexpression host and plasmid, as well as the incubation time, were different from those used in the current work. In addition, they found that the method of purification used can result in loss of the six N-terminal residues. Another study on the purification of Dps from a different bacterium (Wei *et al.*, 2007) demonstrated that the overexpression of *Cyanobacterium anabaena* Dps protein in BL21/DE3 using pET21a to produce a His-tagged Dps, resulted in a soluble overexpressed protein upon at low temperature expression, and thus the problem of insolubility was overcome. Unfortunately, this was not the case in this work and it is unclear why Dps was soluble when overexpressed in the previous work.

6.2.5 Protein solubilisation and an ion-exchange chromatography

In order to solubilize the Dps protein the pellet taken from large-scale overexpression (section 2.15.3) were defrosted (~2 g of cell pellet from 1 litre of LB), from -80 °C, and re-suspend in 25 ml of resuspension buffer (50 mM Tris, 15 mM mannitol, 5% glycerol, 1 mM DTT, pH 8.0). The homogenous suspension was then lysed by passage through the French presser cell press at 20,000 psi three times (section 2.15.4). The resultant lysate was treated by centrifugation at 51,428 x g at 4 °C for 20 min to pellet the insoluble material. After resuspension in the above buffer containing 8 M urea, the sample was then renatured by dialysis against refolding buffer (50 mM Tris, 15 mM mannitol, 1 mM DTT, 0.1 M arginine, pH 8.0) containing 0.1 M arginine. The resultant solution was again treated by centrifugation at 51,428 x g at 4 °C for 20 min to pellet insoluble material, and the supernatant was dialysed against 50 mM Tris buffer (pH 8.0) to remove the refolding buffer (section 2.15.6). Following dialysis, the sample was centrifuged at 6,090 x g at 4 °C for 20 min to pellet any precipitated protein. The soluble supernatant was subsequently applied to a column packed with 20 ml of DEAE-Sepharose^{TM}, an ion exchange chromatography, using buffer A for binding and equilibration (50 mM Tris, 1 mM DTT, pH 8.0) and buffer B for elution (as buffer A but with 1 M NaCl). Elution was carried out using a linear gradient of 0-1 M NaCl (section 2.15.5). Two peaks were observed at the middle stages of the elution profile spanning across fractions 9-22 (Fig. 6.5). Absorbance values dropped to low levels are the two elution peaks.
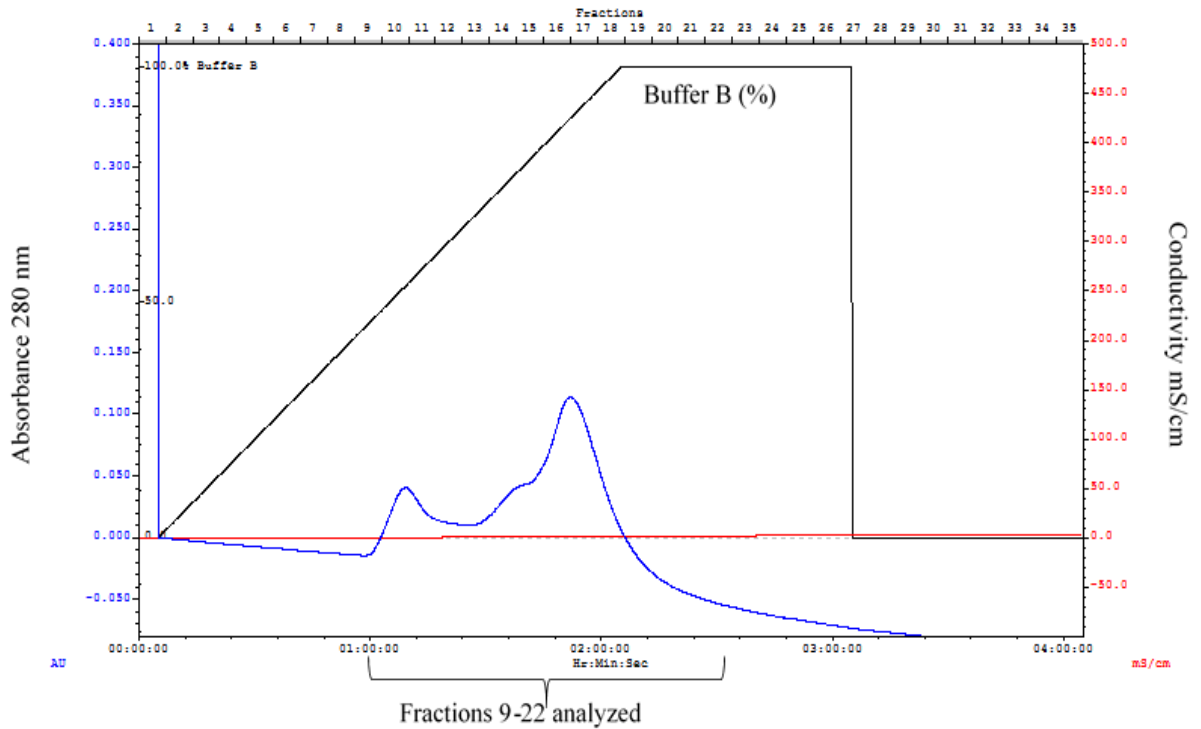
Figure 6.5 Elution profile of resolubilised Dps protein during an ion-exchange chromatography. A DEAE-Sepharose™ column was used as described in Methods (2.15.5). Fractions 9-22 were analysed by 15% SDS-PAGE (Fig. 6.6).
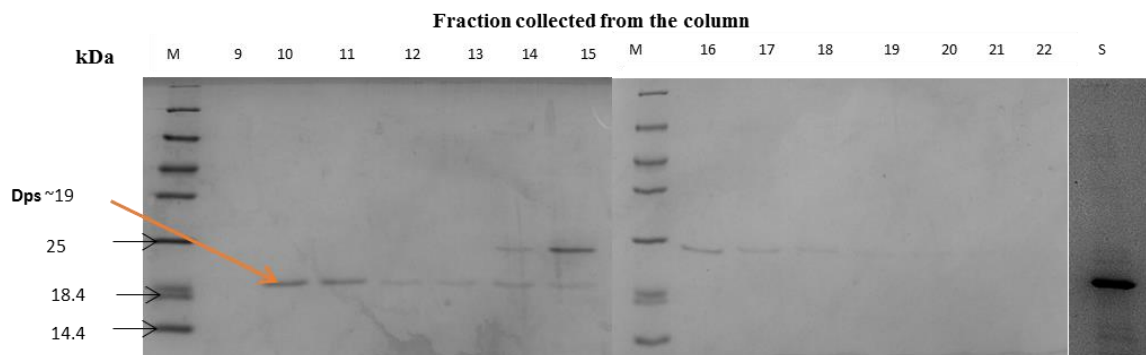
Figure 6.6 SDS-PAGE analysis of fractions obtained from purification of refolded Dps following the chromatography. 5 µl of each fraction (7 ml volume; see Fig. 6.5) were loaded and analysed by 15% SDS-PAGE. The Dps protein, at 18.7 kDa as indicated with the arrow, can be seen in fractions 10-15, S represent the starting sample.

After the SDS-PAGE analysis, the Dps protein was observed eluting across fractions 10-15, fractions 14-15 were excluded from subsequent pooling as they had a higher molecular weight contaminant (Fig. 6.6). Thus, fractions 10-13 were pooled (28 ml) for concentrating using a Vivaspin centrifugal concentrator (5,000 MWCO, Sartorius Stedim Biotech) until an approximate 1 ml final volume was obtained. This was analysed by SDS-PAGE for comparison with the sample before concentration and for determination of purity (Fig. 6.7), before further analysis by ESI-MS analysis and the production of polyclonal antibody. The SDS-PAGE showed a single band of the expected size that appear homogenous. The concentration was estimated as 0.7 mg/ml by Bradford assay. The Dps protein was isolated again by repeating the same process in this section.
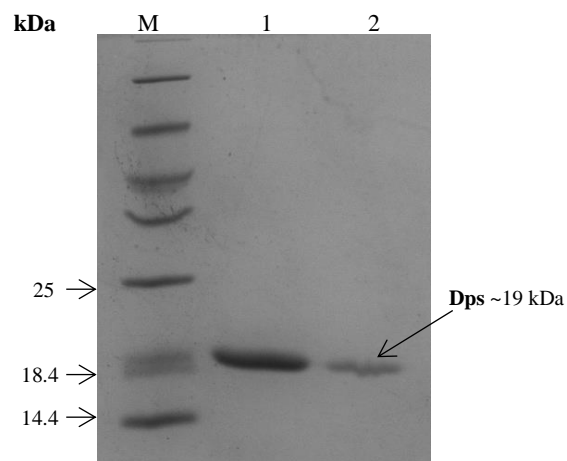
Figure 6.7 Refolded, concentrated and purified Dps protein. A Vivaspin-20 centrifugal concentrator was used for Dps protein concentration. 5 µl of the Dps protein after and before concentration (Lane 1 and 2, respectively) were loaded and analysed by 15% SDS-PAGE. The corresponding size of the molecular weight marker (M) can be seen on the right hand side of the figure.

6.3 Molecular characterisation of the recombinant purified Dps

6.3.1 Determination of Dps Protein Molecular Mass
a. Analysis by SDS-PAGE

The relative migration of a protein band during SDS-PAGE is associated with its molecular mass, thus, the molecular mass of the purified Dps protein was estimated based on its relative mobility with respect to protein standards of known molecular mass. The accuracy of the molecular mass determination is dependent on the linearity of the curve (Figure 6.8). The curve fit shows that there is a strong linear association ($R^2 = 0.97$) between mobility of the standards and their mass, which suggests strong reliability in estimating the molecular mass of the Dps protein. The standard curve gave an estimated mass of 20.2 kDa for Dps which is a reasonable approximation to the mass predicted (18.7 kDa) from its amino acid sequence.
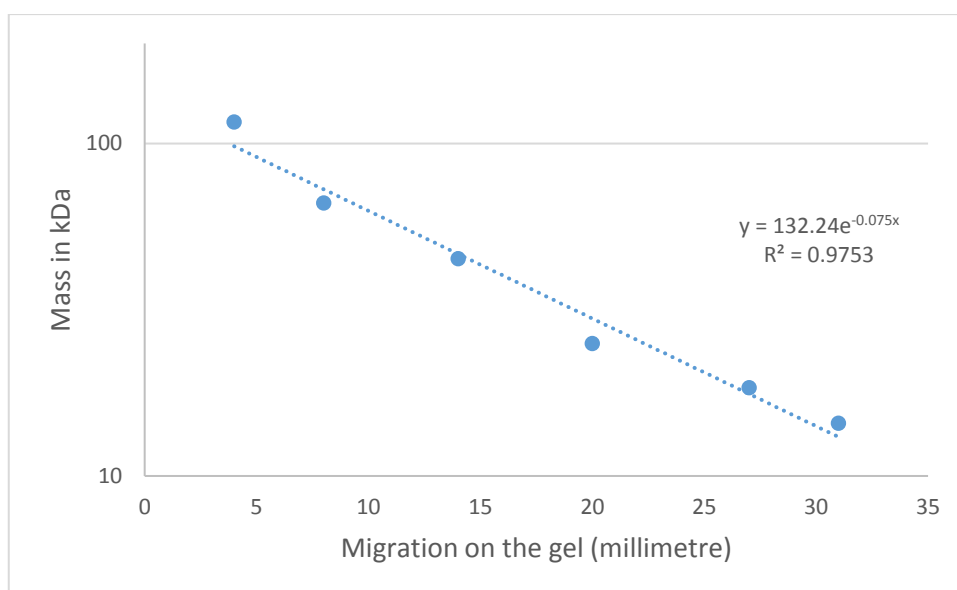
Figure 6.8 Estimation of the molecular mass of the putative Dps protein by SDS-PAGE. Calibration curve of the SDS-PAGE analysis using the 116 kDa unstained Page Ruler Protein Ladder as a size marker. The graph has been plotted using a semi-logarithmic scale.

b. Electrospray ionization mass spectroscopy (ESI-MS)

The Dps protein sample, purified by an ion-exchange chromatography as above, was analysed for true mass by ESI-MS, at the Department of Chemistry (University of Birmingham) by Dr Louise Male after dialysing the protein sample against 20 µM

ammonium acetate to de-salt the protein sample. The mass of the recombinant purified Dps, as found by ESI-MS, was 18,567.0 Da (Fig. 6.9) is similar to the theoretical mass for the Dps protein (18,695.31 Da). The ESI-MS determined mass is 128.3 Da below that predicted. This difference is likely due to the removal of the N-terminal methionine (131.2 Da). Thus, it would appear that the Dps of *E. coli* is subject to the post-translational removal of its N-terminal Met by methionine aminopeptidase (MAP). This is consistent with the presence of Ser at position 2, which has a relatively small side chain that would not therefore be expected to inhibit MAP activity (Frottin *et al*., 2006) and also matches the 91% likelihood Met cleavage prediction of the TermiNator tool (https://bioweb.i2bc.paris-saclay.fr/terminator3).

MAP is one member of a group of enzymes that have an important role in protein N-terminal methionine excision via a co-translational mechanism. In *E. coli*, this the removal of the N-formyl group is achieved by the peptide deformylase enzyme which results in the stimulation of MAP cleavage. Research shows that the probability of this process is increased in the presence of one of a group of amino acids in the second residue including Pro, Ser, Lys, Cys and Ala. Hirel *et al*. (1989) also found that the presence of these residues, as well as Gly, as a second residue of the *E. coli* protein (immature form) have a significant positive association with the N-terminal methionine excision. They also proposed that a substantial portion of the methionine in the cell is provided by MAP in a recycling process.
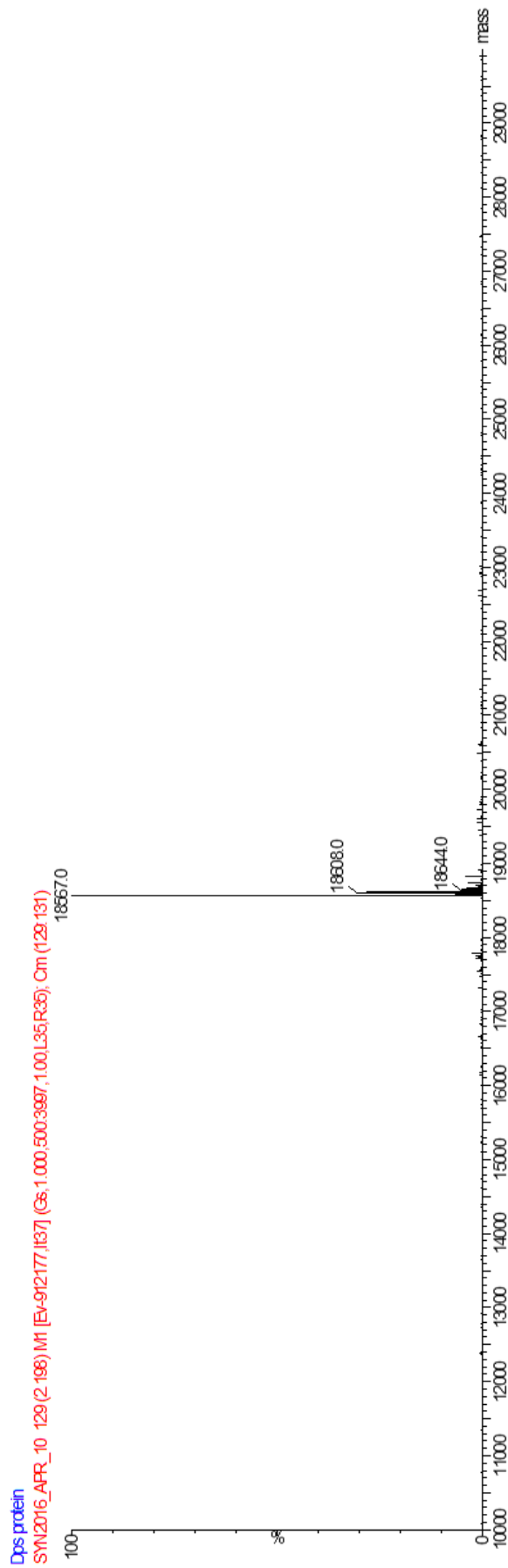
Figure 6.9 Protein mass estimated by ESI-MS for recombinant purified Dps. The protein was injected into the mass spectrometer and the charged protein fragments were then separated according to their m/z ratio. The MS analysis for the recombinant Dps protein give 100% peak with a 18567.0 mass collected in linear mode this. This suggests that N-terminal methionine excision; see predicted mass for residues 2-167 of Dps, as below:

18564.11 (average mass), 18552.70 (monoisotopic mass).

6.4 Does the overexpressed, refolded and purified Dps form a 12-mer capable of iron storage?

Since the purified Dps protein had been subject to denaturation and refolding, the potential remains that it is not properly assembled or may lack iron storage activity. To assess the ability of the purified recombinant Dps protein to store iron, an iron uptake assay was conducted (see Methods 2.21). Dps treated with ferrous ammonium sulphate (FAS), without and with hydrogen peroxide, in 20 mM HEPES (pH 7.0) failed to generate any convincing indication of iron core formation (i.e. soluble brown colour formation in the presence of Dps). Thus, the reassembled protein appeared to be inactive in iron uptake. This contrasts with previous work with *E. coli* Dps showing *in vitro* core formation driven by hydrogen peroxide (Zhao, *et al*., 2002)).

Further experiment was conducted to assess the Dps assembly status, whereby the Dps protein was subject to native PAGE alongside two other proteins of high native mass. The Dps protein was visualised by Coomassie staining as two closely migrating and poorly resolved bands of low mobility at the top of the native gel, of roughly equal intensity. However, the staining pattern also suggests that a major proportion of the Dps protein failed to enter the gel (possibly due to poor solubility or very high mass). The Dps bands were of lower mobility than horse spleen ferritin (450 kDa) which in turn had a lower mobility than bovine serum albumin (198 kDa, for the predominant trimeric form) (Fig 6.10 B). The Dps protein, pre-incubated with 1 mM of FAS (Method 2.21,) failed to generate a Prussian blue stained band following non-denaturing-PAGE stained (Fig. 6.10A) whereas the horse-spleen ferritin (positive control) produced a band as expected. The native-PAGE analysis thus suggest that Dps may be assembled (and hence of low mobility), but no evidence for core formation was obtained. Further, TEM analysis of urinyl acetate negatively stained Dps failed to reveal any particles corresponding to Dps (section 2.16) indicating that the Dps protein may not have assembled correctly.
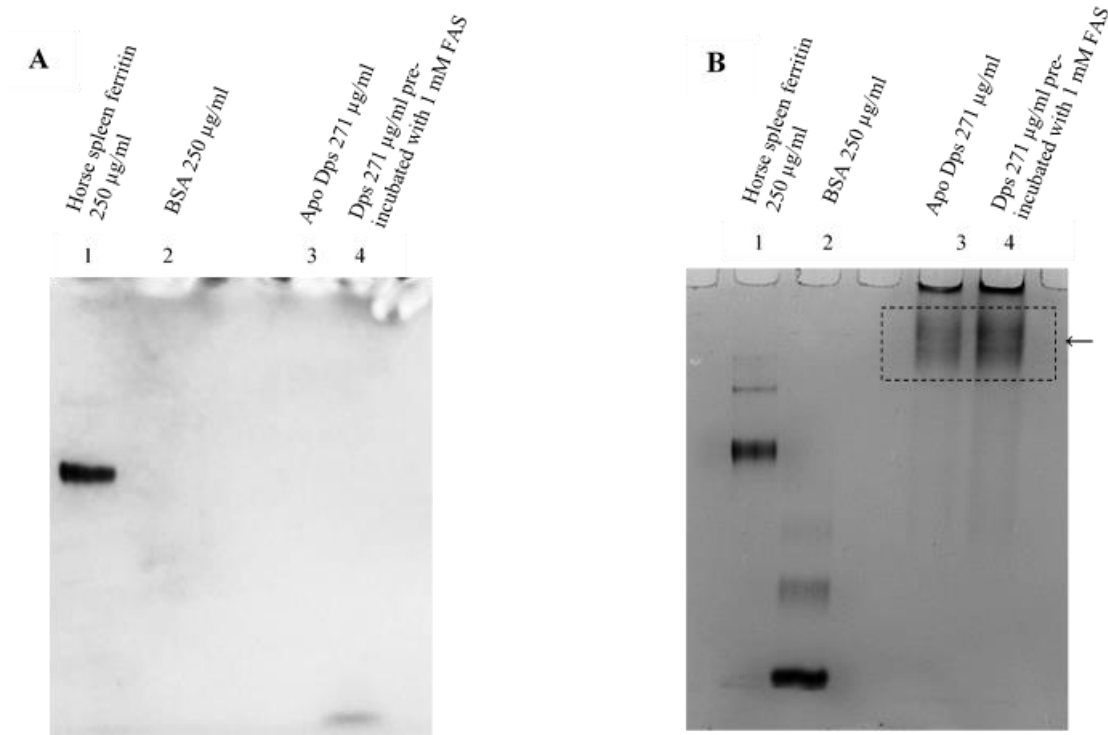
Figure 6.10. Non-denaturing-PAGE analysis of the purified apo-Dps and Fe-Dps (pre-incubated with ferrous ammonium sulphate). Dps protein, with and without pre-incubation with FAS, was subjected to non-denaturing gel electrophoresis and was visualised by ferric-iron and Coomassie Blue staining. **A, iron stained**: lane 1, horse spleen ferritin (Fe-loaded, positive control); lane 2, bovine serum albumin (negative control); lane 3, Dps protein; lane 4, Dps protein pre-incubated with iron (FAS); **B, Commassie stained for protein**: lane 1, horse spleen ferritin (positive control); lane 2, bovine serum albumin (positive control); lane 3, Dps protein; lane 4, Dps protein pre-incubated with iron (FAS). The name of corresponding proteins are indicated. Low mobility Dps protein bands indicated with arrow.

6.5 Immune-detection of Dps using antiserum raised in rabbits against purified *E. coli* Dps.

The purified Dps protein (3.5 mg/ml) was used to raise anti-Dps antibodies in two white New Zealand rabbits in Dundee Cell products Ltd. (see section 2.20). The antisera from the third bleeds were used for western blot analysis of whole-cell samples for all iron storage proteins mutant and the wild type. The results showed that the polyclonal antiserum from rabbit one gave a high background staining in comparison with the polyclonal antisera raised in the second rabbit (data not shown) So the antiserum of the second rabbit was used in the western-blot analysis study in all further work. All cell

pellets from the overnight cultures of all mutants and the wild type strain were re-suspended in 1x SDS digestion buffer. The samples were incubated at 95 °C for 10 min before loading onto 15% polyacrylamide gels for electrophoresis (section 2.13.1). The separated proteins were blotted onto a nitrocellulose membrane (section 2.13.2) which was then subject to immune-detection using anti-Dps antibodies (rabbit one) and anti-rabbit IgG secondary antibody conjugated to alkaline phosphatase. A clear prominent band was seen in the strains possessing the *dps* gene but not in the *dps* mutant strains. The molecular weight of the band was a good matching for the expected mass, 18.7 kDa, of the *E. coli* Dps protein (Fig. 6.11). Thus, the *dps* mutants created in chapter three appear to be genuine.
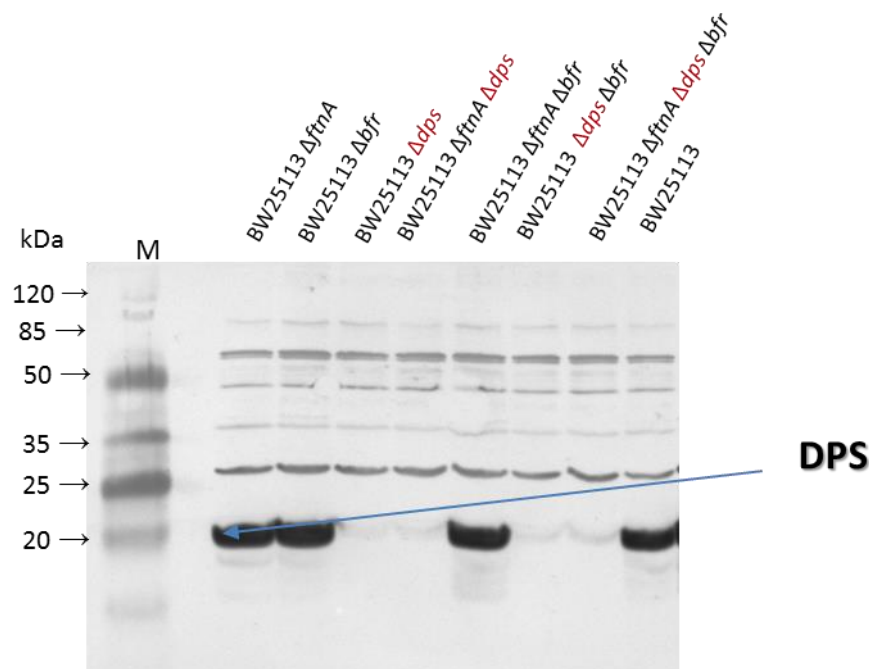
Figure 6.11 Anti-Dps western blot analysis of the mutant and wild strains to evaluate the specificity of the anti-Dps sera generated in the rabbit immunised with the purified recombinant overexpressed Dps protein, and to confirm the identity of the *dps* mutants. Whole-cell extracts of single mutants (BW25113 Δ*ftnA*, BW25113 Δ*bfr*, and BW25113 Δ*dps*), double mutants (BW25113 Δ*ftnA* Δ*dps*, BW25113 Δ*ftnA* Δ*bfr*, BW25113 Δ*dps* Δ*bfr*) the triple mutant (BW25113 Δ*ftnA* Δ*dps* Δ*bfr*) and the wild type (BW25113) were grown overnight in LB at 37 °C and 250 rpm prior to harvesting and western blot analysis. The blots were immunostained using anti-Dps serum from the final bleed of rabbit one. The molecular weight marker (M) can be seen on the right hand side of the figure.

6.6 Phenotypic confirmation of the complementation of the Δ*ftnA* Δ*dps* Δ*bfr* mutant with the pBADrha-*dps* plasmid

The results above confirm the successful generation of polyclonal antibody from the recombinant Dps. Thus, the anti-Dps serum was used to investigate the expression of the *dps* gene in the triple mutant complemented with the pBADrha-*dps* plasmid. BW25113 Δ*ftnA* Δ*dps* Δ*bfr* transformed with pBADrha-*dps* was pre-cultured in M9 supplemented with 20 µM ferric citrate, 50 µg/ml of chloramphenicol and 100 µM of rhamnose. Whole-cell extracts were then subjected to SDS-PAGE followed by western blotting and anti-Dps staining. The resulting western blot clearly shows that the Dps protein is produced in the *dps*-complemented triple mutant (Fig. 6.12). This finding is consistent with the observed production by SDS-PAGE of a protein corresponding to Dps in the *dps*-complemented triple mutant (Chapter 5 Fig. 5.1, D-2) and the increased peroxide resistance exhibited by the triple mutant upon rhamnose induction of *dps* expression (Fig. 4.12, C).

.
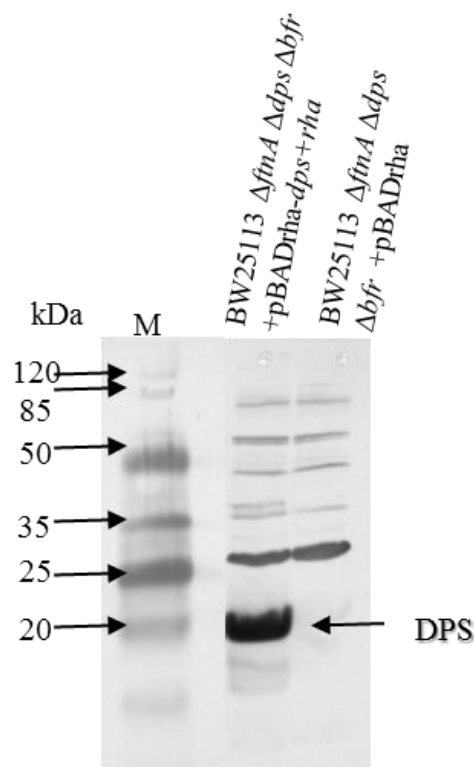
Figure 6.12 Anti-Dps Western blot analysis to identify Dps production in the triple mutant upon induction of pBADrha-*dps*. Whole-cell extracts BW25113 Δ*ftnA* Δ*dps* Δ*bfr* with pBADrha or pBADrha-*dps*. Strains were grown overnight in glucose M9 minimal medium supplemented with 20 µM ferric citrate and 100 µM rhamnose. The molecular weight marker (M) can be seen on the right hand side.

6.7 Discussion

Dps is a member of the ubiquitous Ferritin superfamily which includes ferritin and bacterioferritin which are both are composed of 24 subunits, whereas Dps (also called mini-ferritin) is smaller in size by ~50% since it is composed of just 12 subunits. However, these three types of Ferritin share a common iron sequestration function and share the same cytoplasmic localisation in *E. coli*, as well as certain other bacteria (e.g. *Salmonella*). Dps has an important role in nucleoid formation due to its DNA compaction ability (Talukder & Ishihama, 2014). In some cases, Dps acts to sequester haem to limit haem-induced toxicity (e.g. for anaerobic *Porphyromonas gingivalis*) although this is not known to be the case in general for Dps proteins, and for the Dps of *P. gingivalis* this ability requires a surface Cys residue as a co-axial haem ligand (Gao *et al*., 2012).

In order to perform experiments to further understand the biological function of the Dps protein in *E. coli*, antibodies are required to enable the immunoprecipitation-mediated recovery of Dps protein for analysis of its iron content. In addition, the antibodies would allow quantification of Dps cellular levels and presence/absence in mutant strains. Thus, the anti-Dps serum was used to confirm the identity of *dps* mutants created in chapter three, and to further confirm the ability of pBADrha-*dps* to enable Dps production upon rhamnose induction. To enable production of antibody, Dps protein needed to be isolated. To achieve this, the *dps* gene was amplified and cloned into the overexpression vector pET21a and the cloned *dps* was overexpressed in BL21/DE3*. However, the overproduced protein appeared to be insoluble. Thus, the protein had to be solubilised in order to purify it by chromatography. This problem was overcome by treatment with urea followed by refolding which resulted in soluble Dps protein which was purified by anion-exchange chromatography to a high degree of purity (no contaminants observed by SDS-PAGE). This result was consistence with previous work showing that the overexpression of Dps in *E. coli* results in the aggregation of overexpressed protein as insoluble particles in inclusion bodies (Almiron *et al*., 1992; Azam &Ishihama 1999; Villaverde & Carrió 2003). ESI-MS showed that the protein isolated was of a size very similar to that predicted for Dps followed cleavage of its N-terminal Met residue, which was predicted to be subject to MAP cleavage.

The assembly of the purified Dps protein into 12mer form was investigated by subjecting this protein to a native PAGE in comparison with a high native mass proteins as a control (BSA and ferritin). The native PAGE showed that the Dps protein is of in lower mobility

than the control proteins (Fig. 6.10B), consistent with a 12mer form. However, the recombinant Dps failed to show any ability to form an iron core when treated with FAS in the presence or absence of H_2O_2 (Fig. 6.10A). In addition, TEM analysis did not show any particles indicative of the spherical 12mer form. These results suggest that the purified, resolubilised protein might have lost the ability to take up and oxidise ferrous iron due to failure to assemble correctly. Indeed, it is reported that the reassembly of aggregated, overexpressed recombinant protein (following solubilisation in denaturant) can negatively affect the activity of the protein (Villaverde & Carrió 2003). A previous study showed the formation of a ferric core (~500 iron atoms) with in Dps when ferrous iron was provided, along with and hydrogen peroxide as oxidant, in accordance to the following reaction: $2 Fe (II) + H_2O_2 + 2 H_2O \rightarrow 2 Fe (III) OOH + 4 H^+$. A similar process occurred in the presence of oxygen as an oxidant, but with a lower rate than with H_2O_2 (Almiron et al., 1992). Thus, the failure to generate such an iron core in this work likely reflects the improper assembly of Dps into spherical shells

The main purpose for overexpression and purification of the Dps protein was to generate polyclonal antiserum to test whether the dps mutants were genuine and to enable quantification and recovery of Dps from cell extracts. This target was achieved as the resultant polyclonal antiserum successfully detected the presence of Dps in dps^+ strains but not the dps mutants constructed in chapter 3, by visualization of a prominent band matching the expected mass (18.7 kDa) of the Dps protein of $E. coli$ (Fig 6.11). Controlled Dps protein production in the triple mutant was observed by SDS-PAGE (Chapter 5, Fig. 5.1D-2) as a product equivalent to the expected size of Dps protein, and by western blotting (Fig. 6.12).

Chapter 7

7. Molecular and biological properties of Linocin M18 of *Pyrococcus furiosus*

7.1 Introduction

7.1.1 Nanocompartments

Prokaryotes can compartmentalise enzymes required for reactions that generate a toxic intermediate or benefit from localised concentration of substrate. This mechanism can be accomplished by forming protein shells structures with a central lumen and gates to facilitate substrates/products moving in and out of these particles. Much is understood concerning three types of microcompartment. The first is the carboxysome which is known to be involved in carbon fixation in cyanobacteria; in this case the nanocompartment functions to maintain a high concentration of carbon dioxide inside the particle shell (a carbon dioxide concentrating mechanism) which involves the conversion of internalised bicarbonate into carbon dioxide, followed by reaction of the resultant CO_2 with ribulose bisphosphate by RuBisCO to generate 3-phosphoglyceric acid (3PGA) which is exported out of the carboxysome. There are two types of carboxysome, alpha and beta, which both have the same shape (icosahedral). However they differ from each other in size; the diameter of beta carboxysomes is 300-400 nm which is three times larger than alpha type (80-130 nm) (Rae *et al*., 2013).

The second type of well-studied microcompartment is the propanediol utilisation microcompartment (Pdu), which is used to protect the DNA from the damage caused by toxicity of the reaction intermediate, propionaldehyde. The Pdu microcompartment works by internalizing and restricting the 1,2-propanediol (a major product of sugar fermentation) degradative enzymes and converting propanediol into propionaldehyde which is rapidly converted to propionyl-CoA and 1-propanol (Bobik *et al*., 2015). The genes responsible coding for this compartment are mainly found in intestinal bacteria such as *Citrobacter*, *Klebsiella*, *Shigella* and some *Escherichia coli* strains (Abdul-Rahman *et al*., 2013) Mutations causing the leakage of propionaldehyde outside of the particles has a harmful effect on cellular DNA and increases the lag phase of growth (Sampson & Bobic, 2008). The third well known microcompartment is the ethanolamine utilization microcompartment (Eut), first recognized in *Salmonella enterica*, which is responsible for enzymatic degradation of ethanolamine by a mechanism involving

sequestering the ethanolamine into the protein shell, where it is catabolised into acetaldehyde by the effect of the vitamin B12-dependent ethanolamine ammonia lyase (EutBC) (Roof & Roth, 1989). The function of the Eut microcompartment can be explained in two ways: retention of the toxic intermediate, acetaldehyde, in the shell; and limiting the carbon loss (Chowdhury et al., 2014). The resulting ethanol and acetyl-phosphate then diffuse out of the particles for use in central metabolism (Huseby & Roth, 2013) (Fig. 7.1).
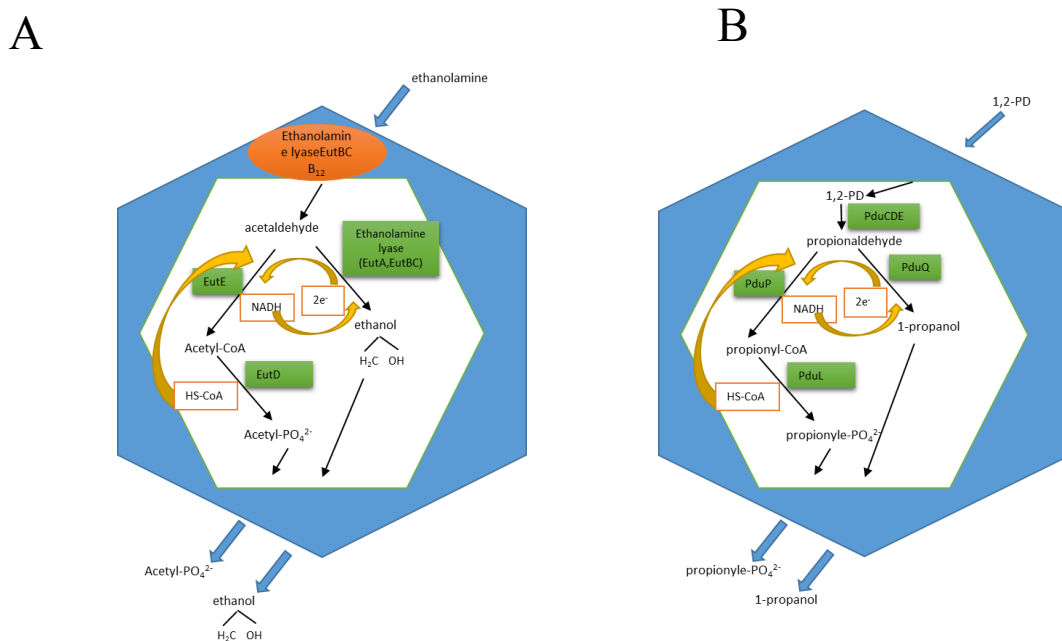
Figuer 7.1 Schematic model representing Eut function (A) and Pdu (B). Adapted from Bobik *et al.*, (2015).

7.1.2 Microcompartment shell assembly

The microcompatment shell proteins are classified as members of Pfam protein family PF00936. They assemble together to form cyclic, planar hexamers with two surfaces, the cytosol and the lumen surfaces. The 'single-domain' proteins form hexamers that make up the facets (BMC-H) of the shell. These bind together at their edges using well-conserved and essential lysine residues; this results in protein sheet formation (Pang *et al.*, 2012 Sinha *et al.*, 2014; Bobik *et al.*, 2015). The pentagonal, five subunit units (BMC-P; EutN/CcmL family proteins) form the vertices of the icosahedral shell. The microcompartment genes are generally encoded at the same locus and can thus can be

transferred horizontally (Sutter *et al.*, 2013). Microcompartments have one or two types of 'gate' within their shells as substrate/product entry/exit points, called tandem-domain proteins (BMC-T) (Tsai *et al.*, 2007). The substrate entry and product escape is driven by diffusion and pore selectivity, and recent studies show that the process of opening and closing the gates is controlled by the substrate binding to the gate (Thompson *et al.*, 2015).

7.1.3 Encapsulins

A new type of 'virus-like' nanocompartment has recently been identified in *Myxococcus xanthus*, described as a ferritin-like iron storage nanocompartment. It is composed of four proteins: EncA, a shell protein resembling the bacteriophage HK97 capsid protein; and EncB, EncC and EncD, which together form the internal core of the encapsulin nanocompartment (Fig. 7.2) with EncB and EncC possessing ferritin-like domains. It can sequester 30,000 iron atoms, nearly ten times more than ferritin. The internal encapsulin proteins are arranged such that capacity remains to accommodate iron atoms, which enter through gates to narrow channels in the shell; the internal core is not continuous and is divided into about 11-19 granules (each of ~5 nm diameter) that together occupy ~1,600 nm^3 of the particle (McHugh *et al.*, 2014).

Mycobacterium tuberculosis also appears to contain an iron storing nanocompartment which encapsulates a dye-decolorizing peroxidase (Mt-DyP) protein through a unique C-terminal extension within the DyP protein. This nanocompartment also encapsulates Mt-BfrB and Mt-FolB (an iron storage ferritin and a folate biosynthesis enzyme, respectively), and appears to have a role in redox-stress resistance (Contreras *et al.*, 2014).
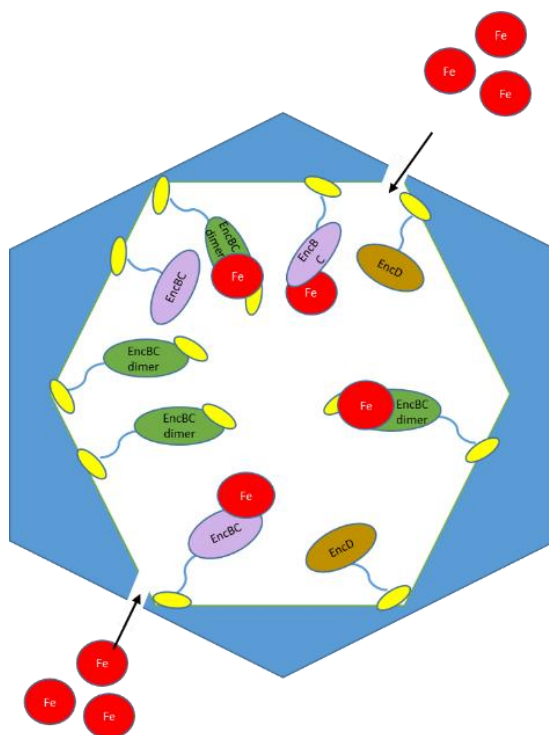
Figure 7.2 Graphical model representing iron encapsulated in the *M. xanthus* nanocompartment. The model shows the binding of the iron atoms to the internal protein anchored into the inner surface of the shell protein by the C-terminal motif (represented by the yellow oval), and attaches to the internal protein through the ferritin-like ruberythrin domain. Adapted from McHugh *et al*. (2014).

Pyrococcus furiosus is a hyperthermophilic archaea species that is anaerobic and nonpathogenic. *It* lives close to hydrothermal vents, at temperatures higher than 100 ˚C and is thus classified as a hyper-thermophilic archaeal organism. It can degrade peptone and utilize both maltose and starch (Fiala & Stetter 1986; *Biller et al., 2002).* It has an important role in biotechnology for its ability to produce highly heat-stable enzymes such as the polymerase enzyme Pfu used in PCR, the *Pyrococcus furiosus* polymerase (Evans *et al*., 2000). This archaea is also known to possess linocin-M18 (an encapsulin) that forms a virus-like particle of 30 nm that is composed of 180 subunits of 38.8kDa (Atika *et al*, 2007). This encapsulin subunit is arranged into two domains, an N-terminal ruberythrin (22-120) and a C-terminal linocin M18 (136-332). It is interesting to note that the ruberythrin domain lacks any rubredoxin domain and only contains two of the four helices normally associated with the di-iron 'erythrin' domain (Fig. 7.3B; Andrews, 2010). This suggest that two erythrin domains combine to allow formation of the four-helix bundle that is required for establishment of the di-iron-binding site of ruberythrins (Andrews, 2010). Interestingly, the linocin-M18 gene sits within a cluster of five iron storage protein genes and a *fur* gene, supporting a role in iron storage (Fig. 7.3A).

However, the purpose of this nanocompartment is unclear as is any potential role in iron storage or redox stress resistance, thus prompting further studies on its function.
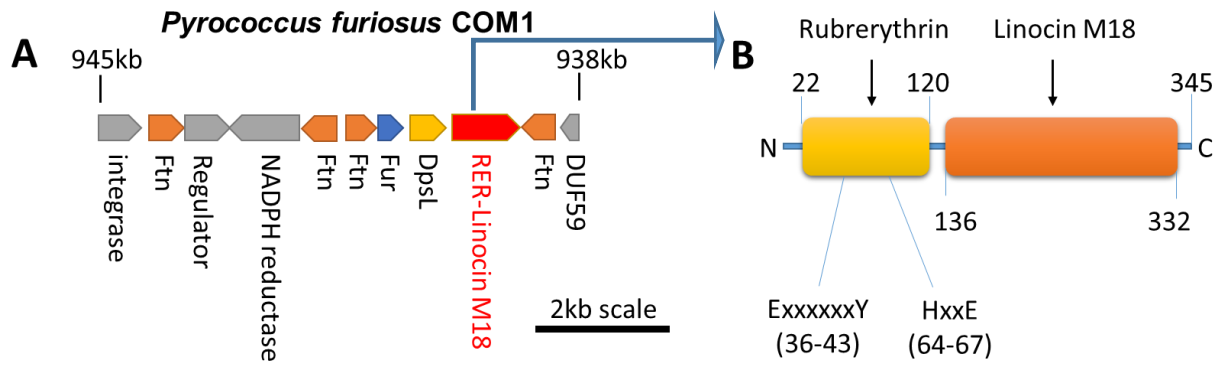
Fig. 7.3. Genetic map of the *P. furiosus* COM1 Linocin locus at ~940 kb (A) and domain organisation of *linocin M18 (B)*. **A**, four *ftnA*-like genes are in orange, one *dps*-like gene is in yellow, and the *fur*-like gene is in blue. **B**, the highly conserved di-Fe centre motifs or rubrerythrins are indicated (just one copy each across two helices, rather than the usual two copies found across four helices) as are the corresponding amino acid residues.

In this chapter, experiments were initiated to study the biological properties of the nanocompartment, encapsulin M18, of *P. furiosus*. Initially, the sequence encoding the linocin M18 protein was codon optimized for expression in *E. coli*. The optimized gene was synthesised and designed with *Nde*I and *BamH*I restriction enzyme sites and supplied in plasmid pMA-T as a transition vector. The synthesised gene was cloned into pET-21a, enabling overexpression in BL21/DE3. The overproduced protein was then purified from the cytoplasmic fraction of the bacterial cells by DEAE chromatography for TEM. The synthesised gene was also cloned into pBADrha to assess any potential for provision of redox stress and low iron resistance in the triple mutant strain, and thus compensate for lack of iron storage capacity.

7.2 Overproduction and purification of the linocin M18 of *P. furiosus* COM1 protein

7.2.1 Codon optimisation of the *P. furiosus* COM1 linocin M18 gene
The nucleotide sequence of linocin M18 gene (*yhjR*) from *P. furiosus* was optimized for expression in *E. coli* by GeneArt, Life Technologies, Invitrogen. The codon optimization manipulates the DNA sequence of the target gene, preserving the encoded amino acid

sequence, whilst the substituting for codons which are frequently used in *E. coli*. The native sequence of *yhjR* had a frequency of optimal codons for *E. coli* of 35% which might delay or arrest translation during overexpression. However, the codon optimised *yhjR* sequence had an increased frequency of 80% (Fig 7.4).
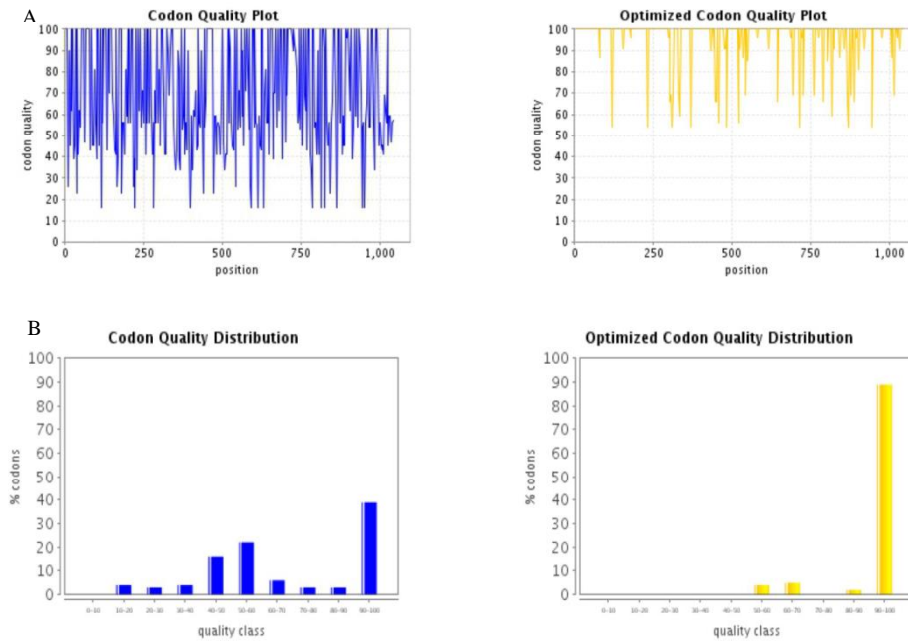
Figure 7.4 Impact of codon optimisation on the nucleotide sequence and expression of *linocin* M18. A, Quality of used codons; B, Codon quality distribution. Native (blue) and synthetic (yellow) linocin M18 gene.

7.2.2 Construction of pET*lin*M18 plasmid

The synthesised linocin M18 gene was designed with *Nde*I and *Bam*HI restriction endonuclease sites at the stop codon and down-stream end (section 2.7), respectively, to facilitate the excision the gene from the pMA-T plasmid (Fig. 7.5). The *Nde*I-*Bam*HI liberated gene fragment was ligated into linearized pET21a plasmid (digested with *Nde*I and *Bam*HI) to give construct pET*lin*M18. The identity of the plasmids thus generated was tested by double digestion with *Nde*I and *Bam*HI (Fig 7.5) and then confirmed by nucleotide sequencing (not shown).
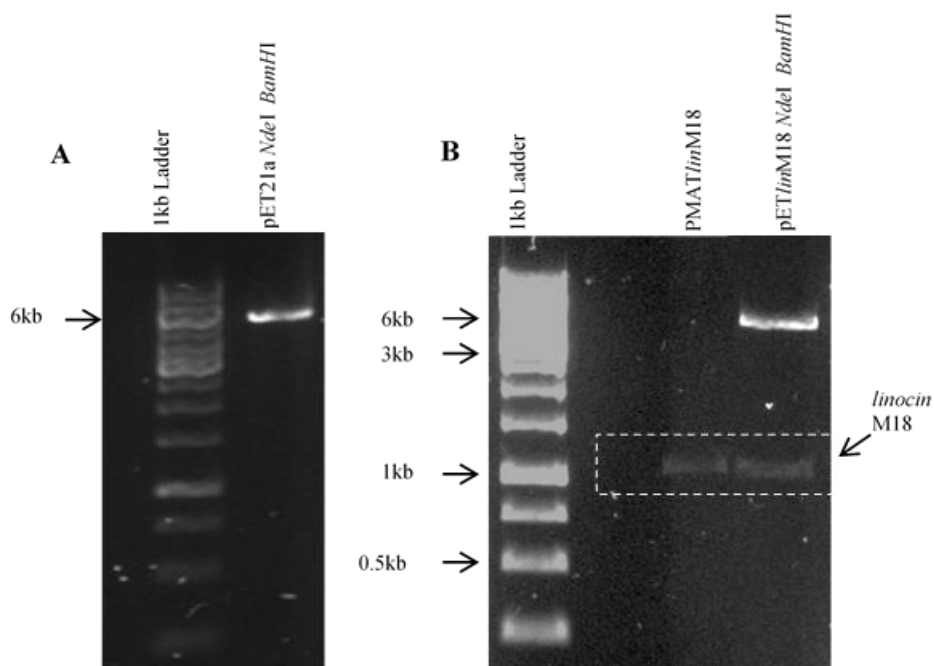
Figure 7.5 Gel electrophoretic analysis of linocin M18 gene cloned into pET21a. A, linearized pET21a plasmid, digested with *Nde*I and *Bam*HI; **B**, the constructed pET-*lin*M18 plasmid digested with *Nde*I and *Bam*HI, and the codon optimised *jhjR* gene from the pMA-T plasmid.

7.2.3 Overexpression of the Linocin M18 protein in BL21/DE3*
7.2.3.1 Small-scale recombinant Linocin M18 protein overproduction

The overproduction of linocin M18 was carried out using pET*lin*M18 transformed in BL21/DE3* at small-scale initially (as described for Dps; section 2.15.1). Both BL21/DE3 (pET21a) and BL21/DE3 (pET21-*lin*M18) strains were grown aerobically at 37 ºC, 250 rpm, in 50 ml LB supplemented with 100 µg/ml of ampicillin. Once the growth reached mid-log (0.5 OD), IPTG was added to induce linicon M18 production. Linocin M18 protein was observed at all time points measured, including at 0 h (pre-induction) (Fig. 7.6).

However, linocin M18 levels were higher at 1-5 h than 0 h, and remained relatively constant over this time period with highest levels apparent in the overnight sample (Fig. 7.6B). In contrast, the empty vector (as a control) induced with IPTG showed no induced band corresponding to that of linocin M18 at ~40 kDa (Fig. 7.6A). Thus, the small-scale overproduction was successful with linocin produced at ~13% of total cell protein according to densitometric analysis.
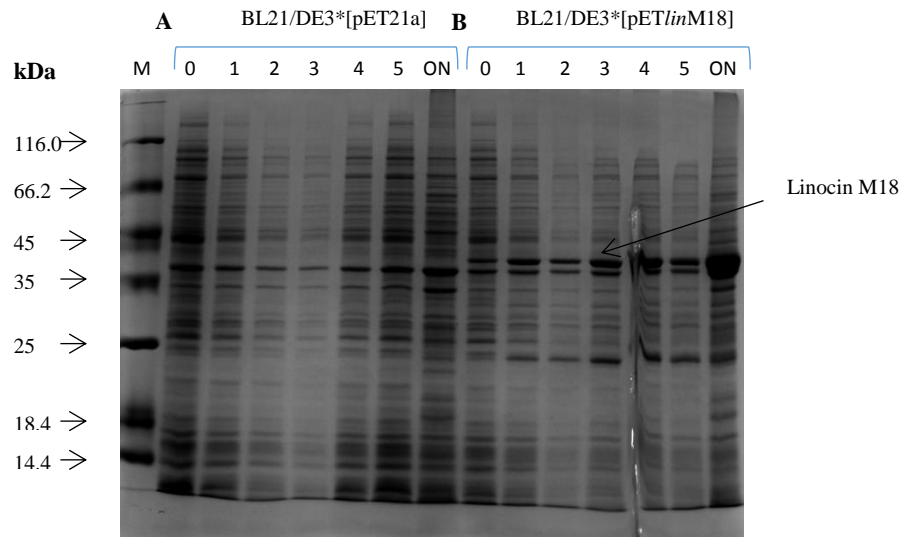
Figure 7.6 Small-scale overexpression of linocin M18 analysed by 15% SDS-PAGE. Growth was carried out in LB containing 100 µg/ml ampicillin at 37 °C. **A**, BL21/DE3*(pET21a) samples at 0-5 h post-induction and after overnight growth (as indicated). **B**; BL21/DE3*(pET*lin*M18) samples, as for A. 0.05 OD units of denatured cells were applied to each lane for all whole-cell samples.

7.2.3.2 Solubility test of the overexpressed recombinant protein

The solubility of the linocin M18 protein was tested before proceeding to large-scale overexpression and purification (as described for Dps; section 2.15.2). This was achieved by addition of B-PER^{TM} to a set of the pellets from a small-scale overexpression to allow rupture of the cells and release of soluble cellular contents. Both the supernatant (soluble fraction) and pelleted cell debris (insoluble fractions) samples were analysed by 15% SDS-PAGE. The linocin M18 presented with ~70% of the protein in the insoluble fraction and ~30% soluble at 3 h post-induction (Fig. 7.7). Thus, the 3 h post-induction time point

appeared to generate the highest quantity of soluble linocin M18 for the range of times tested.
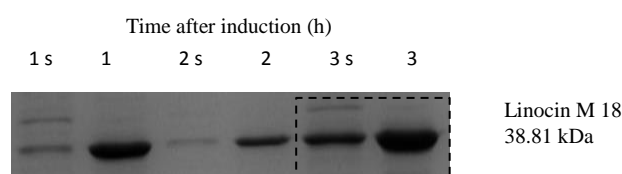
Figure 7.7 Analysis of Linocin M18 solubility. 15% SDS-PAGE analysis of soluble and insoluble fractions of the linocin M18 overproducing strain treated with 'B-PER™ Complete' (Thermo-Scientific). Whole-cell pellets (0.5 OD units) of the BL21/DE3*(pET*lin*M18) strain were harvested at the indicated times (1-3 h) after IPTG induction. These were treated with 100 µl B-PER™ to give insoluble and (S) soluble fractions.

7.2.3.3 Large-scale overexpression of linocin M18 recombinant protein

According to the results, linocin M18 was overproduced in soluble form. Thus, a large–scale overproduction was performed to generate sufficient protein for purification (as described for Dps; section 2.15.3). The cell pellet of the BL21/DE3*(pET*lin*M18), grown as above but in 2 x 500 ml of LB, was harvested 3 h post-induction by centrifugation at 6000 x g (Sorval RC5B+ with SLA-3000 rotor) for 30 min at 4 °C. The harvested pellet (1.88 g) was then maintained at -80 ºC before further treatment.

7.2.3.4 Protein purification

The cell pellet from the large scale overproduction was defrosted and resuspended in 25 ml of resuspension buffer (50 mM Tris, 15 mM mannitol, 5% glycerol, 1 mM DTT, pH 8.0). The homogenous suspension was then lysed by passage through the French pressure cell at 20,000 psi, three times (section 2.15.4). The resultant lysate was subsequently applied to a column packed with 20 ml of DEAE-Sepharose™, for purification by ion-exchange chromatography, using buffer A for binding and equilibration (50 mM Tris, 1 mM DTT, pH 8.0) and buffer B for elution (as buffer A but with 1 M NaCl). It should be

noted that linocin has a theoretical pI of 4.9, so is expected to be well suited to isolation by an anion-exchange chromatography. Elution was carried out using a linear gradient of 0-1 M NaCl (section 2.15.5). Two overlapping major peaks were observed in the elution profile spanning across fractions 9-22 (Fig. 7.8), after which the absorbance dropped. SDS-PAGE analysis was performed for the fractions ranging from 11 to 18 (Fig. 7.9).
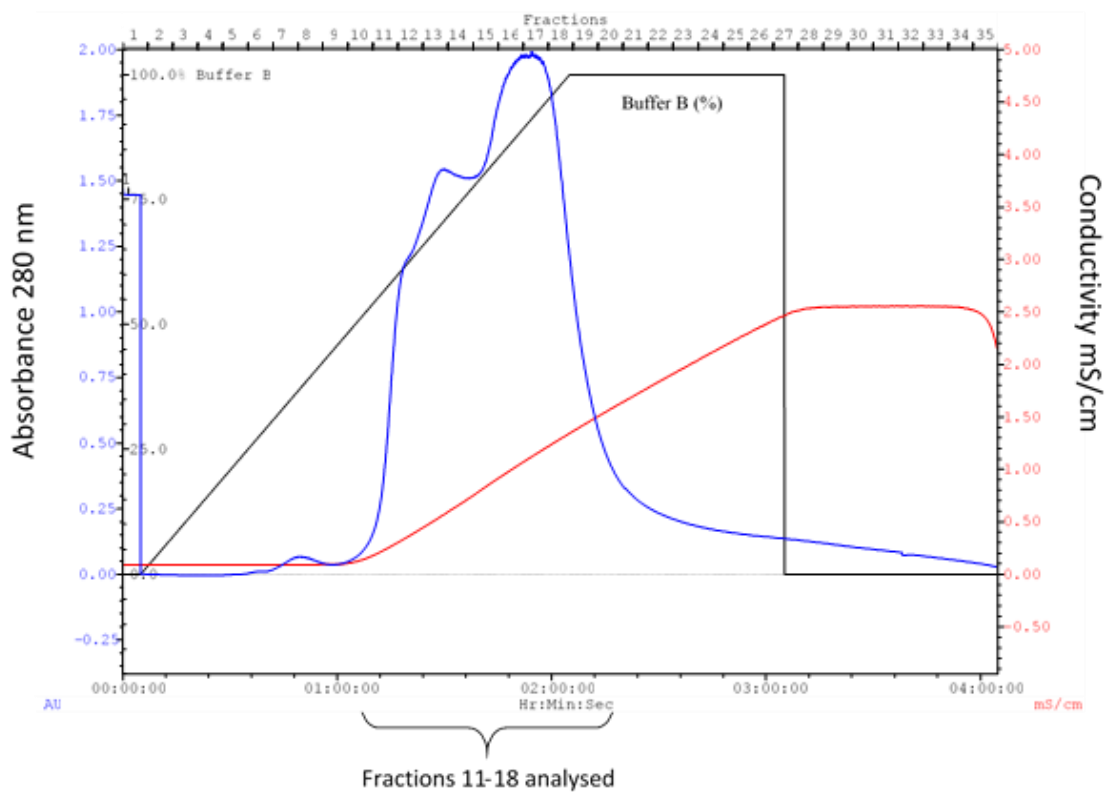
Figure 7.8 Elution profile of linocin M18 protein during ion-exchange chromatography. A DEAE-Sepharose™ column was used as described in methods (Section 2.15.5). Fractions 11-18 were analysed by 15% SDS-PAGE.
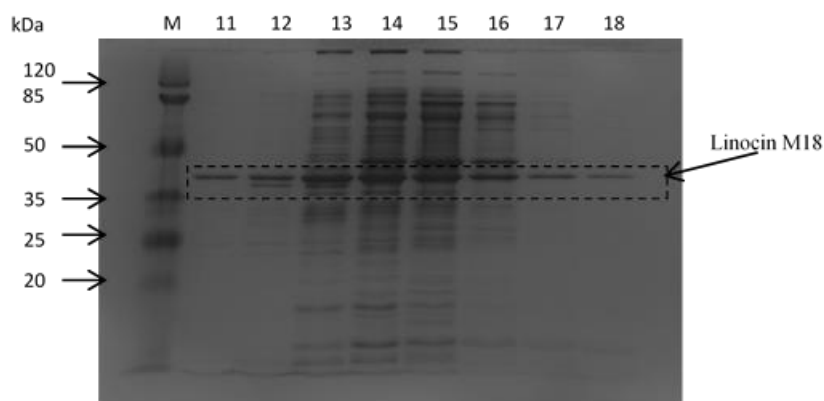
Figure 7.9 SDS-PAGE analysis of fractions obtained for linocin M18 purification by ion-exchange chromatography. 5 µl of each fraction, as indicated, were loaded and analysed by 15% SDS-PAGE. The linocin M18 protein can be seen eluting in 11-18 fractions at a mass of ~40 kDa.

The fractions with the expected ~40 kDa protein were combined into two pools (A, fractions 11-12; B, fractions 13-16) and then analysed again by SDS-PAGE (Fig. 7.10). This showed that pool A had low concentration (208 µg/ml) but appeared relatively pure, whereas pool B has higher concentration (2 mg/ml) but included a number of impurities.

To determine whether these samples (pools A and B) could be stored at -80 ˚C without loss, samples were frozen, defrosted and then centrifuged to remove any precipitated protein, and then compared to non-frozen equivalent samples by SDS-PAGE (Fig. 7.10). No sign of any losses were apparent and so it was assumed that the linocin M18 protein samples could be stored by freezing at -80 ˚C without loss of solubility.
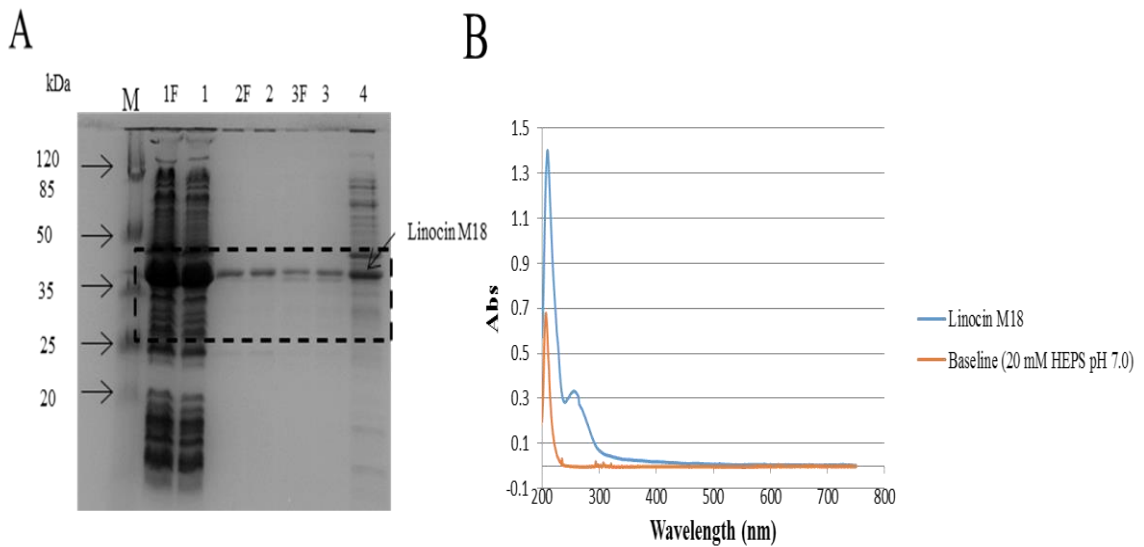
Figure 7.10 SDS-PAGE and spectroscopic analysis of linocin M18 after ion-exchange chromatography. A, 15% SDS-PAGE analysis of linocin M18 samples obtained from anion-exchange chromatography: 1, crude soluble protein sample (4.3 mg/ml; 25 ml) post French press; 2, unbound protein; 3, pooled fractions 11-12 (208 μg/ml; 14 ml); 4, pooled fraction 13-16 (2 mg/ml; 28 ml). 'F' refers to samples obtained after freezing at -80 ℃ followed by centrifugation. **B,** UV-visible spectrum of the semi-purified linocin M18 protein.

7.2.4 Migration of linocin M18 in native PAGE

The migration of protein molecules during electrophoresis is determined by a combination of size and charge. Native-PAGE can used to analyse the charge density and assembly state of proteins in their folded, functional states. This requires the preparation of samples in a buffer without denaturing agents. Under such conditions, proteins will migrate according to their charge to mass ratio. In order to gain some impression of the assembly status of the purified linocin protein, it was thus subjected to native PAGE. However, the linocin M18 protein failed to enter the gel, even when the acrylamide was at just 6% (data not shown), suggesting that it forms a high mass assembly, greater than 1000 kDa. For this reason, a native agarose gel was used (since this type of gel fractionates molecules of higher mass than can be achieved by PAGE), along with BSA and horse-spleen ferritin (450 kDa) as markers. The fully assembled linocin M18 would consist of 180 subunits of 38.9 kDa giving a total mass of ~7,000 kDa. The native agarose gel electrophoretic analysis showed that linocon M18 has a lower mobility than that of ferritin or BSA, which would be consistent with a higher mass than these two proteins

176

(Fig. 7.11). Thus, the native electrophoresis analysis performed here is consistent with assembly of linocin M18 into higher order structures, although could reflect a charge effect.

To test the possible iron uptake capacity of the lincocin M18 complex, ferrous ammonium sulphate (FAS, at 20 or 200 µM final concentration, anaerobically prepared, N_2 purged) was added to the linocin M18 protein (286 µg/ ml) at room temperature under aerobic conditions with or without 1 mM of hydrogen peroxide, the reactions then were incubated for 1 h.

This addition might result in iron core formation as a soluble yellow colour was formed in the presence of linocin M18 protein. The iron treatment had no apparent effect on the mobility of linocin M18 (Fig. 7.11), suggesting no change in aggregation status or surface properties. The linocin M18 sample pre-treated with hydrogen peroxide and FAS showed slightly slower migration indicating a potential change in assembly status or surface properties (Fig. 7.11). However, no clear evidence of iron core formation was obtained. This may reflect the failure of sequestering iron mechanism (in spite of the evidence of form an assembled encapuslin structure; see below), the use of room temperature conditions for core formation rather than the high temperatures at which *P. furiosus* is usually associated, or the impure nature of the linocin M18 preparation.
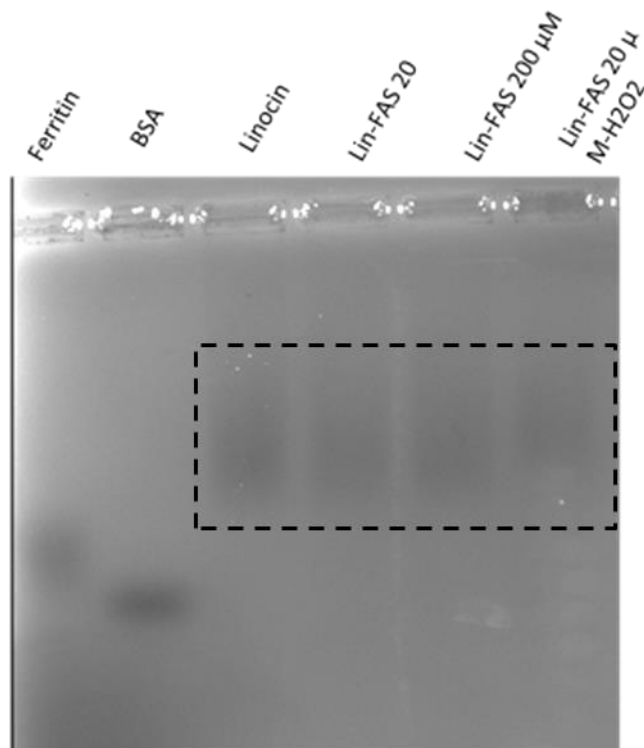
Figure 7.11 Native electrophoresis of linocin M18. Non-denaturing 1% agarose gel electrophoresis (section 2.21) of linocin M18. Samples, as indicated, has been pretreated with 20 or 200 μM FAS or 20 μM FAS plus 1mM H$_2$O$_2$. Protein bands were stained with Coomassie blue. Horse spleen ferritin and bovine serum albumin were included for mobility comparison.

7.2.5 Electron microscopy of the linocin M18 protein

The above analysis indicated that the isolated linocin M18 might form a high order assembly. To determine whether approximately spherical particles of the expected (30 nm) diameter might be formed, a the linocin M18 protein sample was applied to a copper grid, stained with 1% uranyl acetate and then subjected to electron microscopy (Methods 2.16). Transmission electron microscopy (TEM) revealed particles of the size and shape anticipated for the nanocompartment linocin M18 spherical particles, as first reported by Namba *et al*. (2005) which was also expressed in *E. coli* as a C-terminal His-tag. The measurement of the particles imaged by TEM showed that the spherical particles have a diameter of 30 nm (Fig. 7.12) as reported previously (Namba *et al*., 2005; Akita *et al*., 2007). The linocin protein was only partly pure with might explain the presence of 'debris' material with the EM images below. For the FAS treated linocin, the images generated were different in form with a thinner shell exhibited and larger central core.

This preparation had a soluble brown colour associated with it, suggestive of iron core formation.

In summary, the recombinant linocin M18 protein formed spherical particles of the expected size indicating that it had assembled into the 180 subunit complex.   The EM suggests that there may be an iron core associated with the spherical particles upon FAS treatment.
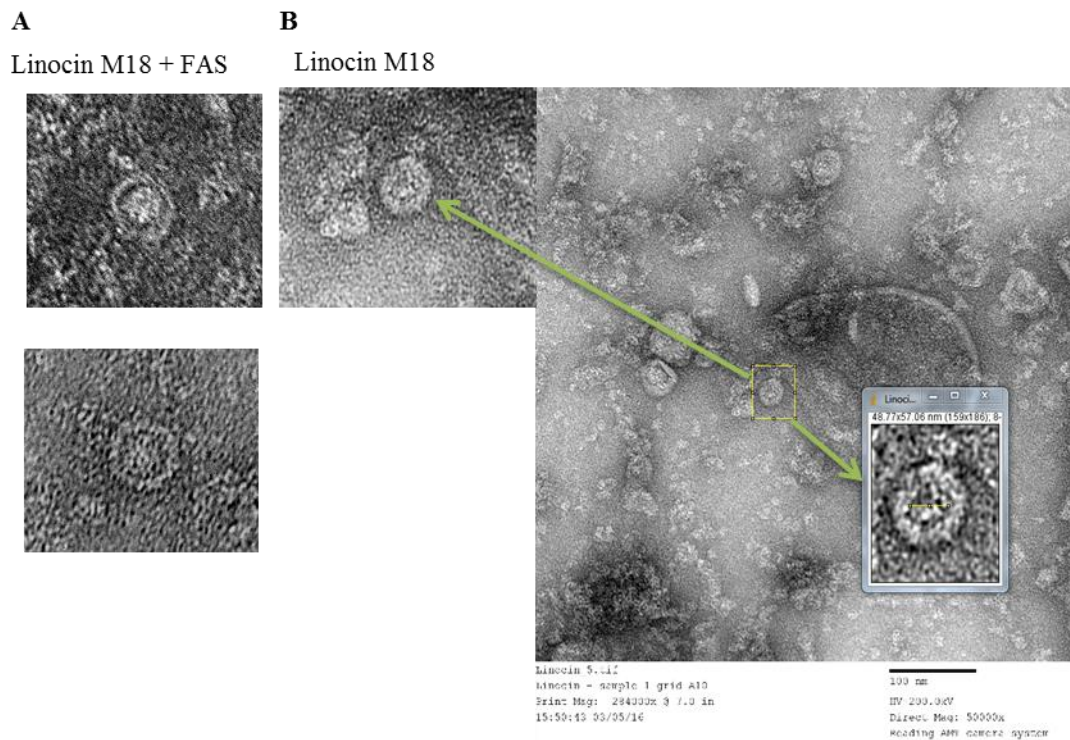
Figure 7.12 Negatively-stained transmission electron micrographs of linocin M18 with and without FAS treatment. TEM analysis of the uranyl acetate stained linocin M18 preparation.

7.3 Cloning of the codon-optimized linocin M18 of *P. furiosus into the pBADrha inducible vector.*

The above experiments failed provide any evidence for iron accumulation by the linocin M18 particle *in vitro*. Thus, the linocin M18 gene was used to complement the triple iron storage mutant of *E. coli* to determine whether it might reverse, partly or completely, the low iron growth and peroxide resistance defect of this mutant.

7.3.1 Isolation of the linocin M18 gene for cloning into pBADrha to form pBAD-*lin*M18.

Thus, the codon-optimised linocin M18 gene was released from pMAT-linocin-M18 by *Nde*I and *Bam*HI digestion (Fig. 7.13A) and purified by gel extraction (Fig. 7.13B). This fragment was then ligated with *Nde*I/*Bam*HI-digested pBADrha and ligations were used to transform *E. coli* TOP10.
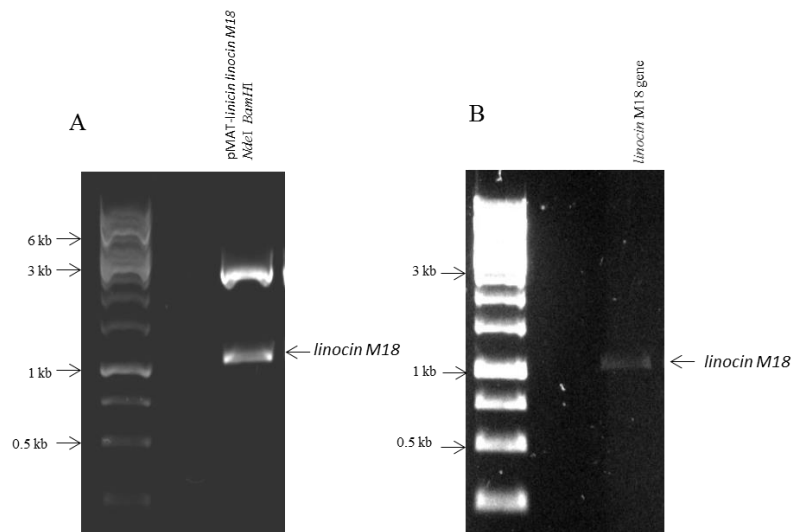
Figure 7.13 Gel electrophoretic analysis of the *Nde*I and *Bam*HI digested linocin M18 DNA fragment. A, *Nde*I and *Bam*HI digested pMAT-linocin-M18 prior to gel purification of the released insert. **B,** gel extracted linocin M18 fragment.

After transformation, plasmid DNA was extracted from Cm^R transformant colonies and all samples were digested with *Bam*HI and *Nde*I. Plasmids with the anticipated restriction pattern (1050 and ~6000 bp) (Fig. 7.14) were selected for confirmation of identity by

nucleotide sequencing. One of these was selected for further work, and was designated pBAD-*lin*M18. This was used to transform the triple iron storage mutant.
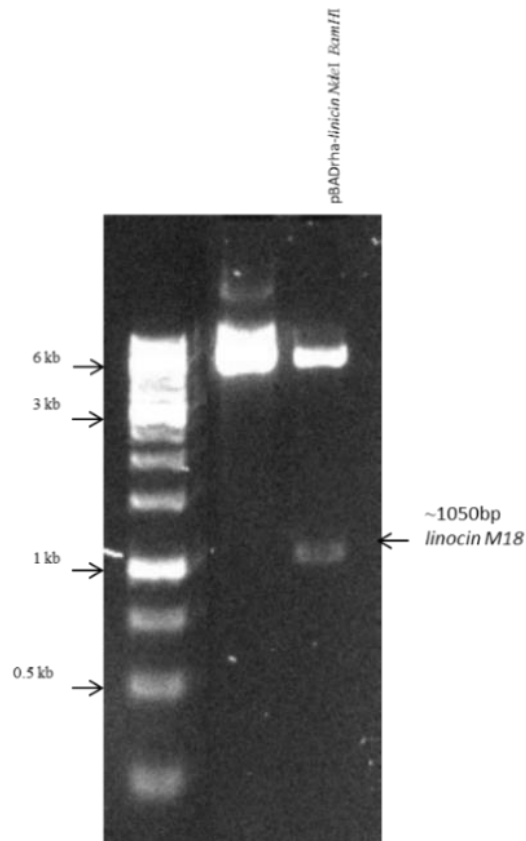
Figure 7.14 Gel electrophoretic analysis of pBADrha-*lin*M18**.** Ladder (left), and undigested (centre) and *Nde*I/*Bam*HI-digested pBAD-*lin*M18 (right).

7.4 Effect of linocin M18 expression in the *E. coli* triple iron-storage mutant

7.4.1 Confirmation of *lin*-M18 expression in *E. coli*

The overexpression work performed above shows that linocin M18 can be produced in a stable fashion when the gene is expressed from a powerful promoter. However, it remains unclear whether significant linocin M18 can be generated when its gene is under control of the *rha* promoter. Thus, to determine whether the linocin M18 gene is induced from pBADrha-*lin*M18 by rhamnose, protein production was assessed through the SDS-PAGE analysis of the whole-cell extracts of overnight cultures of the triple mutant strain

carrying pBAD-*lin*M18 or pBADrha (as a control), with and without rhamnose. The resulting SDS-PAGE showed that a protein band corresponding in size to linocin-M18 is indeed generated in the pBAD*lin*-M18 transformant in the presence of rhamnose (Fig. 7.15). However, this was not produced in the absence of inducer or in the vector control. Thus, pBAD*lin*-M18 can be used for investigating the phenotype conferred by linocin-M18 expression in *E. coli* in the future work of the phenotype experiment.
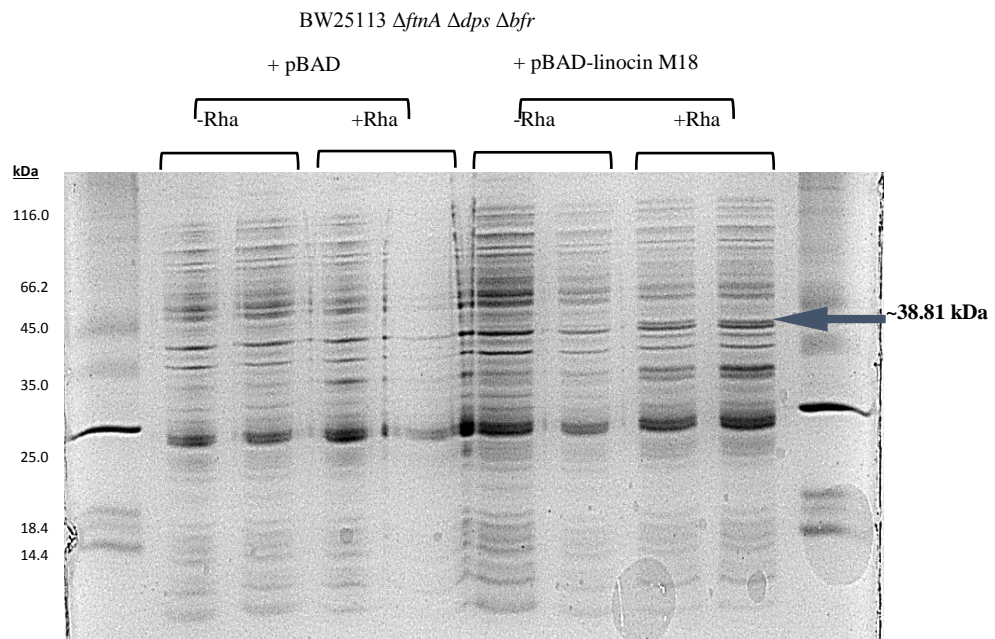
Figure 7.15 SDS-PAGE analysis of expression of the codon optimized linocin M18 gene from pBADrha-*lin*M18. Transformants of *E. coli* BW25113 Δ*ftnA* Δ*dps* Δ*bfr* were grown overnight with and without rhamnose in LB.

7.4.2 The effect of the complementation of BW25113Δ*ftnA*Δ*dps*Δ*bfr* with the linocin M18 gene under low-iron and redox-stress conditions

In an attempt to observe a phenotypic influene of the linocin M18 protein in *E. coli*, the complemented triple mutant was grown under redox stress and low iron conditions. The expectation was that the proposed ability of linocin particls to incorporate iron into its lumen would result in an iron storage effect leading to increased resistance to H_2O_2 and enhanced low-iron growth. The triple iron-storage mutant was employed for this purpose since it lacks any other source of iron-storage capacity.

The BW25113 Δ*ftnA* Δ*dps* Δ*bfr* strain carrying pBAD-*lin*M18 exhibited an increase in resistance to 200 µM hydrogen peroxide upon rhamnose induction (Fig. 7.16 B). At 19 h, culture OD was at 0.21 whereas the vector controls showed no growth by this stage when peroxide was present (Fig. 7.16A), as was also the case for the non-induced pBAM-*lin*M18 culture. The induction of the linocin protein caused a decrease in peroxide-induced lag phase by ~6 h compared to the un-induced control, and to the vector controls (Fig. 7.16). The exact mechanism by which linocin M18 enables this effect is unclear. It could result from iron sequestration within the hollow centre of the linocin particle or from decomposition of H_2O_2 in a process resembling that of Dps. Indeed, the linocin M18 particle may function similarly to the *M. xanthus* and *M. tuberculosis* encapsulin systems; deletion of the corresponding genes resulted in increased hydrogen peroxide sensitivity in *M. xanthus* (McHugh *et al*., 2014) and reduced survival in host cells from *M. tuberculosis* (Contreras *et al*., 2014).

Expression of linocin M18 also provided a low-iron growth advantage in minimal medium (no iron added) (Fig. 7.16B). The induction of linocin protein production caused a growth enhancement by ~20% compared to the uninduced control, and to the vector controls (by ~40%) (Fig. 7.16). Interestingly, the uninduced control also showed increased growth compared to the vector control.

These results suggest that the expression of *P. furiosus* linocin M18 resultst in provision of both redox stress resistance and low iron growth enhancement; these effects are presumed to result from the iron sequester of assembled linocin particles.
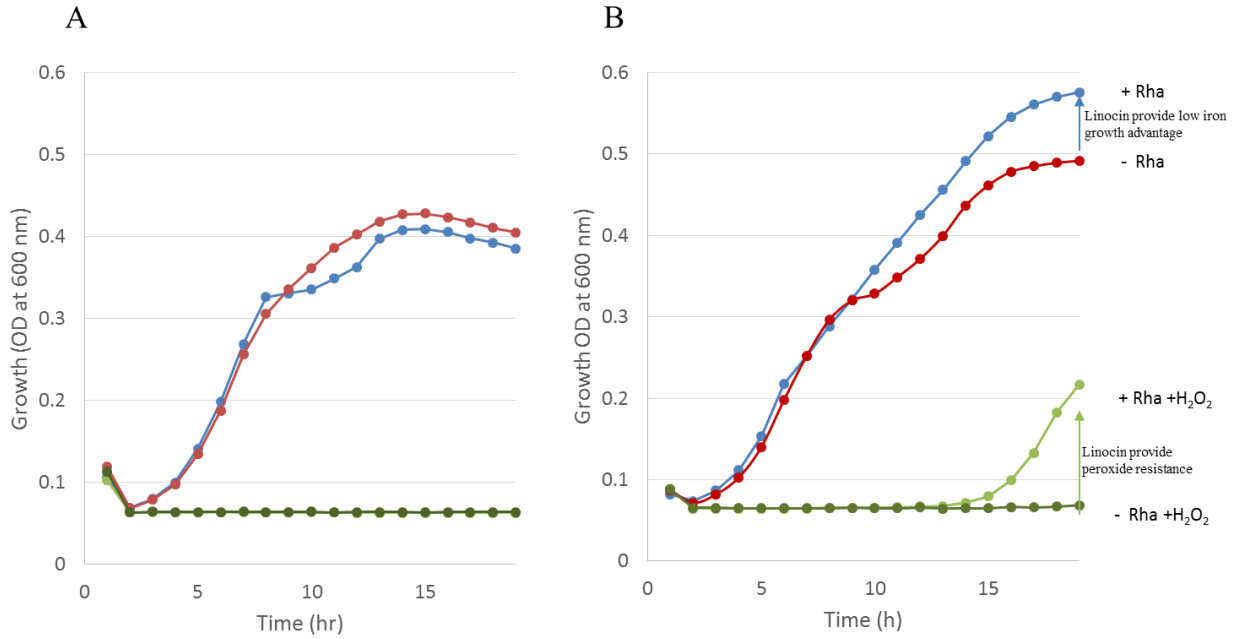
Figure 7.16 Effect of linocin production on growth under redox-stress conditions.
Strain BW25113 Δ*ftnA* Δ*dps* Δ*bfr* carried either the pBAD vector (A) or pBAD-*lin*M18
(B). Strains were grown in glucose M9 minimal medium with or without 200 µM H_2O_2.
Pre-cultures were grown in the same medium but with 20 µM ferric citrate, with/without
100 µM rhamnose, as indicated (there was no rhamnose in the final culture). Data are
the average of duplicate cultures. Repeated once with similar results.

7.5 Discussion

To summarize the experiments carried out in this chapter, these experiments were focused on the archaeal encapsulin (Linocin M18) of the hyperthermophile *Pyrococcus furiosus*. Overproduction of the authentic protein (non-modified with tags) was achieved and the protein was subsequently isolated in partly pure form *E. coli*. The linocin gene was generated by synthesis and codon optimization by GeneArt[TM]; the optimisation was performed to increase the overexpression potential in *E. coli* by limiting any potential problems caused by rare codons. The synthesised gene then cloned into the overexpression plasmid pET21a and overexpression was performed in BL21/DE3 successfully in that a protein of the expected size was generated in abundance (~13% of total protein) and in partly (~30%) soluble from. Large-scale purification from 1 litre of LB yielded a total of ~3 mg of partially pure linocin M18 protein following anion-exchange chromatography. TEM analysis of uranyl acetate stained samples showed that the shape and size of the recombinant linocin M18 protein were as expected, with spherical particles of 30 nm diameter apparent, this result is largely in agreement with the shape of nanocompartment particles isolated previously from *T. maritima*, *P. furiosus* and *M. xanthus* (McHugh *et al*., 2014; Sutter *et al*., 2008; Akita *et al*., 2007; Namba *et al*., 2005).

The isolated linocin M18 protein slowly migrated during the native electrophoresis, supporting formation of a high-order oligomeric structure. No evidence for iron core formation was obtained through in vitro approaches. The shape of the protein sample was not affected with the addition of the FAS as shown in the protein migration in non-denatured PAGE. The linocin M18 protein function was also explored *in vivo* through complementation of the triple iron-storage mutant. SDS-PAGE analysis suggested that the linocin M18 protein was generated at low level in the triple mutant upon induction from a plasmid-specified *rha* promoter. *E. coli* BW25113 Δ*ftnA* Δ*dps* Δ*bfr* carrying pBAD-*lin*M18 exhibited enhanced hydrogen peroxide resistance upon rhamnose induction. This suggests that the *P. furiosus* encapsulin system can provide a protective function similar to that observed for the *M. xanthus* encapsulin (McHugh *et al*., 2014) and *Mycobacterium* Enc nanocompartment systems (Manca & Paul *et al*., 1999; Contreras *et al*., 2014). The induction of linocin M18 in the triple iron-storage mutant appears to support the growth in low iron condition.

Chapter 8

8 General discussion

8.1 Generation of a set of isogenic iron-storage mutants. The work described in this thesis largely focuses on the specific functions of the three iron-storage proteins of *E. coli*. The first requirement for this research was to produce a set of isogenic single, double and triple mutants for comparison and for complementation. Thus, the corresponding Kn^R mutations were transferred from the relevant donor strain to a recipient strain by P1 transduction. This proved to be a challenging process due to contamination of the available P1 phage stocks. This problem was eventually solved by securing a fresh stock from another lab. Recipient strains were first treated with pCP20 to enable the removal of the Kn^R cassette associated with each marked iron-storage-gene mutants; the pCP20 plasmid mediates the thermal induction of FLP synthesis that drives the non-homologous recombination at the FRT sites flanking the Kn^R cassette. This reiterative process of cassette removal and horizontal gene transfer by transduction generated the desired set of iron-storage gene mutants that were confirmed by PCR and anti-FtnA/Bfr/Dps western blotting.

8.2 Establishing phenotypes for the *E. coli* iron-storage mutant strains. The mutants thus generated were analysed for their redox-stress resistance using hydrogen peroxide. The results showed that the H_2O_2 sensitivity of the Δbfr, $\Delta ftnA$ and Δbfr $\Delta ftnA$ mutants was unaffected with respect to that of the wild type. This finding matches that of previous work (Abdul-Tehrani *et al.,* 1999; Keyer and Imlay, 1996). However, the mutants lacking Dps showed a reduced capacity to withstand challenge by hydrogen peroxide, and the raised sensitivity of the $\Delta ftnA$ Δdps strain was approximately the same as that of the Δdps mutant. Thus, FtnA does not appear to contribute to redox-stress resistance (against H_2O_2). This observation is consistent with the perceived protective role of Dps under redox stress (Almiron *et al.,* 1992; Choi *et al.,* 2000; Frenkiel-Krispin *et al*., 2004; Velayudhan *et al*., 2007) and matched previous work indicating no major role for FtnA of *E. coli* in peroxide resistance (Abdul-Tehrani *et al.,* 1999; Keyer and Imlay, 1996). Surprisingly, the presence of *bfr* enhanced sensitivity to peroxide stress in LB when *dps* was nullified. However, in minimal medium the reverse effect was obtained – the absence of *bfr* enhanced peroxide stress in a Δdps background. Thus, it appears that Bfr can assist in combating H_2O_2 toxicity, in the absence of Dps, in minimal medium but in LB the

presence of Bfr raises peroxide sensitivity when Dps is also absent. The reason for this difference between rich and defined medium is unclear.

The effect of low iron conditions on the mutants was assessed by monitoring growth in minimal medium. Results showed that the deletion of *dps* does not affect growth in the presence of DTPA. However, the *ftnA* mutant grew less well in comparison to the wild type, which is consistence with Abdul-Tehrani *et al.* (1999) who also found that the absence of *ftnA* reduces the rate of growth under iron-restricted conditions. The results also showed that there is a role for Bfr in enhancing iron-restricted growth and this matches results obtained for *S. typhimurium* (Velayudhan *et al.*, 2007). The double *ftnA bfr* mutant was more growth impaired than the other double and single mutants under iron restriction. The lack of all three iron-storage proteins gave the greatest growth impairment under iron-restriction, ~60% reduction cf. the wild type. This result suggests that, in the absence of both Bfr and FtnA, the additional absence of Dps reduces iron-restricted growth still further. Thus, it appears that Dps can contribute to iron-restricted growth, but only when no other iron-storage protein is available. This is somewhat consistent with the results of Velaydhan *et al.* (2007) who found that the additional absence of Dps in a *Salmonella* iron-storage triple mutant reduced the total iron content further than observed for the *ftnA bfr* double mutant.

In order to determine the effect of the iron-storage mutations on the capacity of *E. coli* to store iron and to indicate the relative functions of the iron-storage proteins in this process, total cellular iron contents were measured by ICP-OES. The deletion of all three iron-storage proteins genes gave a significant reduction (78% of wild type) in the total iron content in stationary phase upon growth with sufficient iron in rich medium (LB). Upon growth in minimal medium supplemented with iron, the reduction in the cellular iron content of the triple mutant was even greater (at 35% of wild type). In combination, these results further indicate the roles of iron-storage proteins in maintaining iron in the bacterial cell in a safe form and their iron-homeostatic contribution in supporting both iron-restricted growth and redox-stress resistance.

In summary, both Bfr and FtnA make major contributions to the total iron stores of *E. coli* K-12 in stationary phase following aerobic growth in iron-supplemented M9 medium, with Dps contributing relatively little except in the absence of Bfr and FtnA. Up to 62% of cellular iron can be stored in the wild type by a combination of Bfr, FtnA and

Dps. Furthermore, the whole-cell iron contents of the mutant strains (Fig. 3.30) correlate well with the iron-restricted growth phenotypes determined (Fig. 3.26-28) which is fully consistent with the notion that the poor growth for the iron-storage mutants under low-iron conditions is proportion to the loss of iron storage capacity.

8.3 Complementation of the triple iron-storage mutant with inducible versions of each of the iron-storage protein genes of *E. coli*. The work above generated and characterised the triple iron-storage mutant required for complementation with inducible forms of *ftnA*, *bfr* or *dps*. The next aim was to determine to what degree the corresponding proteins are functionally interchangeable, and whether their distinct roles in storage and redox stress resistance are dictated by differences in their degrees and patterns of expression – such factors should be equivalenced by controlled expression from the inducible pBADrha plasmid. The results showed that the expression of the *bfr* or *dps* (but not *ftnA*) genes significantly enhanced the resistance of the triple mutant to hydrogen peroxide. These results support the capacity of Dps to act in redox stress resistance. The protective function of Dps against hydrogen peroxide in *E. coli* is consistence with its function as determined previously (e.g. Almiron *et al.,* 1992; Chiancone *et al*., 2004; Ceci *et al*., 2007; Choi *et al*., 2000) in bacteria such as *Helicobacter pylori* and in *E. coli* O157. Induction of Bfr production supported both iron-restricted growth and redox-stress resistance, indicating that Bfr both provides a source of intracellular iron to promote iron-restricted growth and limits the harmful effects of cytoplasmic iron under redox stress. The redox-stress effect could be mediated by sequestration of free cellular iron or by supporting the synthesis of peroxidases, Fe-SOD and catalases that require iron (or haem) for function. Indeed, such a role has been suggested for Bfr in *Pseudomonas aeruginosa* and *Salmonella enterica* (Ma *et al*., 1999; Velayudhan *et al*., 2007). In contrast to the results here, previous research (Keyer & Imlay 1996; Abdul-Tehrani *et al*., 1999) indicated that Bfr has no notable role in redox stress or iron storage in *E. coli*. Such findings might be caused by weaker expression for *bfr* in wildtype *E. coli* with respect to that achieved when *bfr* is under control of the inducible promoter used here, or due to the combined absence of both Dps and FtnA which provides Bfr with an opportunity to compensate for lack of Dps. The ability of induced Bfr in the triple mutant to engage in iron storage and redox-stress resistance was further supported by the positive impact of *bfr* induction on cellular iron content. Lack of inducer resulted in a very limited effect for the plasmid-encoded *bfr*, indicating that good expression of *bfr* is required for any major

positive impact to be realised. The weak impact of FtnA induction on cellular iron content in the triple mutant is consistent with the results of Liu *et al*. (2016); this weak effect was assumed to reflect low FtnA levels (see below). On the other hand, Dps expression raised total cellular iron levels similar to those achieved by Bfr, which indicates that Dps stores cellular iron but that this is not readily available to counter iron restriction. This may reflect a high iron uptake activity, but relatively weak iron release activity.

8.4 FtnA is subject to the N-end rule. To investigate the reason for the lack of any complementation by the plasmid-borne *ftnA*, experiments to assess the levels of the three iron-storage proteins in the BW25113 Δ*ftnA* Δ*dps* Δ*bfr* triple mutant strain complemented with the pBAD-*ftnA*, -*bfr* or -*dps* plasmid were performed. The results showed that the levels of FtnA are much weaker than those for Bfr and Dps, which would explain the inability of the plasmid expressed *ftnA* to complement the triple mutant. It was considered that this effect could be due to a higher rate of turnover for FtnA, and the possibility that FtnA is subject to enhanced degradation according to the 'N-end rule' was investigated (Varshavsky, 1996; Bivone *et al*., 2010). Thus, the second residue (Leu) was substituted with Ala or Lys ('stabilising' residues). This alteration elevated FtnA (L2K and L2A substitutions) levels to a degree similar to those of plasmid-dependent Bfr and Dps. When the triple mutant was complemented with pBAD-*ftnA*L2→A (or pBAD-*ftnA*L2→K) there was a clear increased growth under iron restriction, but no enhanced resistance to redox stress was achieved. Thus, the lack of complementation obtained before with plasmid-encoded *ftnA* appears due to the low stability of the encoded protein.

The possibility that the FtnA protein might be selectively targeted by one or more proteases for degradation was assessed by comparison the levels of FtnA in the wild type and a series of protease mutants (Δ*ftsH*, Δ*clpS*, Δ*clpA*, Δ*clpP*, Δ*clpX* and Δ*lon*). The results showed that the *ftsH* mutant was the only protease mutant that gave an increase in the level of FtnA; this result is in keeping with previous work showing that FtsH not only degrades integral membrane proteins but can also degrade those that are soluble and cytosolic (Langklotz *et al*., 2012).

8.5 Dps overproduction and purification. A requirement of the research work was the overproduction and purification of the Dps protein to allow generation of polyclonal antibodies. To enable this, the *dps* gene from *E. coli* was cloned into a high copy number

plasmid, pET21a, which contains a T7 RNA polymerase promoter. The constructed plasmid containing *dps* was used to produce a recombinant Dps protein. This was followed by purification by anion exchange chromatography, which was preceded by a step of solubilisation by treatment with urea followed by refolding, due to the production of the recombinant protein in an insoluble form. The purified Dps protein obtained appeared homogenous and enabled further investigation, such as ESI-MS, iron core formation and the generation of polyclonal antibodies. Characterisation of the purified recombinant protein was carried out by electrospray ionization mass spectrometry (ESI-MS), which showed that the protein was of a size 128.3 Da below that predicted. This difference is likely due to the removal of the N-terminal methionine (131.2 Da). Thus, it would appear that the Dps of *E. coli* is subject to the post-translational removal of its N-terminal Met by methionine aminopeptidase (MAP). This is consistent with the presence of Ser at position 2, which has a relatively small side chain that would not therefore be expected to inhibit MAP activity (Frottin *et al*., 2006) and also matches the 91% likelihood Met cleavage prediction of the TermiNator tool. There was no evidence for iron core formation and it is possible that the protein failed to properly assemble. This conclusion was partly based upon the result which showed that the purified recombinant Dps had higher migration than horse spleen ferritin, with poorly resolved bands of low mobility at the top of the native gel in the native PAGE, of roughly equal intensity. The iron storing capacity was also assessed with results indicating that the protein does not show iron-sequestering activity as no band was observed for the Dps protein preincubated with 1 mM of ferrous ammonium sulphate (FAS) in the non-denatured-PAGE stained with iron stain. This might be due to the effect of the denaturation and refolding during the purification process, as it is possible that the aggregation of the overexpressed recombinant protein in insoluble form has a consequence on the activity of the encoded protein (Villaverde & Carrió 2003). Although, there was no evidence that the purified Dps protein formed a 12-mer capable of iron storage, the purified Dps protein was be able to generate polyclonal antiserum. This aim was achieved in Dundee Cell products Ltd. A 90-day protocol was performed for polyclonal antibody production white New Zealand rabbits. In summary, the Dps protein was injected into a rabbit in two separate doses, then the serum was collected after three months of immunisation. This in turn allowed the successful detection of Dps in *dps*⁺ strains but not *dps* mutants. Thus, the *dps* mutants were genuine. The polyclonal antibody from the recombinant Dps was used to assess the expression of the gene in the triple mutant complemented with the pBADrha-

dps plasmid by western blotting. The result indicated the production of the Dps protein; this was consistent with the production by SDS-PAGE of a protein corresponding to Dps in the *dps*-complemented triple mutant. These observation together reflect the ability of the Dps expression upon rhamnose of the triple mutant to increase peroxide resistance.

8.6 Linocin-M18 overproduction and purification. The linocin-M18 of *Pyrococcus furiosus (*a hyper-thermophilic aerobic archaeal organism) is a *virus-like particle of 30 nm that is composed of 180 subunits of 38.8 kDa (Atika et al, 2*007), encoded by a gene situated within a cluster of five iron-storage protein genes and a *fur* gene, supporting a role in iron storage. The function of this nanocompartment (or 'encapsulin') is unclear although its structure is partially solved (Akita *et al.*, 2007). Experiments were performed to further investigate the role of linocin-M18 as a potential iron-storage nanocompartment. The work was initiated by cloning the codon optimised linocin-M18 gene of *P. furiosus* into a high copy number plasmid, pET21a, which contained a T7 RNA polymerase promoter, creating the plasmid containing linocin-M18 gene enabling the overexpression of linocin-M18 in BL21/DE3. The induction resulted in the production of a protein with the expected molecular weight. The 3 h post-induction time point appeared to generate the highest quantity of soluble linocin M18 for the range of times tested. This step, followed by large-scale purification by anion-exchange chromatography, yielded partially pure linocin-M18 protein. This enabled further characterisation.

To determine the size and the shape of the purified nanocompartment, the linocin M18 protein sample was applied to a copper grid, and stained with 1% uranyl acetate for TEM analysis. Results showed that the shape and size of the recombinant linocin M18 protein were as expected, with spherical particles of 30 nm diameter apparent, consistent with the shape of nanocompartment particles isolated previously from *T. maritima*, *P. furiosus* and *M. xanthus* (McHugh *et al.*, 2014; Sutter *et al.*, 2008; Akita *et al.*, 2007; Namba *et al.*, 2005). The recombinant purified protein thus appeared to form a high-order oligomeric structure, that was further illustrated as the purified protein slowly migrated during native electrophoresis.

To assess whether the linocin M18 gene is induced from pBADrha-*lin*M18 by rhamnose and can compensate for lack of iron-storage capacity in *the E. coli* triple mutant, the linocin-M18 gene was cloned into the pBADrha controllable expression vector using Gibson cloning then transformed to allow the observation of protein expression. It

appeared from the SDS-PAGE analysis that the linocin M18 protein was generated at low level in the triple mutant upon induction from a plasmid-specified *rha* promoter. This observation supports the ability of the linocin M18 expressed in the triple iron-storage mutant upon rhamnose to provide peroxide resistance and enhance growth under low iron conditions.

Appendix

1. Schematic representation of *E. coli* mutant construction. Mutant creation by replacing the gene target with the Kn^R cassette flanked by FRT sites, followed by Kn^R cassette removal by site-specific recombination at FTR sites. Adapted from Datsenko &Wanner (2000) and Baba *et al.*, (2006).
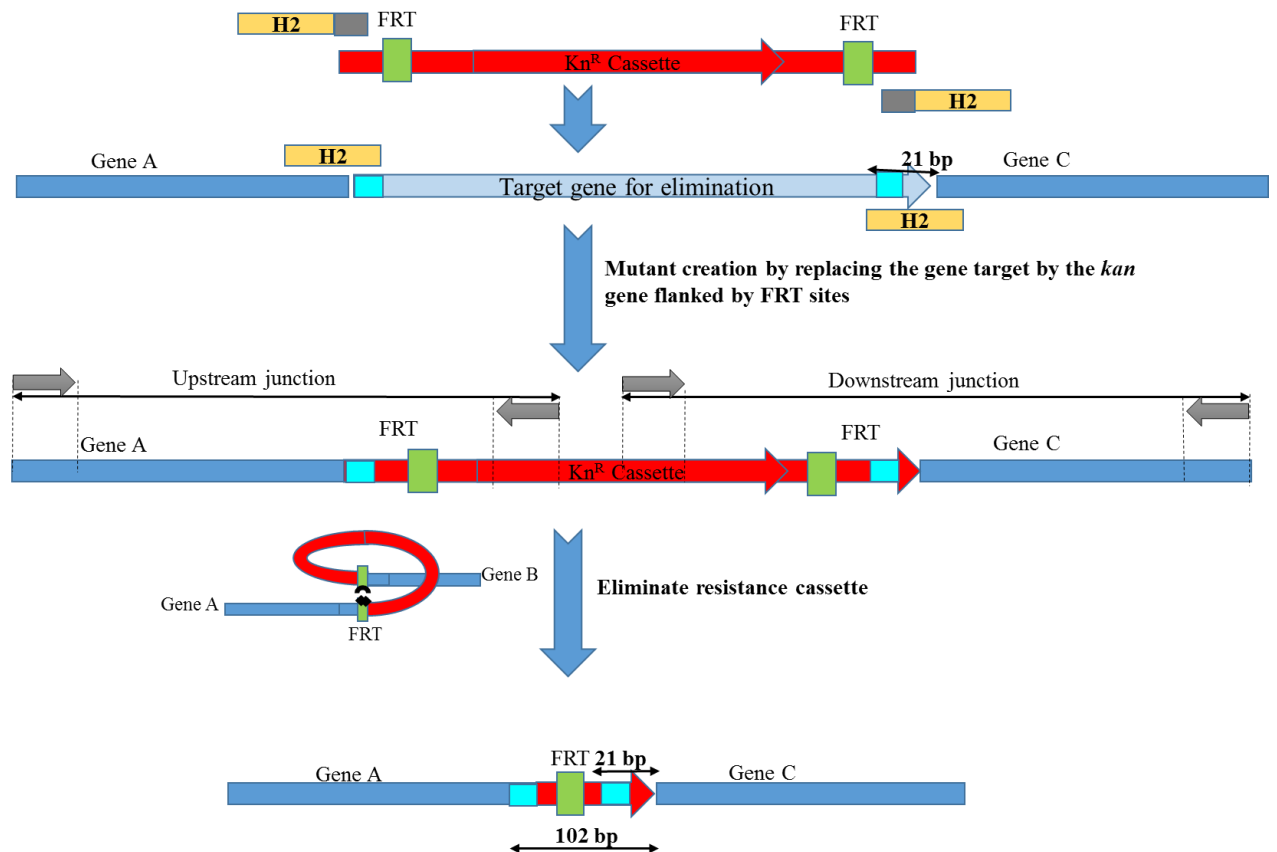
2. Determination the molecular weight of the Bfr (A); and FtnA (B) protein by Western blot. Calibration curve of the Western blot analysis, of figure 5.1-A and 5.1-B, using the 120 kDa pre-stained PageRuler Protein Ladder as a size marker. The graph has been plot using a semi-logarithmic scale. The standard curve gave an estimated mass of 17.3 kDa and 18.9 kDa for FtnA and Bfr, respectivel, proteins which are a reasonable approximation to the mass predicted (18-18.49 kDa for FtnA and Bfr, respectively) from its amino acid sequence.
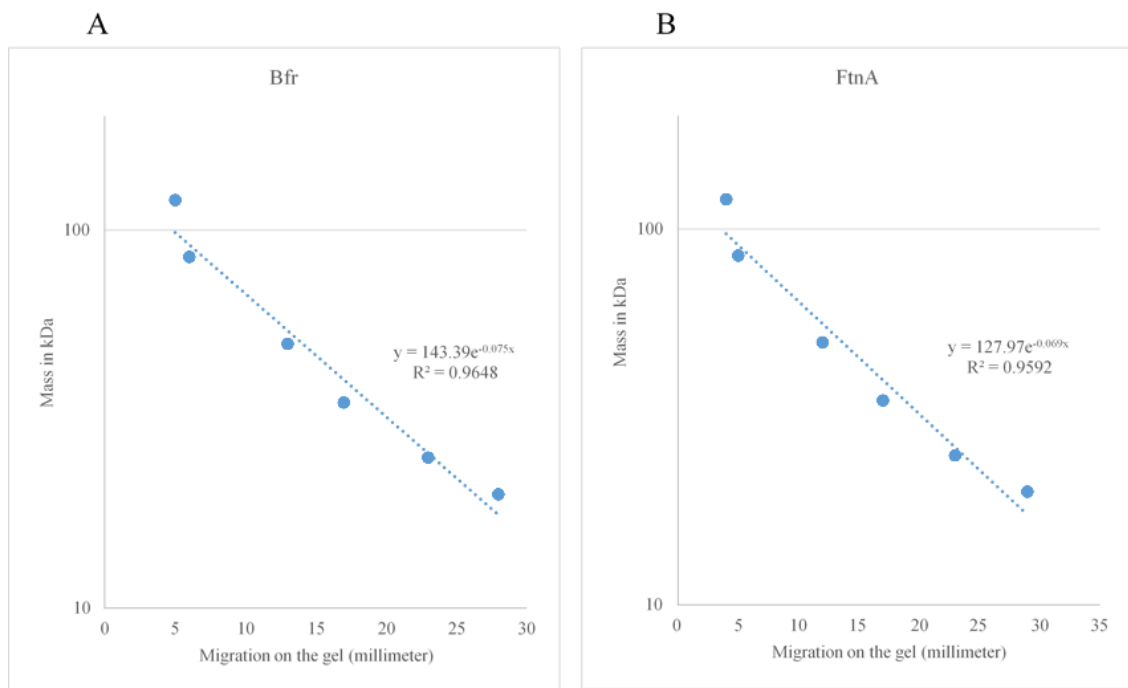
3.Determination the molecular weight of the Dps (A); and Bfr (B) protein by SDS-PAGE. Calibration curve of the SDS-PAGE analysis, of figure 5.1-D.1 and 5.1-D.2, using the 120 kDa pre-stained PageRuler Protein Ladder as a size marker. The graph has been plot using a semi-logarithmic scale. The standard curve gave an estimated mass of 17.3 kDa and 17.1 kDa for Dps and Bfr, respectively, proteins which are a reasonable approximation to the mass predicted (18.7-18.49 kDa for Dps and Bfr, respectivly) from its amino acid sequence.

4. The most frequent amino acid at position 2 among the group of aligned bacterial iron storage proteins (FtnA, Bfr and Dps).

Iron storage proteins	more frequent second residues	Less frequent second residues
FtnA	Leu 90%	(Trp, Ile, Ser, Lys) 10%
Bfr	Lys 90%	(Gln, Phe and Ser) 10%
Dps	Ser 45%, Arg 22% and Lys 9%	(His, Gly, Val, Gln, Pro, Phe, Thr, Asn, Cys, Tyr, Ala and Leu) 24%

5. Western blotting analysis showing that ClpS, the ClpAP 'N-end rule' targeting component, also does not participate in FtnA degradation. The bacterial strains including the wild type BW25113 and Δ *clps* mutant (each one complemented with pBAD-*ftnA* of the wild type/ pBAD-*ftnA* L→A or pBAD-*ftnA* L →K) inoculated in 50 ml (M9 +Cm 50 μM+ Fe 20 μM), once the O.D reached 0.5 unit 100 μM rhamnose was added. Pellet samples were collected in different time points (1, 2, 4, and 6 h, overnight sample of the post culture in addition to the overnight sample of the pre-culture were also collected. The pre-culture in M9 suplemented with 20 μM of ferric citrate and 50 μM of chloramphenecole.

4 h post-culture
Δ*clps* +pBADrha+

ftnA L to K   *ftnA* LtoA   *ftnA* wild type

4 h post-culture
BW25113 +pBADrha+

ftnA L to K   *ftnA* LtoA   *ftnA* wild type

2 h post-culture
Δ*clps* +pBADrha+

ftnA L to K   *ftnA* LtoA   *ftnA* wild type

2 h post-culture
BW25113 +pBADrha+

ftnA L to K   *ftnA* LtoA   *ftnA* wild type

M

O.N post-culture
Δ*clps* +pBADrha+

ftnA L to K   *ftnA* L to A   *ftnA* wild type

O.N post-culture
BW25113 +pBADrha+

ftnA L to K   *ftnA* LtoA   *ftnA* wild type

6 h post-culture
Δ*clps* +pBADrha+

ftnA L to K   *ftnA* L to A   *ftnA* wild type

6 h post-culture
BW25113 +pBADrha+

ftnA L to K   *ftnA* L to A   *ftnA* wild type

M

References

Abdul-Rahman, F., Petit, E., & Blanchard, J. L. (2013). The distribution of polyhedral bacterial microcompartments suggests frequent horizontal transfer and operon reassembly. *Journal of Phylogenetics & Evolutionary Biology*, 1-7.

Abdul-Tehrani, H., Hudson, A. J., Chang, Y. S., Timms, A. R., Hawkins, C., Williams, J. M., . . . Andrews, S. C. (1999). Ferritin mutants of Escherichia coli are iron deficient and growth impaired, and fur mutants are iron deficient. *Journal of Bacteriology , 181*(5), 1415-1428.

Adhikari, P., Kirby, S. D., Nowalk, A. J., Veraldi, K. L., Schryvers, A. B., & Mietzner, T. A. (1995). Biochemical characterization of a Haemophilus influenzae periplasmic iron transport operon. *Journal of Biological Chemistry, 270*(42), 25142-25149.

Akita, F., Chong, K. T., Tanaka, H., Yamashita, E., Miyazaki, N., Nakaishi, Y., . . . Tsukihara, T. (2007). The crystal structure of a virus-like particle from the hyperthermophilic archaeon Pyrococcus furiosus provides insight into the evolution of viruses. *Journal of Molecular Biology, 368*(5), 1469-1483.

Almiron, M., Link, A. J., Furlong, D., & Kolter, R. (1992). A novel DNA-binding protein with regulatory and protective roles in starved Escherichia coli. *Genes and Development, 6*(12b), 2646-2654.

Almirón, M. A., & Ugalde, R. A. (2010). Iron homeostasis in Brucella abortus: the role of bacterioferritin. *The Journal of Microbiology, 48*(5), 668-673.

Anderson, E. S., Paulley, J. T., Gaines, J. M., Valderas, M. W., Martin, D. W., Menscher, E., . . . Roop, R. M., 2nd. (2009). The manganese transporter MntH is a critical virulence determinant for Brucella abortus 2308 in experimentally infected mice. *Infection and Immunity, 77*(8), 3466-3474. doi:10.1128/iai.00444-09

Anderson, J. E., Sparling, P. F., & Cornelissen, C. N. (1994). Gonococcal transferrin-binding protein 2 facilitates but is not essential for transferrin utilization. *Journal of Bacteriology , 176*(11), 3162-3170.

Andrews, S. C. (2010). The Ferritin-like superfamily: Evolution of the biological iron storeman from a rubrerythrin-like ancestor. *Biochimica et Biophysica Acta (BBA)-General Subjects, 1800*(8), 691-705.

Andrews, S. C., Robinson, A. K., & Rodriguez-Quinones, F. (2003). Bacterial iron homeostasis. *FEMS Microbiology Reviews, 27*(2-3), 215-237.

Andrews, S. C., Smith, J., Hawkins, C., Williams, J. M., Harrison, P. M., & Guest, J. R. (1993). Overproduction, purification and characterization of the bacterioferritin of Escherichia coli and a C-terminally extended variant. *The FEBS Journal, 213*(1), 329-338.

Baba, T., Ara, T., Hasegawa, M., Takai, Y., Okumura, Y., Baba, M., . . . Mori, H. (2006). Construction of Escherichia coli K-12 in-frame, single-gene knockout mutants: the Keio collection. *Molecular System Biology, 2*, 2006.0008. doi:10.1038/msb4100050

Beinert, H., Holm, R. H., & Munck, E. (1997). Iron-sulfur clusters: nature's modular, multipurpose structures. *Science, 277*(5326), 653-659.

Biller, K. F., Kato, I., & Märkl, H. (2002). Effect of glucose, maltose, soluble starch, and CO_2 on the growth of the hyperthermophilic archaeon Pyrococcus furiosus. *Extremophiles, 6*(2), 161-166.

Bittner, L.-M., Westphal, K., & Narberhaus, F. (2015). Conditional proteolysis of the membrane protein YfgM by the FtsH protease depends on a novel N-terminal degron. *Journal of Biological Chemistry, 290*(31), 19367-19378.

Bivona, L., Zou, Z., Stutzman, N., & Sun, P. D. (2010). Influence of the second amino acid on recombinant protein expression. *Protein Expression and Purification, 74*(2), 248-256.

Blair, J. M., Richmond, G. E., Bailey, A. M., Ivens, A., & Piddock, L. J. (2013). Choice of bacterial growth medium alters the transcriptome and phenotype of Salmonella enterica Serovar Typhimurium. *PLoS One, 8*(5), e63912.

Bobik, T. A., Lehman, B. P., & Yeates, T. O. (2015). Bacterial microcompartments: widespread prokaryotic organelles for isolation and optimization of metabolic pathways. *Molecular Microbiology, 98*(2), 193-207.

BOLANN, B. J., & ULVIK, R. J. (1990). On the limited ability of superoxide to release iron from ferritin. *The FEBS Journal, 193*(3), 899-904.

Bou-Abdallah, F., Yang, H., Awomolo, A., Cooper, B., Woodhall, M., Andrews, S., & Chasteen, N. (2014). Functionality of the three-site ferroxidase center of Escherichia coli bacterial ferritin (EcFtnA). *Biochemistry, 53*(3), 483-495.

Boughammoura, A., Matzanke, B. F., Böttger, L., Reverchon, S., Lesuisse, E., Expert, D., & Franza, T. (2008). Differential role of ferritins in iron metabolism and virulence of the plant-pathogenic bacterium Erwinia chrysanthemi 3937. *Journal of Bacteriology, 190*(5), 1518-1530.

Bozzi, M., Mignogna, G., Stefanini, S., Barra, D., Longhi, C., Valenti, P., & Chiancone, E. (1997). A novel non-heme iron-binding ferritin related to the DNA-binding proteins of the Dps family in Listeria innocua. *Journal of Biological Chemistry , 272*(6), 3259-3265.

Bradley, J. M., Moore, G. R., & Le Brun, N. E. (2017). Diversity of Fe2+ entry and oxidation in ferritins. *Current Opinion in Chemical Biology, 37*, 122-128.

Braun, V., & Braun, M. (2002). Iron transport and signaling in Escherichia coli. *FEBS Letters, 529*(1), 78-85.

Braun, V., Hantke, K., & Koster, W. (1998). Bacterial iron transport: mechanisms, genetics, and regulation. *Metal Ions in Biological Systems , 35*, 67-145.

Braun, V., & Wolff, H. (1973). Characterization of the receptor protein for phage T5 and colicin M in the outer membrane of E. coli B. *FEBS Letters, 34*(1), 77-80.

Brock, J. H., Williams, P. H., Liceaga, J., & Wooldridge, K. G. (1991). Relative availability of transferrin-bound iron and cell-derived iron to aerobactin-producing and enterochelin-producing strains of Escherichia coli and to other microorganisms. *Infection and Immunity, 59*(9), 3185-3190.

Bullen, J., Griffiths, E., & Edmiston, C. E. (1999). Iron and infection: molecular, physiological and clinical aspects: LWW.

Byers, B. R., & Arceneaux, J. E. (1998). Microbial iron transport: iron acquisition by pathogenic microorganisms. *Metal Ions in Biological Systems, 35*, 37-66.

Calhoun, L. N., & Kwon, Y. M. (2011). The ferritin-like protein Dps protects Salmonella enterica serotype Enteritidis from the Fenton-mediated killing mechanism of bactericidal antibiotics. *International Journal of Antimicrobial Agents, 37*(3), 261-265. doi:10.1016/j.ijantimicag.2010.11.034

Cao, J., Woodhall, M. R., Alvarez, J., Cartron, M. L., & Andrews, S. C. (2007). EfeUOB (YcdNOB) is a tripartite, acid-induced and CpxAR-regulated, low-pH Fe2+ transporter that is cryptic in Escherichia coli K-12 but functional in E. coli O157:H7. *Molecular Microbiology, 65*(4), 857-875. doi:10.1111/j.1365-2958.2007.05802.x

Carrondo, M. A. (2003). Ferritins, iron uptake and storage from the bacterioferritin viewpoint. *The EMBO Journal, 22*(9), 1959-1968.

Ceci, P., Ilari, A., Falvo, E., & Chiancone, E. (2003). The Dps Protein of Agrobacterium tumefaciens does not bind to DNA but protects it toward oxidative cleavage x-ray crystal structure, iron binding, and hydroxyle-radical scavenging properties. *Journal of Biological Chemistry, 278*(22), 20319-20326.

Čepl, J., Blahůšková, A., Cvrčková, F., & Markoš, A. (2014). Ammonia produced by bacterial colonies promotes growth of ampicillin-sensitive Serratia sp. by means of antibiotic inactivation. *FEMS Microbiology Letters, 354*(2), 126-132.

Chen, C. Y., & Morse, S. A. (1999). Neisseria gonorrhoeae bacterioferritin: structural heterogeneity, involvement in iron storage and protection against oxidative stress. *Microbiology, 145 (Pt 10)*, 2967-2975. doi:10.1099/00221287-145-10-2967

Chen, S., Bleam, W. F., & Hickey, W. J. (2010). Molecular analysis of two bacterioferritin genes, bfrα and bfrβ, in the model rhizobacterium Pseudomonas putida KT2440. *Applied and Environmental Microbiology, 76*(16), 5335-5343.

Cherepanov, P. P., & Wackernagel, W. (1995). Gene disruption in Escherichia coli: TcR and KmR cassettes with the option of Flp-catalyzed excision of the antibiotic-resistance determinant. *Gene, 158*(1), 9-14.

Chiancone, E., Ceci, P., Ilari, A., Ribacchi, F., & Stefanini, S. (2004). Iron and proteins for iron storage and detoxification. *Biometals, 17*(3), 197-202.

Chiba, S., Akiyama, Y., Mori, H., Matsuo, E. i., & Ito, K. (2000). Length recognition at the N-terminal tail for the initiation of FtsH-mediated proteolysis. *EMBO Reports, 1*(1), 47-52.

Chimento, D. P., Kadner, R. J., & Wiener, M. C. (2005). Comparative structural analysis of TonB-dependent outer membrane transporters: implications for the transport cycle. *Proteins, 59*(2), 240-251. doi:10.1002/prot.20416

Choi, S. H., Baumler, D. J., & Kaspar, C. W. (2000). Contribution of dps to acid stress tolerance and oxidative stress tolerance in Escherichia coli O157:H7. *Applied and Environmental Microbiology, 66*(9), 3911-3916.

Chowdhury, C., Sinha, S., Chun, S., Yeates, T. O., & Bobik, T. A. (2014). Diverse bacterial microcompartment organelles. *Microbiology and Molecular Biology Reviews, 78*(3), 438-468.

Christensen, D. G., Orr, J. S., Rao, C. V., & Wolfe, A. J. (2017). Increasing growth yield and decreasing acetylation in Escherichia coli by optimizing the carbon-to-magnesium ratio in peptide-based media. *Applied and Environmental Microbiology, 83*(6), e03034-03016.

Chu, C.-Y., Stewart, P. E., Bestor, A., Hansen, B., Lin, T., Gao, L., . . . Rosa, P. A. (2016). Function of the Borrelia burgdorferi FtsH homolog is essential for viability both in vitro and in vivo and independent of HflK/C. *MBio, 7*(2), e00404-00416.

Claverys, J. P. (2001). A new family of high-affinity ABC manganese and zinc permeases. *Research in Microbiology, 152*(3-4), 231-243.

Clermont, O., Bonacorsi, S., & Bingen, E. (2001). The Yersinia high-pathogenicity island is highly predominant in virulence-associated phylogenetic groups of Escherichia coli. *FEMS Microbiology Letters , 196*(2), 153-157.

Contreras, H., Joens, M. S., McMath, L. M., Le, V. P., Tullius, M. V., Kimmey, J. M., . . . Goulding, C. W. (2014). Characterization of a Mycobacterium tuberculosis nanocompartment and its potential cargo proteins. *Journal of Biological Chemistry, 289*(26), 18279-18289.

Cornelis, P., & Andrews, S. C. (2010). *Iron uptake and homeostasis in microorganisms*: Horizon Scientific Press.

Coulton, J. W., Mason, P., Cameron, D. R., Carmel, G., Jean, R., & Rode, H. N. (1986). Protein fusions of beta-galactosidase to the ferrichrome-iron receptor of Escherichia coli K-12. *Journal of Bacteriology , 165*(1), 181-192.

Crichton, R. (2016). *Iron metabolism: from molecular mechanisms to clinical consequences*: John Wiley & Sons.

Datsenko, K. A., & Wanner, B. L. (2000). One-step inactivation of chromosomal genes in Escherichia coli K-12 using PCR products. *Proceedings of the National Academy of Sciences of U S A, 97*(12), 6640-6645. doi:10.1073/pnas.120163297

Daugherty, A., Suvarnapunya, A. E., & Runyen-Janecky, L. (2012). The role of oxyR and soxRS in oxidative stress survival in Shigella flexneri. *Microbiological Research, 167*(4), 238-245. doi:10.1016/j.micres.2011.09.004

de Paiva, J. B., da Silva, L. P. M., Casas, M. R. T., Conceição, R. A., Nakazato, G., de Pace, F., . . . da Silveira, W. D. (2016). In vivo influence of in vitro up-regulated genes in the virulence of an APEC strain associated with swollen head syndrome. *Avian Pathology, 45*(1), 94-105.

Debut, A. J., Dumay, Q. C., Barabote, R. D., & Saier, M. H., Jr. (2006). The iron/lead transporter superfamily of Fe/Pb2+ uptake systems. *Journal Molecular Microbiology and Biotechnology, 11*(1-2), 1-9. doi:10.1159/000092814

Delany, I., Spohn, G., Rappuoli, R., & Scarlato, V. (2001). The Fur repressor controls transcription of iron-activated and -repressed genes in Helicobacter pylori. *Molecular Microbiology, 42*(5), 1297-1309.

Deng, Z., Shan, Y., Pan, Q., Gao, X., & Yan, A. (2013). Anaerobic expression of the gadE-mdtEF multidrug efflux operon is primarily regulated by the two-component system ArcBA through antagonizing the H-NS mediated repression. *Frontiers in Microbiology, 4*, 194.

Dougan, D. A., Mogk, A., Zeth, K., Turgay, K., & Bukau, B. (2002). AAA+ proteins and substrate recognition, it all depends on their partner in crime. *FEBS letters, 529*(1), 6-10.

Dougan, D. A., Weber-Ban, E., & Bukau, B. (2003). Targeted delivery of an ssrA-tagged substrate by the adaptor protein SspB to its cognate AAA+ protein ClpX. *Molecular Cell, 12*(2), 373-380.

Douglas, T., & Ripoll, D. R. (1998). Calculated electrostatic gradients in recombinant human H-chain ferritin. *Protein Science, 7*(5), 1083-1091. doi:10.1002/pro.5560070502

Earhart, C. (1996). Uptake and metabolism of iron and molybdenum. *Escherichia coli and Salmonella: cellular and molecular biology, 2nd ed. ASM Press, Washington, DC*, 1075-1090.

Ebrahimi, K. H., Hagedoorn, P. L., & Hagen, W. R. (2013). A conserved tyrosine in ferritin is a molecular capacitor. *ChemBioChem, 14*(9), 1123-1133.

Eshelman, K., Yao, H., Hewage, A. N. P., Deay, J. J., Chandler, J. R., & Rivera, M. (2017). Inhibiting the BfrB: Bfd interaction in Pseudomonas aeruginosa causes irreversible iron accumulation in bacterioferritin and iron deficiency in the bacterial cytosol. *Metallomics, 9*(6), 646-659.

Evans, S. J., Fogg, M. J., Mamone, A., Davis, M., Pearl, L. H., & Connolly, B. A. (2000). Improving dideoxynucleotide-triphosphate utilisation by the hyper-thermophilic DNA polymerase from the archaeon Pyrococcus furiosus. *Nucleic acids research, 28*(5), 1059-1066.

Fabian, M., Solomaha, E., Olson, J. S., & Maresso, A. W. (2009). Heme transfer to the bacterial cell envelope occurs via a secreted hemophore in the Gram-positive

pathogen Bacillus anthracis. *Journal of Biological Chemistry , 284*(46), 32138-32146. doi:10.1074/jbc.M109.040915

Fan, R., Boyle, A. L., Cheong, V. V., Ng, S. L., & Orner, B. P. (2009). A helix swapping study of two protein cages. *Biochemistry, 48*(24), 5623-5630.

Fiala, G., & Stetter, K. O. (1986). Pyrococcus furiosus sp. nov. represents a novel genus of marine heterotrophic archaebacteria growing optimally at 100 C. *Archives of Microbiology, 145*(1), 56-61.

Fischbach, M. A., Lin, H., Liu, D. R., & Walsh, C. T. (2006). How pathogenic bacteria evade mammalian sabotage in the battle for iron. *Nature Chemechal Biology, 2*(3), 132-138. doi:10.1038/nchembio771

Fischbach, M. A., Lin, H., Zhou, L., Yu, Y., Abergel, R. J., Liu, D. R., . . . Smith, K. D. (2006). The pathogen-associated iroA gene cluster mediates bacterial evasion of lipocalin 2. *Proceedings of the National Academy of Sciences of U S A , 103*(44), 16502-16507. doi:10.1073/pnas.0604636103

Ford, D. C., Ireland, P. M., Bullifent, H. L., Saint, R. J., McAlister, E. V., Sarkar-Tyson, M., & Oyston, P. C. (2014). Construction of an inducible system for the analysis of essential genes in Yersinia pestis. *Journal of Microbiological Methods, 100*, 1-7. doi:10.1016/j.mimet.2014.01.017

Foster, J. W., & Hall, H. K. (1992). Effect of Salmonella typhimurium ferric uptake regulator (fur) mutations on iron- and pH-regulated protein synthesis. *Journal of Bacteriology , 174*(13), 4317-4323.

Frenkiel-Krispin, D., Levin-Zaidman, S., Shimoni, E., Wolf, S. G., Wachtel, E. J., Arad, T., . . . Minsky, A. (2001). Regulated phase transitions of bacterial chromatin: a non-enzymatic pathway for generic DNA protection. The *Embo journal, 20*(5), 1184-1191. doi:10.1093/emboj/20.5.1184

Frenkiel-Krispin, D., Ben-Avraham, I., Englander, J., Shimoni, E., Wolf, S. G., & Minsky, A. (2004). Nucleoid restructuring in stationary-state bacteria. *Molecular Microbiology, 51*(2), 395-405.

Fu, Y., Lee, H., Collins, M., Tsai, H. F., Spellberg, B., Edwards, J. E., Jr., . . . Ibrahim, A. S. (2004). Cloning and functional characterization of the Rhizopus oryzae high affinity iron permease (rFTR1) gene. *FEMS Microbiology Letters, 235*(1), 169-176. doi:10.1016/j.femsle.2004.04.031

Führer, F., Langklotz, S., & Narberhaus, F. (2006). The C-terminal end of LpxC is required for degradation by the FtsH protease. *Molecular Microbiology, 59*(3), 1025-1036.

Gancz, H., & Merrell, D. S. (2011). Acid Survival Mechanisms of Bacterial Pathogens of the Digestive Tract. *Stress Response in Pathogenic Bacteria, 19*, 135.

Gao, J.-L., Lu, Y., Browne, G., Yap, B. C.-M., Trewhella, J., Hunter, N., & Nguyen, K.-A. (2012). The role of heme binding by DNA-protective protein from starved cells (Dps) in the tolerance of Porphyromonas gingivalis to heme toxicity. *Journal of Biological Chemistry, 287*(50), 42243-42258.

Gao, Q., Wang, X., Xu, H., Xu, Y., Ling, J., Zhang, D., . . . Liu, X. (2012). Roles of iron acquisition systems in virulence of extraintestinal pathogenic Escherichia coli: salmochelin and aerobactin contribute more to virulence than heme in a chicken infection model. *BMC Microbiology, 12*, 143. doi:10.1186/1471-2180-12-143

Gauss, G. H., Reott, M. A., Rocha, E. R., Young, M. J., Douglas, T., Smith, C. J., & Lawrence, C. M. (2012). Characterization of the Bacteroides fragilis bfr gene product identifies a bacterial DPS-like protein and suggests evolutionary links in the ferritin superfamily. *Journal of Bacteriology, 194*(1), 15-27.

Ge, Z., & Taylor, D. E. (1996). Sequencing, expression, and genetic characterization of the Helicobacter pylori ftsH gene encoding a protein homologous to members of a novel putative ATPase family. *Journal of Bacteriology, 178*(21), 6151-6157.

Genco, C. A., & Dixon, D. W. (2001). Emerging strategies in microbial haem capture. *Mol Microbiol, 39*(1), 1-11.

Ghysels, B., Ochsner, U., Mollman, U., Heinisch, L., Vasil, M., Cornelis, P., & Matthijs, S. (2005). The Pseudomonas aeruginosa pirA gene encodes a second receptor for ferrienterobactin and synthetic catecholate analogues. *FEMS Microbiology Letters, 246*(2), 167-174. doi:10.1016/j.femsle.2005.04.010

Gottesman, S. (2003). Proteolysis in bacterial regulatory circuits. *Annual Review of Cell and Developmental Biology, 19*(1), 565-587.

Grass, G., Franke, S., Taudte, N., Nies, D. H., Kucharski, L. M., Maguire, M. E., & Rensing, C. (2005). The metal permease ZupT from Escherichia coli is a transporter with a broad substrate spectrum. *Journal of Bacteriology , 187*(5), 1604-1611. doi:10.1128/jb.187.5.1604-1611.2005

Grass, G., Otto, M., Fricke, B., Haney, C. J., Rensing, C., Nies, D. H., & Munkelt, D. (2005). FieF (YiiP) from Escherichia coli mediates decreased cellular accumulation of iron and relieves iron stress. *Archives of Microbiology, 183*(1), 9-18. doi:10.1007/s00203-004-0739-4

Grass, G., Wong, M. D., Rosen, B. P., Smith, R. L., & Rensing, C. (2002). ZupT is a Zn(II) uptake system in Escherichia coli. *Journal of Bacteriology , 184*(3), 864-866.

Gresock, M. G., Savenkova, M. I., Larsen, R. A., Ollis, A. A., & Postle, K. (2011). Death of the TonB Shuttle Hypothesis. *Frontiers in Microbiology, 2*, 206. doi:10.3389/fmicb.2011.00206

Griffiths, E. (1999). The iron-uptake systems of pathogenic bacteria, fungi and protozoa. *Iron and infetion*, 87-212.

Gupta, S., & Chatterji, D. (2003). Bimodal protection of DNA by Mycobacterium smegmatis DNA-binding protein from stationary phase cells. *Journal of Biological Chemistry , 278*(7), 5235-5241. doi:10.1074/jbc.M208825200

Halliwell, B., & Gutteridge, J. M. (1986). Oxygen free radicals and iron in relation to biology and medicine: some problems and concepts. *Archives of Biochemistry and Biophysics, 246*(2), 501-514.

Halsey, T. A., Vazquez-Torres, A., Gravdahl, D. J., Fang, F. C., & Libby, S. J. (2004). The ferritin-like Dps protein is required for Salmonella enterica serovar Typhimurium oxidative stress resistance and virulence. *Infection and Immunity, 72*(2), 1155-1158.

Hansen, E. B. (1989). Structure and regulation of the lytic replicon of phage P1. *Journal of Molecular Biology , 207*(1), 135-149.

Hantke, K. (1987). Selection procedure for deregulated iron transport mutants (fur) in Escherichia coli K 12: fur not only affects iron metabolism. *Molecular and General Genetics, 210*(1), 135-139.

Hantke, K. (1997). Ferrous iron uptake by a magnesium transport system is toxic for Escherichia coli and Salmonella typhimurium. *Journal of Bacteriology , 179*(19), 6201-6204.

Hantke, K. (2001). Iron and metal regulation in bacteria. *Current Opinion in Microbiology, 4*(2), 172-177.

Hantke, K., Nicholson, G., Rabsch, W., & Winkelmann, G. (2003). Salmochelins, siderophores of Salmonella enterica and uropathogenic Escherichia coli strains,

are recognized by the outer membrane receptor IroN. *Proceedings of the National Academy of Sciences of U S A, 100*(7), 3677-3682. doi:10.1073/pnas.0737682100

Heller, K., Mann, B. J., & Kadner, R. J. (1985). Cloning and expression of the gene for the vitamin B12 receptor protein in the outer membrane of Escherichia coli. *Journal of Bacteriology , 161*(3), 896-903.

Henle, E. S., Luo, Y., & Linn, S. (1996). Fe2+, Fe3+, and oxygen react with DNA-derived radicals formed during iron-mediated Fenton reactions. *Biochemistry, 35*(37), 12212-12219. doi:10.1021/bi961235j

Herman, C., Prakash, S., Lu, C. Z., Matouschek, A., & Gross, C. A. (2003). Lack of a robust unfoldase activity confers a unique level of substrate specificity to the universal AAA protease FtsH. *Molecular cell, 11*(3), 659-669.

Higgs, P. I., Larsen, R. A., & Postle, K. (2002). Quantification of known components of the Escherichia coli TonB energy transduction system: TonB, ExbB, ExbD and FepA. *Molecular Microbiology, 44*(1), 271-281.

Ho, T. D., & Waldor, M. K. (2007). Enterohemorrhagic Escherichia coli O157:H7 gal mutants are sensitive to bacteriophage P1 and defective in intestinal colonization. *Infection and Immunity, 75*(4), 1661-1666. doi:10.1128/iai.01342-06

Hsueh, K. L., Yu, L. K., Chen, Y. H., Cheng, Y. H., Hsieh, Y. C., Ke, S. C., . . . Huang, T. H. (2013). FeoC from Klebsiella pneumoniae contains a [4Fe-4S] cluster. *Journal of Bacteriology , 195*(20), 4726-4734. doi:10.1128/jb.00687-13

Hudson, A. J., Andrews, S. C., Hawkins, C., Williams, J. M., Izuhara, M., Meldrum, F. C., . . . Guest, J. R. (1993). Overproduction, purification and characterization of the Escherichia coli ferritin. *The FEBS Journal, 218*(3), 985-995.

Humbard, M. A., Surkov, S., De Donatis, G. M., Jenkins, L. M., & Maurizi, M. R. (2013). The N-degradome of Escherichia coli limited proteolysis in vivo generates a large pool of proteins bearing N-degrons. *Journal of Biological Chemistry, 288*(40), 28913-28924.

Ilari, A., Ceci, P., Ferrari, D., Rossi, G. L., & Chiancone, E. (2002). Iron incorporation into Escherichia coli Dps gives rise to a ferritin-like microcrystalline core. *Journal of Biological Chemistry , 277*(40), 37619-37623. doi:10.1074/jbc.M206186200

Jabado, N., Jankowski, A., Dougaparsad, S., Picard, V., Grinstein, S., & Gros, P. (2000). Natural resistance to intracellular infections: natural resistance-associated macrophage protein 1 (Nramp1) functions as a pH-dependent manganese transporter at the phagosomal membrane. *Journal of Experimental Medicine, 192*(9), 1237-1248.

Jayasekera, M. M., Foltin, S. K., Olson, E. R., & Holler, T. P. (2000). Escherichia coli requires the protease activity of FtsH for growth. *Archives of Biochemistry and Biophysics, 380*(1), 103-107.

Jordan, L. D., Zhou, Y., Smallwood, C. R., Lill, Y., Ritchie, K., Yip, W. T., . . . Klebba, P. E. (2013). Energy-dependent motion of TonB in the Gram-negative bacterial inner membrane. *Proceedings of the National Academy of Sciences of U S A, 110*(28), 11553-11558. doi:10.1073/pnas.1304243110

Kadir, F. H., & Moore, G. R. (1990). Bacterial ferritin contains 24 haem groups. *FEBS Letters, 271*(1-2), 141-143.

Kammler, M., Schon, C., & Hantke, K. (1993). Characterization of the ferrous iron uptake system of Escherichia coli. *Journal of Bacteriology , 175*(19), 6212-6219.

Kehres, D. G., & Maguire, M. E. (2003). Emerging themes in manganese transport, biochemistry and pathogenesis in bacteria. *FEMS Microbiology Reviews, 27*(2-3), 263-290.

Kehres, D. G., Zaharik, M. L., Finlay, B. B., & Maguire, M. E. (2000). The NRAMP proteins of Salmonella typhimurium and Escherichia coli are selective manganese transporters involved in the response to reactive oxygen. *Molecular Microbiology, 36*(5), 1085-1100.

Keyer, K., & Imlay, J. A. (1996). Superoxide accelerates DNA damage by elevating free-iron levels. *Proceedings of the National Academy of Sciences, 93*(24), 13635-13640.

Keyer, K., & Imlay, J. A. (1996). Superoxide accelerates DNA damage by elevating free-iron levels. *Proceedings of the National Academy of Sciences of U S A, 93*(24), 13635-13640.

Kihara, A., Akiyama, Y., & Ito, K. (1995). FtsH is required for proteolytic elimination of uncomplexed forms of SecY, an essential protein translocase subunit. *Proceedings of the National Academy of Sciences, 92*(10), 4532-4536.

Kim, H., Lee, H., & Shin, D. (2013). The FeoC protein leads to high cellular levels of the Fe(II) transporter FeoB by preventing FtsH protease regulation of FeoB in Salmonella enterica. *Journal of Bacteriology, 195*(15), 3364-3370. doi:10.1128/jb.00343-13

Kim, J. N., & Kwon, Y. M. (2013). Identification of target transcripts regulated by small RNA RyhB homologs in Salmonella: RyhB-2 regulates motility phenotype. *Microbiology Research, 168*(10), 621-629. doi:10.1016/j.micres.2013.06.002

Koebnik, R., Locher, K. P., & Van Gelder, P. (2000). Structure and function of bacterial outer membrane proteins: barrels in a nutshell. *Molecular Microbiology, 37*(2), 239-253.

Koster, W. (2001). ABC transporter-mediated uptake of iron, siderophores, heme and vitamin B12. *Research in Microbiology, 152*(3-4), 291-301.

Kowit, J. D., & Goldberg, A. L. (1977). Intermediate steps in the degradation of a specific abnormal protein in Escherichia coli. *Journal of Biological Chemistry, 252*(23), 8350-8357.

Krewulak, K. D., & Vogel, H. J. (2008). Structural biology of bacterial iron uptake. *Biochimica et Biophysica Acta, 1778*(9), 1781-1804. doi:10.1016/j.bbamem.2007.07.026

Lafont, J. P., Dho, M., D'Hauteville, H. M., Bree, A., & Sansonetti, P. J. (1987). Presence and expression of aerobactin genes in virulent avian strains of Escherichia coli. *Infection and Immunity, 55*(1), 193-197.

Langklotz, S., Baumann, U., & Narberhaus, F. (2012). Structure and function of the bacterial AAA protease FtsH. *Biochimica et Biophysica Acta (BBA)-Molecular Cell Research, 1823*(1), 40-48.

Le Brun, N., Andrews, S. C., Guest, J., Harrison, P., Moore, G., & Thomson, A. (1995). Identification of the ferroxidase centre of Escherichia coli bacterioferritin. *Biochemical Journal, 312*(Pt 2), 385.

Liu, X., Lopez, P. A., Giessen, T. W., Giles, M., Way, J. C., & Silver, P. A. (2016). Engineering Genetically-Encoded Mineralization and Magnetism via Directed Evolution. *Scientific Reports, 6*, 38019.

Lukat-Rodgers, G. S., Rodgers, K. R., Caillet-Saguy, C., Izadi-Pruneyre, N., & Lecroisey, A. (2008). Novel heme ligand displacement by CO in the soluble hemophore HasA and its proximal ligand mutants: implications for heme uptake and release. *Biochemistry, 47*(7), 2087-2098. doi:10.1021/bi7019518

Lundrigan, M. D., & Kadner, R. J. (1986). Nucleotide sequence of the gene for the ferrienterochelin receptor FepA in Escherichia coli. Homology among outer

membrane receptors that interact with TonB. *Journal of Biological Chemistry , 261*(23), 10797-10801.

Lysenko, E., Ogura, T., & Cutting, S. M. (1997). Characterization of the ftsH gene of Bacillus subtilis. *Microbiology, 143*(3), 971-978.

Ma, J. F., Ochsner, U. A., Klotz, M. G., Nanayakkara, V. K., Howell, M. L., Johnson, Z., . . . Hassett, D. J. (1999). Bacterioferritin A modulates catalase A (KatA) activity and resistance to hydrogen peroxide in Pseudomonas aeruginosa. *Journal of Bacteriology, 181*(12), 3730-3742.

Mademidis, A., Killmann, H., Kraas, W., Flechsler, I., Jung, G., & Braun, V. (1997). ATP-dependent ferric hydroxamate transport system in Escherichia coli: periplasmic FhuD interacts with a periplasmic and with a transmembrane/cytoplasmic region of the integral membrane protein FhuB, as revealed by competitive peptide mapping. *Molecular Microbiology , 26*(5), 1109-1123.

Makui, H., Roig, E., Cole, S. T., Helmann, J. D., Gros, P., & Cellier, M. F. (2000). Identification of the Escherichia coli K-12 Nramp orthologue (MntH) as a selective divalent metal ion transporter. *Molecular Microbiology , 35*(5), 1065-1078.

Manca, C., Paul, S., Barry, C. E., Freedman, V. H., & Kaplan, G. (1999). Mycobacterium tuberculosis catalase and peroxidase activities and resistance to oxidative killing in human monocytes in vitro. *Infection and Immunity, 67*(1), 74-79.

Marlovits, T. C., Haase, W., Herrmann, C., Aller, S. G., & Unger, V. M. (2002). The membrane protein FeoB contains an intramolecular G protein essential for Fe(II) uptake in bacteria. *Proceedings of the National Academy of Sciences of U S A, 99*(25), 16243-16248. doi:10.1073/pnas.242338299

Masse, E., & Gottesman, S. (2002). A small RNA regulates the expression of genes involved in iron metabolism in Escherichia coli. *Proceedings of the National Academy of Sciences of U S A, 99*(7), 4620-4625. doi:10.1073/pnas.032066599

McHugh, C. A., Fontana, J., Nemecek, D., Cheng, N., Aksyuk, A. A., Heymann, J. B., . . . Steven, A. C. (2014). A virus capsid-like nanocompartment that stores iron and protects bacteria from oxidative stress. *The EMBO Journal, 33*(17), 1896-1911.

McHugh, J. P., Rodriguez-Quinones, F., Abdul-Tehrani, H., Svistunenko, D. A., Poole, R. K., Cooper, C. E., & Andrews, S. C. (2003). Global iron-dependent gene regulation in Escherichia coli. A new mechanism for iron homeostasis. *Journal of Biological Chemistry , 278*(32), 29478-29486. doi:10.1074/jbc.M303381200

Messenger, A. J., & Barclay, R. (1983). Bacteria, iron and pathogenicity. *Biochemistry and Molecular Biology Education, 11*(2), 54-63.

Miller, J. H. (1992). *A Short Course in Bacterial Genetics: Laboratory Manual. Labo*: Cold Spring Harbor Laboratory Press.

Moeck, G. S., & Coulton, J. W. (1998). TonB-dependent iron acquisition: mechanisms of siderophore-mediated active transport. *Molecular Microbiology, 28*(4), 675-681.

Namba, K., Hagiwara, K., Tanaka, H., Nakaishi, Y., Chong, K. T., Yamashita, E., . . . Omura, T. (2005). Expression and molecular characterization of spherical particles derived from the genome of the hyperthermophilic euryarchaeote Pyrococcus furiosus. *Journal of Biochemistry, 138*(2), 193-199.

Nandal, A., Huggins, C. C., Woodhall, M. R., McHugh, J., Rodriguez-Quinones, F., Quail, M. A., . . . Andrews, S. C. (2010). Induction of the ferritin gene (ftnA) of Escherichia coli by Fe(2+)-Fur is mediated by reversal of H-NS silencing and is

RyhB independent. *Molecular Microbiology, 75*(3), 637-657. doi:10.1111/j.1365-2958.2009.06977.x

Nassif, X., & Sansonetti, P. J. (1986). Correlation of the virulence of Klebsiella pneumoniae K1 and K2 with the presence of a plasmid encoding aerobactin. *Infection and Immunity, 54*(3), 603-608.

Neilands, J. B. (1995). Siderophores: structure and function of microbial iron transport compounds. *Journal of Biological Chemistry , 270*(45), 26723-26726.

Nevo, Y., & Nelson, N. (2006). The NRAMP family of metal-ion transporters. *Biochimica et Biophysica Acta, 1763*(7), 609-620. doi:10.1016/j.bbamcr.2006.05.007

Nies, D. H., & Herzberg, M. (2013). A fresh view of the cell biology of copper in enterobacteria. *Molecular Microbiology, 87*(3), 447-454.

Ogura, T., Inoue, K., Tatsuta, T., Suzaki, T., Karata, K., Young, K., . . . Raetz, C. R. (1999). Balanced biosynthesis of major membrane components through regulated degradation of the committed enzyme of lipid A biosynthesis by the AAA protease FtsH (HflB) in Escherichia coli. *Molecular Microbiology, 31*(3), 833-844.

Pandey, R., & Rodriguez, G. M. (2012). A ferritin mutant of Mycobacterium tuberculosis is highly susceptible to killing by antibiotics and is unable to establish a chronic infection in mice. *Infection and Immunity, 80*(10), 3650-3659. doi:10.1128/iai.00229-12

Pang, A., Liang, M., Prentice, M. B., & Pickersgill, R. W. (2012). Substrate channels revealed in the trimeric Lactobacillus reuteri bacterial microcompartment shell protein PduB. *Acta Crystallographica Section D: Biological Crystallography, 68*(12), 1642-1652.

Papp-Wallace, K. M., & Maguire, M. E. (2006). Manganese transport and the role of manganese in virulence. *Annu Rev Microbiol, 60*, 187-209. doi:10.1146/annurev.micro.60.080805.142149

Patzer, S. I., & Hantke, K. (1999). SufS is a NifS-like protein, and SufD is necessary for stability of the [2Fe-2S] FhuF protein in Escherichia coli. *Journal of bacteriology , 181*(10), 3307-3309.

Patzer, S. I., & Hantke, K. (2001). Dual repression by Fe(2+)-Fur and Mn(2+)-MntR of the mntH gene, encoding an NRAMP-like Mn(2+) transporter in Escherichia coli. *Journal of bacteriology , 183*(16), 4806-4813. doi:10.1128/jb.183.16.4806-4813.2001

Pawelek, P. D., Croteau, N., Ng-Thow-Hing, C., Khursigara, C. M., Moiseeva, N., Allaire, M., & Coulton, J. W. (2006). Structure of TonB in complex with FhuA, E. coli outer membrane receptor. *Science, 312*(5778), 1399-1402. doi:10.1126/science.1128057

Payne, S. M., & Mey, A. R. (2010). Iron uptake in Shigella and Escherichia coli. *Iron uptake and homeostasis in microorganisms*, 87-100.

Pecqueur, L., D'Autreaux, B., Dupuy, J., Nicolet, Y., Jacquamet, L., Brutscher, B., . . . Bersch, B. (2006). Structural changes of Escherichia coli ferric uptake regulator during metal-dependent dimerization and activation explored by NMR and X-ray crystallography. *Journal of Biological Chemistry , 281*(30), 21286-21295. doi:10.1074/jbc.M601278200

Pilpa, R. M., Robson, S. A., Villareal, V. A., Wong, M. L., Phillips, M., & Clubb, R. T. (2009). Functionally distinct NEAT (NEAr Transporter) domains within the Staphylococcus aureus IsdH/HarA protein extract heme from methemoglobin.

Journal of Biological Chemistry , 284(2), 1166-1176. doi:10.1074/jbc.M806007200

Posey, J. E., & Gherardini, F. C. (2000). Lack of a role for iron in the Lyme disease pathogen. *Science, 288*(5471), 1651-1653.

Price, N. M., & Morel, F. M. (1998). Biological cycling of iron in the ocean. *Metal Ions in Biological Systems , 35*, 1-36.

Quail, M. A., Jordan, P., Grogan, J. M., Butt, J. N., Lutz, M., Thomson, A. J., . . . Guest, J. R. (1996). Spectroscopic and Voltammetric Characterisation of the Bacterioferritin-Associated Ferredoxin ofEscherichia coli. *Biochemical and biophysical research communications, 229*(2), 635-642.

Rae, B. D., Long, B. M., Badger, M. R., & Price, G. D. (2013). Functions, compositions, and evolution of the two types of carboxysomes: polyhedral microcompartments that facilitate CO2 fixation in cyanobacteria and some proteobacteria. *Microbiology and Molecular Biology Reviews, 77*(3), 357-379.

Rajasekaran, M. B., Nilapwar, S., Andrews, S. C., & Watson, K. A. (2010). EfeO-cupredoxins: major new members of the cupredoxin superfamily with roles in bacterial iron transport. *Biometals, 23*(1), 1-17. doi:10.1007/s10534-009-9262-z

Ratledge, C. (2004). Iron, mycobacteria and tuberculosis. *Tuberculosis, 84*(1), 110-130.

Ratledge, C., & Dover, L. G. (2000). Iron metabolism in pathogenic bacteria. *Annu Rev Microbiol, 54*, 881-941. doi:10.1146/annurev.micro.54.1.881

Reddy, P. V., Puri, R. V., Khera, A., & Tyagi, A. K. (2012). Iron storage proteins are essential for the survival and pathogenesis of Mycobacterium tuberculosis in THP-1 macrophages and the guinea pig model of infection. *Journal of bacteriology, 194*(3), 567-575.

Repine, J., Fox, R. B., & Berger, E. (1981). Hydrogen peroxide kills Staphylococcus aureus by reacting with staphylococcal iron to form hydroxyl radical. *Journal of Biological Chemistry, 256*(14), 7094-7096.

Rivera, M. (2017). Bacterioferritin: structure, dynamics, and protein–protein interactions at play in iron storage and mobilization. *Accounts of chemical research*, *50*(2), 331-340.

Romao, C. V., Louro, R., Timkovich, R., Lubben, M., Liu, M. Y., LeGall, J., . . . Teixeira, M. (2000). Iron-coproporphyrin III is a natural cofactor in bacterioferritin from the anaerobic bacterium Desulfovibrio desulfuricans. *FEBS Letters, 480*(2-3), 213-216.

Roof, D. M., & Roth, J. R. (1988). Ethanolamine utilization in Salmonella typhimurium. *Journal of bacteriology, 170*(9), 3855-3863.

Rotanova, T. V., Melnikov, E. E., Khalatova, A. G., Makhovskaya, O. V., Botos, I., Wlodawer, A., & Gustchina, A. (2004). Classification of ATP-dependent proteases Lon and comparison of the active sites of their proteolytic domains. *The FEBS Journal, 271*(23-24), 4865-4871.

Sampson, E. M., & Bobik, T. A. (2008). Microcompartments for B12-dependent 1, 2-propanediol degradation provide protection from DNA and cellular damage by a reactive metabolic intermediate. *Journal of Bacteriology, 190*(8), 2966-2971.

Sankari, S., & O'Brian, M. R. (2016). Synthetic lethality of the bfr and mbfA genes reveals a functional relationship between iron storage and iron export in managing stress responses in Bradyrhizobium japonicum. *PLoS One, 11*(6), e0157250.

Sauer, R. T., & Baker, T. A. (2011). AAA+ proteases: ATP-fueled machines of protein destruction. *Annual review of Biochemistry, 80*, 587-612.

Schramm, E., Mende, J., Braun, V., & Kamp, R. M. (1987). Nucleotide sequence of the colicin B activity gene cba: consensus pentapeptide among TonB-dependent colicins and receptors. *Journal of bacteriology , 169*(7), 3350-3357.

Schröder, I., Johnson, E., & de Vries, S. (2003). Microbial ferric iron reductases. *FEMS Microbiology Reviews, 27*(2-3), 427-447.

Sigdel, T. K., Easton, J. A., & Crowder, M. W. (2006). Transcriptional response of Escherichia coli to TPEN. *Journal of Bacteriology, 188*(18), 6709-6713.

Sriram, S. M., Kim, B. Y., & Kwon, Y. T. (2011). The N-end rule pathway: emerging functions and molecular principles of substrate recognition. *Nature Reviews Molecular Cell Biology, 12*(11), 735.

Stephani, K., Weichart, D., & Hengge, R. (2003). Dynamic control of Dps protein levels by ClpXP and ClpAP proteases in Escherichia coli. *Molecular Microbiology, 49*(6), 1605-1614.

Sutter, M., Boehringer, D., Gutmann, S., Günther, S., Prangishvili, D., Loessner, M. J., . . . Ban, N. (2008). Structural basis of enzyme encapsulation into a bacterial nanocompartment. *Nature Structural and Molecular Biology, 15*(9), 939.

Sutter, M., Wilson, S. C., Deutsch, S., & Kerfeld, C. A. (2013). Two new high-resolution crystal structures of carboxysome pentamer proteins reveal high structural conservation of CcmL orthologs among distantly related cyanobacterial species. *Photosynthesis Research, 118*(1-2), 9-16.

Talukder, A. A., & Ishihama, A. (2014). Dps Is a Stationary Phase-Specific Protein of Escherichia coli Nucleoid. *Advances in Microbiology, 4*(15), 1095.

Tam, R., & Saier, M. H., Jr. (1993). Structural, functional, and evolutionary relationships among extracellular solute-binding receptors of bacteria. *Microbiology Reviews, 57*(2), 320-346.

Thompson, M. C., Cascio, D., Leibly, D. J., & Yeates, T. O. (2015). An allosteric model for control of pore opening by substrate binding in the EutL microcompartment shell protein. *Protein Science, 24*(6), 956-975.

Tobias, J. W., Shrader, T. E., Rocap, G., & Varshavsky, A. (1991). The N-end rule in bacteria. *Science, 254*(5036), 1374-1377.

Tomoyasu, T., Gamer, J., Bukau, B., Kanemori, M., Mori, H., Rutman, A., . . . Niki, H. (1995). Escherichia coli FtsH is a membrane-bound, ATP-dependent protease which degrades the heat-shock transcription factor sigma 32. *The EMBO Journal, 14*(11), 2551-2560.

Tomoyasu, T., Yamanaka, K., Murata, K., Suzaki, T., Bouloc, P., Kato, A., . . . Ogura, T. (1993). Topology and subcellular localization of FtsH protein in Escherichia coli. *Journal of Bacteriology, 175*(5), 1352-1357.

Torres, A. G., & Payne, S. M. (1997). Haem iron-transport system in enterohaemorrhagic Escherichia coli O157:H7. *Molecular Microbiology, 23*(4), 825-833.

Torres, A. G., Redford, P., Welch, R. A., & Payne, S. M. (2001). TonB-dependent systems of uropathogenic Escherichia coli: aerobactin and heme transport and TonB are required for virulence in the mouse. *Infection and Immunity , 69*(10), 6179-6185. doi:10.1128/iai.69.10.6179-6185.2001

Touati, D., Jacques, M., Tardat, B., Bouchard, L., & Despied, S. (1995). Lethal oxidative damage and mutagenesis are generated by iron in delta fur mutants of Escherichia coli: protective role of superoxide dismutase. *Journal of Bacteriology, 177*(9), 2305-2314.

Treffry, A., Zhao, Z., Quail, M. A., Guest, J. R., & Harrison, P. M. (1998). How the presence of three iron binding sites affects the iron storage function of the ferritin (EcFtnA) of Escherichia coli. *FEBS Letters, 432*(3), 213-218.

Tsai, Y., Sawaya, M. R., Cannon, G. C., Cai, F., Williams, E. B., Heinhorst, S., . . . Yeates, T. O. (2007). Structural analysis of CsoS1A and the protein shell of the Halothiobacillus neapolitanus carboxysome. *PLoS Biology, 5*(6), e144.

Tsilibaris, V., Maenhaut-Michel, G., & Van Melderen, L. (2006). Biological roles of the Lon ATP-dependent protease. *Research in Microbiology, 157*(8), 701-713.

Tsolis, R. M., Baumler, A. J., Heffron, F., & Stojiljkovic, I. (1996). Contribution of TonB- and Feo-mediated iron uptake to growth of Salmonella typhimurium in the mouse. *Infection and Immunity, 64*(11), 4549-4556.

Velayudhan, J., Castor, M., Richardson, A., Main-Hester, K. L., & Fang, F. C. (2007). The role of ferritins in the physiology of Salmonella enterica sv. Typhimurium: a unique role for ferritin B in iron-sulphur cluster repair and virulence. *Molecular Microbiology, 63*(5), 1495-1507. doi:10.1111/j.1365-2958.2007.05600.x

Velayudhan, J., Hughes, N. J., McColm, A. A., Bagshaw, J., Clayton, C. L., Andrews, S. C., & Kelly, D. J. (2000). Iron acquisition and virulence in Helicobacter pylori: a major role for FeoB, a high-affinity ferrous iron transporter. *Molecular Microbiology, 37*(2), 274-286.

Villaverde, A., & Carrió, M. M. (2003). Protein aggregation in recombinant bacteria: biological role of inclusion bodies. *Biotechnology Letters, 25*(17), 1385-1395.

Winkelmann, G. (2002). Microbial siderophore-mediated transport. *Biochemical Society Transactions, 30*(4), 691-696. doi:10.1042/

Wirth, C., Meyer-Klaucke, W., Pattus, F., & Cobessi, D. (2007). From the periplasmic signaling domain to the extracellular face of an outer membrane signal transducer of Pseudomonas aeruginosa: crystal structure of the ferric pyoverdine outer membrane receptor. *Journal of Molecular Biology, 368*(2), 398-406. doi:10.1016/j.jmb.2007.02.023

Wong, S. G., Abdulqadir, R., Le Brun, N. E., Moore, G. R., & Mauk, A. G. (2012). Fe-haem bound to Escherichia coli bacterioferritin accelerates iron core formation by an electron transfer mechanism. *Biochemical Journal, 444*(3), 553-560.

Wong, S. G., Grigg, J. C., Le Brun, N. E., Moore, G. R., Murphy, M. E., & Mauk, A. G. (2015). The B-type channel is a major route for iron entry into the ferroxidase center and central cavity of bacterioferritin. *Journal of Biological Chemistry, 290*(6), 3732-3739.

Woodmansee, A. N., & Imlay, J. A. (2002). Reduced flavins promote oxidative DNA damage in non-respiring Escherichia coli by delivering electrons to intracellular free iron. *Journal of Biological Chemistry , 277*(37), 34055-34066. doi:10.1074/jbc.M203977200

Yamamoto, K., Ishihama, A., Busby, S. J., & Grainger, D. C. (2011). The Escherichia coli K-12 MntR miniregulon includes dps, which encodes the major stationary-phase DNA-binding protein. *Journal of Bacteriology, 193*(6), 1477-1480. doi:10.1128/jb.01230-10

Yang, X., Le Brun, N. E., Thomson, A. J., Moore, G. R., & Chasteen, N. D. (2000). The iron oxidation and hydrolysis chemistry of Escherichia coli bacterioferritin. *Biochemistry, 39*(16), 4915-4923.

Yasmin, S., Andrews, S. C., Moore, G. R., & Le Brun, N. E. (2011). A new role for heme, facilitating release of iron from the bacterioferritin iron biomineral. *Journal of Biological Chemistry , 286*(5), 3473-3483. doi:10.1074/jbc.M110.175034

Yukl, E. T., Jepkorir, G., Alontaga, A. Y., Pautsch, L., Rodriguez, J. C., Rivera, M., & Moenne-Loccoz, P. (2010). Kinetic and spectroscopic studies of hemin acquisition in the hemophore HasAp from Pseudomonas aeruginosa. *Biochemistry, 49*(31), 6646-6654. doi:10.1021/bi100692f

Zhao, G., Ceci, P., Ilari, A., Giangiacomo, L., Laue, T. M., Chiancone, E., & Chasteen, N. D. (2002). Iron and hydrogen peroxide detoxification properties of DNA-binding protein from starved cells. A ferritin-like DNA-binding protein of Escherichia coli. *Journal of Biological Chemistry , 277*(31), 27689-27696. doi:10.1074/jbc.M202094200

Zheng, M., Doan, B., Schneider, T. D., & Storz, G. (1999). OxyR and SoxRS regulation of fur. *Journal of Bacteriology, 181*(15), 4639-4643.